

A ROLE FOR CAVEOLIN-3 IN THE PATHOGENESIS OF THE *MDX* MOUSE

Dean Paul Larner

A thesis submitted to
The University of Birmingham
for the degree of
DOCTOR OF PHILOSOPHY

School of Biosciences
The University of Birmingham
B15 2TT

September 2011

UNIVERSITY OF
BIRMINGHAM

University of Birmingham Research Archive

e-theses repository

This unpublished thesis/dissertation is copyright of the author and/or third parties. The intellectual property rights of the author or third parties in respect of this work are as defined by The Copyright Designs and Patents Act 1988 or as modified by any successor legislation.

Any use made of information contained in this thesis/dissertation must be in accordance with that legislation and must be properly acknowledged. Further distribution or reproduction in any format is prohibited without the permission of the copyright holder.

ABSTRACT

Duchenne muscular dystrophy (DMD) is a muscle-wasting disease caused by the loss of sarcolemmal protein dystrophin. In DMD and the mouse model of the disease *mdx*, there is an increase in an associated protein, caveolin-3. In this study, *mdx* mice with deficiencies in caveolin-3 were generated to allow a distinction to be made between the pathology caused by the loss of dystrophin and that caused by an excess of caveolin-3.

It was found that in late gestation embryos, there were perturbations in skeletal muscle stem cell populations and depletion of respiratory muscles in *mdx* and *mdx/cav3^{+/-}*, both of which were more severe in *mdx/cav3^{+/-}* embryos. In post natal skeletal muscles, there was a trend in that the level of regeneration, believed to be indicative of previous degeneration, was consistently greater in *mdx* than *mdx/cav3^{+/-}*. Taken together it would appear whereas increased caveolin-3 may compensate for the lack of dystrophin in embryonic *mdx* muscle; post natally, it may contribute to the muscle regeneration observed in *mdx*.

The data presented in this thesis should help towards clarifying the contribution of caveolin-3 in the pathogenesis of DMD and in doing so expand on the understanding of the molecular aetiology of the disease.

ACKNOWLEDGEMENTS

I would like to thank my supervisor Dr Janet Smith for all the help and advice she has given me over the last four years, it is very much appreciated. I would also like to thank Dr Chris Bunce for his valuable input during the times we have met throughout the course of my project.

A big thank you to Professor John Heath and all of the P.I.s, post-docs and Ph.D. students from the 5th and 8th floors, your input and suggestions have been invaluable.

Lastly, I would like to thank my family and close friends for the support they have given me, in particular my wife, who always does everything she can to help me succeed in everything I do.

My appreciation goes to BBSRC for funding my project.

TABLE OF CONTENTS

CHAPTER 1 – INTRODUCTION	1
1.1 - Muscular dystrophy	1
1.1.1 - Duchenne muscular dystrophy	3
1.1.2 - Limb-girdle muscular dystrophy	5
1.1.3 - Limb-girdle muscular dystrophy type 1C (LGMD1C)	6
1.2 - Skeletal muscle	7
1.2 - Dystrophin-associated glycoprotein complex	8
1.2.1 - Dystrophin	10
1.2.2 - Caveolin-3	11
1.3 - Myogenesis	13
1.4 - Myogenic regulatory factors	16
1.5 - Growth factors	17
1.5.1 - Insulin-like growth factors	18
1.5.2 - Myostatin	19
1.6 - Myosin	20
1.7 - Satellite cells	21
1.8 - Paired box transcription factors	23
1.8.1 - Pax7	24
1.9 - Animal models for DMD	24
1.9.1 - Rodent models of muscular dystrophy	25
1.9.2 - The <i>dy/dy</i> mouse and cardiomyopathic Syrian hamster	25
1.9.3 - The <i>mdx</i> mouse	26
1.9.4 - The <i>mdx/utrn</i> ^{-/-} mouse	27
1.9.5 - GRMD dog	27
1.10 - Treatments for Duchenne muscular dystrophy	29
1.10.1 - Corticosteroids	29
1.10.2 - Non-invasive ventilation	30
1.10.3 - Ataluren (PTC-124)	31

1.10.4	- Exon skipping	31
1.10.5	- Myostatin gene therapy	32
1.10.6	- Utrophin upregulation	32
1.10.7	- A matter of time	33
1.11	- Aims and objectives	34
1.11.1	- Aim	34
1.11.2	- Objectives	34

CHAPTER 2 - MATERIALS AND METHODS 36

2.1	- Introduction	36
2.2	- Mouse models used	37
2.3	- Generation of DM mice	40
2.4	- Collection of embryos	41
2.5	- Excision of adult skeletal muscles	43
2.6	- Extraction of DNA from tissues	43
2.6.1	- Isopropanol extraction of DNA	44
2.6.2	- Phenol-chloroform extraction of DNA	45
2.7	- Spectrophotometry	46
2.8	- Polymerase chain reaction	48
2.9	- Gel electrophoresis	50
2.10	- DNA sequencing	51
2.11	- Processing for paraffin wax embedding	53
2.12	- Microtome sectioning of paraffin blocks	56
2.13	- Immunohistochemistry (IHC)	56
2.13.1	- De-waxing, rehydration and antigen retrieval	57
2.13.2	- Peroxidase quenching, blocking and incubation with primary antibodies	58
2.13.3	- Incubation in secondary antibodies and signal amplification	59
2.13.4	- Antigen localisation, counter staining, dehydration and mounting	61
2.14	- Haematoxylin and eosin staining	61

2.15	- Protein extraction	61
2.15.1	- Protein extraction from embryos	62
2.15.2	- Protein extraction from neonate mice, muscle samples and frozen samples	62
2.16	- Protein assay	64
2.17	- Western blotting	64
2.17.1	- Gel casting	66
2.17.2	- Protein sample preparation, loading and running of gels	67
2.17.3	- Transfer to membrane	69
2.17.4	- Membrane probing	70
2.17.5	- Antigen detection	70
2.17.5.1	- Detection using ECL	71
2.17.5.2	- Detection using fluorescence	71
2.17.5.3	- Detection using Streptavidin	72
2.18	- Analysis of regenerating areas in adult muscle	74
2.19	- Statistical analysis	

CHAPTER 3 - GENERATION OF DOUBLE-MUTANTS AND CHARACTERISATION OF DMHET EMBRYOS

		75
3.1	- INTRODUCTION	75
3.2	- RESULTS	77
3.2.1	- Generation of DM litters	77
3.2.1.1	- Litters produced via <i>mdx</i> and <i>cav3</i> ^{-/-} crosses	77
3.2.1.2	- <i>mdx</i> and DMhet littermates	80
3.2.1.3	- Sequencing to confirm the presence of the <i>mdx</i> mutation	84
3.2.2	- Caveolin-3 protein levels are reduced in DMhet embryos	87
3.2.3	- Pax7 ^{+ve} cells are severely attenuated in DMhets	90
3.2.4	- Reduced fibre-density in dystrophin-deficient intercostal muscles	93
3.2.5	- MF20 and MY32 labelled diaphragms	96
3.2.5	- α -tubulin appears perturbed in dystrophic embryos	99

3.3	- DISCUSSION	102
3.3.1	- Generation of caveolin-3 deficient <i>mdx</i> mice	102
3.3.2	- Embryonic phenotype of DMhet	103
3.3.2.1	- Attrition of pax7 ⁺ ve cells in DMhets	103
3.3.2.2	- Fibre loss in intercostals of dystrophin-deficient mutants	105
3.3.3	- Tubulin upregulation	106

CHAPTER 4 - CORRELATION OF CAVEOLIN-3 TO THE OBSERVED PATHOLOGY IN POST NATAL DYSTROPHIN-DEFICIENT MICE

4.1	- INTRODUCTION	107
4.2	- RESULTS	110
4.2.1	- IHC and immunoblotting confirms the loss of caveolin-3 in the DM	110
4.2.2	- Macroscopic analysis of the DM	116
4.2.3	- Regeneration of dystrophin-deficient proximal limb muscles	121
4.2.3.1	- Histology of four weeks triceps and quadriceps	121
4.2.3.2	- Histology of nine weeks triceps and quadriceps	131
4.2.3.3	- Histology of nine months triceps and quadriceps	140
4.2.4	- Respiratory muscles	149
4.2.4.1	- Intercostals	149
4.2.4.2	- Diaphragm	153
4.2.5	- Fibre diameter variation in dystrophin-deficient mutants	156
4.2.6	- Quantification of muscle regeneration	162
4.2.6.1	- Hypercellular aggregation	162
4.2.6.2	- Centrally located myonuclei	165
4.2.6.3	- Extra-myonuclei in dystrophin-deficient mutants	165
4.3	- DISCUSSION	169
4.3.1	- The macroscopic analysis of dystrophin-deficient mice	169
4.3.1.1	- Mobility and general appearance	169
4.3.1.2	- Muscle mass	170
4.3.1.3	- Fat deposition	172

4.3.2	- Muscle regeneration in caveolin-3 dystrophin-deficient mice	173
4.3.2.1	- Cell infiltration into regenerating areas	173
4.3.2.2	- Centrally nucleated fibres are more prevalent in <i>mdx</i>	175
4.3.3	- The histopathogenesis of respiratory muscles in dystrophin-deficient mutants	177
4.3.4	- Muscle fibre calibre variations in dystrophin-deficient mutants	178
CHAPTER 5 - CONCLUSIONS AND FUTURE WORK		181
5.1	- Conclusions	181
5.1.1	- Caveolin-3 in embryonic myogenesis	181
5.1.2	- Caveolin-3 in adult myoregeneration	181
5.1.3	- Heterogeneity of muscle fibre calibres	182
5.2	- Future work	183
	REFERENCES	185
	APPENDIX	199

TABLE OF FIGURES

1.1	- Illustration showing five different types of muscular dystrophy	2
1.2	- Two signs synonymous with DMD	5
1.3	- Diagrammatic representation of the macro-to-micro structure of muscle	8
1.4	- The dystrophin-associated glycoprotein complex	10
1.5	- Caveolin-3 is an integral protein of caveolae	13
1.6	- Illustrated representation of a transverse view of an early stage embryo	14
1.7	- Myostatin deficiency causes excessive skeletal muscle growth	20
1.8	- Schematic illustration showing regeneration of a myofibre following myotrauma	23
1.9	- Muscular dystrophy in the Golden Retriever	28
1.10	- DMD patient using a non-invasive ventilator	30
2.1	- Diagram of a pregnant female mouse with opened abdomen prior to embryo collection showing bi-lateral uterus	41
2.2	- Images of skinned fore and hindlimbs	42
2.3	- Electrophoresis gel apparatus	50
2.4	- Microtome used for the cutting of paraffin wax embedded sections	55
2.5	- Representative illustration of a protein assay plate	63
2.6	- Gel casting	66
2.7	- Illustrated representation of cassette 'sandwich'	68
2.8	- Early stage regeneration at x 20 magnification	73
3.1	- Generation of caveolin-3 deficient <i>mdx</i> mice (DM)	78
3.2	- Genotyping of F2, F3 and F4 litters	82
3.3	- Sequencing of the <i>Dmd</i> gene to confirm the presence of the <i>mdx</i> mutation in DM	85
3.4	- Caveolin-3 probed membranes and sections of WT, <i>mdx</i> , <i>cav3</i> ^{-/-} and DMhets	88
3.5	- Pax7 labelled intercostal muscles	91

3.6	- E17.5 WT, <i>mdx</i> and DMhet MF20 labelled intercostal muscles	94
3.7	- Diaphragm muscles of E17.5 WT, <i>mdx</i> and DMhets	97
3.8	- Immunoblots of E13.5 – E17.5 WT, <i>mdx</i> , <i>cav3</i> ^{-/-} and DMhet membranes probed for caveolin-3, α -tubulin and β -actin	100
4.1	- Stages of muscle regeneration in <i>mdx</i>	109
4.2	- Membranes probed with antibodies to caveolin-3 and α -tubulin	112
4.3	Caveolin-3 protein levels and localisation in WT, <i>mdx</i> , <i>cav3</i> ^{-/-} , DMhet and DM	114
4.4	- Macroscopic analysis of nine month old WT, <i>mdx</i> , <i>cav3</i> ^{-/-} and DM somatotypes	117
4.5	- Line graphs showing live bodyweights of adult WT, <i>mdx</i> , <i>cav3</i> ^{-/-} and DM colonies	119
4.6	- H&E stained four weeks old triceps	123
4.7	- H&E stained four weeks old quadriceps	125
4.8	- Images of four weeks old H&E stained triceps muscles	127
4.9	- Images of four weeks old H&E stained quadriceps muscles	129
4.10	- H&E stained nine weeks old triceps	132
4.11	- H&E stained nine weeks old quadriceps	134
4.12	- Images of nine weeks old H&E stained triceps	136
4.13	- Images of nine weeks old H&E stained quadriceps	138
4.14	- H&E stained nine months old triceps	141
4.15	- H&E stained nine months old quadriceps muscles	143
4.16	- Images of nine months old H&E stained triceps	145
4.17	- Images of nine months old H&E stained quadriceps	147
4.18	- H&E stained intercostal muscles	151
4.19	- H&E stained diaphragm muscle	154
4.20	- Graphical representation of fibre diameter sizes of nine weeks triceps muscles	158
4.21	- Pie charts showing proportions of small, medium, large and extra-large muscle fibres in nine weeks old WT, <i>mdx</i> , <i>cav3</i> ^{-/-} and DM triceps muscles	160

4.22	Regeneration in <i>mdx</i> and DM triceps and quadriceps muscles	163
4.23	- Graphical representation of central nucleated myofibres and extra-myonuclei	167

TABLE OF TABLES

2.1	- Mice used and the dystrophic models they represent	37
2.2	- Generation of DM mice	39
2.3	- Primers used for the purposes of genotyping and sequencing	48
2.4	- Processes involved in paraffin embedding of embryonic and neonate mice and adult muscle samples	53
2.5	- Antibodies used for IHC during the course of this project	58
2.6	- Antibodies used for western blotting during the course of this project	69
3.1	- Summary of results	106
4.1	- Summary of results	180

ABBREVIATIONS USED

APS	ammonium persulphate
bHLH	basic helix-loop-helix
BMD	Becker muscular dystrophy
BMSU	biomedical services unit
BSA	bovine serum albumin
Cav3	caveolin-3
DAB	diaminobenzidine tetrahydrochloride
dATP	deoxyadenosine triphosphate
dCTP	deoxycytidine triphosphate
DGC	dystrophin-associated glycoprotein complex
dGTP	deoxyguanosine triphosphate
dH ₂ O	distilled water
DM	double-mutant
DMD	Duchenne muscular dystrophy
DMhet	double-mutant heterozygous
DNA	deoxyribonucleic acid
dTTP	deoxythymidine triphosphate
ECL	enhanced chemiluminescence
EDTA	ethylenediaminetetra acetic acid
EtOH	ethanol
FGF	fibroblast growth factor
FMyHC	fast myosin heavy chain
GH	growth hormone
H&E	haematoxylin and eosin
HCl	hydrochloric acid
H ₂ O	water
H ₂ O ₂	hydrogen peroxide
HRP	horse-radish peroxidase
IGF	insulin-like growth factor
IGF-1R	type 1 igf receptor
IGF-2R	type 2 igf receptor

IHC	immunohistochemistry
IR	insulin receptor
kDa	kilo-Dalton
LGMD	limb-girdle muscular dystrophy
LN ₂	liquid nitrogen
MD	muscular dystrophy
Mdx	X-linked muscular dystrophy (mouse)
MeOH	methanol
MgCl ₂	magnesium chloride
MRF	myogenic regulatory factor
MSTN	myostatin
MyHC	myosin heavy chain
NaCl	sodium chloride
NaOH	sodium hydroxide
Neo	neomycin
nNOS	neuronal nitric oxide synthase
PAGE	polyacrylamide gel electrophoresis
PBS	phosphate-buffered saline
PCR	polymerase chain reaction
PFA	paraformaldehyde
RNA	ribonucleic acid
rpm	revolutions per minute
sdH ₂ O	sterile distilled water
SMSc	skeletal muscle stem cells
sPBS	sterile phosphate buffered saline
TBS	tris-buffered saline
TGF	transforming growth-factor
TSA	tyramide signal amplification
UTRN	utrophin
UV	ultra-violet
VP	vaginal plug
WT	wild-type

CHAPTER 1 – INTRODUCTION

This thesis focuses on the muscle-specific protein caveolin-3 and the histological pathogenesis of the *mdx* mouse, an animal model for Duchenne muscular dystrophy (DMD). It has been known for more than a decade that caveolin-3 is upregulated in both *mdx* mouse and males' suffering with DMD and was suggested the upregulation of caveolin-3 contributed to the observed pathogenesis. In order to investigate this further, *mdx* mice with hypophysiological levels of caveolin-3 and *mdx* mice deficient in caveolin-3 were generated and analyses made using haematoxylin and eosin staining, immunohistochemistry and immunoblotting (which shall be referred to as western blotting throughout this thesis) on embryonic and adult tissues. The analyses of embryonic tissue in a disease that is generally believed to initially present with the dystrophic phenotype postnatally is justified in light of recent data, that suggests the dystrophic phenotype has an embryonic origin.

1.1 - Muscular dystrophy

The muscular dystrophies are a group of around seventy inheritable skeletal muscle-specific diseases distinct from other myopathies in that there is no associated neuro-degeneration, they are characterised by progressive muscle degeneration and subsequent loss of strength. Like other myopathies, there is usually an increase in serum creatine kinase. Histologically, dystrophic muscle tissue contains areas of degeneration/regeneration and necrosis with fibres of varying sizes and areas of connective and adipose tissue. Many muscular dystrophies are the result of genetic

mutations of the genes encoding proteins of the dystrophin-associated glycoprotein complex (DGC). Muscular dystrophies were initially classified into three principal groups; Duchenne – the most common and severe type (section 1.1.1), limb-girdle and facioscapulohumeral and three rarer groups; distal, oculopharyngeal and congenital, depending on the anatomical location of the affected muscles. They are classified today following histological, molecular and genetic analysis of the patient (Edmondson and Olson, 1989).

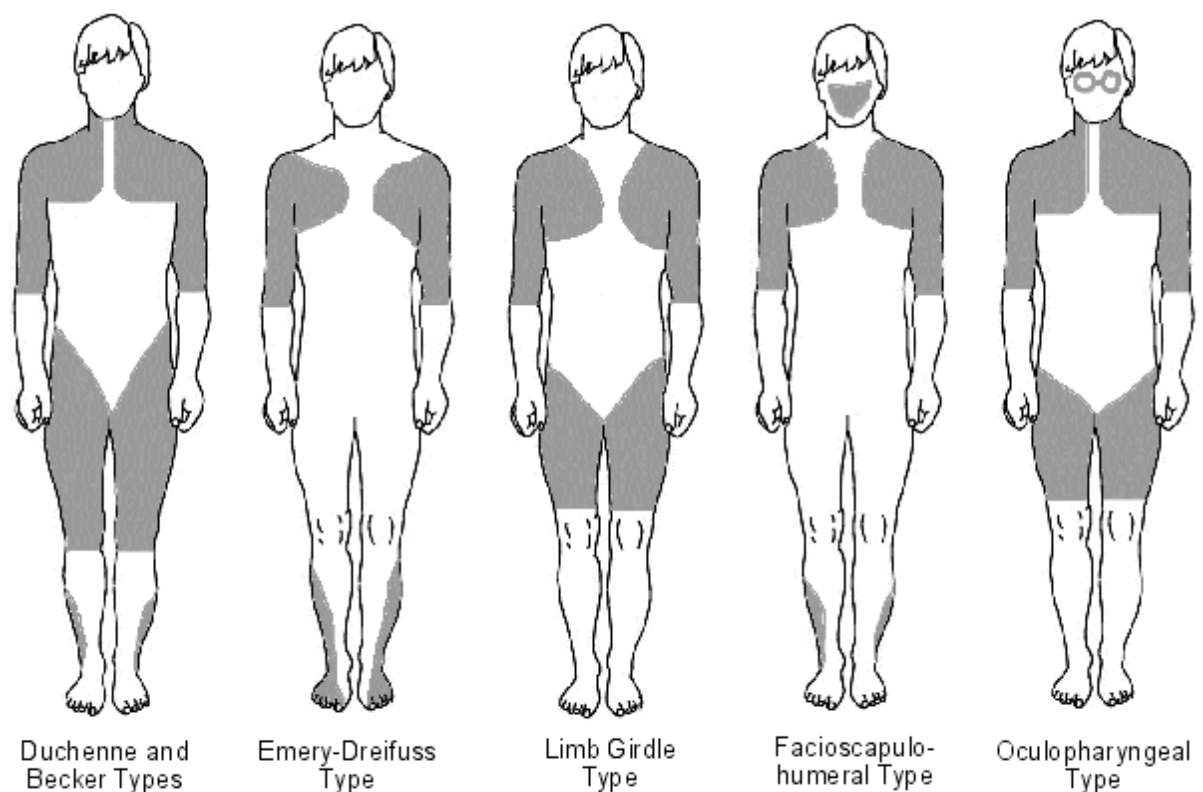


Image from - <http://www.patient.co.uk/health/Muscular-Dystrophies-An-Overview.htm>

Figure 1.1 - Illustration showing five different types of muscular dystrophy.

DMD, the most severe of all the muscular dystrophies affects most of the muscles in the body, while others affect specific areas. Many present with cardiomyopathy also.

1.1.1 - Duchenne muscular dystrophy

Duchenne muscular dystrophy (DMD) is the most common and debilitating of all muscular dystrophies, it is characterised by progressive global muscle degeneration resulting in subsequent loss of strength and impaired mobility (Meryon, 1851). Although eponymously named after Guillaume-Benjamin Amand Duchenne de Boulogne following his report in 1861, the disease was initially described by Edward Meryon ten years previously. Prior to the disease being known as Duchenne dystrophy or Meryon's disease, it was referred to as pseudohypertrophic muscular dystrophy due to the pronounced calf enlargement exhibited by many with the disease; this name however was not accurate as not all displayed the pseudohypertrophic phenotype and this particular phenotype was also seen in other types of muscular dystrophy (Walton, 1956). DMD occurs as a result of a mutation of the *dystrophin* (*DMD*) gene, located on chromosome Xp21, which results in the absence of sarcolemmal protein dystrophin (section 1.3.1). Dystrophin is an integral protein of the DGC (section 1.3) and its absence results in the breakdown of the DGC. There is also a concomitant increase in DGC associated protein caveolin-3 (section 1.3.2) (Repetto *et al.*, 1999). Microarray analysis has provided data showing that many genes are differentially expressed in DMD muscle compared to healthy muscle and that there is a correlation between pathological severity and the degree of differential gene expression (Haslett *et al.*, 2002; Porter *et al.*, 2002; Noguchi *et al.*, 2003). DMD affects 1/3,500 live male births, making it the second most common single gene disorder thus far identified next to cystic fibrosis (Repetto *et al.*, 1999). Although an inheritable genetic disorder, one third of all cases arise via spontaneous mutations within the *DMD* gene. As the disease is X-linked, far more males than females are affected by the disease however, between 1993 and 1999, four of the

three hundred and fifty-five deaths due to DMD in England and Wales were female (Calvert *et al.*, 2006). This figure represents 1.1 % of mortalities recorded. Symptoms usually manifest when the infant exhibits difficulty with ambulation and in the absence of any familial history of the disease, a diagnosis given between the ages of three and five; by which time the disease has had a profound effect on the child's mobility. Disease progression is such that loss of independent ambulation occurs at an average age of nine (Eagle *et al.*, 2002). If left untreated death usually occurs in the mid-to-late teens, 56 % of mortalities due to respiratory failure although in 95 % of cases there is also cardiomyopathy (Walton and Nattrass, 1954; Cox and Kunkel, 1997; Calvert *et al.*, 2006). Though the general consensus that the malady of DMD becomes symptomatic during the child's early ambulatory years, knowledge of increased serum creatine kinase levels in DMD neonates has been known for many years and more efficient means of identifying the disease developed, with a view to earlier treatments (Zellweger and Antonik, 1975).

One aspect of DMD that has received far less research is the effect the loss of dystrophin has on brain physiology. Studies evaluating cognitive function have shown that DMD boys have cognitive impairment and a lower average IQ than healthy subjects; moreover, incidents of autism spectrum disorder/persuasive developmental disorder are far more prevalent in DMD boys than in the general population (Anderson *et al.*, 2002; Wu *et al.*, 2005).

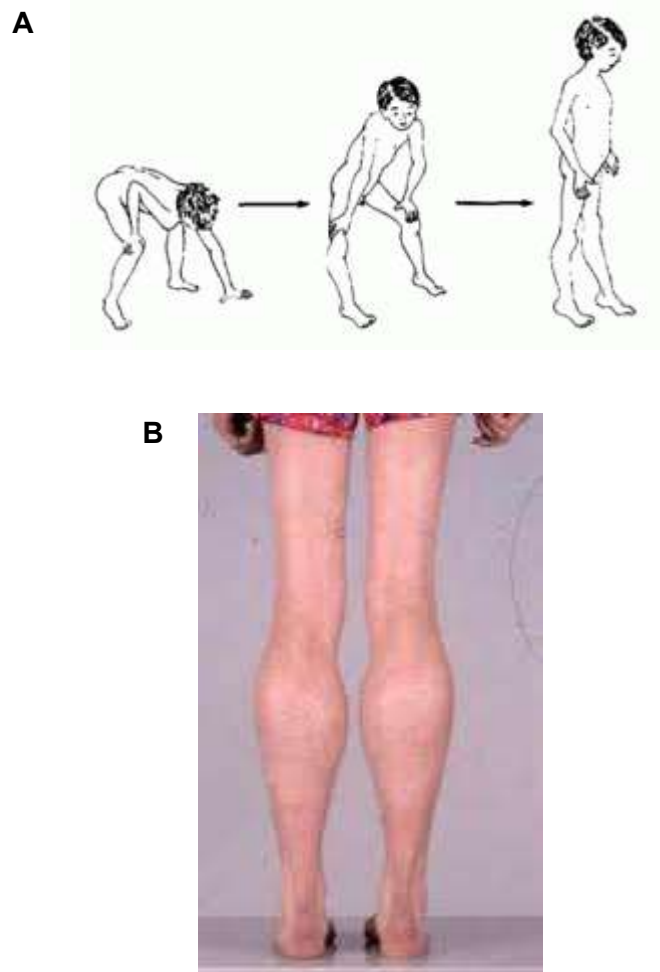


Figure 1.2 - Two signs synonymous with DMD. (A) To rise from the floor, ambulatory DMD boys must use what is referred to as the 'Gower's sign', a manoeuvre whereby the arms are used to help straighten the legs and trunk until an upright position is achieved. (B) Enlarged calf muscles are a common feature of DMD, but as the enlargement is due to an accumulation of adipose and connective tissue rather than muscular hypertrophy, the condition is referred to as 'pseudohypertrophy'.

1.1.2 - Limb-girdle muscular dystrophy

The limb-girdle muscular dystrophies (LGMD) are a heterogeneous group of muscular dystrophies that affect skeletal muscles of the shoulders, hips and proximal limbs. As

with all muscular dystrophies this manifests in the degeneration of effected muscles and subsequent loss of strength; cardiomyopathy may or may not accompany the disease (Mathews and Moore, 2003). There are a total of twenty-two limb-girdle muscular dystrophies thus far identified, which are sub-divided into types 1 and 2; type-1 are inherited in an autosomal dominant manner and includes the caveolinopathy LGMD type 1C (LGMD-1C) whereas type-2 are inherited in an autosomal recessive manner and includes the sarcoglycanopathies (LGMD-2C-F) (Gordon *et al.*, revised 2009). Cardiomyopathy is often present in all sarcoglycanopathies, with the exception of LGMD-2D (α -sarcoglycanopathy), perhaps due to the substitution of α -sarcoglycan with ϵ -sarcoglycan in smooth muscle and as a consequence no loss of sarcoglycan complex integrity in the plasma membrane of the coronary artery endothelium (Straub *et al.*, 1999).

1.1.3 - Limb-girdle muscular dystrophy type 1C (LGMD-1C)

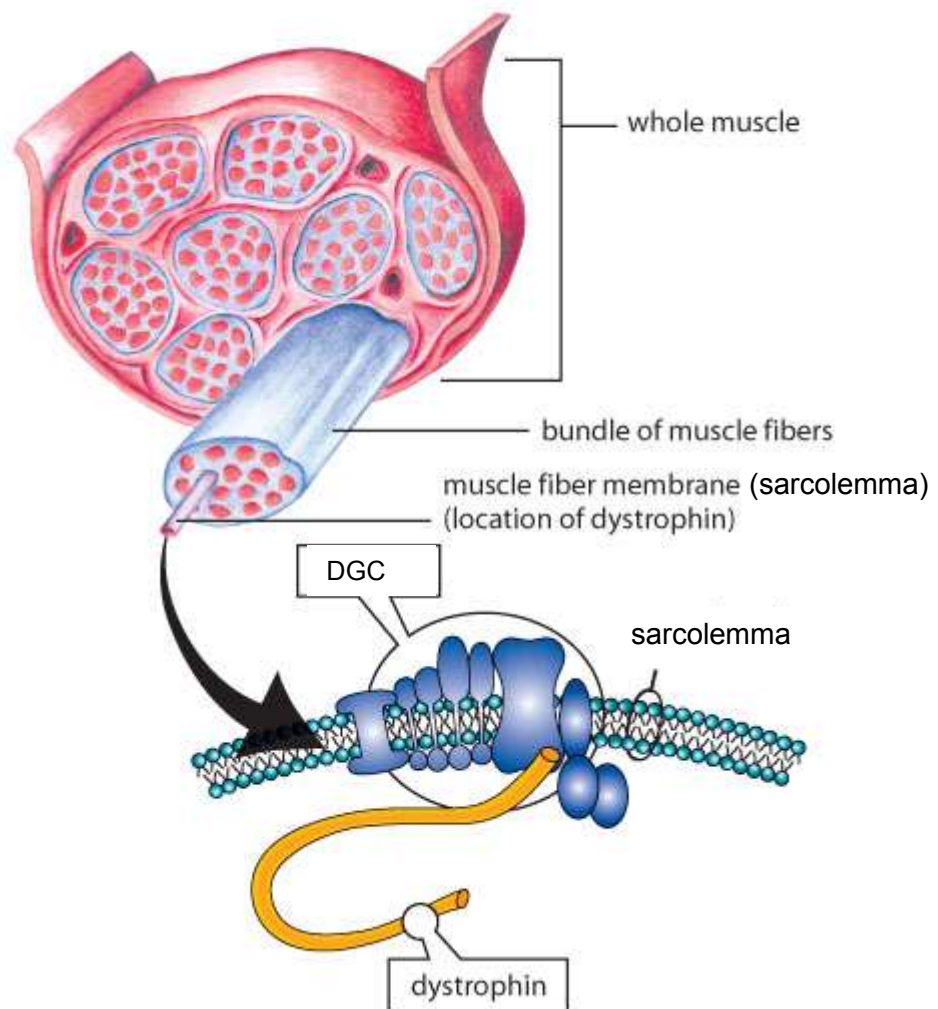
LGMD-1C was the third of the autosomal dominant limb-girdle muscular dystrophies to be recognised and is caused by the absence of sarcolemmal protein caveolin-3 (McNally *et al.*, 1998; Minetti *et al.*, 1998). The disease generally progresses at a far slower rate than the more severe DMD and muscle degeneration and weakness is limited to muscles of the shoulders, hips and proximal limbs; mortality as a consequence of LGMD-1C is rare. There are several mutations associated with LGMD-1C, the first two identified were a missense mutation that substitutes a proline for a leucine (P104L) in the transmembrane domain of caveolin-3 and a micro-deletion of nine base pairs that result in the removal of the amino acid sequence of threonine, phenylalanine, threonine (TFT) in the scaffolding region of the protein (Minetti *et al.*, 1998). Other mutations identified

include a G55S and a C71W (McNally *et al.*, 1998). Oddly, three distinctly separate phenotypes can occur as a result of the same mutation in the human *CAV3* gene; LGMD-1C, hyperCKaemia and hereditary muscle rippling disease, suggesting epigenetic factors may play a role in the progression of caveolinopathy.

1.2 – Skeletal muscle

Skeletal muscle accounts for approximately 38 % and 31 % of total body mass for male and female adult humans respectively (Janssen *et al.*, 2000). It is a dynamic tissue that has the ability to adapt according to the demands placed upon it. Strenuous physical exercise, or to be more precise, intense anaerobic exercise such as weight resistance training, can result in dramatic increases in muscular size and strength through muscle fibre hypertrophy. Conversely, disuse through inactivity results in muscular atrophy; which may also occur due to senescence, referred to as sarcopenia and often manifests as a result of cancer cachexia (reviewed in (Baracos, 2001; Doherty, 2003)).

Skeletal muscles provide bodily movement through their attachment to skeletal bones via tendons of origin and tendons of insertion. It is the bone to which the insertions are attached that is moved during muscular contractions. Skeletal muscle is comprised of bundles of individual fibres (refer to **Figure 1.3**), each of which is formed via the fusion of multiple myotubes, a process mediated by metalloproteases referred to as meltrins; muscle fibres are therefore multi-nucleated (Yagami-Hiromasa *et al.*, 2002). Dystrophin and the proteins of the DGC are associated with the plasma membrane of the muscle fibre, which is referred to as the sarcolemma by muscle physiologists (Zubrzycka-Gaarn *et al.*, 1988; Ervasti and Campbell, 1991).



Adapted from MDA Publications 2011

Figure 1.3 - Diagrammatic representation of the macro-to-micro structure of muscle. Skeletal muscles are comprised of bundles of muscle fibres, each fibre resulting from the fusion of multiple myotubes. Dystrophin and the proteins of the DGC are associated with the sarcolemma of muscle fibres.

1.3 - Dystrophin-associated glycoprotein complex

Associated with the sarcolemma is a complex of proteins referred to as the Dystrophin-associated glycoprotein complex (DGC) (Ervasti and Campbell, 1991). The complex

consists of sarcoglycans, dystroglycans, syntrophins, sarcospan, dystrobrevin and dystrophin. The sarcoglycan complex consists of subunits α , β , γ and δ which are glycosylated single-pass transmembrane proteins (Ervasti and Campbell, 1991). Their function within the complex is to stabilise, along with sarcolemmal bound tetraspanin family member sarcospan, the dystroglycan complex and afford the complex protection against mechanical stress during muscular contractions. Although absence of any of the sarcoglycans results in autosomal-recessive LGMD, sarcospan deficiency has no apparent detrimental effect (Lebakken *et al.*, 2000). Dystroglycans α and β are also glycosylated, α -dystroglycan, a large extracellular 156 kDa protein, binds laminin-2 of the extracellular matrix (Ervasti and Campbell, 1991; Corrado *et al.*, 1994). β -dystroglycan is a 43 kDa transmembrane spanning glycoprotein that binds dystrophin at its C-terminus via a PPxY motif (Jung *et al.*, 1995; Rentschler *et al.*, 1999). Absence of β -dystroglycan is embryonic lethal, with the embryo reabsorbed by E10.5 (Williamson *et al.*, 1997).

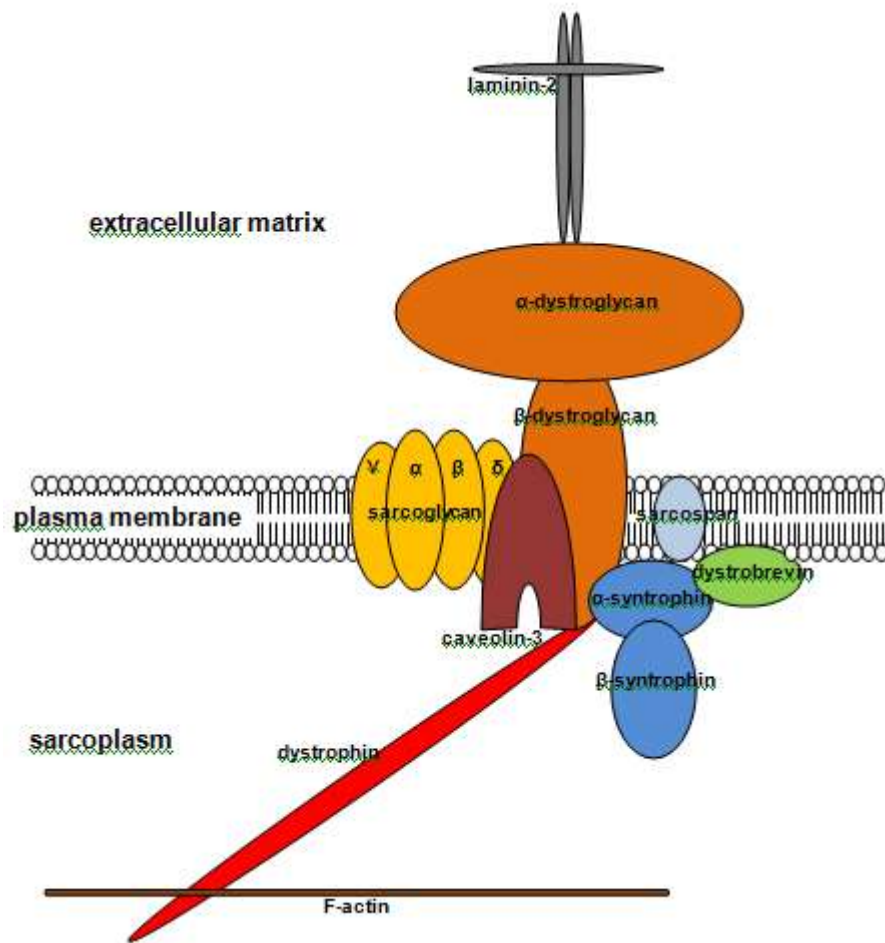


Figure 1.4 - The dystrophin-associated glycoprotein complex. Rod-like dystrophin, via the dystroglycans, anchors the DGC to the sarcolemma affording protection against mechanical stress. The proteins of the DGC are believed to be involved in cell-signalling and their mutations' often result in myopathies referred to as muscular dystrophies. Caveolin-3 is not an integral protein of the DGC but localises with dystrophin, where both bind to β -dystroglycan.

1.3.1 - Dystrophin

The *DMD* gene is the largest in the human genome; spanning 2.4 Mb over 79 exons, its mRNA is 14 kb in length and takes 16 hours to transcribe (Tennyson *et al.*, 1995). The

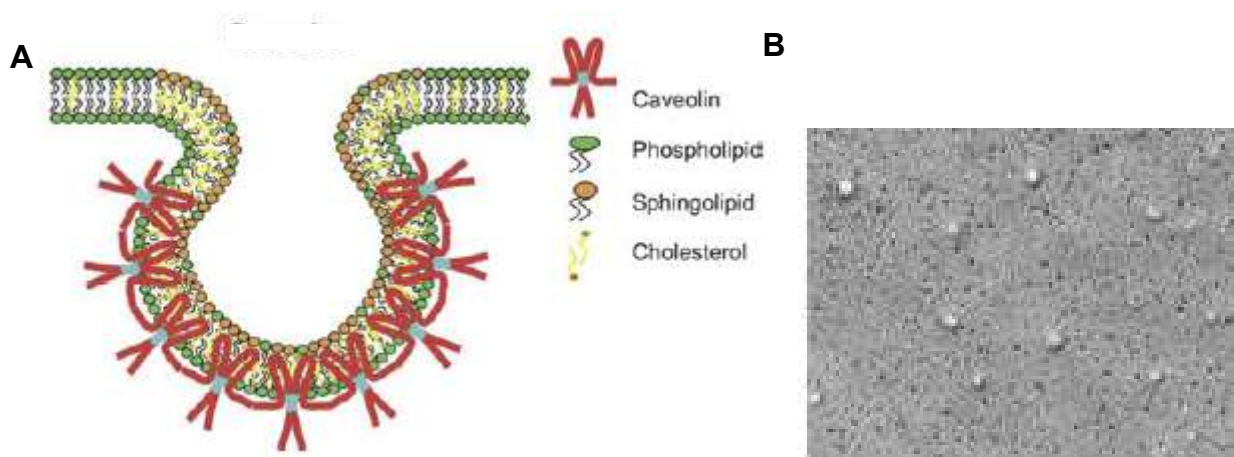
dystrophin protein accounts for 0.002 % of total skeletal muscle protein and 5 % of sarcolemmal protein, consists of 3685 amino acid residues and has a molecular weight of 427 kDa (Hoffman *et al.*, 1987; Tennyson *et al.*, 1995). The *DMD* gene is located on the X chromosome; Xp21-Xp223 and was identified as the *DMD* protein in 1987 by Hoffman and colleagues and as its absence or truncation was associated with Duchenne and Becker muscular dystrophies respectively, was named dystrophin (Lindenbaum *et al.*, 1979; Zatz *et al.*, 1981; Murray *et al.*, 1982; Davies *et al.*, 1983). Its four domains consist of an N-terminal of 240 amino acids, a second domain of 25 triplehelices, a cysteine-rich third domain and a C-terminal of 420 amino acid residues, affording dystrophin a rod-like structure of 150 nm in length (Koenig *et al.*, 1988). An integral component of the DGC, a group of sarcolemmal associated proteins that function in cell signalling (reviewed in (Rando, 2001)), dystrophin localises to the sarcolemma, where it binds via a WW domain of its C-terminus to a PPxY motif of the β sub-unit of trans-sarcolemmal DGC protein dystroglycan (Zubrzycka-Gaarn *et al.*, 1988; Jung *et al.*, 1995). An N-terminal domain of dystrophin, consisting of 90 amino acid residues, binds to f-actin of the cytoskeleton, dystrophin therefore anchors the DGC to the sarcoplasm, to which it is believed to afford protection against mechanical stress (Petrof *et al.*, 1993; Corrado *et al.*, 1994). The absence of dystrophin results in a breakdown of the DGC, compounding its importance in maintaining the integrity of the complex (Ervasti *et al.*, 1990; Ohlendieck and Campbell, 1991).

1.3.2 - Caveolin-3

Associated with, but not an integral DGC protein is caveolin-3 or M-caveolin; the muscle-specific isoform of the caveolin family is expressed in smooth, cardiac and skeletal

muscle (Song *et al.*, 1996; Tang *et al.*, 1996; Crosbie *et al.*, 1998). The *CAV3* gene is located on chromosome 3p25 in humans and consists of 2 exons spanning 12 kb of DNA, which encodes a 1.5 kb transcript translating to a 151 amino acid protein with a molecular weight of around 17 kDa (McNally *et al.*, 1998; Minetti *et al.*, 1998). Caveolin-3 homo-oligomerises and as hydrophobic residues are present within the central region of the protein, both N and C terminals position on the sarcoplasmic side of the cell; resulting in hairpin-like structures (refer to **Figure 1.5 A**). Caveolin-3 is an integral component of caveolae that form 50-100 nm invaginations within the sarcolemma of myofibres, where it acts as a scaffolding protein for lipid-modified proteins (reviewed in (Smart *et al.*, 1999)). Caveolins function in cell signalling often playing inhibitory roles; and in endocytosis (Hulit *et al.*, 2000; Rodriguez *et al.*, 2009). Caveolin-3 directly interacts with neuronal nitric oxide synthase (nNOS) where it inhibits signalling (Venema *et al.*, 1997). Mutations in the *CAV3* gene result in three distinct pathological phenotypes: LGMD-1C, inheritable rippling muscle disease (RMD) and hyperCKaemia (Minetti *et al.*, 1998). LGMD-1C is a muscular dystrophy that effects predominantly muscles of the hips, shoulders and proximal limbs, although cardiomyopathy is also a condition of the disease, it is inherited through the autosomal dominant mode of transmission (Minetti *et al.*, 1998). Caveolin-3 initially appears at the sarcolemma during the differentiation of myocytes, where it co-localises with dystrophin and via WW domains, competitively binds to a PPxY motif located at the C-terminus of β -dystroglycan, a DGC glyco-protein vital for embryonic survival (Song *et al.*, 1996; Williamson *et al.*, 1997; McNally *et al.*, 1998; Rentschler *et al.*, 1999; Sotgia *et al.*, 2000). *CAV3* is upregulated in DMD and *mdx* mouse and transgenic mice that over-express *Cav3* exhibit a Duchenne-like phenotype; suggesting caveolin-3 may contribute to the

pathogenesis of the disease, although recent data suggests a compensatory rather than contributory role to the pathogenesis of DMD (Vaghy *et al.*, 1998; Repetto *et al.*, 1999; Galbiati *et al.*, 2000; Merrick *et al.*, 2009). Transgenic mice exhibiting autosomal recessive and dominant forms of inheritance, *cav3*^{-/-} and TgCAV3M1 respectively, have been generated as animal models for LGMD-1C (Hagiwara *et al.*, 2000; Ohsawa *et al.*, 2004).



Razani & Lisanti (2002) *Reviews in Undergraduate Research*. 1: 44-50

Hagiwara *et al.* (2000) *Hum. Mol. Gen.* 9: 3047-33054

Figure 1.5 - Caveolin-3 is an integral protein of caveolae. (A) Caveolin-3 homooligomerises to form hairpin-like structures in caveolae, where it associates with cholesterol and sphingolipids. (B) Freeze-fracture electron micrograph of the soleus of a WT mouse shows sarcolemmal caveolae.

1.4 - Myogenesis

The process of muscle generation is referred to as myogenesis and is derived from the Greek *mys* (muscle) and *genesis* (origin). Although myogenesis is usually used in

reference to the development of the musculature in the embryo, the process is recapitulated in postnatal muscle tissue following myotrauma. Following fertilisation, cleavage and multiple cell divisions of the mammalian ovum, the blastula undergoes gastrulation; establishing the three germ layers and anterioposterior axis of the embryo. Epithelialisation of paraxial mesoderm in a rostral to caudal direction results in the formation of pairs of mesodermic blocks adjacent to the neural tube, called somites (Christ and Ordahl, 1995). Somitic mesoderm differentiates to form the sclerotome and the dermomyotome, which as the name suggests, is comprised of dermatomal and myotomal cells; it is the myotome from which cells destined for the myogenic lineage are derived. Cells of the dermatome give rise to the dermis of the back and those derived from the sclerotome the vertebrae and ribs (Christ and Ordahl, 1995).

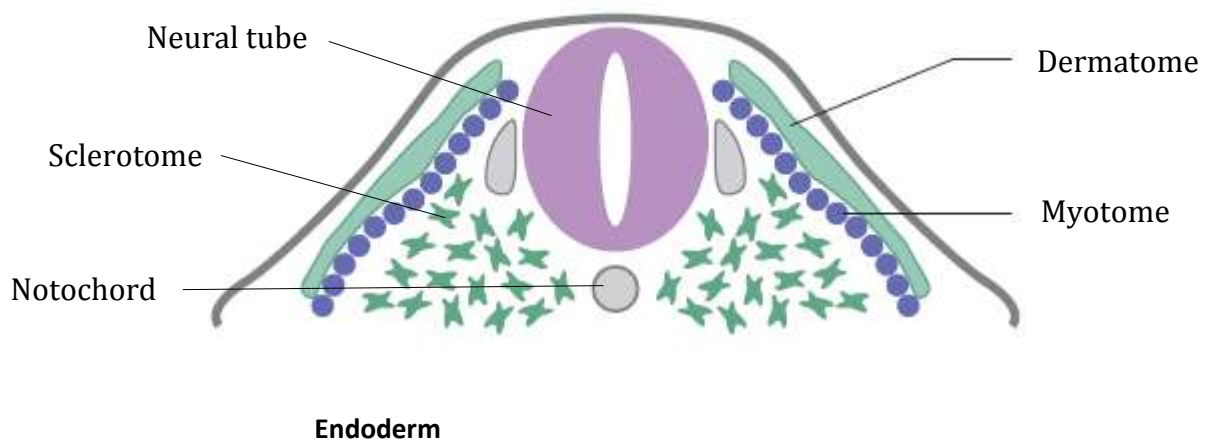


Image adapted from Somitogenesis in Vertebrate Development Yoshiko Takahashi *ENCYCLOPEDIA OF LIFE SCIENCES* © 2004, John Wiley & Sons Ltd.

Figure 1.6 - Illustrated representation of a transverse view of an early stage embryo. Blocks of somites arranged in pairs develop laterally to the neural tube and notochord. It is from the myotome that cells destined to form the musculature are derived. The image represents a two day old chick embryo.

Myogenesis is under the control of transcription factors called myogenic regulatory factors (MRFs), MRFs are themselves activated by transcription factors which include pax-3 and pax-7 (reviewed in (Pownall *et al.*, 2002)). Other regulators essential to the myogenic programme include mef2, six, eya, wnt, sonic hedgehog and the notch ligand delta-like 1; there is also evidence that micro-RNAs (miRNA) play a role in myogenic regulation (Naidu *et al.*, 1995; Cossu and Borello, 1999; Chen *et al.*, 2005; Giordani *et al.*, 2007; Grifone *et al.*, 2007; Sun *et al.*, 2008). Myogenesis takes place in two stages; primary and secondary. Primary myogenesis in the mouse occurs between embryonic day (E) 9.5 and E13.5 during which time a scaffold of short thick myotubes is established throughout the developing musculature of the embryo. During secondary myogenesis, which commences around E11.5 in the mouse and continues into neonatal life, longer thinner myotubes are established around the primary myotubes. Primary and secondary myotubes not only differ in their morphology but also in the myosin heavy chain (MyHC) isoform they express; primary express the slow type 1 and secondary express the fast type 2. During the later stages of secondary myogenesis, around E14.5 in the mouse, fibre-type switching occurs, where some MyHC-1 switch to MyHC-2 and vice versa, resulting in varying mixed fibre-types within muscle groups. The ratio of type 1 to type 2 MyHC varies dependent on their anatomical position. Fibre-type switching is an important process as muscles that are required to contract for longer periods of time e.g. soleus, must have a greater ratio of MyHC-1 to MyHC-2 fibres, as although type 2 fibres are more explosive, they are not as efficient at continued contractions as the slower MyHC-1 fibres.

1.5 - Myogenic regulatory factors

There are four members of the myogenic regulatory factor (MRF) family; *Myf-5* (myogenic factor 5) and *MyoD* (myogenic differentiation) are expressed in undifferentiated myoblasts, whereas *Myog* (myogenin) and *MRF4* (muscle-specific regulatory factor 4) are expressed in post-mitotic differentiated myotubes; all MRFs are defined by their ability to induce a wide variety of cells into the myogenic programme (Davis *et al.*, 1987; Braun *et al.*, 1989; Edmondson and Olson, 1989; Rhodes and Konieczny, 1989; Wright *et al.*, 1989; Braun *et al.*, 1990; Choi *et al.*, 1990; Miner and Wold, 1990). All MRFs have a basic helix-loop-helix (bHLH) motif and as is typical of most transcription factors with this motif, MRFs form heterodimers with enhancer box sequences (E-boxes) of gene promoter regions of DNA (reviewed in (Weintraub *et al.*, 1991; Olson and Klein, 1994)). MRFs are sequentially expressed spatiotemporally during embryogenesis with *Myf-5* transcripts in mouse somites appearing at E8, followed by *Myog* at E8.5, *MRF4* is expressed biphasically, first between E9 and E12 and the second wave of expression coinciding with fibre-type specification and innervation at E14.5, although work from the Rigby group suggested *MRF4* may be contemporaneously expressed with *Myf-5*; the final member, *MyoD* is expressed at E10.5 and continues into adulthood (Sassoon *et al.*, 1989; Bober *et al.*, 1991; Ott *et al.*, 1991; Summerbell *et al.*, 2002). There has been extensive research employed in an effort to ascertain the role each MRF family member plays during myogenesis and to elucidate whether any functional redundancy may exist within these transcription factors (reviewed in (Arnold and Braun, 1996)). Although *MyoD* may have some functional redundancy, as *MyoD*^{-/-} mice display no adverse muscle phenotype or aberration in the expression of any muscle-specific genes, an increase in *Myf-5* expression in these mice

suggests a regulatory role for MyoD in the expression of *Myf-5* (Rudnicki *et al.*, 1992). Skeletal muscle development is also normal in *Myf-5*^{-/-} mice, although myotomal expression of *Myf-5* is delayed by two days, E10.5 as opposed to E8.5 in WT, and there are distal rib developmental defects; consequently *Myf-5*^{-/-} mice die shortly after birth, a similar phenotype is observed in *MRF4*^{-/-} mutant-mice (Braun *et al.*, 1992; Braun and Arnold, 1995; Patapoutian *et al.*, 1995; Zhang *et al.*, 1995). Initial work with double-mutant *Myf-5*^{-/-}/*MyoD*^{-/-} mice found roles for Myf-5 and MyoD in the specification of muscle progenitor cells to the myogenic programme as these mice are amyoplastic, with loose mesenchymal tissue and fluid replacing muscle tissue (Rudnicki *et al.*, 1993). More recently, it was shown that MRF4 could compensate for the loss of Myf-5 and MyoD as long as MRF4 was not compromised, suggesting that rather than functioning only as a post-mitotic transcription factor, MRF4 is conducive to inducing myogenic specification in the same way as Myf-5 and MyoD (Kassar-Duchossoy *et al.*, 2004). Evidence to support the indispensable role myogenin has in completing the process of myogenesis is evident in that mutant *Myog*^{-/-} mice are void of any muscle fibres, instead their musculature is comprised of undifferentiated myoblasts; these mice are immobile and die soon after birth (Hasty *et al.*, 1993; Nabeshima *et al.*, 1993).

1.6 - Growth factors

Several growth factors have roles throughout the myogenic programme; fibroblast growth factor (FGF) stimulates myoblast proliferation and inhibits differentiation; IGF-2 establishes the optimum proportion of FMyHC⁺ myotubes during fibre-type specification and myostatin negatively regulates muscle growth (Moore *et al.*, 1991; McPherron *et al.*, 1997; Merrick *et al.*, 2007). The endocrine hormone insulin has roles in

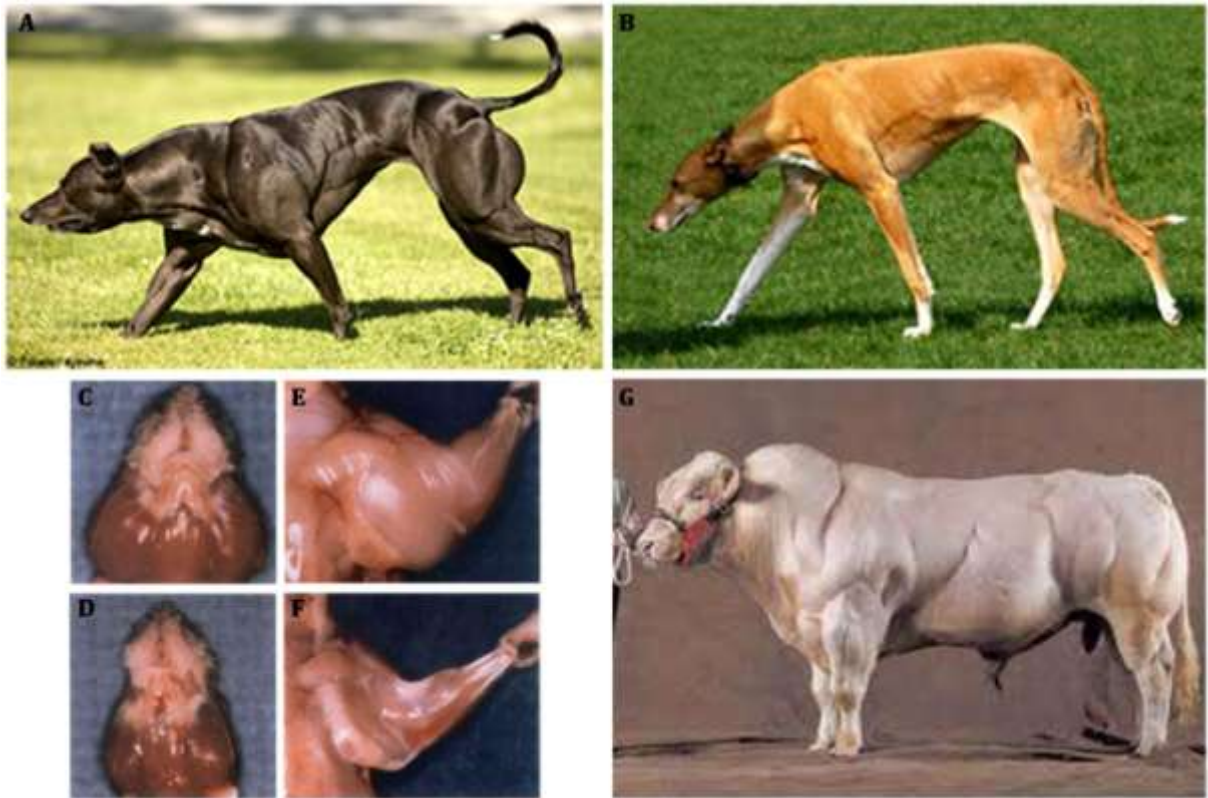
glycogenesis, adipogenesis and blood-glucose homeostasis; it also has a profound anabolic effect on skeletal muscle. Insulin and insulin-like growth factors (IGF-1 and IGF-2) share structural homology and can all mediate signals via insulin-receptors (IR) or type-1 IGF receptors (IGF-1R). IR and IGF-1R mediated signalling is attenuated by adaptor protein Grb10 (Liu and Roth, 1995; Ooi *et al.*, 1995; Dey *et al.*, 1996), conversely, caveolin-3 has been shown to enhance insulin signalling (Oshikawa *et al.*, 2004). Epidermal growth-factor (EGF) like family member delta-like 1 (Dlk1) has roles in cell-cell communication and development and in contrast to Grb10 has a role in IGF-1 signal amplification (Nueda *et al.*, 2008). Although virtually absent in healthy adult muscle, Dlk1 is found in all myopathic muscle tissue (Andersen *et al.*, 2009).

1.6.1 - Insulin-like growth factors

It has been shown that IGF-2 (insulin-like growth factor 2), is an important peptide in the maintenance of MyHC-2 and the switching of MyHC-1 to MyHC-2 during secondary myogenesis (Merrick *et al.*, 2007). IGF-2 along with IGF-1 belongs to the insulin-like growth factor family (previously called somatomedins) so named for their close structural homology with the endocrine hormone insulin. IGF-2 is an imprinted gene, with expression from the paternal allele. IGF-2 is primarily produced during embryogenesis and unlike IGF-1, which is expressed postnatally; is not regulated by growth hormone (GH). IGF-2 signals via the IR and IGF-1R; it also binds the type-2 insulin-like growth factor receptor (IGF-2R) also referred to as the mannose 6-phosphate receptor.

1.6.2 - Myostatin

Transforming growth-factor β (TGF- β) super-family member myostatin, or growth/differentiation factor-8, is a negative regulator of skeletal muscle growth that inhibits myogenesis through repression of myoblast proliferation and downregulation of myoD and myogenin; myostatin mutant animals exhibit extreme muscularity (refer to **Figure 1.7**) (McPherron *et al.*, 1997; Thomas *et al.*, 2000; Ríos *et al.*, 2001). Myostatin also has a role in the regulation of a population of skeletal muscle stem cells (SMSc), referred to as satellite cells, where via *pax7* downregulation, negative regulation of satellite cell activation and self-renewal occurs (McCroskery *et al.*, 2003; McFarlane *et al.*, 2008). Caveolin-3 negatively regulates myostatin signalling through suppression of its type-1 receptor (Ohsawa *et al.*, 2006). Upregulated caveolin-3 is accompanied by downregulated myostatin in MD, although there is evidence to refute that there is any change in the expression levels of myostatin in dystrophic muscles (Repetto *et al.*, 1999; Zhu *et al.*, 2000; Castro-Gago *et al.*, 2006).



A, B, G - copyright-free-pictures.org.uk; C-F - (McPherron *et al.*, 1997)

Figure 1.7 - Myostatin deficiency causes excessive skeletal muscle growth. (A) A mutation in the *MSTN* gene is responsible for the extreme muscularity seen in this dog, referred to as a 'bully whippet', the usual somatotype for a whippet is shown in B. (C, E) Mutant *Mstn*^{-/-} mice show such extreme muscle hypertrophy it earned them the name 'mighty-mice', the images are of jaw and forelimb muscles; WT littermates are shown in panels D and F. (G) Beef cattle farmers unknowingly bred myostatin-deficient double-muscling mutant the 'Belgian blue'.

1.7 - Myosin

Myosins are a family of around twenty cytoplasmic motor proteins that act in concert with actin to provide cell motility in processes such as cytokinesis, phagocytosis and muscular contractions; they are ubiquitously expressed in all eukaryotic cells (reviewed

in (Weiss and Leinwand, 1996)). Each myosin molecule consists of two 200 kDa heavy chains and two pairs of 17-23 kDa light chains, the heavy chains consist of a coiled-coil rod domain and a globular head domain which binds actin and hydrolyses ATP (reviewed in (Weiss and Leinwand, 1996)). There are six myosin heavy chain (MyHC) isoforms expressed in skeletal muscle; MyHC-embryonic, MyHC-neonatal (also referred to as perinatal), MyHC- β (also referred to as slow or type-1) and three adult fast isoform; FMyHC-2a (oxidative), FMyHC-2b (glycolytic) and FMyHC-2dx (oxidative/glycolytic) (reviewed in (Weiss and Leinwand, 1996)). During mouse myogenesis the first isoforms to be expressed are *MyHC-e* and *MyHC- β* between E9 and E10 in the myotome of rostral somites, *MyHC-neo* is expressed at E10.5 and by E15.5 MyHC-neo is the most abundant isoform, expressed only in fibres destined to become adult fast-type fibres (Lyons *et al.*, 1990). Although 70 % of adult skeletal muscle is comprised of FMyHC-2b, it is the loss of FMyHC-2dx that presents with the more severe phenotype in *FMyHC-2b* and *FMyHC-2dx* knockout mice (Acakpo-Satchivi *et al.*, 1997).

1.8 - Satellite cells

The existence of a population of cells with little cytoplasm, juxtaposed to muscle fibres was established in 1961, during electron microscopy of frog tibialis anterior and it was proposed that they were responsible for myo-regeneration in all vertebrates; they were named 'satellite' cells because of their peripheral positions around muscle fibres (Mauro, 1961). The theory of mono-nucleated cells fusing to form multi-nucleated fibres was first suggested over a century earlier by Theodor Schwann; but as it was fervently contested by leading muscle physiologists of the time, was not accepted (reviewed in (Schmalbruch, 2006)). Postnatal regeneration of damaged muscle-fibres occurs via the

activation of SMSc and subsequent initiation of myogenic processes that recapitulate embryonic myogenesis. Satellite cells contribute significantly to this pool of SMSc and reside between the sarcolemma and basal lamina of the muscle fibre where they remain in quiescence until activated (Mauro, 1961; Schultz *et al.*, 1978). Recent studies suggest heterogeneity within the satellite cell population; $pax7^+/myf5^-$ cells remain undifferentiated SMSc thereby maintaining the satellite cell population and $pax7^+/myf5^+$ cells, committed to become differentiated myoblasts upon stimulation. To which sub-set the cell is destined is determined by apical-basal orientation, whereby cells adjacent to the basal lamina become $pax7^+/myf5^-$ and those adjacent to the sarcolemma become $pax7^+/myf5^+$ (Kuang *et al.*, 2007). Satellite cells express specific genes that can be used as markers; *pax7*, a transcription factor of the paired box family of genes is expressed in quiescent satellite cells and cell-adhesion molecule M-cadherin, which is expressed in both quiescent and activated satellite cells are two used for this purpose (Wernig *et al.*, 2004).

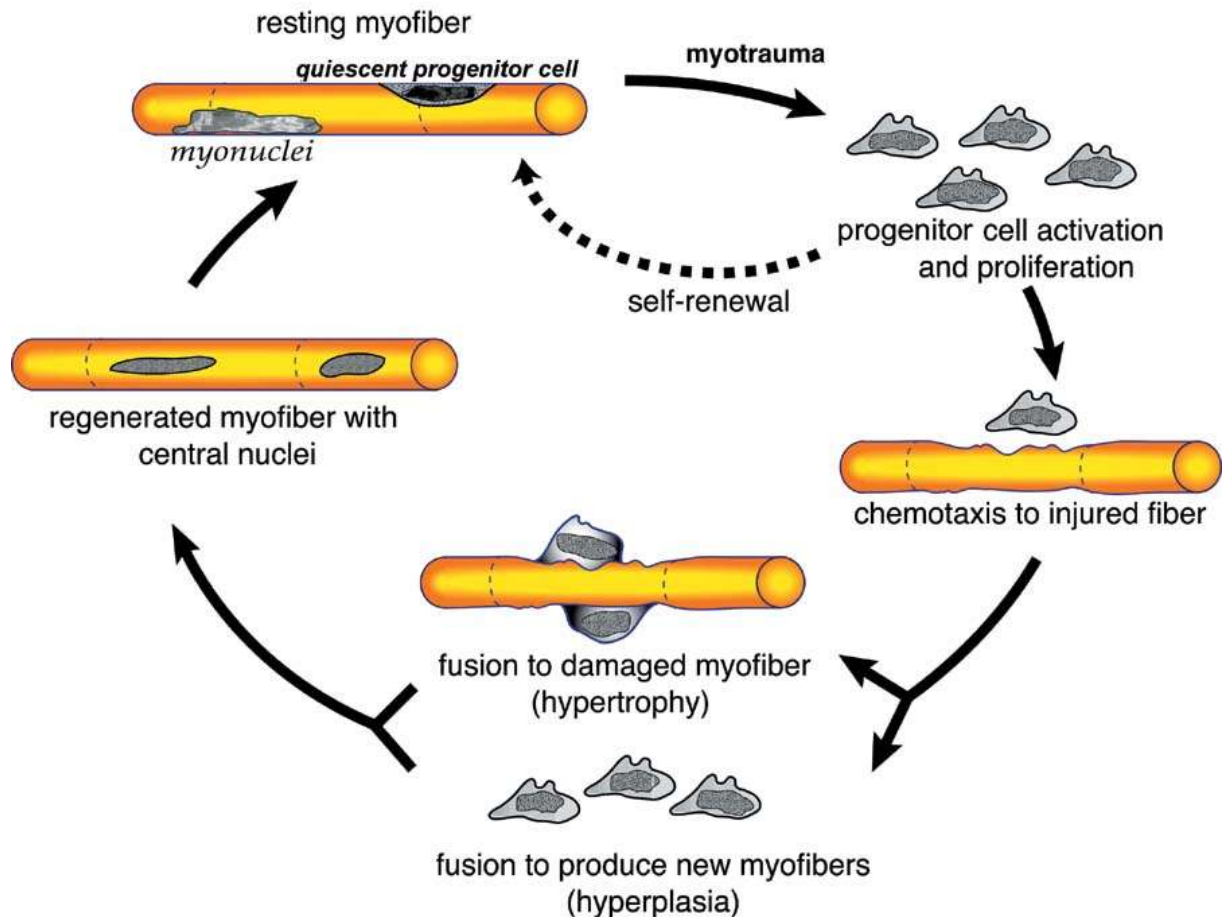


Image from - pimm.wordpress.com

Figure 1.8 - Schematic illustration showing regeneration of a myofibre following myotrauma. (Top left of illustration) Activated satellite cells (referred to in the illustration as progenitor cells) proliferate and migrate to a damaged myofibre where differentiation and fusion occurs. Proliferation ensures the pool of satellite cells are not depleted. Satellite cells remain in quiescence until required.

1.9 - Paired box transcription factors

The importance of pax-3 and pax-7 is illustrated in that cells destined to become myoblasts in *Pax-3/Pax-7* double-mutant null mice, die or assume a different cell lineage (Relaix *et al.*, 2005). Although pax proteins are paralogues of one another as they share

structural homology, their function during myogenesis occurs during different phases of development. *Pax-3* is expressed predominantly during embryogenesis where it is an important migratory factor for myogenic progenitor cells and *Pax-7* is expressed in satellite cells where it functions in their maintenance. *Pax-7* can also substitute effectively if *Pax-3* is absent (Relaix *et al.*, 2005).

1.9.1 - Pax7

The transcription factor *pax7* is a repressor of myogenesis and is expressed in satellite cells where it functions in their maintenance (Seale *et al.*, 2000; Olguin and Olwin, 2004; Oustanina *et al.*, 2004). Recent data suggests an age-related dependency for *pax7* in the maintenance of satellite cells, as *Pax7* inactivated satellite cells of adult mice are not compromised in their ability to proliferate or regenerate muscle following cardiotoxin induced injury (Lepper *et al.*, 2009). *Pax7* belongs to a family of nine transcription factors necessary for development and along with *Pax3*, is expressed in muscle and neuronal tissues (reviewed in (Buckingham and Relaix, 2007)). *Pax7* is a repressor of myogenesis, upregulation of *Pax7* downregulates *MyoD* and *Pax7* and *Myog* expression have been shown to be mutually exclusive (Seale *et al.*, 2000; Olguin and Olwin, 2004; Oustanina *et al.*, 2004).

1.10 - Animal models for DMD

The use of dystrophic animal models, whether they arose naturally or were developed through genetic manipulation, have proven to be invaluable research tools for scientists working in the field of muscular dystrophy. If research was reliant solely on human subjects, our understanding of the aetiology, molecular mechanisms and natural history

of the disease would be incredibly retarded, due to sample size and ethical restrictions. A wide range of animals have been used for research including nematodes, zebrafish, cats, dogs and rodents; of the mammalian models, the hypertrophic feline muscular dystrophy (HFMD) cat has been the least used (reviewed in (Collins and Morgan, 2003)). A brief description of the canine and rodent animal models used shall be given.

1.10.1 - Rodent models of muscular dystrophy

1.10.2 - The *dy/dy* mouse and cardiomyopathic Syrian hamster

Prior to the identification of dystrophin as the protein product of the *DMD* gene in 1987, there were three dystrophic rodent strains used as models for DMD; two murine models, *dy/dy* and *mdx* and a cricetine model BIO.14.6, better known as the cardiomyopathic Syrian hamster (Michelson *et al.*, 1955; Hoffman *et al.*, 1987). Of the murine models the *dy/dy* mouse was preferred by some as it presented with a more severe phenotype than *mdx* (Michelson *et al.*, 1955; Bullfield *et al.*, 1984; Dangain and Vrbova, 1984). After four decades of use as a model for DMD, the malady of the *dy/dy* mouse was shown to be caused by a deficiency in merosin, due to a mutation in the *Lama2* gene; the *dy/dy* mouse was a murine model for merosin deficient congenital muscular dystrophy (Xu *et al.*, 1994). In a similar vein to that of the *dy/dy* mouse, it was shown that the cardiomyopathic Syrian hamster's dystrophy was caused by a mutation in the *Sgcd* gene, which resulted in a deficiency in DGC protein δ -sarcoglycan; this made it a model for LGMD-2F (Nigro *et al.*, 1997). The *mdx* mouse was accepted as the mouse model best representative of DMD and has been widely used since.

1.10.3 - The *mdx* mouse

The *mdx* mouse has been the preferred animal model of choice for most working in the field of muscular dystrophy since its introduction in the mid 1980's; it arose via a spontaneous mutation within exon 23 of the *Dmd* gene of the WT mouse line C57BL/10 (Bullfield *et al.*, 1984). This resulted in a premature STOP codon and subsequent loss of the protein dystrophin in the sarcolemma (Sicinski *et al.*, 1989). Testament to its unparalleled use as a research model for DMD is evident in the fact that there are currently (at the time of writing) 2100 articles on PubMed.gov's data base relating to the *mdx* mouse (US National Library of Medicine National Institutes of Health) and this is by no means exhaustive. When compared to the 44 papers archived for the canine model of DMD (GRMD/*CXMD*), the significance of the *mdx* mouse cannot be overstated.

Although extensively used as the primary animal model for DMD, the myopathy observed in *mdx* does not accurately represent the pathogenesis and progression that manifests with the human form of the disease; mobility is not impaired and life-span is not curtailed, although one study found there was an 18 % reduction in *mdx* lifespan (Dangain and Vrbova, 1984; Carnwath and Shotton, 1987; Chamberlain *et al.*, 2007). Muscle tissue regenerated in the *mdx* mouse, although abnormal in architecture; variations in fibre sizes and centrally located nuclei, functions perfectly sufficiently and is void of the connective and adipose tissue associated with the human form of the disease.

1.10.4 - The *mdx/utrn*^{-/-} mouse

The pathogenesis of the dystrophin/utrophin double-deficient mouse perhaps most closely resembles that of DMD. Not only does the histopathogenesis appear more severe than that of *mdx*, but *mdx/utrn*^{-/-} mice present with pronounced kyphosis, colloquially referred to as 'hunch-back' and marked muscular impairment when compared to *mdx*, there is also a substantial reduction in their lifespan; death occurring at around twenty weeks of age (Deconinck *et al.*, 1997). However, as utrophin is upregulated and not absent in DMD muscles, these mice do not provide a true molecular model for the study of DMD (Kleopa *et al.*, 2006).

1.10.5 - GRMD dog

There have been several breeds of dog shown to have canine X-linked muscular dystrophy (*CXMD*) including the Rottweiler, the German short-haired pointer, the Beagle and the Golden Retriever (reviewed in (Collins and Morgan, 2003)). It is the Golden Retriever muscular dystrophy (GRMD) dog that has been studied most extensively (reviewed in (Collins and Morgan, 2003)). The histopathological and physiopathological homology between GRMD and DMD makes the GRMD dog the most accurate animal model available for the study of DMD (Cooper *et al.*, 1988). The pathogenesis of GRMD begins *in utero* and at birth necrosis of quadriceps limbs, neck and trunk muscles are seen; by the age of six months severe necrosis of muscle tissues are evident with carpus/tarsus contractures severely impeding mobility (refer to **Figure 1.9**) (reviewed in (Collins and Morgan, 2003)). As is the case with DMD, premature death of GRMD dogs often occurs as a result of respiratory or cardiac failure (reviewed in (Collins and Morgan, 2003)). Although a seemingly perfect animal model for DMD, there are several

drawbacks to using the GRMD dog. There are great phenotypic variations between GRMD dogs of different litters although littermates are phenotypically similar, thus trans-litter experiments are more difficult to evaluate (Cooper *et al.*, 1988). Also, the comparable size to DMD boys which makes GRMD dogs excellent models for the testing of new research strategies and therapies that have shown to be successful in *mdx* mice, makes the practicality of husbandry very difficult (reviewed in (Collins and Morgan, 2003)).



<http://www.ncdmd.org/index.cfm> National Centre for Canine Models of Duchenne Muscular Dystrophy

Figure 1.9 - Muscular dystrophy in the Golden Retriever. (A) At three months of age the puppy appears to be perfectly normal, with no sign of any dystrophy. (B) The aggressive progression of the disease is clearly evident just three months later, the dog is no longer able to walk on its toes due to carpus/tarsus contractures and the muscles of its hindlimbs appear incapable of supporting its weight for any considerable length of time. Young GRMD dogs often succumb to respiratory or cardiac failure.

1.11 - Treatments for Duchenne muscular dystrophy

There are no curative treatments for DMD at the moment, however the administration of corticosteroid therapy has helped slow disease progression and along with the application of non-invasive ventilation, the life expectancies of DMD patients has been prolonged by around a decade (Simonds *et al.*, 1998; Manzur *et al.*, 2008). Although these two treatments are the only ones available at the moment, there are new therapies that are being developed which look very promising. A brief account of available treatments and of some of those being developed shall follow.

1.11.1 - Corticosteroids

Corticosteroids, notably prednisolone and deflazacort, have been used in the treatment of DMD for decades, although the mechanism of action that makes them effective is still unknown (reviewed in (Muntoni *et al.*, 2002)). Prolonged use of these drugs is not desirable, as side effects including weight gain and growth suppression are common, with weight gain more prevalent with prednisolone use (Bonifati *et al.*, 2000). They are still the only pharmaceutical treatments available that consistently improve muscle strength, muscle functional performance, pulmonary functional performance and if they are administered prior to the onset of ventricular dysfunction, have been shown to retard the development of this particular cardiac condition (Wong and Christopher, 2002; Markham *et al.*, 2008). Although boys as young as one year of age have been given these drugs, a review of the scientific and clinical evidence conducted in 2002 recommended corticosteroid treatment between the ages of four and seven years of age would be of best benefit and that their administration prolonged ambulation by three years (reviewed in (Wong and Christopher, 2002)).

1.11.2 - Non-invasive ventilation

Along with corticosteroid drugs, non-invasive ventilation has increased the life expectancies of those with DMD. In a study conducted in 2002, the impact of non-invasive nocturnal ventilation on the average ages of deaths of patients whose care had been managed by the Newcastle Muscle Centre, between the years 1967 and 2002 was reviewed. It found the chances of DMD patients surviving to 25 years of age since the use of non-invasive nocturnal ventilation had risen by 41 % (Eagle *et al.*, 2002).



Figure 1.10 - DMD patient using a non-invasive ventilator. The use of assisted ventilation is often necessary as the degeneration of respiratory muscles makes it increasingly more difficult for those with DMD to breathe independently. In conjunction with corticosteroids, non-invasive ventilation has increased the life expectancies for sufferers of DMD by around a decade.

1.11.3 - Ataluren (PTC-124)

Ataluren (formally known as PTC-124) is a therapeutic agent that is in phase two of clinical trials. Like the aminoglycoside antibiotic gentamicin, Ataluren promotes ribosomal readthrough of premature nonsense stop codons in mRNA, enabling the process of translation to continue in diseases such as DMD and cystic fibrosis, where premature translational termination results in protein deficiencies and the manifestation of their associated diseases (Welch *et al.*, 2007). Like many potential therapies, Ataluren has shown promising results in the laboratory when administered to *mdx* mice.

1.11.4 - Exon skipping

The potential for exon skipping as a therapy for DMD was evident as soon as results were shown of dystrophin localisation to the sarcolemma of *mdx* mice who had been administered drugs that promote exon skipping (Mann *et al.*, 2001). Since then it has been developed further to enable the skipping of duplicated and deleted exons in human DMD subjects, which account for around 80 % of mutations, resulting in the restoration of WT dystrophin (Aartsma-Rus *et al.*, 2006 ; Aartsma-Rus *et al.*, 2007). Exon skipping employs the use of antisense oligonucleotides (AON), which complement regions of pre-mRNA upstream or downstream of mutated regions which are subsequently 'skipped' without affecting the reading frame. This prevents mRNA translation prematurely terminating and a truncated, yet functional dystrophin protein is synthesised. This results in a milder Becker-like muscular dystrophy. Although this sounds incredibly auspicious, exon skipping has been shown to be unsuccessful with multiple exon

duplications (Aartsma-Rus *et al.*, 2007). Clinical trials for exon skipping are now in stage three, so treatments should be imminent.

1.11.5 - Myostatin gene therapy

Ever since the effects of myostatin deficiency on the muscle mass of mutant mice was shown, myostatin inhibition as a potential therapeutic treatment for those with muscle wasting diseases has been a subject of intense research (McPherron *et al.*, 1997; Ohsawa *et al.*, 2006; Cash *et al.*, 2009; Kota *et al.*, 2009; Foley *et al.*, 2010). The pharmaceutical company Acceleron Pharma are currently developing a myostatin inhibitor called ACE-031, it is a soluble form of activin receptor type 2B (ActRIIB), for which myostatin is a ligand and recent research has shown ACE-031 to be effective in increasing the strength and muscle mass of *mdx* mice (George Carlson *et al.*, 2011; Pistilli *et al.*, 2011). Phase two trials have already been conducted on DMD patients in Canada using this drug.

1.11.6 - Utrophin upregulation

The autosomal homologue of dystrophin, utrophin, when upregulated in *mdx* and *CXMD* muscles, has been shown to ameliorate the dystrophic condition and has therefore been the subject of extensive research over the past two decades (Tinsley *et al.*, 1996; Tinsley *et al.*, 1998; Cerletti *et al.*, 2003). Retro-viral vectors were initially employed to introduce *Utrn* transgenes into the muscle tissues of animal models used for the research, but more recently work has progressed with an orally administered drug that has been shown to upregulate endogenous utrophin (Cerletti *et al.*, 2003; Tinsley *et al.*, 2011). The drug is called SMT1100 and although recent phase one clinical trials

produced disappointing results, the drug shows immense promise as a pharmaceutical therapy for DMD.

1.11.7 – A matter of time

The last two decades of research in the field of treatments for DMD have resulted in therapeutic agents that could potentially change the prognosis of the disease for those affected with DMD in the future. The progressive, debilitating and ultimately lethal disease of today could be replaced with one that is manageable, with little impairment to the quality of life of those affected. Exon skipping, ribosomal readthrough and utrophin upregulation are likely to be ready for general use in the next few years, but the timing of administration is of paramount importance for the optimal efficacy of these treatments. Speaking to the Times in June of 2011, Professor Dame Kay Davies said, “Anyone on these therapies is going to have to be treated more or less from birth to get maximum benefit. I’m not sure whether we’re there yet but we need to be ready to introduce a screening programme the moment that these treatments start to come through...that means piloting and planning now”.

Wales has been screening for DMD for the past 21 years as part of the heel-prick test performed on neonates, it is about time we did too.

1.12 - Aims and objectives

1.12.1 - Aim

The aim of this project was to establish a role for caveolin-3 in the pathogenesis of the *mdx* mouse.

1.12.2 - Objectives

The first objective was to generate a line of mice that were deficient in both dystrophin and caveolin-3, i.e. caveolin-3 deficient *mdx* mice. Caveolin-3 is upregulated in DMD and its mouse model *mdx*, yet very little work has been done to distinguish between the pathogenesis caused by a loss of dystrophin and that caused as a result of an increase in caveolin-3. In order to develop a line of mice deficient in dystrophin and caveolin-3, a series of crosses were employed beginning with *mdx* and *cav3*^{-/-}, with each subsequent generation requiring genotyping and careful pairing of offspring to ensure the genetic requirements were eventually met. These genetic requirements were *mdx* with hypophysiological levels of caveolin-3 (*mdx/cav3*^{+/-}) and *mdx* with a complete deficiency in caveolin-3 (*mdx/cav3*^{-/-}). DNA sequencing of a selected region of the murine *Dmd* gene was used to confirm the presence of the *mdx* mutation in dystrophin-deficient mutants.

The second objective was to confirm that phenotypes were consistent with genotypes, in regards to levels of caveolin-3 in the three dystrophin-deficient mutants, thus western blotting and immunohistochemistry (IHC) were used to establish caveolin-3 protein levels and localisation.

The third objective was to ascertain the effects of reduced caveolin-3 in the musculature of developing *mdx* embryos, in view of establishing a role for caveolin-3 during myogenesis. This was achieved through IHC using muscle and muscle cell specific antibodies. Caveolin-3 levels were confirmed with western blotting.

The fourth objective was to correlate observed dystrophic pathogenesis with levels of caveolin-3 in postnatal muscles. Aside from examination of the gross histology of muscle sections, regenerating areas were calculated as percentages of total areas and centronucleated fibres, a hallmark of cumulative regeneration, were counted and comparisons made between the three dystrophin-deficient mutants. Haematoxylin and eosin (H&E) staining was employed for the histological analysis of postnatal muscle tissues.

CHAPTER 2 - MATERIALS AND METHODS

2.1 - Introduction

This chapter contains all of the methodology along with materials that have been used during the course of the project. Protocols have been written with enough detail included to allow for reproducibility of all experiments. Where the same methodology has been used for different protocols, a detailed description of the protocol has been written for the first instance and is cross-referenced where used in the remainder of the thesis. To avoid repetitious and superfluous text, names of suppliers of any chemicals and equipment used have been included when initially mentioned; this also applies to the chemical ingredients of any reagents used.

2.2 - Mouse models used

Three mouse strains were used for all work during this project; wild-type (WT) C57BL/10, DMD mouse model *mdx* and LGMD-1C mouse model *cav3*^{-/-}. In addition, two double-mutant strains were generated for use during this project through crossing *mdx* and *cav3*^{-/-}; namely *mdx/cav3*^{+/-} and *mdx/cav3*^{-/-} (see section 2.3). Throughout the remainder of this thesis *mdx/cav3*^{+/-} (mice with the *mdx* mutation which are heterozygous for *Cav3*) shall be referred to as double-mutant (DM) hets and *mdx/cav3*^{-/-} (mice with the *mdx* mutation which are homozygous negative for *Cav3*) referred to as DMs. Animal husbandry was employed at the Biomedical Services Unit (BMSU), University of Birmingham. All mouse strains used were isogenic, on a C57BL/10 background. *Cav3*^{-/-} were originally generated and provided by Yoshito Hagiwara

(Hagiwara *et al.*, 2000) and *mdx* from the Bullfield laboratory in 1991 (Bullfield *et al.*, 1984).

Table 2.1 – Mice used and the dystrophic models they represent. Denotations **X** – WT *dystrophin*, **X^d** – *mdx* mutation, **Y** – no contribution to the dystrophic genotype, **A** – WT *cav3*, **a** – mutant *cav3*.

Mouse strain	Genotype (M/F)	Mutated gene	Effected protein	Model of
C57BL/10	XYAA/XXAA	N/A	N/A	Wild-type
<i>mdx</i>	X ^d YAA/X ^d X ^d AA	<i>Dmd</i>	Dystrophin	DMD
<i>cav3</i> ^{-/-}	XYaa/XXaa	<i>Cav3</i>	Caveolin-3	LGMD-1C
DMhet (<i>mdx/cav3</i> ^{+/-})	X ^d Yaa/X ^d X ^d Aa	<i>Dmd</i> , <i>Cav3</i> (1 allele)	Dystrophin, Caveolin-3 (het)	N/A
DM (<i>mdx/cav3</i> ^{-/-})	X ^d Yaa/X ^d X ^d aa	<i>Dmd</i> , <i>Cav3</i>	Dystrophin, Caveolin-3	N/A

2.3 - Generation of DM mice

Natural matings were set up between *cav3*^{-/-} males and *mdx* females. Females were checked for vaginal plugs (VP) daily until the presence of a plug indicated a successful pregnancy and was taken as embryonic stage 0.5 days (E0.5). This strategy ensured all resultant males were hemizygous and all females heterozygous for *mdx*, as the gene has an X-chromosome location; all littermates produced via these crosses were heterozygous for *Cav3*, as it is an autosomal gene. The next stage was to backcross DMhet males with *mdx* females to produce litters that were all dystrophin deficient. Approximately half of these were, according to Mendelian principles of genetic

inheritance, expected to be DMhets and half *mdx*. Genotypes of resultant progeny were established by polymerase chain reaction (PCR) to identify their *neo* status. *Cav3*^{-/-} mice were generated through the deletion of exon 2 of the *Cav3* gene which was replaced with a phosphoglycerate kinase promoter-driven neomycin-resistant cassette (Hagiwara *et al.*, 2000), therefore those *neo* positive mice would be DMhets and those *neo* negative, *mdx*. The penultimate stage of the breeding programme was to cross DMhet males and DMhet females to produce progeny with three possible genotypes; *mdx*, DMhet and DM. In order to identify the genotypes from these crosses, *neo* and *cav3* PCRs were performed; *mdx* would be *Cav3* positive/*neo* negative, DMhets would be positive for both genes and DMs *Cav3* negative/*neo* positive. Finally, DMs were crossed to produce entire DM litters (**Table 2.2**).

Table 2.2 - Generation of DM mice. Stage 1: *cav3*^{-/-} males (XYaa) were crossed with *mdx* females (X^dX^dAA) to produce F1 DMhet males (X^dYAa) and *mdx* carrier, *cav3*het females (X^dXAa) in the Mendelian ratio of 1:1. **Stage 2:** F1 DMhet males (X^dYAa) were backcrossed with *mdx* females (X^dX^dAA) to produce F2 progeny of two expected genotypes (males and females); *mdx* (X^dYAA/X^dX^dAA) and DMhets (X^dYAa/X^dX^dAa) in the Mendelian ratios of 1:1. **Stage 3:** DMhet males (X^dYAa) were crossed with F2 DMhet females (X^dX^dAa) to produce F3 progeny of three expected genotypes (males and females); *mdx* (X^dYAA/X^dX^dAA), DMhets (X^dYAa/X^dX^dAa) and DMs (X^dYaa/X^dX^daa) in the Mendelian ratios of 1:2:1. **Stage 4:** F3 DM males and females were crossed to produce litters of a single genotype, DM (X^dYaa/X^dX^daa). **X** – WT *dystrophin*, **X^d** – *mdx* mutation, **Y** – no contribution to the dystrophic genotype, **A** – WT *Cav3*, **a** – mutant *Cav3*.

Stage 1

	X^dA	X^dA
Xa	X ^d XAa	X ^d XAa
Ya	X ^d YAa	X ^d YAa

Stage 2

	X^dA	X^dA
X^dA	X ^d X ^d AA	X ^d X ^d AA
X^da	X ^d X ^d Aa	X ^d X ^d Aa
YA	X ^d YAA	X ^d YAA
Ya	X ^d YAa	X ^d YAa

Stage 3

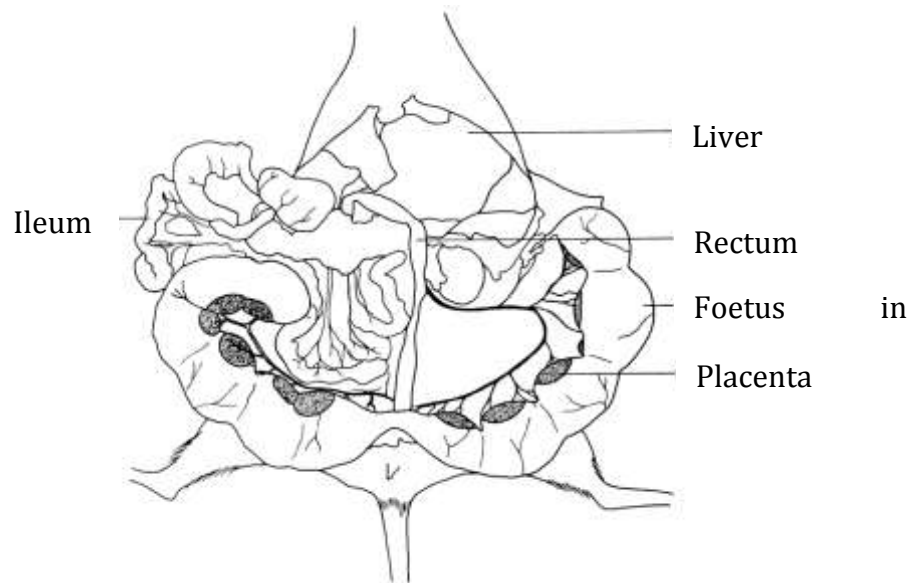
	X^dA	X^da
X^dA	X ^d X ^d AA	X ^d X ^d Aa
X^da	X ^d X ^d Aa	X ^d X ^d aa
YA	X ^d YAA	X ^d YAa
Ya	X ^d YAa	X ^d Yaa

Stage 4

	X^da	X^da
X^da	X ^d X ^d aa	X ^d X ^d aa
Ya	X ^d Yaa	X ^d Yaa

2.4 - Collection of embryos

Pregnant female mice of the required gestational stage were sacrificed via cervical dislocation (schedule 1 killing) by trained BMSU staff in accordance with the Animal Welfare (Scientific Procedures) Act 1986, placed supine and secured to cork dissecting boards via quadrupedally inserted hypodermic needles (Terumo). Their abdomens were then sprayed with 70 % ethanol (EtOH) for the purpose of sanitisation, opened using sterile dissecting tools and their uteri removed (**Figure 2.1**). Upon removal, the uteri were immediately placed into Universal tubes containing sterile phosphate buffered saline (sPBS) kept on ice. Embryos were promptly liberated from uteri via the removal of deciduas' and amnion in Petri-dishes (Nunc) under an inverted dissecting Stemi 1000 microscope (Zeiss) using sterile forceps and processed for either paraffin wax embedding (section **2.11**) or protein extraction (section **2.15.1**). Simultaneous to the removal of embryos, the dissected placentas and amnion were placed into eppendorf tubes, snap-frozen in liquid nitrogen (LN₂) and later stored at -70 °C until required for genotyping. All waste uterine tissue was placed into Universal tubes and disposed of using specially designated bins at BMSU.



Adapted from - Cook, M.J. (1965) *The Anatomy of the Laboratory Mouse*

Figure 2.1 – Diagram of a pregnant female mouse with opened abdomen prior to embryo collection showing bi-lateral uterus. The liver and intestines were either excised or moved enough to allow for the removal of the uterus. The uterus lies laterally in the mouse abdomen, to prevent mobility problems as gestation progresses and contains ‘pods’ of embryos, each embryo having its own placenta.

2.5 - Excision of adult skeletal muscles

Skeletal muscles and organs were excised from four weeks, nine weeks and nine months old mice for the purpose of analysis via immunohistochemistry and western blotting.

Adult mice were sacrificed as described in section 2.4, pinned and sprayed with 70 % EtOH to sanitise. Using disposable scalpels (Swann-Morton), fur was removed from relevant areas before the commencement of any surgery (as shown in Merrick *et al.*, 2010). Cutaneous incisions were made using sterilised dissecting scissors and skins

covering relevant muscles removed, with care taken not to cut into underlying muscles. For the removal of triceps and quadriceps, upper proximal limb joints humerus/radioulna and femur/tibiofibular were flexed and using sterile dissecting scissors, muscles excised. Sections of thoracic cage containing four of five ribs were also removed for the purpose of intercostal histological analysis. Samples that were excised for the purpose of analysis via immunohistochemistry were fixed in ice-cold 4 % paraformaldehyde (PFA) (Sigma-Aldrich) and processed as described in section 2.11; samples taken for the purpose of western blotting were snap frozen in LN₂ and stored at -70 °C until required.

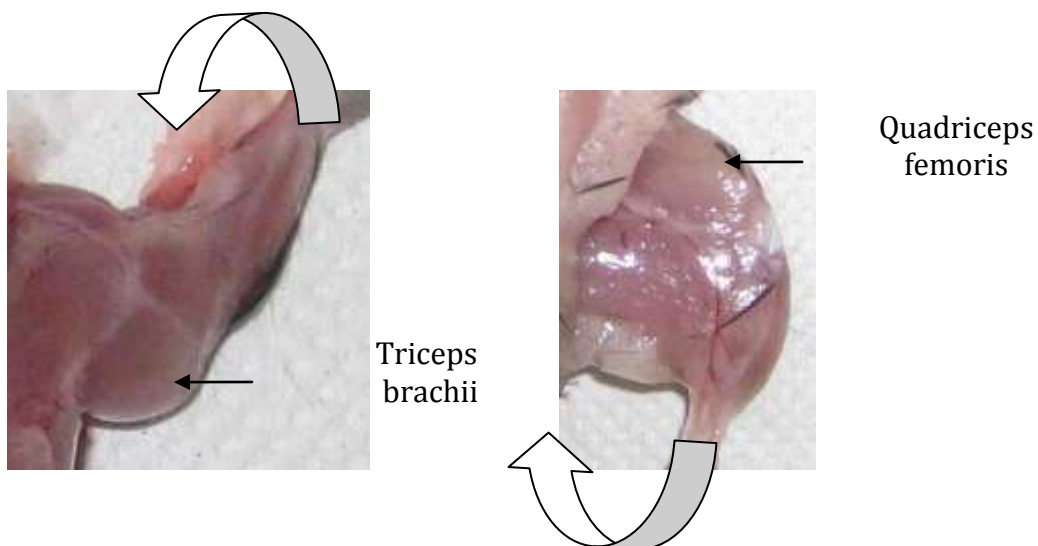


Figure 2.2 – Images of skinned fore and hindlimbs. To excise triceps and quadriceps from fore and hindlimbs respectively, skinned limbs were first flexed (direction of arrows), to allow ease of access to the full length of the muscles. Muscles taken were then processed for either protein extraction or paraffin wax embedding.

2.6 – Extraction of DNA from tissues

The acquisition of tissue for the purpose of genotyping was a consistent requirement of this project. Ear-clips from adult mice and placentas, amnion and tail-clips from embryos were used to establish genotypes; tail-clips were also used when genotyping neonate mice. Upon their removal, tissues were immediately placed in labelled eppendorf tubes, snap-frozen in LN₂ and stored at -70 °C until required. There were two protocols used for the extraction of DNA; the first used isopropanol as a precipitate and the second phenol-chloroform. Of the two methods, phenol-chloroform produced the cleanest DNA samples, but as isopropanol was a much simpler and faster method to employ, the majority of DNA samples were extracted using this method.

2.6.1 - Isopropanol extraction of DNA

Tissue samples required for genotyping were removed from storage at -70 °C and thawed on ice. To each eppendorf, 200 µL of lysis buffer (100 mM Tris HCl (Fisher scientific) pH 8.5; 5 mM EDTA (Fisher scientific); 200 mM NaCl (BDH laboratory supplies)) and 5 µL (20 mg mL⁻¹) Proteinase-K (VWR) was added and samples incubated for several hours at 50 °C with agitation at 600 revolutions per minute (rpm) using a Thermomixer Compact (Eppendorf). The digested samples were then centrifuged at 13,000 rpm for 60 seconds in a Hettich Mikro 20 centrifuge (DJB Labcare Ltd.) and the resultant supernatants transferred to new eppendorf tubes leaving pellets of hair and debris (if any) to be discarded. Some embryonic tissues did not require centrifugation as the samples were free from hair or debris. Volumes of isopropanol (Fisher Scientific) equal to that of the supernatants were then added to the supernatants in each eppendorf which were vigorously shaken to precipitate the DNA from their solutions. Using fresh

yellow pipette tips (Gilson) for each sample, DNA aggregates were removed from their supernatants and placed in fresh labelled eppendorf tubes and placed in a heat block (Techne) set at 50 °C for approximately 10 minutes to allow for the evaporation of residual isopropanol. If there was no DNA aggregate visible following the addition of isopropanol and shaking, the tubes were subjected to centrifugation for 20 minutes at 13,000 rpm. The supernatants were then carefully aspirated from the eppendorfs which were then placed in a heat block set at 50 °C for approximately 10 minutes to allow for the evaporation of residual isopropanol. Finally, DNA pellets were re-suspended in 50 – 100 µL sterile distilled H₂O (sdH₂O), the volumes of which were dependant on the size of the DNA aggregates. The process of re-suspension was hastened via the use of a heat block set at 50 °C. Once dissolved the samples were stored at -20 °C until they were required for genotyping.

2.6.2 - Phenol-chloroform extraction of DNA

Although the phenol/chloroform method of DNA extraction from tissues was a more onerous process than that of the isopropanol extraction method, the purity of DNA attained via this method was far superior. 500 µL of lysis buffer (1 % SDS (Fisher Scientific); 50 mM Tris pH 7.5; 50 mM EDTA; 100 mM NaCl) and 5 µL (20 mg mL⁻¹) Proteinase-K was added to tissues and samples incubated for several hours at 50 °C with agitation at 600 rpm using a Thermomixer Compact, to allow digestion. Once digested, samples were removed from the heat block, vortexed thoroughly using a Vortex genie-2 (Scientific Industries) and centrifuged for 5 minutes at 13,000 rpm to separate hair and debris from the supernatants. Eppendorf tubes were tipped and supernatants poured into fresh tubes; pouring supernatants from debris pellets was preferred to pipetting

supernatants from debris pellets as the latter invariably resulted in disturbance of pellets and subsequent supernatant contamination. To each tube, 500 μ L of the bottom layer of a 1:1 phenol (Sigma-Aldrich)/chloroform (Fisher Scientific) solution was aliquoted and tubes once more vortexed thoroughly. The tubes were then centrifuged at 13,000 rpm for 5 minutes after which upper aqueous phases were removed using wide-bore yellow pipette tips (200 μ L Gilson with tips removed and autoclaved for sterility) and added to 500 μ L chloroform. Using fresh wide-bore pipette tips once more, upper aqueous phases were removed and added to 1 mL 100 % ethanol (EtOH) and left overnight at -20 °C in order to precipitate the DNA from their solutions. The following day the samples were removed from the freezer and centrifuged at 13,000 rpm for the 30 minutes at 4 °C after which supernatants were removed and eppendorfs were left uncapped to allow for the evaporation of residual EtOH from the samples. Once the EtOH had evaporated from the samples, DNA pellets were resuspended in 50 μ L sdH₂O and allowed to dissolve for approximately 10 minutes at 50 °C before being stored at -20 °C until required for genotyping.

2.7 - Spectrophotometry

Following all DNA extractions the concentration and purity of DNA in each sample was quantified using a double-beamed U-1800 spectrophotometer (Digilab Hitachi) which read at λ 260 nm and λ 280 nm, for DNA and protein absorbency wavelengths respectively. For ease of calculation, 5 μ L DNA of each sample was added to 95 μ L sdH₂O which meant the resultant reading at λ 260 nm equated to the concentration of DNA in μ g per μ L. The concentration of DNA afforded through the use of spectrophotometry

would ultimately determine the volumes of DNA aliquoted per PCR mix, with 1 µg DNA being the maximum amount aliquoted per reaction mix.

2.8 – Polymerase chain reaction (PCR)

Several different suppliers' products of PCR reagents were tried during the course of the project including GoTaq (Promega), Amplitaq (Applied Biosystems), Biotherm (Gene Craft) and Dreamtaq (Fermentas). The majority of PCR work was employed using GoTaq or Amplitaq, of which the preferred buffer of choice was GoTaq flexi green, by virtue of the dyes added to the buffer, which negated the need to add loading dyes and therefore saved time. All of the DNA polymerases used were of thermophilic bacterium, *Thermus aquaticus* origin. 25 µL of a PCR master mix was added to 0.2 mL nuclease-free PCR tubes (ABgene® PCR plates, Thermo Scientific). Each PCR reaction mix consisted of 5 µL (5x) GoTaq flexi green buffer; 3 µL (25 mM) magnesium chloride (MgCl₂), for a final concentration of 3 mM; 0.05 µL (100 mM) of deoxynucleotides dATP, dGTP, dCTP and dTTP (Invitrogen), for a final concentration of 200 µM; 1 µL of target-specific primers (Alta biosciences) consisting of 10 % forward primer, 10 % reverse primer (stock solutions 100 pmol µL⁻¹) and 80 % sdH₂O, for a final concentration of 400 nM of each primer; sdH₂O to 24 µL and GoTaq or Amplitaq polymerase (5 U µL⁻¹), aliquoted at 0.1 µL per 25 µL reaction mix. All reagents were thawed on ice except for the DNA polymerase, which was used directly from -20 °C and returned immediately afterwards. Finally 1 µL (200–1000 ng) of sample DNA was added per PCR tube.

All PCRs were performed with the following standard protocol using either Verity (Applied Biosystems) or PCR Express (Hybaid) machines.

1 cycle

- 94 °C for 3 minutes
- Optimal annealing temperature for 45 seconds (dependent on T_m)
- 72 °C for 45 seconds

n cycles

- 94 °C for 30 seconds
- Optimal annealing temperature for 45 seconds (dependent on T_m)
- 72 °C for 45 seconds

A further extension of 72 °C for 10 minutes, followed by a period of cooling at 4 °C completed the process.

Table 2.3 - Primers used for the purposes of genotyping and sequencing.

Gene target	Forward	Reverse	Amplicon length (bp)	Design Source
SRY	5' TCT-TAA- ACT-CTG-AAG- AAG-AGA-C- 3'	5' GTC-TTG-CCT- GTA-TGT-GAT- GG- 3'	404	(Kunieda <i>et al.</i> , 1992)
CAV3	5' ATT-CCT-GTT- CGC-CTG-TAT-C- 3'	5' AGG-ACC-AAC- CGA-ATC-TTC- TG- 3'	670	(Hagiwara <i>et al.</i> , 2006)
NEO	5' GCA-CGC-AGG- TTC-TCC-GGC- 3'	5' GTC-CTG-ATA- GCC-GTC-CGC-C- 3'	639	Provided for by Craig Hughs (UoB medical school)
Dystrophin mdx	5' CTT-CTG-TGA- TGT-GAG-GAC- ATA- 3'	5' CTA-GCT-TTT- GGC-AGC-TTT- CC- 3'	587	Designed by myself

2.9 - Gel electrophoresis

All gel electrophoreses during the course of this project were performed using Horizon® Horizontal Gel Electrophoresis apparatus (Life Technologies) and PCR products were resolved in 1-1.2 % agarose (Bioline) in 0.5 x TBE (9.3 g EDTA; 55 g Boric Acid (Fisher Scientific) and 108 g Tris, made up to 1 L with dH₂O to give a 5 x solution).

The agarose was dissolved in the TBE via heating in an NN-E442W microwave oven (Panasonic) and ethidium bromide (EtBr) (Life Technologies) added to the molten agarose gel at a concentration of $1 \mu\text{L } 50\text{mL}^{-1}$ ($0.2 \mu\text{L mL}^{-1}$). The gel apparatus was pieced together (**Figure 2.3**) and the molten agarose solution poured into the gel mould and allowed to set. Once set, the wedges and gel comb/s were carefully removed, a scalpel was used to remove the wedges in order to ensure no tearing of the gel occurred. TBE at 0.5 x was then carefully poured into the apparatus chamber, enough to barely cover the gel but ensuring wells were free of any air pockets that may have impeded the loading of PCR products. $6 \mu\text{L}$ of a 100 base-pair (bp) DNA ladder (Biolabs) was then aliquoted into the first lane of the gel, followed by 10-25 μL of each PCR sample, which were aliquoted to subsequent wells. The volume of PCR sample aliquoted was dependent on the size of the wells. Once loaded, the apparatus was connected to a power source (Hoefer Scientific Instruments) and gels were run at 80-130 V until DNA ladders had separated sufficiently enough to identify base-pair graduations. Once the gels had been run, they were carefully removed from the electrophoresis apparatus and viewed under ultra-violet (UV) light using a Chromato-Vue Transiluminator (UVP). Safety precautions regarding UV light exposure and the handling of gels containing EtBr required the wearing of a lab coat, gloves and face visor. Images of gels were printed immediately and scanned using a CanoScan LiDE 200 (Canon) and saved as JPEG computer files.

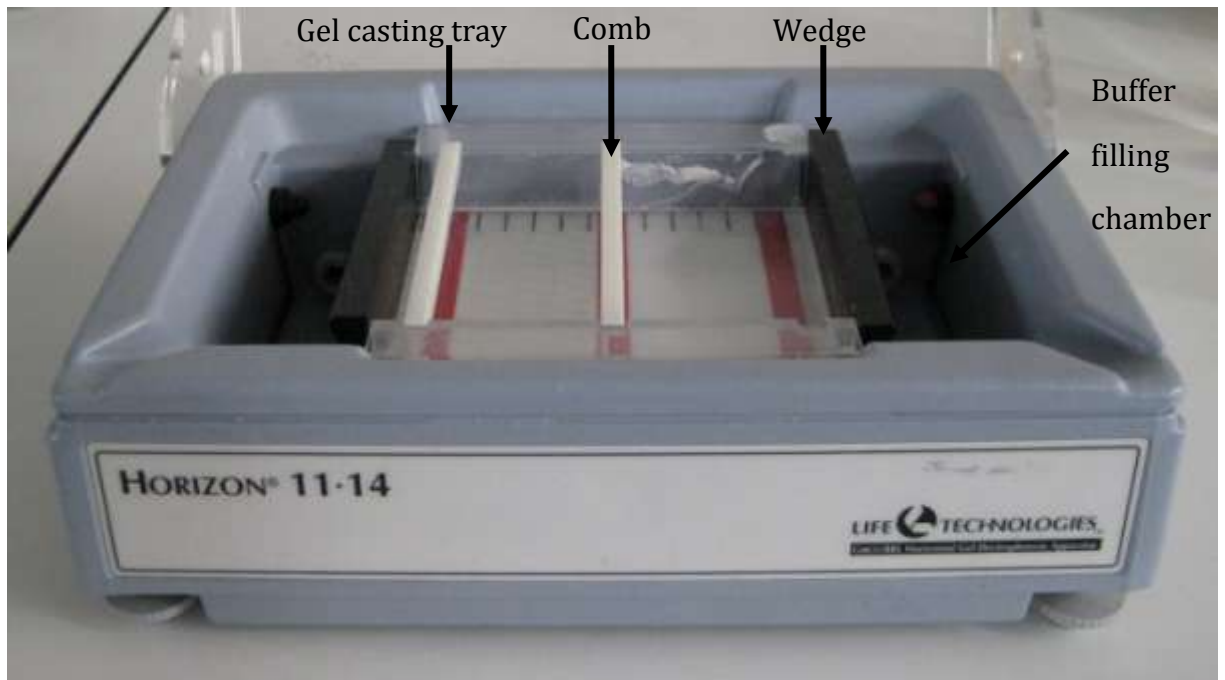


Figure 2.3 - Electrophoresis gel apparatus. Wedges were placed either side of the casting tray and molten agarose poured in to a depth of approximately 1 cm, this depth would accommodate 25 μ L of PCR product per well without spilling over. After pouring enough TBE into the filling chamber to barely cover the gel, the gel was run at 80–130 V until the ladders' graduations had separated sufficiently.

2.10 - DNA sequencing

The application of PCR and visualisation of PCR products via gel electrophoresis was a simple and clear method used to identify male from female embryos and *cav3*^{-/-} from WT and *cav3*^{hets}. However, PCR to identify the *mdx* point mutation was notoriously difficult and was unsuccessful when tried. In order to confirm the presence of the *mdx* mutation in the DM animals that had been generated, DNA sequencing had to be employed; therefore primers were designed to amplify the region of DNA containing the C-T base-pair change that was present in *mdx*. 2 μ L of PCR product from each sample was

aliquoted into a PCR tube, along with 3.2 pmol. dystrophin *mdx* forward primer (5' CTT-CTG-TGA-TGT-GAG-GAC-ATA 3') and 4.8 µL nuclease-free H₂O (Sigma-Aldrich), for a total volume of 10 µL. Samples were then taken to the Functional Genomics and Proteomics Unit, University of Birmingham for sequencing, where they were run on a capillary sequencer ABI 3730 (Applied Biosystems). DNA sequences were analysed using Sequence Scanner Software v1.0 (Applied Biosystems).

2.11 - Processing for paraffin wax embedding

All samples, whether embryonic or muscles from adult mice used for immunohistochemical analysis were processed using a 10 step protocol. Once removed from uteri (section 2.4) or excised, samples were promptly placed in ice-cold 4 % PFA (4 g PFA; 100 mL sPBS) for fixing. The fixation time period was dependent on the sample being processed (**Table 2.4**). Following fixation, samples were washed twice for 10 minutes per wash in sPBS prior to undergoing dehydration in serial EtOH solutions of 40 %, 70 %, 95 % and 100 % (EtOH diluted with tap water). An additional step of decalcification in 0.5 M EDTA pH 7.5 was necessary for E17.5 embryos and sections of adult thoracic cages. Decalcification was followed by an overnight wash in dH₂O prior to dehydration in EtOH. All of the above steps were employed at 4 °C on a gyro-rocker. Following dehydration, samples were placed into either 10 or 25 mL glass jars for xylene clearing, a process that was undertaken in a fume hood. Following clearing for the appropriate time (**Table 2.4**), the xylene was replaced with molten (60 °C) paraffin wax (Paraplast, BDH), with the use of a wax dispenser (Bavimed). Following wax dispensation, jars were then placed in a slowly rocking hybridisation oven/shaker SI 20H (Stuart Scientific) set at 60 °C for the required duration (**Table 2.4**). For the final

stage of the process, molten wax was dispensed into the bottom of 22 mm x 22 mm plastic moulds with peel-away sides (Polysciences Inc.), samples removed from glass jars using heated forceps and placed into moulds. Embryos were oriented into the moulds right-side down and adult muscle samples carefully placed so that muscles fibres would be oriented vertically through the wax to allow for cross-sectional cutting. Once the samples were satisfactorily aligned, the moulds were filled with more molten wax. Filter paper (Fisher Scientific) labels stating the age of the sample, mouse strain, date of sacrifice and if a muscle sample, which particular muscle, were inserted into the molten wax of the mould. Blocks were then allowed to solidify at room temperature for several hours before being stored at 4 °C until required for sectioning (section **2.12**). Although processes in the protocol were the same for all stages of mice (additional steps for E17.5 and thoracic cages mentioned previously), durations of processes varied according to the developmental stage of the mice. **Table 2.4** shows a summary of all processes and their respective duration for each developmental stage (adapted from Deborah Merrick's 2006 thesis).

Table 2.4 - Processes involved in paraffin embedding of embryonic and neonate mice and adult muscle samples

Stage of Process	E11.5	E13.5	E15.5	E17.5	Adult muscle*
4 % PFA	3 h	20 h	20 h	24 h	24 h
sPBS wash	2x10 m	2x10 m	2x10 m	2x10 m	2x10 m
0.5 M EDTA pH 7.5	NA	NA	NA	3 days	3 days
dH ₂ O	NA	NA	NA	Overnight	Overnight
40 % EtOH	30 m	1 h	1.5 h	1 day	1 day
70 % EtOH	30 m	1 h	1.5 h	1 day	1 day
95 % EtOH	30 m	1 h	1.5 h	1 day	1 day
100 % EtOH	3x30 m	3x1 h	3x1.5 h	2 days	2 days
Xylene	3x30 m	3x1 h	3x1.5 h	3 days	3 days
Paraffin wax	2 in 24 h	2 in 24 h	3 in 48 h	3 in 48 h	3 in 48 h

2.12 - Microtome sectioning of paraffin blocks

A Medax water-bath (Camlab), which was set at 40 °C was filled with tap water and allowed to reach the required temperature. Paraffin wax blocks containing embryos or muscle samples were selected and removed from cold storage individually for sectioning; this ensured the wax remained cold during cutting, making the process of sectioning far easier than with a warmer block. Excess wax adjacent to specimens was removed using a razor blade and blocks securely clamped in an 1150/Autocut

microtome (Reichert-Jung (**Figure 2.4**)); though care was taken not to damage blocks through excessive tightening of the clamp. Blocks were aligned parallel to the blade and vertical to the floor and micro-adjustments of the alignment screws of the microtome ensured blocks were cut evenly across their surfaces. Wax sections of 20 μm were initially cut from fresh blocks which were reduced to 5-8 μm once the samples had been reached. When cutting embryos, sagittal sections were cut to the mid-line of the sample in accordance with *The Atlas of Mouse Development* (M. H. Kaufmann, 1992, Elsevier Academic Press); muscle samples were cut at the muscles' belly. Cut sections were carefully placed on the water's surface using two artist's fine paint brushes to allow any creases within the wax to unfold. Individual muscle samples did not have to be so meticulously aligned as fibre direction was easily ascertained macroscopically and sagittal and transverse sections cut accordingly. Sections were 'scooped' onto Superfrost® Plus electrostatically charged microscope slides (VWR) from the water's surface and comprehensively labelled using a pencil. Ink could not be used as it would have been washed off during the process of IHC (section **2.13**). Any excess water trapped between the wax and slides was drained with paper towels and slide mounted sections incubated for a minimum of 1 hour or left overnight at 37 °C in a Heraeus electronic incubator (Thermo Scientific) to ensure adherence of sections onto slides.

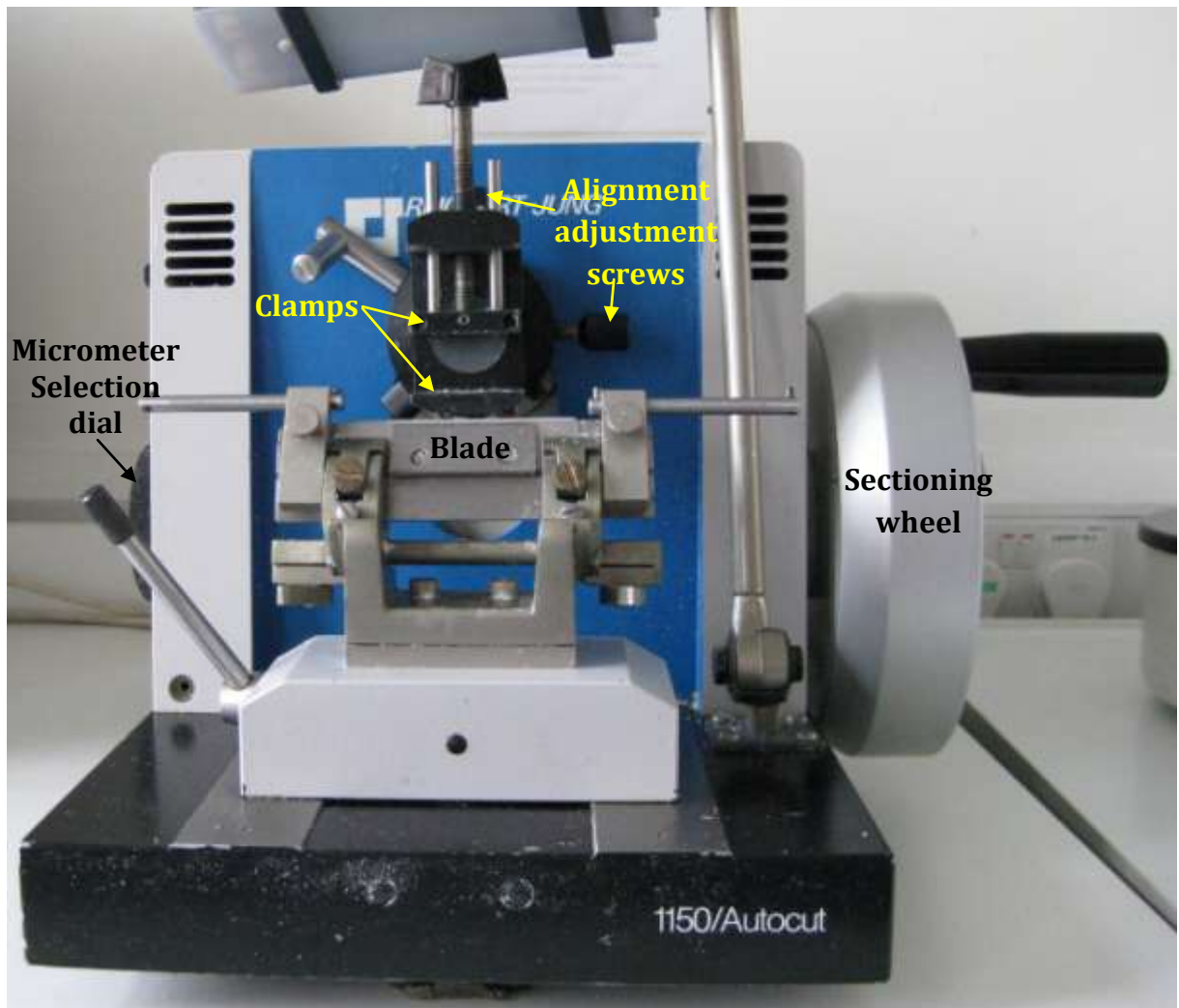


Figure 2.4 - Microtome used for the cutting of paraffin wax embedded sections. Paraffin wax blocks containing samples were clamped into position and aligned using the adjustment screws. Section thickness was selected using the micrometer dial and sections were cut with smooth clockwise rotations of the sectioning wheel.

2.13 – Immunohistochemistry (IHC)

Embryos and adult muscle tissues processed for paraffin wax embedding were analysed using IHC. The streptavidin/biotin method of signal amplification was employed for all IHC performed during the course of this project (as described in Merrick *et al.*, 2007).

2.13.1 - De-waxing, rehydration and antigen retrieval

Slide mounted sections were placed into metal slide racks and de-waxed with two washes in the solvent xylene; one 5 minutes wash and one 10 minutes wash, which were performed in the confinements of a fume-hood. Separate glass vessels were used for the two washes which were labelled 'A' (5 minutes) and 'B' (10 minutes). Following de-waxing of the sections, they were then rehydrated using serial dilutions of EtOH (Fisher Scientific), beginning with two x 2 minutes' immersions in 100 % EtOH, followed by further immersions in 95 %, 90 %, 70 %, 50 % and 30 % EtOH solutions, all for a period of 2 minutes. EtOH solutions were diluted using tap water. While in the EtOH, the metal slide racks were tapped against the bottom of the glass vessels every 30-60 seconds, this helped to eliminate any air bubbles from the sections which if left, may have impeded the rehydration process. Following rehydration, slides were then washed for 10 minutes in PBS-using a Gyro-Rocker® STR9 shaker (Bibby Sterlin Ltd.). The next stage involved an antigen retrieval step which was necessary to break the amino acid cross-linkage bonds that had been made during fixation of the samples in PFA. Without this step any antigens of interest in the samples would be unrecognisable to their respective antibodies and as a consequence, immunodetection of proteins impossible. A buffer consisting of 4.7 g sodium citrate (Fisher Scientific), dissolved in 1.6 L dH₂O at pH 6 was used for the process of antigen retrieval, which was poured into a Smart-plus pressure

cooker (Prestige) and brought to boiling on a hot plate (Russell Hobbs). The slides were then placed into the solution, the lid locked and the solution brought to pressure on setting II, which was maintained for 90 seconds. The cooker was then promptly removed from the heat and cooled under cold running tap water for approximately 3 minutes; while cooling, the lid of the pressure cooker was removed upon depressurising of the cooker (by releasing steam) as soon as was possible. Slides were then washed for 10 minutes in fresh PBS as previously.

2.13.2 - Peroxidase quenching, blocking and incubation with primary antibodies

To enable adjacent sections of slides to be immunolabelled using different antibodies without cross-incubation and to contain reagents aliquoted to areas immediately surrounding sections, an ImmEdge™ wax barrier pen (Vector Laboratories) was used to draw around each section. Care was taken during this process to ensure sections did not dry out, as this would have impaired the quality of staining. Having drawn around each section on a slide, the slide was then placed into a separate slide rack in PBS. When all of the slides had been completed, they were placed into coplin jars containing 3 % hydrogen peroxide (H_2O_2)(Sigma Aldrich) in tap water for 5 minutes followed by 1 hour in 0.5 % H_2O_2 in 100 % methanol (MeOH)(Fisher Scientific), in order to quench endogenous peroxidase activity. Peroxidase quenching was then followed by three washes in PBS +0.05 % Tween20 (Sigma Aldrich), 10 minutes per wash. Sections were then blocked in TNB (0.1 M Tris pH 7.5; 0.15 M NaCl (BDH); 0.25 g blocking reagent (TSA kit Perkin-Elmer)) for 30 minutes, after which the TNB was removed by tapping the slides on their sides. For the final stage of day one, sections were incubated in primary antibodies; all of which were diluted in TNB. Where possible, one section per

slide was aliquoted TNB in place of primary antibody, as a control. Sections were incubated with primary antibodies overnight at 4 °C in a humidity chamber, which consisted of a lidded tray lined with PBS-soaked filter paper, sealed with masking tape.

Table 2.5 - Antibodies used for IHC during the course of this project. Primary and secondary antibodies are listed along with their working concentration and immunoglobulin (Ig) isotypes.

Name	Antigen	Host	Ig class	Dilution
MF20	Pan-myosin	Mouse	IgG	1/1,000
MY32	Fast-myosin	Mouse	IgG	1/1,000
PAX7	Pax7	Mouse	IgG	1/1,000
CAV3	Caveolin-3	Mouse	IgG	1/1,000
Biotinylated anti-mouse IgG	Mouse IgG	Goat	N/A	1/1,000

2.13.3 - Incubation in secondary antibodies and signal amplification

Following overnight incubation in primary antibodies, antibodies were carefully removed from sections via tapping the slides on the base tray of the humidity chamber. To eliminate the possibility of unintentional cross-incubation with neighbouring antibodies while washing, slides were individually dipped in fresh PBS before commencing with three washes for 10 minutes each in PBS +0.05 % Tween20. Sections were then incubated in secondary biotinylated antibodies for 1 hour at room

temperature after which they were washed three times for 10 minutes each wash in PBS +0.05 % Tween20. Streptavidin conjugated with horse-radish peroxidase (SA-HRP) (Perkin-Elmer), diluted 1/100 in TNB was then aliquoted to sections and incubated for 30 minutes, followed by three more 10 minutes washes in PBS +0.05 % Tween. The next stage was signal amplification, which was achieved using biotinyl tyramide (TSA kit, Perkin-Elmer), diluted 1/50 with the kit diluent, aliquoted to sections and incubated at room temperature for between 8 and 10 minutes (dependent on antibodies used). After three more 10 minutes washes in PBS+0.05 % Tween20, sections were incubated for a second time for 30 minutes with SA-HRP followed by three final 10 minutes washes in PBS+0.05 % Tween20.

2.13.4 - Antigen visualisation, counter staining, dehydration and mounting

Antigen visualisation was achieved using the chromogen 3, 3' diaminobenzidine tetrahydrochloride (DAB, Dako) at 1 mg ml⁻¹ dissolved in sPBS. To 1 mL of the DAB solution, 1 µL of a 30 % H₂O₂ stock solution was added, to give a working solution of 0.03 % H₂O₂. DAB was then aliquoted to sections using a Pasteur pipette (Sarstedt) and incubated for 5-8 minutes, after which slides were washed twice for 5 minutes per wash in tap water. DAB is a suspected carcinogen and irritant; therefore its use and disposal have strict protocols that must be adhered to. All work involving DAB was carried out in a designated foil-lined tray and all equipment that had direct contact with DAB (i.e. Pasteur pipette, pipette tips and bijoux tube that contained DAB) were placed into sodium hypochlorite (VWR) for 24 hours to de-activate the DAB. Tap water from the first wash had sodium hypochlorite (NaClO) added and could be safely disposed of down a sink with copious amounts of water after 24 hours; tap water from the second wash

was safe to be poured down the sink immediately after use; again with copious amounts of water. In addition to a lab coat, two pairs of gloves were also worn and they too were soaked in NaClO for 24 hours before being deposited into a specially designated hazardous waste bin. Following antigen visualisation, slides were counterstained in haematoxylin (Gills) for 2 minutes before being washed in Scott's tap water (50 µL 10 M NaOH (BDH); 400 mL tap water) for a further 5 minutes. Slides were then briefly (<1 second) dipped in an acid alcohol solution (0.5 % HCl (Fisher Scientific) in 70 % EtOH) then immediately washed once more for 5 minutes in Scott's tap water. The washing process was concluded with 5 minutes under running tap water; care was taken during this process to ensure sections were not damaged by leaving the lid to the vessel on, but open ajar and water delivered to the vessel via a hose connection. Sections were then dehydrated with the same serial EtOH concentrations as were used in the rehydration process; 30 %, 50 %, 70 %, 90 % and 95 % each for 2 minutes and finally twice for 2 minutes in 100 % EtOH. Xylene washes for 5 and 10 minutes, using vessels 'B' and 'A' respectively were used to clear the EtOH from sections. Having been cleared, slides could now have coverslips mounted on them. DePex mounting medium (Gurr, BDH) was used to mount the 22 mm x 64 mm (VWR) coverslips, which after a small amount of the medium had been applied, were pressed firmly enough to dissipate the DePex over the sections. Both xylene washes and mounting of slides were carried out in a fume-hood; in which slides were left to dry overnight before being visualised using an Eclipse E600 light microscope (Nikon). Images of all IHC runs were taken using an E995 digital camera (Nikon) and saved as JPEG files.

2.14 - Haematoxylin and eosin staining (H&E)

Tissue histology was employed on postnatal muscle sections using H&E staining; fibre morphology, myonuclei positioning and fibre regeneration were analysed using this method of tissue staining. Slide-mounted sections were first de-waxed in xylene and rehydrated in EtOH as previously described (section 2.13.1), before being placed in haematoxylin for 2 minutes. Slides were then washed in Scott's water for 5 minutes after which they were dipped briefly in acid alcohol and washed once more in Scott's water for 5 minutes. Sections were then partially dehydrated in EtOH solutions of 30 %, 50 %, 70 % and 90 % for 2 minutes each followed by immersion in eosin (0.5 % eosin (Gurr, BDH); 0.5 % acetic acid (Fisher Scientific); 90 % EtOH) also for 2 minutes. The dehydration step was completed using a 95 % and two 100 % EtOH solutions, again for 2 minutes each. Xylene clearing and mounting as has been previously described (section 2.13.4) completed the process.

2.15 - Protein extraction

2.15.1 - Protein extraction from embryos

Embryonic proteins were taken from all mouse strains at E11.5, E13.5, E15.5 and E17.5 and used for analysis via western blotting. Uteri were removed and embryos liberated as previously described (section 2.4), placed in a glass homogeniser and enough RIPA buffer (50 mM Tris; 150 mM NaCl; 1 % Nonidet-P40 or Igepal CA-630 (Sigma-Aldrich); 0.5 % deoxycolic acid (Sigma-Aldrich); to 100 mL with sdH₂O) added to barely cover the embryos. In order to inhibit endogenous protease activity, 1 protease inhibitor tablet (Complete mini, Roche), which had been dissolved in 1.5 mL sdH₂O while on ice, was added to the RIPA buffer and used at 1.5:8.5, protease inhibitors: RIPA buffer. Embryos

were homogenised and poured into 5 mL bijoux tubes, homogenates drawn into Plastipak syringes (BD) using 18 gauge hypodermic needles to shear genomic DNA and promptly aliquoted into 1.5 mL eppendorf tubes. Tubes were then spun for 30 minutes, 14,000 RPM at 4 °C in a 5415C centrifuge (Eppendorf) after which the supernatants were removed from the debris, aliquoted to fresh labelled eppendorfs and stored at -20 °C until required.

2.15.2 - Protein extraction from fresh muscle samples and frozen samples

Adult muscle tissue and all samples that had been snap frozen and stored at -20 °C could not be readily homogenised using a glass homogeniser as was used for embryos freshly taken from uteri. Instead, samples were ground together with RIPA, using a pestle and mortar. The process of grinding was performed on ice to minimise protein degradation and was a very time consuming and onerous task. Once ground, homogenates were drawn into syringes using 18 gauge hypodermic needles to shear genomic DNA and processed as described previously (section 2.15.1).

2.16 - Protein assay

Once proteins had been extracted from the samples, it was necessary to quantify the concentration of protein in each sample, in order to allow for equal loading when performing western blotting. Samples were removed from storage at -20 °C and placed on ice to thaw (proteins were always kept on ice to prevent degradation). Bovine serum albumin (BSA) standards (Pierce) of 1, 2, 5, 10, 15, 25 and 50 µg mL⁻¹ were made from a stock solution of 2 mg mL⁻¹ and 100 µL of each was aliquoted in duplicate to the first two rows of a 96 well plate (Nunc). Two wells of sterile distilled water (sdH₂O) were also

aliquoted as blank controls. The protein samples were diluted to 1/100 and 1/400 with sdH_2O and 100 μL of each sample were aliquoted in duplicate alongside the blank and BSA standards. To which wells standards and samples were aliquoted was recorded. 100 μL of Coomassie® Protein Assay Reagent (Pierce) was then added to each well and the plate left at room temperature for 20 minutes on an SO1 Orbital Shaker (Stuart Scientific). Protein concentrations were then calculated using an E max microplate reader (Molecular Devices), which read protein concentrations at a wavelength of 595 nm. Results from the microplate reader were printed using a Laserjet 4ML (Hewlett Packard) and loading volumes required for western blotting were then calculated from the results provided.


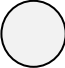











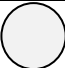













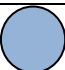

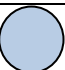



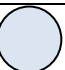

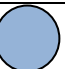



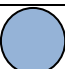

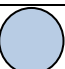



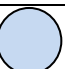



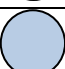

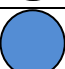

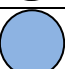







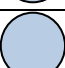



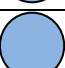







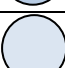

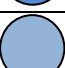

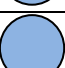









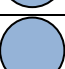

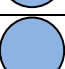






	1	2	3	4	5	6	7	8	9	10	11	12
A												
B												
C												
D												
E												
F												
G												
H												

Figure 2.5 – Representative illustration of a protein assay plate. Serial dilutions of BSA standards were aliquoted in duplicate to the first two rows of a 96 well plate (columns 2-8, rows A/B); dH₂O was also aliquoted as blank controls (column 1, rows A/B). Protein samples were diluted 1/100 and 1/400 and aliquoted also in duplicates; 1/400 dilutions were aliquoted laterally adjacent to 1/100 dilutions (rows C-H). An equal volume of Coomassie assay reagent was added to each well and the plates were subjected to colourimetric analysis. The deeper the blue colouration in the illustration is indicative of a greater concentration of protein in the sample. Dotted circles represent empty wells. The example shown is merely for illustration purposes and does not represent any actual protein assay performed during the project.

2.17 - Western blotting

The quantification of proteins of interest from embryonic, neonatal and adult muscle tissue of all murine strains studied was ascertained via SDS polyacrylamide gel electrophoresis (PAGE) and western blotting. All western blotting was performed using equipment from the mini PROTEAN system® (Bio-Rad Laboratories) using standard protocols.

2.17.1 - Gel casting

Glass plates were selected ensuring that front plates was shorter than outer plates for ease of loading and were swilled in hot water and dried with clean paper towel before being cleaned using isopropanol. Once residual isopropanol had evaporated, plates were clamped into gel casting apparatus (figure 2.6) and a 12 % resolving gel (4 mL 30 % Ultra pure ProtoGel® acrylamide (Geneflow); 2.5 mL 1.5 M Tris pH 8.8; 100 µL 10 %

SDS; 3.3 mL sdH₂O; 100 µL 10 % ammonium persulfate (Sigma-Aldrich); 4 µL TEMED (Sigma-Aldrich)) pipetted to approximately $\frac{3}{4}$ the height of the outer plate. As proteins of interest had molecular masses of between 17.5 and 60 kilodaltons (kDa), 12 % gels were used for their resolution. Both resolving and stacking gels were made up in 50 mL Falcon tubes (BD Biosciences), with ammonium persulfate and TEMED added immediately prior to being pipetted between the plates. The setting of gels in the Falcon tubes was indicative that the gels between the plates had also set. A layer of isopropanol was then added to the resolving gel solution in order to eliminate any air bubbles from the gel's surface. The gel was then allowed to set. Once set, the isopropanol was carefully decanted from the gel and any residual isopropanol removed with the use of filter paper. The plates were then clamped back into the gel casting apparatus and the stacking gel added (1.4 mL 30 % acrylamide; 100 µL 10 % SDS; 1.2 mL 0.5 M Tris pH 6.8; 5.62 mL sdH₂O; 85 µL 10 % ammonium persulfate; 8.5 µL TEMED) to the top of the inner plate. A comb of the appropriate size (dependent on number of samples being analysed) was then carefully inserted between the plates, ensuring there were no bubbles of air trapped between the comb and stacking gel.

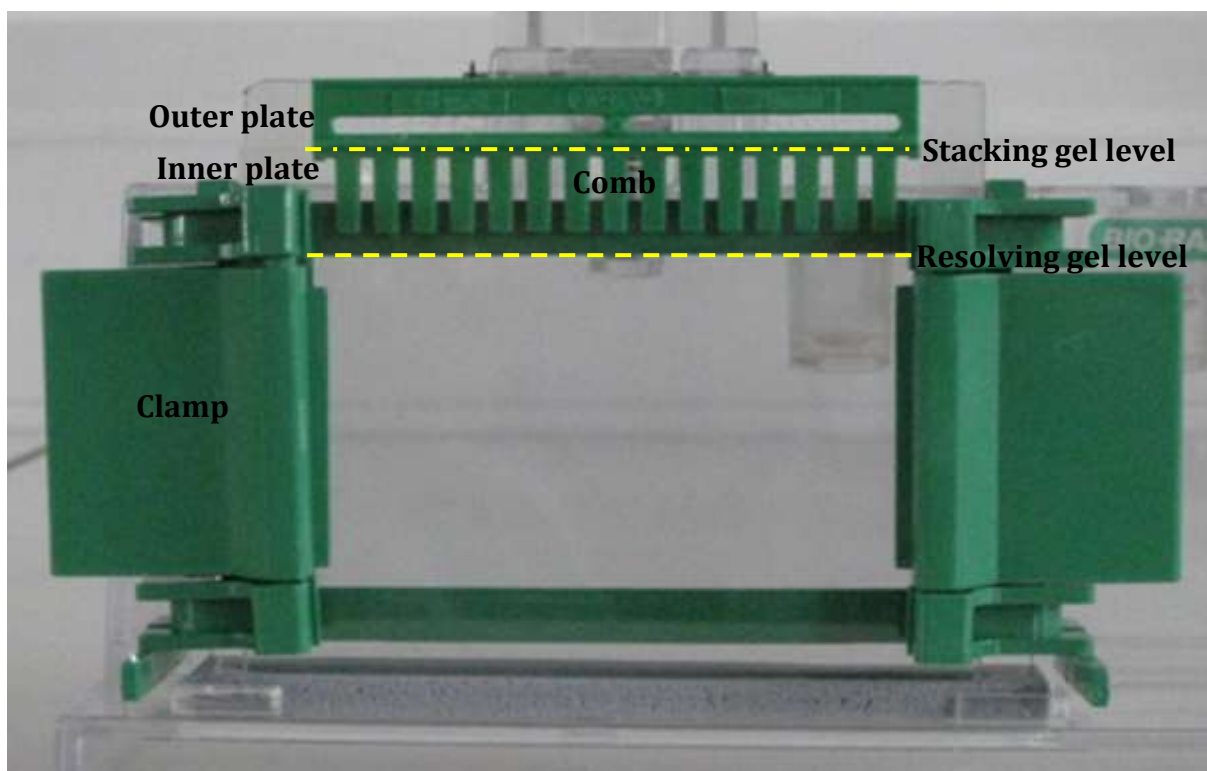


Figure 2.6 - Gel casting. Glass plates were assembled and clamped into casting apparatus as shown. Resolving gel was pipetted between the plates to the level indicated and setting allowed, after which stacking gel was added to the top of the inner plate and a comb carefully inserted between the plates.

2.17.2 - Protein sample preparation, loading and running of gels

While the gels were setting the protein samples, which had been removed from storage at $-20\text{ }^{\circ}\text{C}$ and thawed on ice, were prepared. Proteins, unlike DNA are very labile molecules and must therefore be kept on ice at all times. Protein concentrations had been ascertained prior (section 2.16) and were diluted with sdH_2O to $1\text{ }\mu\text{g }\mu\text{L}^{-1}$, of this stock dilution, $7.5\text{ }\mu\text{L}$ of each sample was aliquoted into eppendorfs. An equal volume of 2x Laemmli sample buffer (Sigma-Aldrich) was also added to the eppendorfs to give a

total volume of 15 μ L and the samples were then boiled for 5-10 minutes in an SBH200D digital block heater (Stuart Scientific) set at 95 °C. After boiling, the samples were removed from the heating block and placed on ice until required for loading into the gel. Once the stacking gel had set, it could be loaded with the protein samples. The gel comb was carefully removed from the stacking gel and the gel chamber clamped into the electrophoresis apparatus, ensuring the front of the chamber was facing inwards. The inner chamber of the electrophoresis apparatus was then filled with running buffer (3 g Tris; 14.4 g glycine (Fisher Scientific); 10 mL 10 % SDS; dH₂O to 1 L) until it over spilled into the outer chamber. Bubbles were then removed from the power filament at the bottom of the apparatus through positioning and gently tapping the apparatus on the laboratory bench until all visible bubbles were released to the surface. Following this, the inner chamber was topped up with running buffer ready for protein loading. Into the first lane, 8 μ L of a Prestained Broad Range marker (Biolabs) was loaded using long thin pipette tips, followed by 15 μ L of each of the samples. After checking and filling the inner chamber with running buffer, the PS 500X power source (Hoefer Scientific Instruments) was run at 100 V. The gel was left to run until the dyes from the Laemmli buffer had migrated to the bottom of the gel, upon which the run was terminated.

2.17.3 - Transfer to membrane

While the run was concluding, items required for the transfer step were prepared. For each gel, two sponges and four pieces of filter paper were soaked in transfer buffer (3 g Tris; 14.4 g glycine; 200 mL MeOH; to 1 L with dH₂O) and a piece of Amersham™ Hybond™ - ECL nitrocellulose membrane (GE Healthcare) was soaked in dH₂O for 1 minute before being soaked in transfer buffer. Once the run had been completed, the

plates were removed from the apparatus and separated using a scalpel, which was also used to cut the stacking gel from the resolving gel. Transfer cassettes were opened and laid clear side down onto a tray. A sponge, two pieces of filter paper, the membrane, gel, two more pieces of filter paper and the remaining sponge were placed on the clear side of the cassette (**Figure 2.7**) and a pipette (Costar) rolled across the surface to eliminate any bubbles. The cassette was then closed and the 'sandwich' placed into the cassette holder ensuring the black-side of the cassette faced toward the black-side of the cassette holder. An ice block was also added to assist with cooling and the transfer chamber filled with transfer buffer. Membrane transfer was performed at 4 °C and run at 100 V for 1 hour 15 minutes using an EV231 power pack (Consort).

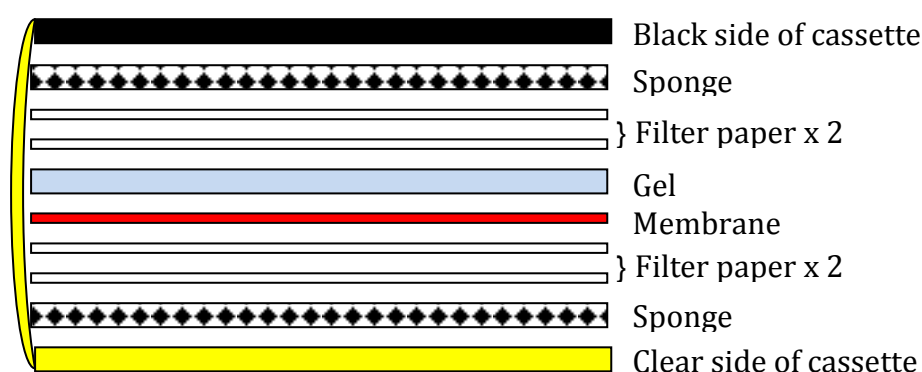


Figure 2.7 - Illustrated representation of cassette 'sandwich'. Transfer cassettes were assembled as shown, starting from the clear side of the cassette and all components were soaked in transfer buffer prior. When completed, a pipette was rolled across the sandwich to eliminate any air bubbles which could have impeded the transfer of membranes from the gel to the membrane. Cassettes were closed and sealed before being placed in a cassette holder, ensuring the black side of the cassette was adjacent to the black side of the cassette holder.

2.17.4 - Membrane probing

Transfer cassettes were removed from 4 °C and filter paper and gels discarded as non-hazardous waste. As a means of identifying the side of the membrane onto which the proteins had been transferred, the top left corners of the membranes (adjacent to marker) were removed and the membranes incubated in blocking buffer (PBS+ 0.1 % Tween® 20; 5 % dried skimmed milk, Marvel, Premier International Foods) for 1 hour at room temperature with gentle agitation. Following blocking, the membranes were incubated in primary antibodies diluted in blocking buffer either overnight at 4 °C, or for 2 hours at room temperature, both with violent agitation. For economy of antibodies, membranes were incubated with primary antibodies in sealed plastic bags, which were cut according to the size of the membrane and securely taped to trays.

Table 2.6 - Antibodies used for western blotting during the course of this project.

Primary and secondary antibodies are listed along with their working concentration and immunoglobulin (Ig) isotype.

Name	Host	Ig Class	Used at
Anti-pax7	Mouse	IgG	1/1,000
Anti-NTP-2	Rabbit	IgG	1/1,000
Anti- caveolin-3	Mouse	IgG	1/500
Anti- α -tubulin	Mouse	IgG	1/1,000
Anti- β -actin	Mouse	IgG	1/20,000
Biotinylated anti-mouse IgG	Goat	N/A	1/1,000
Biotinylated anti-Rabbit Ig	Donkey	N/A	1/1,000
Anti-mouse IgG-HRP	Goat	N/A	1/1,000
Anti-rabbit IgG-HRP	Goat	N/A	1/1,000

2.17.5 – Antigen detection

There were two different methods used for antigen detection; enhanced chemiluminescence (ECL) and fluorescence, of which the latter utilised two protocols; the first of which employed the use of fluorescently conjugated secondary antibodies and the second the biotin/streptavidin system of signal amplification. Both methods shall be described separately for ease of reading.

2.17.5.1 - Detection using ECL

Following incubation in primary antibodies, the membranes were swilled with and then washed four times for 5 minutes each wash in PBS + 0.1 % Tween® 20 (PBST) with gently shaking. The membranes were then incubated in secondary horse-radish peroxidase (HRP) conjugated antibodies diluted in blocking buffer for 1 hour at room temperature with violent agitation, again in sealed plastic bags and then swilled and washed four times for 5 minutes in PBST. Following washing, the membranes were dabbed on tissue paper and incubated in SuperSignal® West Pico chemiluminescence substrate (Pierce) for approximately 30 seconds (500 µL of each substrate was mixed together immediately prior to use), dabbed dry and placed face down onto cling-film. The cling-film wrapped membranes were then taped face up into x-ray cassettes and developed onto photographic film (Scientific Laboratory Supplies) using an X-Ograph compact X2 (X-Ograph Imaging Systems Ltd). Exposure times ranged from a few seconds to several hours.

2.17.5.2 - Detection using fluorescence

Following incubation in primary antibodies, membranes were swilled with and then washed four times for 5 minutes in PBST with gently shaking before incubation for 1 hour at room temperature with Odyssey (LI-COR® Biosciences) secondary antibodies diluted in blocking buffer (fluorescence conjugated antibodies are light sensitive, therefore incubations were carried out in either LI-COR® dark boxes or wrapped in aluminium foil). Following four more 5 minutes washes in PBST, the membranes were washed for 5 minutes in PBS before visualisation using the Odyssey Infrared Imaging System.

2.17.5.3 - Detection using Streptavidin

Some proteins were difficult to visualise using fluorescently conjugated secondary antibodies alone and in these cases an intermediate step was added to enhance signalling. The membranes were washed four times for 5 minutes in PBST following incubation in primary antibodies and then incubated for 1 hour at room temperature in biotinylated secondary antibodies diluted in blocking buffer. Following four more washes for 5 minutes in PBS, the membranes were then incubated in Dylight™ 800 Conjugated Streptavidin (Thermo Scientific) diluted 1/15,000 in PBS for 30 minutes. As was employed for incubation in Odyssey secondary antibodies, incubation with streptavidin was performed using LI-COR® dark boxes. Following four final 5 minutes washes in PBS, the membranes were visualised using the Odyssey Infrared Imaging System.

All images were saved as high quality JPEG images on the Odyssey system and transferred to a removable storage device.

2.18 - Analysis of regenerating areas in adult muscle

Quantification of regenerating areas in postnatal derived skeletal muscle tissue was calculated with the use of an Eclipse E600 light microscope with a 10 x 10 square grid integrated into the eyepiece. The objective of choice utilised for this was x20. The numbers of squares covered with areas of regeneration on the grid were counted for each section analysed, as were those squares not covered with regenerating areas (**Figure 2.8**). This was repeated across the whole section and regenerating areas calculated as percentages of the total area of the section. Grid areas were calculated using a 1 mm/100 stage mounted scale micrometer (C. Baker, London).

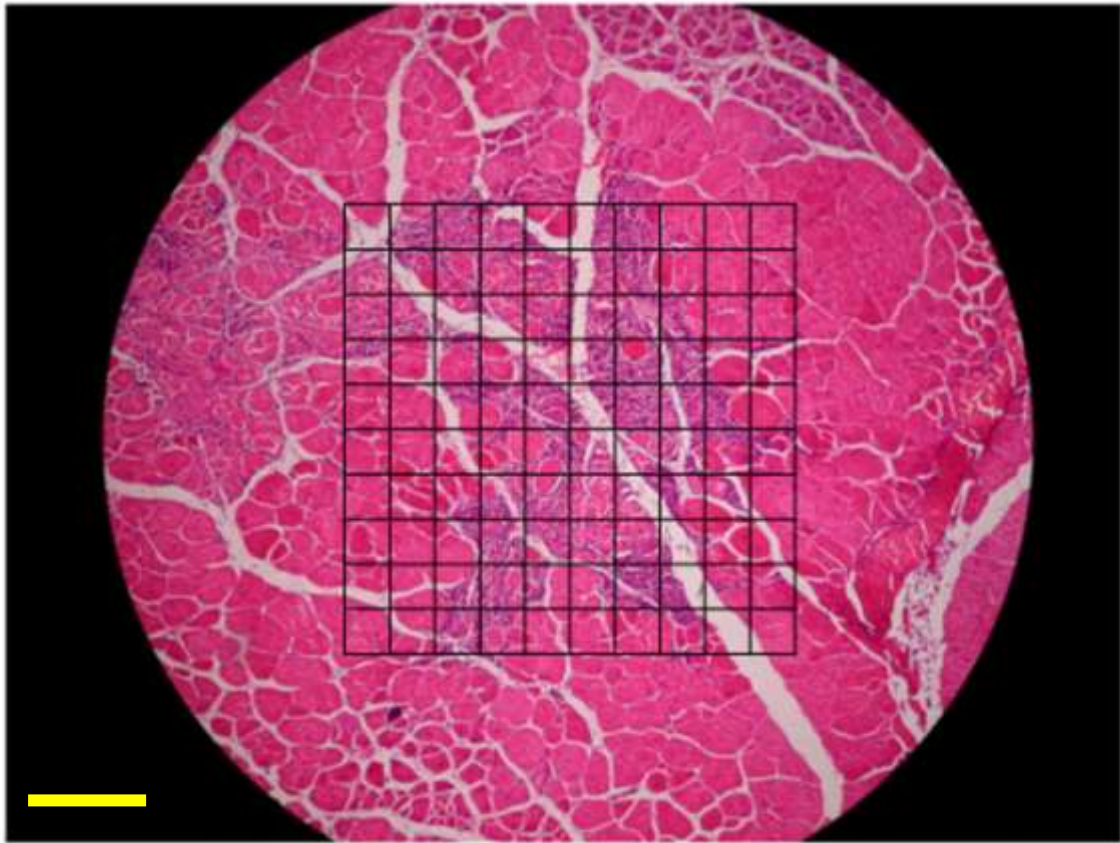


Figure 2.8 - Early stage regeneration at x 20 magnification. Areas of regeneration were calculated using an eyepiece integrated 10 x 10 square grid. The numbers of squares covered with areas of regeneration on the grid were counted, as were those squares not covered with regenerating areas. In the example given for the top row, left to right, this would be as follows; square #1, no regeneration; #2, $\frac{3}{4}$ regeneration; #3, whole square regeneration; #4, $\frac{1}{4}$ regeneration; #5, no regeneration; #6, $\frac{1}{3}$ regeneration; #7, $\frac{2}{3}$ regeneration; #8; #9; #10, no regeneration, for a total of 3 regenerating squares out of 10. This was repeated across the whole section and regenerating areas calculated as percentages of total section areas. Scale bar: 100 μ m.

2.19 - Statistical analysis

All statistical analyses were performed using two-tailed student's *t*-tests and where appropriate asterisks designated as follows; $P < 0.05 = *$, $P < 0.01 = **$, $P < 0.001 = ***$.

CHAPTER 3 - GENERATION OF DOUBLE-MUTANTS AND CHARACTERISATION OF DMHET EMBRYOS

This chapter focuses on the generation of DM (*mdx* mouse deficient in caveolin-3) and DMhet (*mdx* mouse with reduced caveolin-3) mice, the analysis of which allowed a distinction to be made between the pathology caused by the loss of dystrophin and that caused by an excess of caveolin-3. Prenatal studies were employed using DMhets due to dystrophic phenotypes shown in *mdx* and *cav3*^{-/-} embryos.

3.1 – INTRODUCTION

The global degeneration of muscle tissue in DMD has long been believed to manifest during infancy, although elevated serum creatine kinase levels and abnormalities in foetal muscle histology were shown many years ago (Emery, 1977). The DMD mouse model, *mdx*, was thought to initially present with the dystrophic malady at around three weeks of age, based on a histopathological phenotype which includes abnormal variation in fibre-size, centralised myonuclei, raised levels of serum creatine kinase and fibre necrosis (Bullfield *et al.*, 1984; Fletcher *et al.*, 2007). Postnatal phenotypes observed in a mouse model for LGMD-1C, *cav3*^{-/-}, include fibre degeneration between five and eight weeks of age, centralised myonuclei and mononuclear cell infiltration,

restricted to the muscles of distal hindlimbs, or to be more specific, soleus muscles (Hagiwara *et al.*, 2000; Hagiwara *et al.*, 2006). Research from the Smith group established that dystrophic phenotypes for both *mdx* and *cav3*^{-/-} have embryonic origins; with increased cell proliferation and apoptosis evident as early as E11.5 and E15.5 for *mdx* and *cav3*^{-/-} respectively; perturbations in the SMSc populations of dystrophic mutants were also observed (Merrick *et al.*, 2009). These data, pertaining to the onset of a dystrophic phenotype in immature muscle, are supported by abnormalities that were found in *mdx* derived undifferentiated myoblasts, where perturbed mitochondrial physiology and a reduction in proteins of the mitochondrial respiratory machinery were observed (Onopiuk *et al.*, 2009).

3.2 – RESULTS

3.2.1 – Generation of DM litters

3.2.1.1 - Litters produced via *mdx* and *cav3*^{-/-} crosses

Initial matings between *cav3*^{-/-} males and *mdx* females resulted in litters in which males were hemizygous and females heterozygous for *mdx* and both males and females were heterozygous for *Cav3* (**Figure 3.1 A**). F1 progeny genotypes from these initial crosses were therefore *mdx/cav3*^{+/-} and *mdx*^{+/-}/*cav3*^{+/-}, for males and females respectively. Only male embryos were required for analysis, thus F1 embryos were sexed from tail-clips, placenta or amnion using the following *sry* (sex-determining region Y) specific primers; forward – 5' TCT-TAA-ACT-CTG-AAG-AAG-AGA-C 3' and reverse – 5' GTC-TTG-CCT-GTA-TGT-GAT-GG 3'. **Figure 3.1 E** is an image of a gel with EtBr stained products from a *sry* PCR. In the example given, there were three males and five females in the litter; the controls' DNA was extracted from adult tail-clips; 'm' and 'f' in reference to male and female respectively. An additional control consisting of PCR reaction mix minus any DNA is labelled as '0 DNA' in the figure.

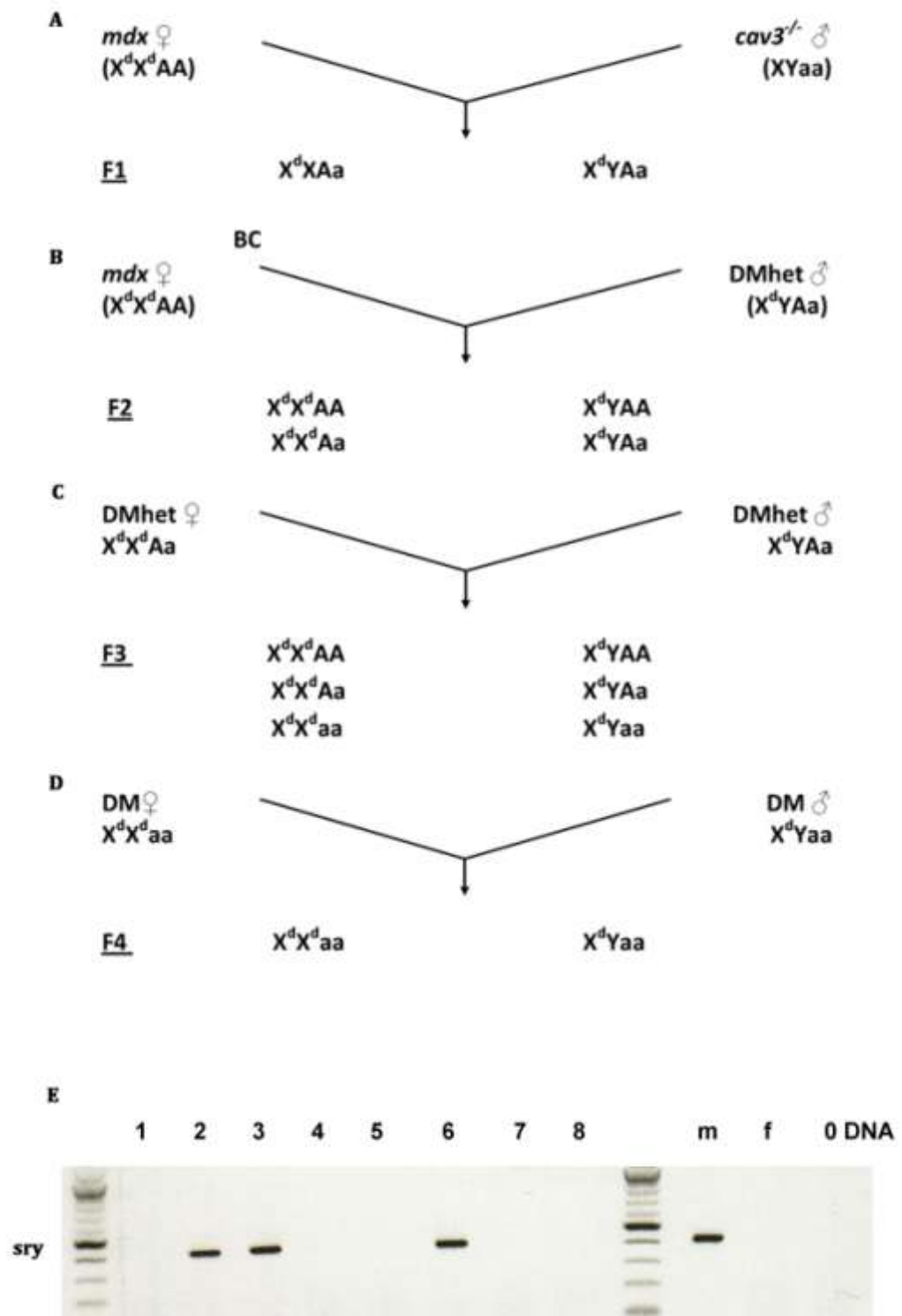


Figure 3.1

Generation of caveolin-3 deficient *mdx* mice (DM). (A) Crosses between *mdx* females and *cav3*^{-/-} males resulted in F1 progeny where all males were hemizygous (X^dY) and females heterozygous (X^dX) for *mdx*; both males and females were heterozygous for *Cav3* (Aa). (B) F1 males (DMhets) were backcrossed with *mdx* females to produce F2 progeny where 50 % (males and females) were *mdx* and 50 % (males and females) were DMhets. (C) F2 DMhet females were crossed with DMhet males to produce F3 litters comprising of three possible different genotypes; *mdx* (25 %), DMhet (50 %) and DM (25 %). (D) Sibling F3 DM males and DM females were then crossed to establish a pure F4 DM strain. (E) F1 embryos were sexed using primers to Y-chromosome specific *sry* as only males were DMhets; the gel shown is a typical example. Denotations: X, WT X-chromosome located *Dmd* gene; X^d, mutated *Dmd* (*mdx*) gene; Y, Y-chromosome; A, WT *Cav3* autosomal gene; a, mutated *Cav3* gene.

3.2.1.2 – *mdx* and DMhet littermates

F2 litters, resulting from backcrossing DMhet males with *mdx* females, consisted of two possible genotypes; *mdx* (males and females) and DMhets (males and females), in the expected ratios of 1:1 (**Figure 3.1 B**). F2 embryos' and adults' genotypes were ascertained via *neo* PCR using the following primers; forward - 5' GCA-CGC-AGG-TTC-TCC-GGC 3' and reverse - 5' GTC-CTG-ATA-GCG-GTC-CGC-C 3'. Male and female embryos of both genotypes were processed for either paraffin wax embedding for immunohistochemical analysis or proteins were extracted to be used for western blotting. Adult DMhets were crossed to produce offspring consisting of entire DM litters.

The next stage of the breeding programme involved crossing DMhet males and DMhet females (**Figure 3.1 C**). As there were expected to be three possible genotypes from matings between DMhet males and DMhet females; *mdx*, DMhets and DM, in the Mendelian ratios of 1:2:1 or 25 % : 50 % : 25 % respectively; both *Cav3* and *neo* statuses of littermates had to be ascertained via PCR. The *Cav3* primers used were as follows; forward - 5' ATT-CCT-GTT-CGC-CTG-TAT-C 3' and reverse - 5' AGG-ACC-AAC-CGA-ATC-TTC-TG 3'. Genotyping of the first litter to be born from successfully crossing a DMhet male and DMhet female is shown in an image of an electrophoresis gel (**Figure 3.2 A**). Of nine live pups from a litter of ten, one was *mdx* (#4; *Cav3* positive, *neo* negative), six were DMhets (#3, #5-9; *Cav3* positive, *neo* positive) and there were two DM (#1, #2 *Cav3* negative, *neo* positive), affording ratios of 1:6:2, or 11.1 % : 66.7 % : 22.2 % for *mdx*, DMhet and DM respectively. The genotype of the deceased pre-weaned pup is not known, so the ratios and percentages of genotypes stated are not wholly accurate as a comparison to the expected. The two DMs were both males and these were paired with

DMhet females from which one litter of two DM female pups (#10 and #11) were born (sired by DM male #2). These DM females were paired with the DM males; #1 with #10 and #2 with #11 and a litter of three pups (#12, #13, #14; all *Cav3* negative, *neo* positive) born to DM pair #2 and #11. The DM genotypes of pair #2 and #11 were confirmed (**Figure 3.2 B**) and re-confirmed along with their progeny (**Figure 3.2 C**). Samples from WT, *mdx*, *cav3*^{-/-}, DMhet and PCR reaction mix only were among those used as controls. Subsequent litters proved to be DM (**Figure 3.2 D**).

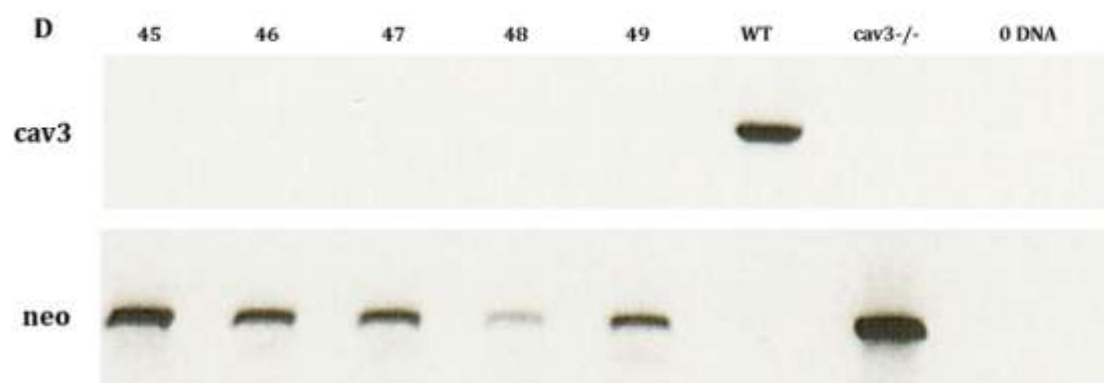
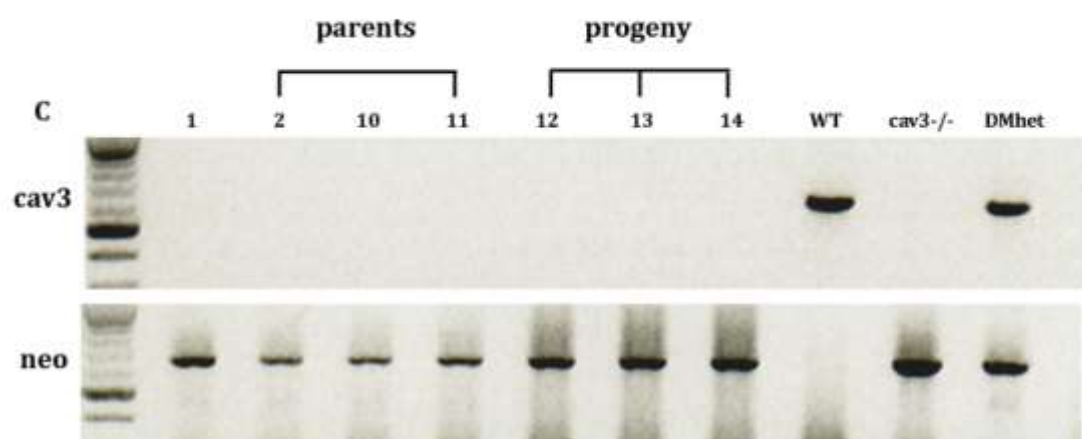
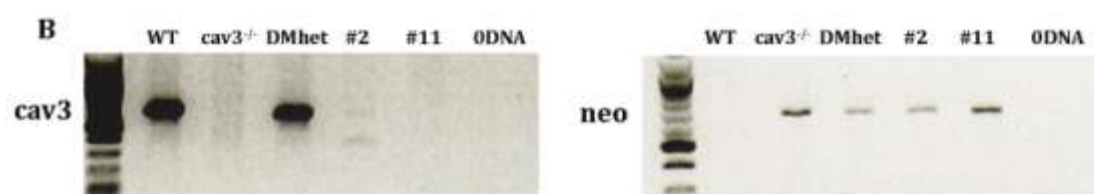
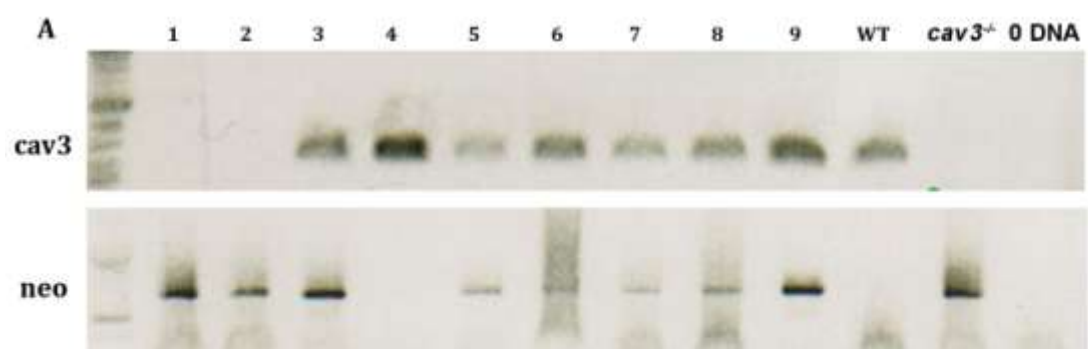


Figure 3.2

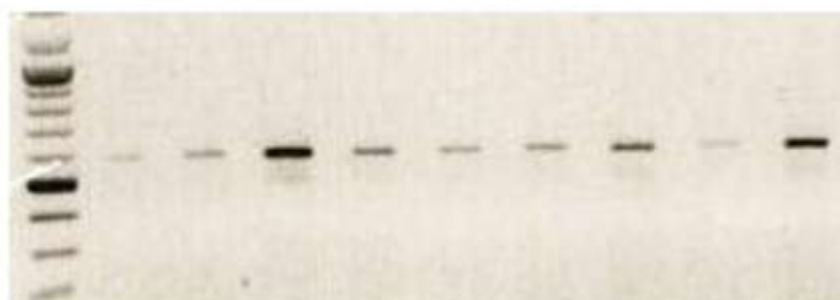
Genotyping of F2, F3 and F4 litters. F2 litters resulting from crosses between DMhet males and *mdx* females were of two possible genotypes; *mdx* and DMhet and F3 litters, resulting from crosses between DMhet males and females, were of three possible genotypes; *mdx*, DMhet and DM. Genotypes of both were ascertained via establishment of *Cav3* and *neo* statuses. The figure shows images of EtBr stained amplicons from *Cav3* and *neo* PCRs. **(A)** Electrophoresis gel image of genotyping the first litter to be born from successfully crossing a DMhet male with a DMhet female. Of nine littermates, one was *mdx* (#4), six were DMhet (#3, #5-9) and two were DM (#1, #2). From this litter, mating pairs were set up with #1 and #2 (both males) and DMhet females resulting in two pups, both of which were DM and both of which were female. These DM females were paired with DM males #1 and #2 and one litter of three pups was born to pair #2 and #11. **(B)** Confirmation of DM genotypes of pair #2 and #11 shows an absence of *Cav3* bands and presence of *neo* bands for both. Controls were provided by WT, *cav3*^{-/-} and 0 DNA samples. **(C)** Gel showing confirmation of DM genotypes of F3 and F4 mice. Parents (#2, #11), progeny (#12-14) and pair #1 and #10 are shown with WT, *cav3*^{-/-} and 0 DNA controls. **(D)** Genotyping of subsequent litters confirmed the DM line had been established.

3.2.1.3 – Sequencing to confirm the presence of the *mdx* mutation

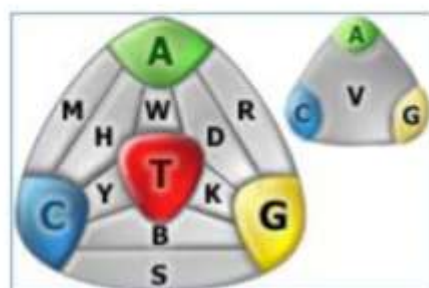
The establishment of *Cav3* and *neo* statuses in F2, F3 and F4 mice identified littermates that were homozygous positive (*cav3^{+/+}*), heterozygous (*cav3^{+/-}*) and homozygous negative (*cav3^{-/-}*) for *Cav3*; it did not confirm that the mice generated were positive for the *mdx* mutation, i.e. dystrophin deficient. Although it was unlikely that the thymine at bp position 3203 of the *Dmd* gene associated with *mdx* would have mutated back to WT cytosine, DNA sequencing was performed on WT, *mdx*, *mdxhets* (F1 females) and DMs. Primers; forward - 5' CTT-CTG-TGA-TGT-GAG-GAC-ATA 3' and reverse - 5' CTA-GCT-TTT-GGC-AGC-TTT-CC 3' were designed to amplify a 587 bp region that contained the *mdx* C-T point mutation and electrophoresis gels ran to confirm the PCRs had been successful in amplifying the target region (**Figure 3.3 A**). Amplicons were then directly aliquoted to reaction mixes for DNA sequencing. Sequence analyses showed the expected cytosine, represented by the letter C, was present in WT at bp position 3203 (**Figure 3.3 C**), thymine, letter T, was present in DM (**Figure 3.3 D**) and a letter Y, denoting the presence of both cytosine and thymine (**Figure 3.3 B**), was present in *mdxhet/cav3het* sequences (**Figure 3.3 E**). Thus, the *mdx* mutation was confirmed to be present in DM mice generated.

A

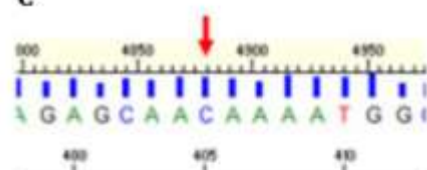
dystrophin *mdx*



B

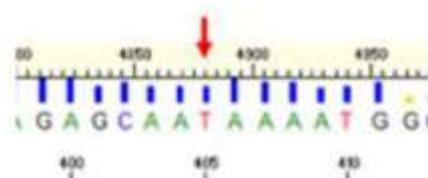


C



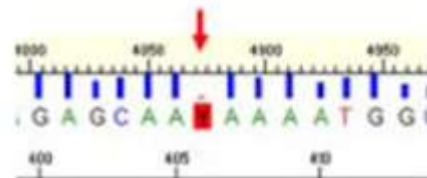
GCGTGTAGTGTAAATGAAC
 3AAAGAGCAACAAAATGGCT
 2CAAGAAAGCACCTTCAGAA

D



GCGTGTAGTGTAAATGAAC
 3AAAGAGCAATCAAAATGGCT
 2CAAGAAAGCACCTTCAGAA

E



GCGTGTAGTGTAAATGAAC
 3AAAGAGCAATCAAAATGGCT
 2CAAGAAAGCACCTTCAGAA

Figure 3.3

Sequencing of the *Dmd* gene to confirm the presence of the *mdx* mutation in DM.

PCRs were performed to amplify a 587 bp region of the *Dmd* gene that contained the *mdx* C-T mutation and electrophoresis gels ran to confirm the PCR had been successful.

(A) A representative example of a gel showing EtBr stained amplicons; PCR products were then directly used for sequencing. (B) Mixed bases diagram (provided by the Functional Genomics and Proteomics Unit, University of Birmingham) showing letters resulting when two different bases, from homologous alleles occupy the same position of DNA; as in the case of an *mdx* heterozygote. (C) WT DNA sequence showing a cytosine (red arrow and red letter) at position 3203. (D) DM DNA showing the C-T *mdx* point mutation. (E) *mdxhet* showing a Y, denoting both a C and a T at base position 3203.

3.2.2 - Caveolin-3 protein levels are reduced in DMhet embryos

To establish the caveolin-3 protein levels of DMhet embryos in respect to WT and *mdx*, whole embryo protein samples of all four strains, WT, *mdx*, *cav3*^{-/-} and DMhet were analysed via western blotting. At E13.5 only the increased caveolin-3 of *mdx* can be clearly seen following western blotting but at E15.5 and E17.5 protein levels of all four strains, except for *cav3*^{-/-}, can be seen (**Figure 3.4 A**). Negative controls were provided for by *cav3*^{-/-} samples, one for each embryonic stage; the very faint E13.5 *cav3*^{-/-} band must therefore be attributed to loading overspill. There is clear upregulation in *mdx* at E17.5 and no protein present in *cav3*^{-/-} as expected. Although caveolin-3 levels of the DMhet appear comparable to WT at E15.5, there is a definite reduction at E17.5 when compared to WT and particularly *mdx* at the same stages; an observation confirmed via the β -actin loading control. Although subtle, immunolabelling of E15.5 sagittal wax-embedded sections with anti-caveolin-3 antibodies shows an increase in staining intensity in *mdx* and a slight reduction in staining intensity of DMhet, when compared to WT of the same embryonic stage (**Figure 3.4 B**). When taken together, these data indicate there is a reduction in caveolin-3 protein of developing DMhet embryos.

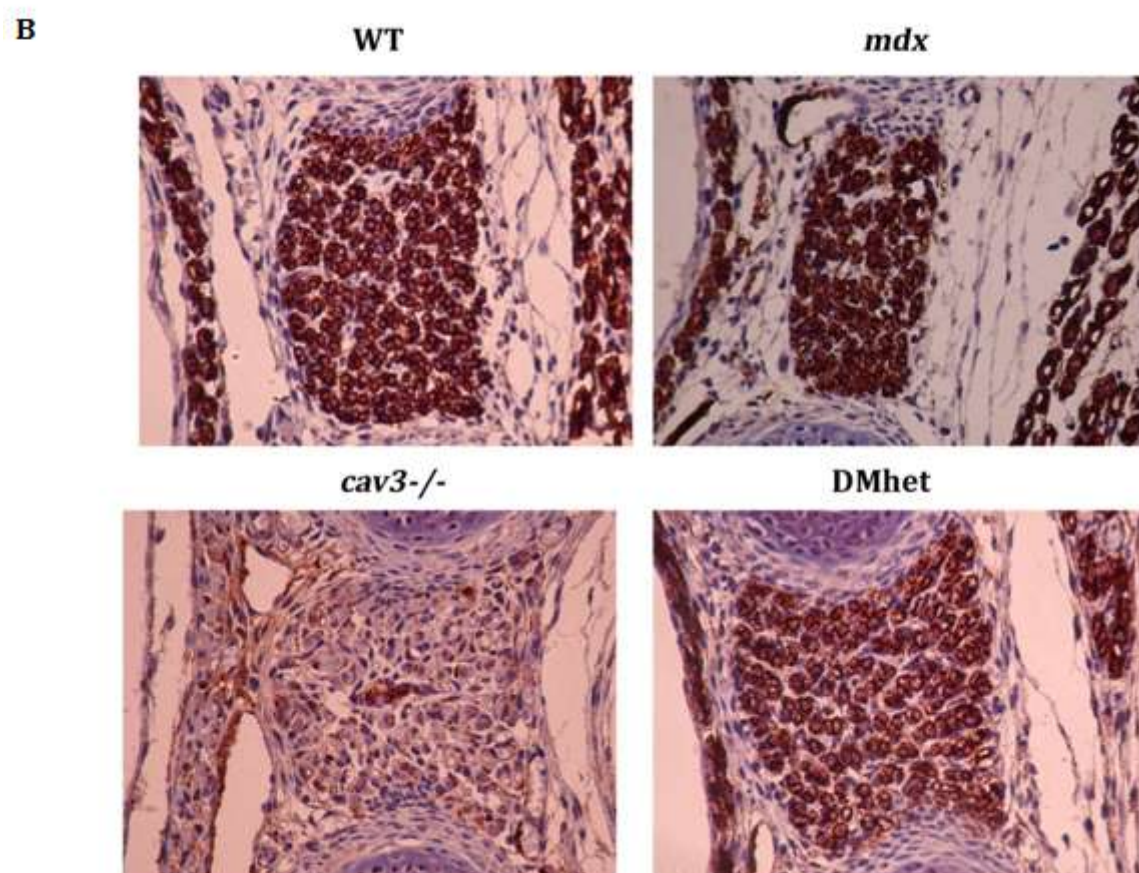
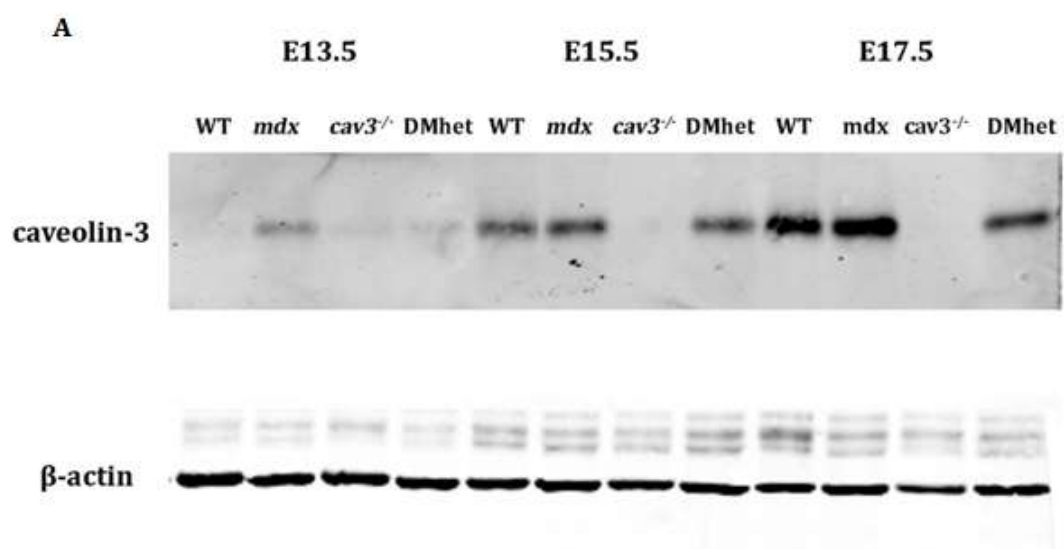


Figure 3.4

Caveolin-3 probed membranes and sections of WT, *mdx*, *cav3*^{-/-} and DMhets. (A) At E13.5 a strong band can only be seen in the lane corresponding to *mdx* but at E15.5 bands can be seen in all except the lane for *cav3*^{-/-}. There is very little difference between protein levels of WT and DMhet at E15.5, with *mdx* protein being slightly increased when compared to WT at this stage. At E17.5 there is an increase in caveolin-3 protein seen in *mdx* and a decrease in DMhet when compared to WT levels; β -actin served as a loading control. (B) 5 μ m paraffin wax embedded sections of E15.5 WT, *mdx*, *cav3*^{-/-} and DMhet intercostals labelled with anti-caveolin-3 antibodies. There is increased intensity of staining in *mdx* and slightly reduced staining in DMhet when compared to WT. The apparent staining seen in *cav3*^{-/-} is due to over-incubation in the tyramide signal amplification reagent as there is no sarcolemmal specific staining.

3.2.3 - Pax7⁺ cells are severely attenuated in DMhets

Sagittal paraffin wax-embedded WT, *mdx*, *cav3*^{-/-} and DMhet sections were immunolabelled with anti-pax7 antibodies in order to examine numbers and distribution of pax7⁺ cells *in situ*. At E17.5 (**Figure 3.5**), the number of pax7⁺ cells in the muscles of the intercostals is reduced in *mdx* (**Figure 3.5 D-F**) and DMhets (**Figure 3.5 G-O**) when compared to WT (**Figure 3.5 A-C**).

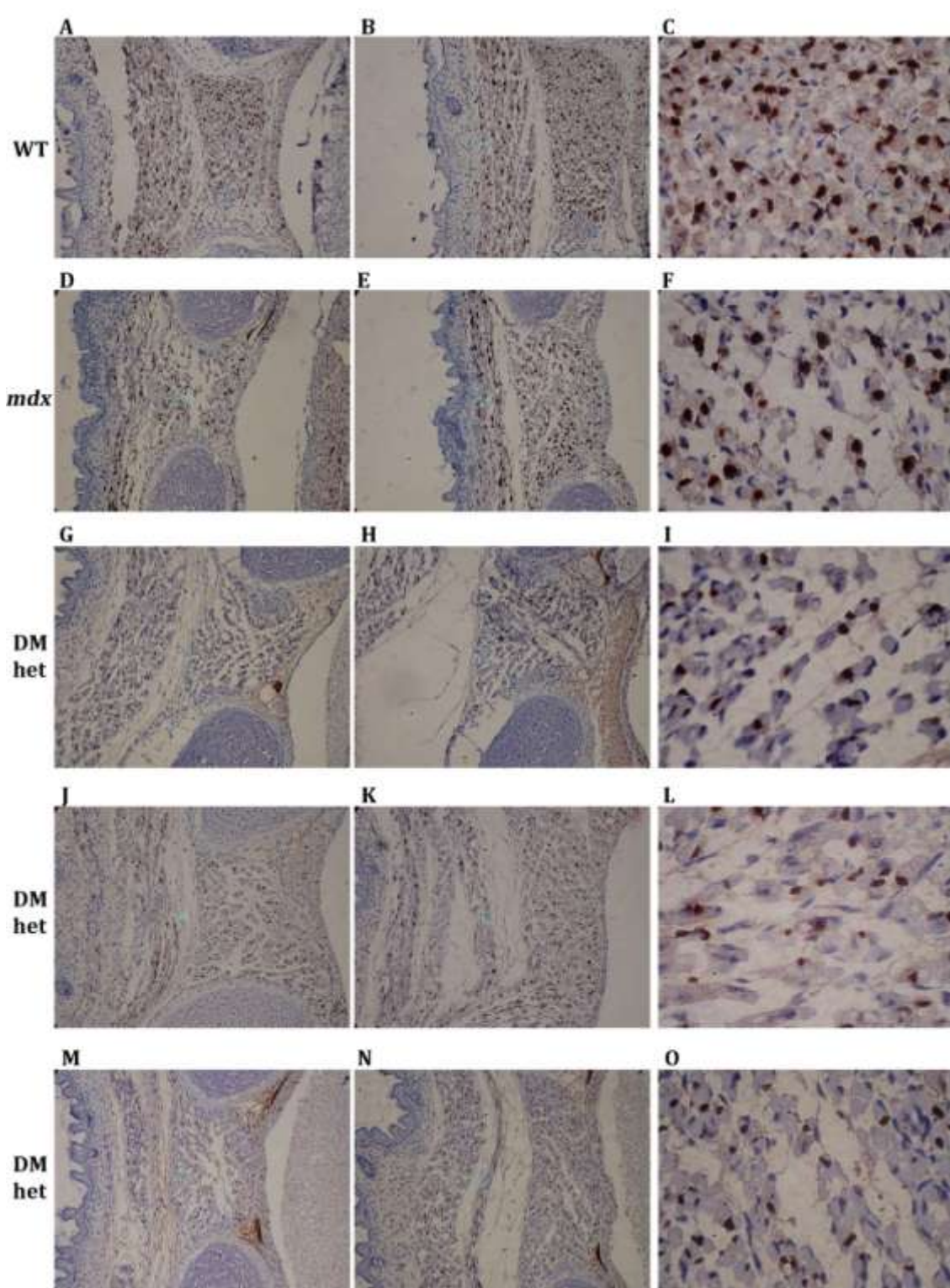
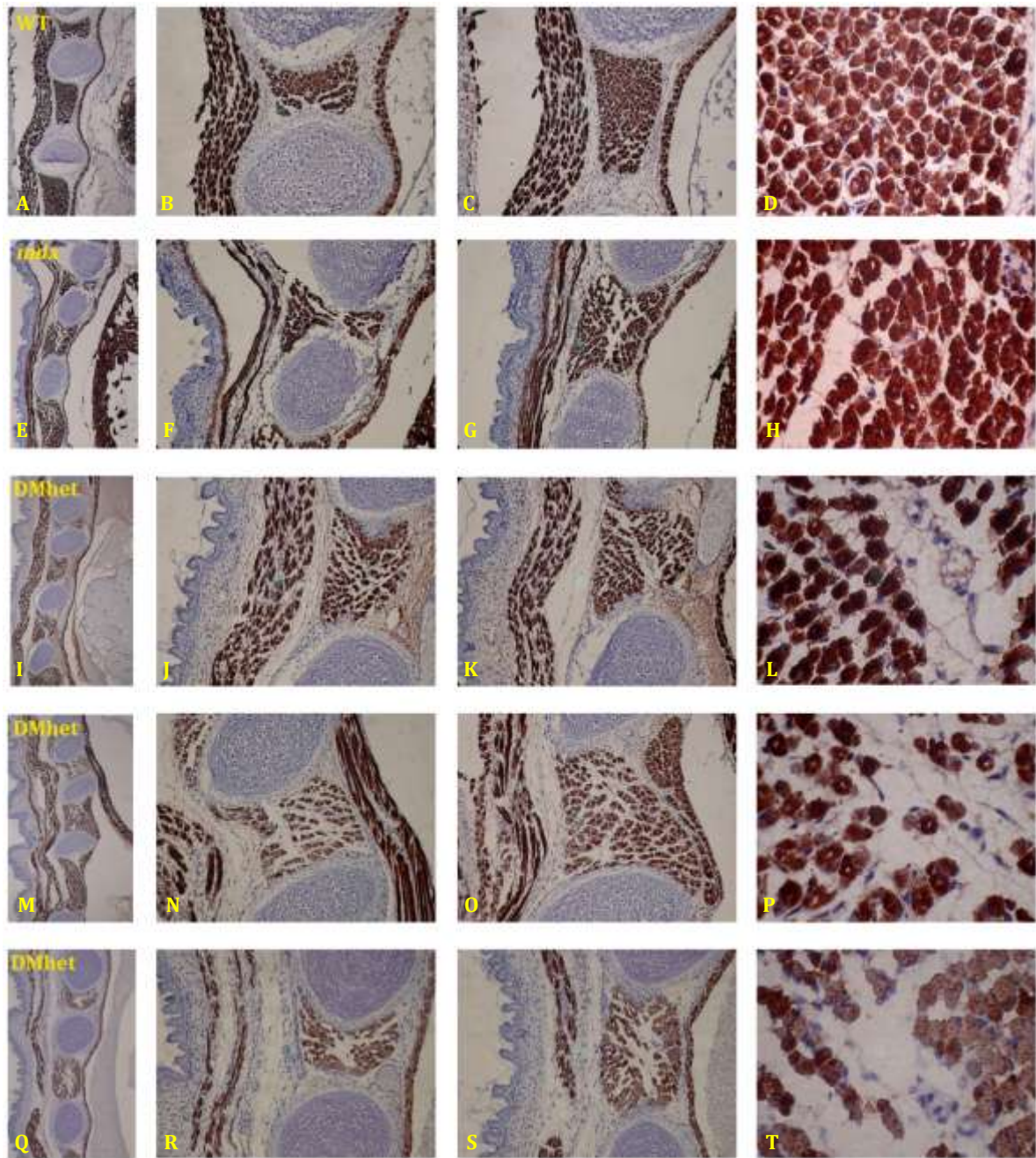


Figure 3.5

Pax7 labelled intercostal muscles. Paraffin wax embedded E17.5 WT, *mdx* and DMhet 5 μ m sections were immunohistochemically labelled with anti-pax7 antibodies. At low magnification images, pax7⁺ cells can be clearly seen in WT (**A, B**) and *mdx* (**D, E**) intercostal muscles, but not so clearly in DMhet intercostals (**G, H, J, K, M, N**). At higher magnification, there is no discernible difference in pax7⁺ cell staining intensity in *mdx* (**F**) when compared to WT (**C**), although there is a greater abundance of pax7⁺ cells in WT, which is consistent with the greater myofibre density shown. The three DMhets have reduced pax7⁺ cell abundance when seen at higher magnification (**I, L, O**).

3.2.4 – Reduced fibre-density in dystrophin-deficient intercostal muscles

Sagittal wax-embedded sections, 5 µm in thickness, were mounted onto slides and immunolabelled with anti-pan-myosin MF20 antibodies in order to compare these proteins in E17.5 WT, *mdx*, *cav3*^{-/-} and DMhets (**Figure 3.6**). There is an observable reduction in fibre-density in the intercostal muscles of *mdx* (**Figure 3.6 E-H**) and DMhet embryos (**Figures 3.6 I-T**), when compared to the intercostals of aged matched WT embryos (**Figures 3.6 A-D**); the reduction is evident through areas of white spaces located in the centre of the intercostal muscles. Intercostal fibre-density is reduced by 37.5 % and 71.2 % for *mdx* and DMhets respectively, when compared to age matched WT sections (**Figure 3.6 X**), n=3 per strain. In contrast, intercostal muscles of age matched *cav3*^{-/-} embryos (**Figure 3.6 U-W**) show densely packed hypertrophic fibres when compared to WT control (**Figure 3.6 A-D**).



X

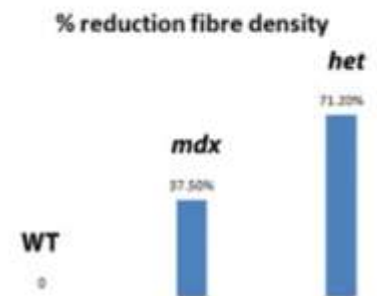
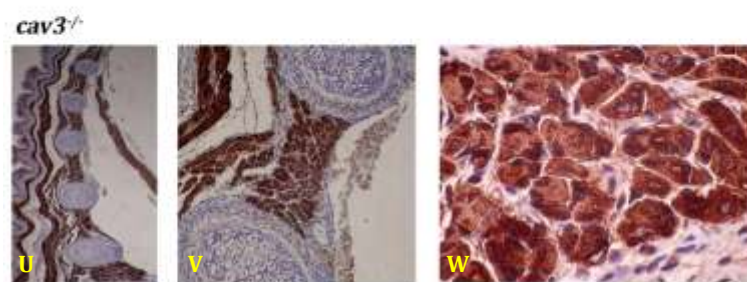


Figure 3.6

E17.5 WT, *mdx* and DMhet MF20 labelled intercostal muscles. Paraffin wax embedded 5 μ m sections were labelled with anti-pan-myosin antibody MF20. Reduced fibre density in both *mdx* (**E-H**) and DMhet (**I-T**) intercostals can be seen when compared to WT (**A-D**) however, there is no such reduction in the intercostals muscles of *cav3^{-/-}* (**U-W**). At higher magnification, extra-myonuclei can be seen in DMhet muscle (**L, P, T**), but not in WT (**D**) or *mdx* (**H**). (**X**) Intercostal muscle-fibre density is reduced by 37.5 % and 71.2 % for *mdx* and DMhet respectively, when compared to WT (graph reproduced from Merrick *et al.*, 2009, quantitative analysis performed by Dr Janet Smith), n= 3.

3.2.5 – MF20 and MY32 labelled diaphragms

Diaphragm muscles of WT, *mdx* and DMhets were also examined for myosin content using MF20 and MY32 antibodies and there were no discernible difference evident between pan-myosin stained and FMyHC stained sections (**Figure 3.7**). In the lower magnification images shown in **Figure 3.7**, the diaphragms of *mdx* (**Figure 3.7 D, E**) and DMhets (**Figure 3.7 G, H, J, K, M, N**) appear substantially reduced in thickness when compared to WT diaphragm (**Figure 3.7 A, B**), but this can be attributed to slight differences in the planes at which sagittal sections of the embryos were cut. At higher magnification the fibres of DMhets show clustering and increased fibre density (**Figure 3.7 I, L, O**) when compared to the WT control (**Figure 3.7 C**). Although no pathology appears to be present in DMhet or *mdx* diaphragm at this embryonic stage, there does seem to be a greater abundance of extra-myonuclei present in DMhet diaphragms (**Figure 3.7 I, L, O**) when compared to WT (**Figure 3.7 C**) and *mdx* (**Figure 3.7 F**).

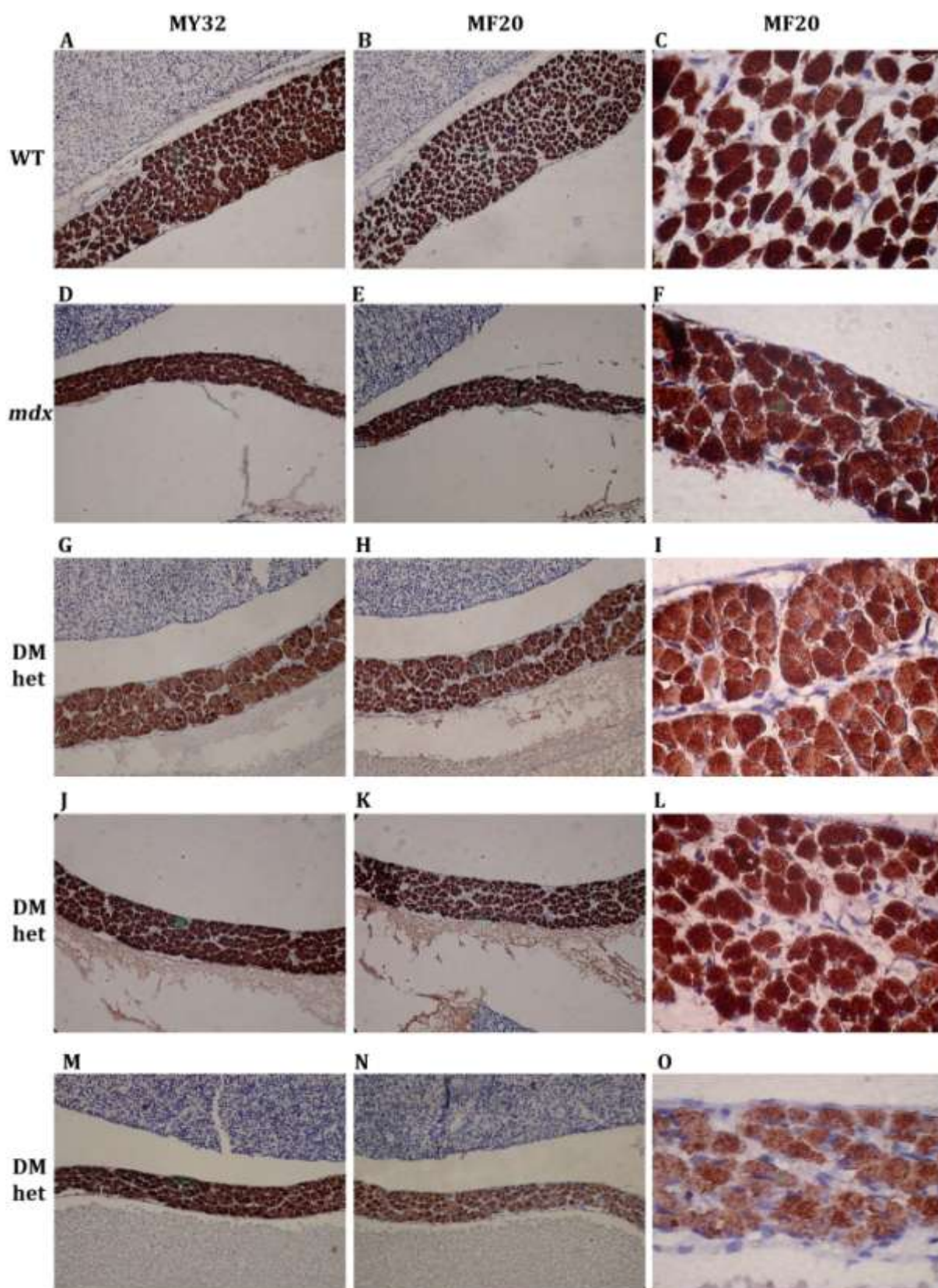


Figure 3.7

Diaphragm muscles of E17.5 WT, *mdx* and DMhets. Sections 5 μm in thickness were immunohistochemically labelled using anti-pan-myosin antibody MF20 and anti-FMyHC antibody MY32. There is no discernible difference seen between pan-myosin stained (**B, E, H, K, N**) and FMyHC stained (**A, D, G, J, M**) images. At lower magnification the thickness of the diaphragm muscles in *mdx* (**D, E**) and DMhets (**G, H, J, K, M, N**) appears reduced when compared to WT diaphragm (**A, B**). The fibres of DMhets at higher magnification show clustering (**I, L, O**), most evident in **I** and although the level of interstitium is greater in WT (**C**), there is no clustering of fibres seen. The fibres of *mdx* at higher magnification (**F**) appear to be more densely packed than those of WT (**C**). Although there appears to be no obvious pathology in the diaphragms of DMhets, there seems to be a greater abundance of extra-myonuclei, when compared to both WT and *mdx*.

3.2.5 - α -tubulin appears perturbed in dystrophic embryos

Western blotting was used to examine specific protein levels in all dystrophic strains compared to WT in embryonic and adult tissue homogenates and initially α -tubulin was used as a loading control for these analyses. Variable lane intensities of α -tubulin on western blots indicative of uneven sample loading was reproved when β -actin was used as a loading control. Consistent downregulation of α -tubulin can be seen in *cav3*^{-/-} at E13.5, E15.5 and E17.5 when compared to WT at the same stages; conversely, upregulation can be seen in *mdx* and DMhets at the same embryonic developmental stages when compared to WT (**Figure 3.8 A, B**). Densitometric analysis shows α -tubulin protein levels in *cav3*^{-/-} mutants to be between 0.5 and 0.75 of WT levels at all three stages, with the greatest difference seen in *mdx* and DMhets at E13.5, with a 2 and 2.5 fold increase respectively above that of WT (**Figure 3.8 C**). As there were no such disturbances of β -actin observed in the protein of dystrophic embryos, β -actin was used as a reliable loading control.

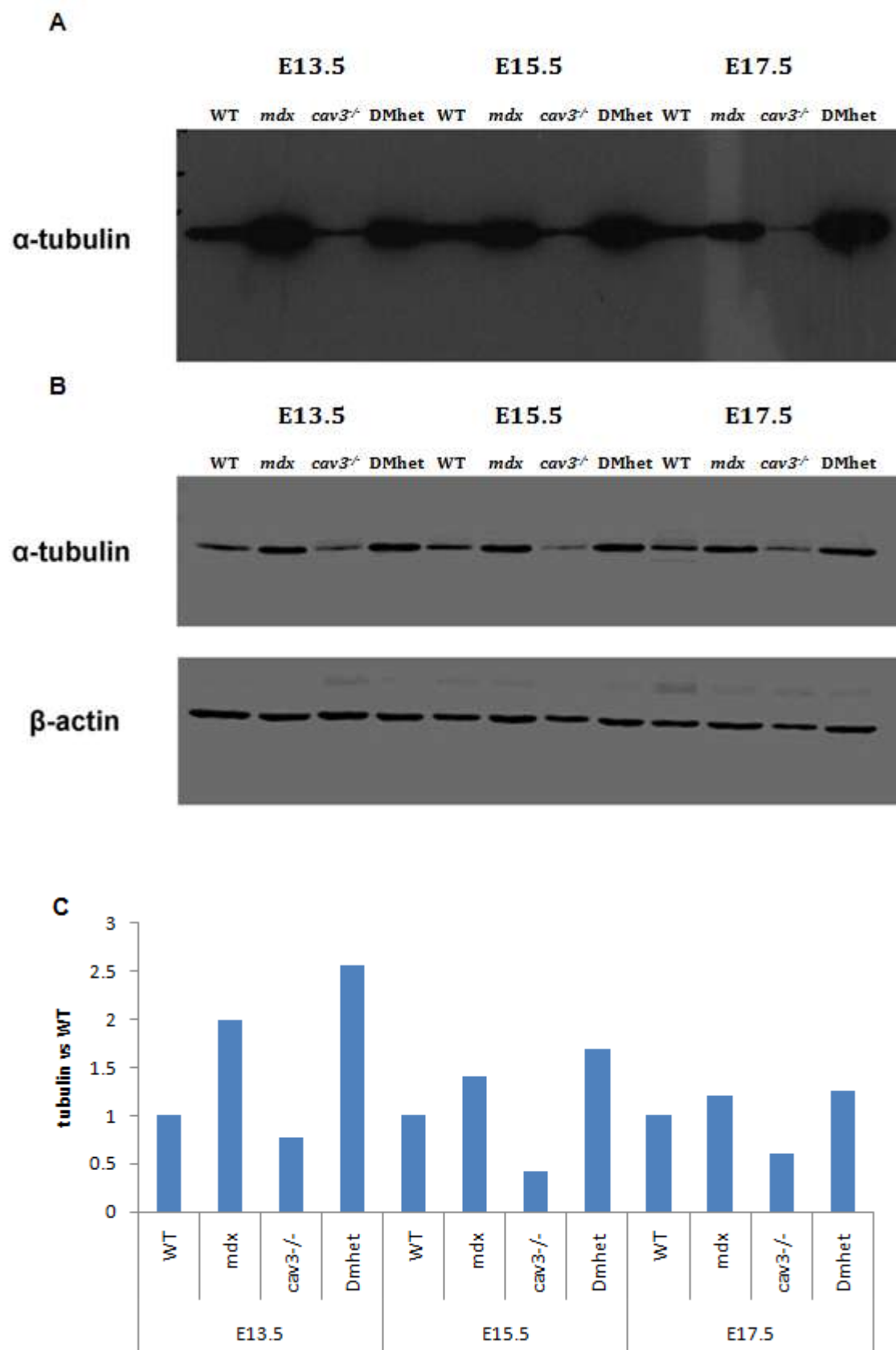


Figure 3.8

Immunoblots of E13.5 – E17.5 WT, *mdx*, *cav3*^{-/-} and DMhet membranes probed for caveolin-3, α -tubulin and β -actin. (A) Initial western blot analysis of membranes probed for α -tubulin show disturbances in dystrophic embryos consistent throughout all stages when compared to WT. (B) Subsequent membrane probing with anti α -tubulin afforded similar results, β -actin appeared unaffected in dystrophic mutants. (C) Densitometric analysis showed increases of α -tubulin in *mdx* and DMhet, whereas there was a reduction in α -tubulin seen in *cav3*^{-/-} protein. The graph shows the fold increase/decreased compared to WT levels.

3.3 – DISCUSSION

3.3.1 - Generation of caveolin-3 deficient *mdx* mice

Although breeding programmes do not usually form part of discussions, the generation of DM mice was such a time consuming and onerous task that a couple of paragraphs are justified.

The initial stage at the commencement of the breeding programme was uncomplicated and free from any problems. Female *mdx* and male *cav3*^{-/-} mice produced litters that were readily sexed using *sry* specific primers and PCR. There were problems however with the next stage of the breeding programme. Although a seemingly straightforward process, the genotyping of F2 mice was fraught with PCR inconsistencies (*sry* genotyping presented with no such problems), initially gel electrophoresis of *neo* PCR products resulted in bands which were too faint to make any genotypic identification of DNA samples. Later and invariably, there would be no bands at all. This problem persisted for a total of seven long, painfully frustrating months and was eventually resolved by the use of a different PCR machine. Unfortunately, mice of the required genotype (DMhets) required to continue with the breeding programme were by this stage too old and as a consequence, DMhet matings did not result in any successful pregnancies. The programme had to be started again and *in vitro* fertilisation (IVF) was performed on female *mdx* and *cav3*^{-/-} mice using sperm taken from a DMhet male; the procedure was performed by BMSU technicians. The decision made by BMSU management to use *mdx* and *cav3*^{-/-} females, rather than DMhet females further setback

the breeding programme. However, a litter of nine re-derived mice were born to an *mdx* female of which two males, # 1 and # 2, which were positive for *neo* and negative for *Cav3* were crossed with DMhet females and a litter of two pups were born; genotyping showed these two females were DM. These two females were backcrossed with males # 1 and # 2 and a litter of three pups were born to male # 2 and female # 11. The DM line had been established.

Had I have been aware that a line of mice deficient in both dystrophin and caveolin-3 had already been generated; I could have looked at acquiring these mice which would have saved hundreds of laboratory hours that could have been used in generating data. Given the opportunity to choose the line of caveolin-3 deficient mice to use, I would prefer the TgCAV3M1 line over the *cav3*^{-/-} line as the P104L mutation of the former results in the autosomal dominant transmission of the disease, rather than recessive transmission (Hagiwara *et al.*, 2000; Ohsawa *et al.*, 2006). The use of the TgCAV3M1 mouse model would not only have saved time in the generation process, but as a model for LGMD-1C it is more akin to the human caveolinopathy than the *cav3*^{-/-} mouse.

3.3.2 - Embryonic phenotype of DMhets

3.3.2.1 - Attrition of pax7^{+ve} cells in DMhets

It has been shown that both pax7 protein and pax7^{+ve} cell numbers are reduced in *mdx* and *cav3*^{-/-} late gestation embryos (Merrick *et al.*, 2009). In DMhet embryos, the attrition of pax7^{+ve} cells is even more severe than that which is seen in *mdx*, with evidence of pax7^{+ve} cell fragmentation suggesting increased apoptosis of pax7^{+ve} cells in these

mutants. The reduced levels of caveolin-3 in late stage (E17.5) DMhet embryos as is shown in western blots could have a detrimental effect on the numbers of $pax7^{+ve}$ cells, through a reduction in the embryonic growth factor Igf-2. A reduction of Igf-2 has been shown previously in *cav3^{-/-}* embryos (unpublished data) and Igf-2 has been shown to have an inhibitory effect on apoptosis of dystrophic SMSc (Smith *et al.*, 2000; Merrick *et al.*, 2007). Pax7 is detected in WT mouse at E11.5, as is caveolin-3; *mdx* and *cav3^{-/-}* both have delayed *pax7* expression and towards late gestation, *pax7* protein levels and $pax7^{+ve}$ cells are significantly reduced in both mutants, although caveolin-3 is increased in *mdx* late gestation embryos; as it is in adult *mdx* and DMD (Vaghy *et al.*, 1998; Repetto *et al.*, 1999; Merrick *et al.*, 2009). This suggests caveolin-3 has a role in the maintenance of *pax7* expression and subsequently $pax7^{+ve}$ satellite cells and that dystrophin may compensate for the absence of caveolin-3. In the absence of dystrophin, with reduced levels of caveolin-3, the attrition of $pax7^{+ve}$ cells is exacerbated in the DMhet. Through which signalling pathway caveolin-3 may mediate *pax7* maintenance, if it does at all, needs to be elucidated, but evidence suggests that transforming growth-factor β (TGF- β) super-family member myostatin may have a role. The reduction of *pax7* protein and attrition of $pax7^{+ve}$ cells in *cav3^{-/-}* mutants complies with data that showed caveolin-3 negatively regulates myostatin signalling through suppression of its type-1 (ALK4/ALK5) receptor (Ohsawa *et al.*, 2006; Merrick *et al.*, 2009). Interestingly, myostatin negatively regulates the expression of Igf-2 (Lalani *et al.*, 2000; Miyake *et al.*, 2010). Taken together these data infer a very real involvement for caveolin-3 in the maintenance of *pax7*, an inference compounded in that upregulated caveolin-3 is accompanied by downregulated myostatin in DMD (Repetto *et al.*, 1999; Zhu *et al.*, 2000).

3.3.2.2 - Fibre loss in intercostal muscles of dystrophin-deficient mutants

It has been shown that FMyHC can be detected in WT at E11.5, whereas there is a delay in *mdx*, this suggests a temporal role for dystrophin in the optimisation of FMyHC expression as although FMyHC is not detected in *cav3*^{-/-} at E11.5, its levels are above that of WT by E13.5 (Merrick *et al.*, 2007). The reduced fibre-density shown in the intercostals of *mdx* is consistent with this developmental delay. DMhet embryos have a greater reduction in intercostal fibre-density than in age matched *mdx* embryos and as no such reduction is present in *cav3*^{-/-}, this suggests a compensatory role for caveolin-3 in the maintenance of dystrophin deficient *mdx* intercostal muscles. Myostatin, of the TGF- β family of growth factors, negatively regulates myoblast proliferation and differentiation through suppression of Igf-2 and research has shown that caveolin-3 inhibits myostatin via binding of its type-2 receptor (Lalani *et al.*, 2000; Thomas *et al.*, 2000; Ríos *et al.*, 2001; Ohsawa *et al.*, 2006; Miyake *et al.*, 2010). The more severe phenotype seen in the DMhet is consistent with these data. It has been shown that FMyHC⁺ fibres are depleted in DMD and *mdx*, with a virtual total loss of FMyHC-2dx⁺ and FMyHC-2b⁺ fibres along with a concomitant 7-fold increase of SMyHC in diaphragm muscle of 22 to 24 month *mdx* (Petrof *et al.*, 1993). The loss of FMyHC-2dx presents a more severe phenotype than the loss of the more abundant FMyHC-2b, including kyphosis, a condition common in DMD and LGMD-1C (Acakpo-Satchivi *et al.*, 1997). The global-loss of FMyHC, when taken with the intercostal fibre-reduction in *mdx* is significant, as more than 70 % of skeletal muscle is comprised of FMyHC-2b and 30-60 % of diaphragm MyHC is the FMyHC-2dx isoform. Understanding the molecular aetiology of respiratory muscle degeneration is crucial to the understanding of the

pathogenesis of DMD, as 56 % of mortalities (Figures for England and Wales) are attributed to respiratory failure (Calvert *et al.*, 2006).

3.3.3 - Tubulin upregulation

The upregulation of α -tubulin seen in *mdx* and in the DMhet concurs with microarray analysis results which found a 2.7 fold increase in the expression of α -tubulin in DMD muscle biopsies compared to healthy muscle biopsy expression of the same gene (Haslett *et al.*, 2002). Results obtained from colleagues using lysates of dystrophic cell-lines also showed α -tubulin to be an unreliable house-keeping protein when analysing proteins from these sources. The molecular mechanisms responsible for the increased protein levels of α -tubulin seen in dystrophin-deficient muscle and the reduction seen in *cav-3^{-/-}* embryos although interesting are beyond the scope of this thesis, but as the increase of α -tubulin seen in *mdx* is echoed in DM, it suggests the involvement of the DGC and not the increase in caveolin-3 as a possible causal factor. Interestingly, α -tubulin is shown to be increased, as opposed to decreased, in postnatal muscle of *cav3^{-/-}* mice so this may infer a role for caveolin-3 in the temporal expression of α -tubulin.

Table 3.1 - Summary of results. The two embryonic dystrophin-deficient mouse strains used along with the results are summarised. All results are compared with WT, therefore – denotes < WT and + denotes >WT.

Mouse	Caveolin-3	Pax7 ^{+ve} cells	Intercostal fibre density	α -tubulin
<i>mdx</i>	+	-	-	+
DMhet	-	--	--	+

CHAPTER 4 - CORRELATION OF CAVEOLIN-3 TO THE OBSERVED PATHOLOGY IN POSTNATAL DYSTROPHIN-DEFICIENT MICE

This chapter looks at the musculo-histopathology of the three dystrophin-deficient mouse strains used during the course of this study, *mdx* and the two double-mutants generated, namely the DM (*mdx/cav3^{-/-}*) and DMhet (*mdx/cav3^{+/-}*); with a view to correlate observed pathology with levels of caveolin-3 protein. Data pertaining to three postnatal time points; four weeks, nine weeks and nine months, shall be presented herein.

4.1 – INTRODUCTION

The *mdx* mouse has been the preferred animal model of choice for most working in the field of muscular dystrophy since its introduction in the mid 1980's (Bullfield *et al.*, 1984). Although extensively used as the primary animal model for DMD, the myopathy observed in *mdx* does not accurately represent the pathogenesis and progression that manifests with the human form of the disease as mobility is not impaired and life-span is comparable to that of WT mice. Muscle tissue regenerated in the *mdx* mouse, although abnormal in architecture as there are variations in fibre sizes and centrally located nuclei, functions perfectly sufficiently and is void of the connective and adipose tissue associated with the human form of the disease.

The loss of dystrophin from the DGC has a profound effect on the complex' integrity and results in its eventual breakdown, there are many genes that have been found to be

differentially expressed in dystrophin-deficient muscle (Ervasti *et al.*, 1990; Haslett *et al.*, 2002; Porter *et al.*, 2002; Noguchi *et al.*, 2003; Turk *et al.*, 2005). DGC associated protein caveolin-3 is one that is upregulated in DMD and *mdx* and it has been suggested that the increase protein content of caveolin-3 may contribute to the pathogenesis observed in *mdx* and DMD (Vaghy *et al.*, 1998; Repetto *et al.*, 1999; Galbiati *et al.*, 2000). The histological analyses of *mdx*, DM and DMhet mice, in essence all dystrophin-deficient mice with hyperphysiological levels of caveolin-3, *mdx*; hypophysiological/WT levels of caveolin-3, DMhet; and a deficiency of caveolin-3, DM would allow for a correlation to be made between varying levels of caveolin-3 and the associated pathology.

The decision to use mice of four weeks, nine weeks and nine months of age was dictated by the progression of the dystrophic condition previously observed in *mdx*. Proximal limb muscles, or to be more specific, triceps brachii and quadriceps femoris, were chosen by virtue of their mixed fibre content and comparative associated workload, as there is a correlation between mechanical stress and muscle degeneration, with no degeneration present in denervated hindlimb muscles (Karpati *et al.*, 1988; Petrof *et al.*, 1993).

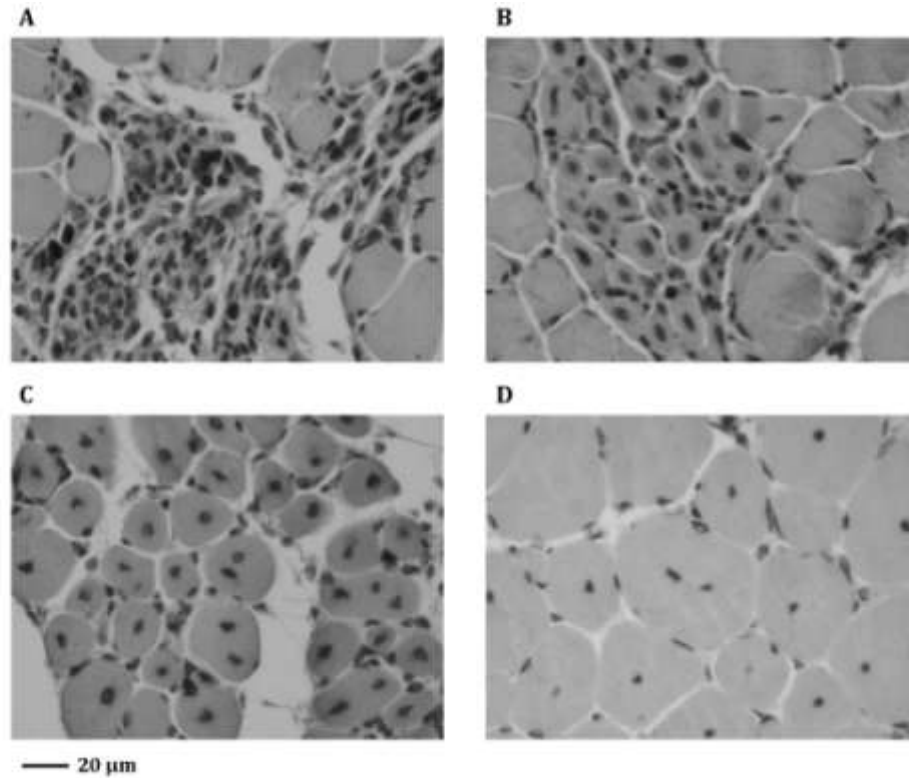


Figure 4.1 – Stages of muscle regeneration in *mdx*. (A) Following degeneration of fibres, infiltration of muscle tissue interstitium with muscle progenitor (satellite) cells, fibroblasts and leukocytes occurs resulting in areas of hypercellularity. (B) Newly regenerating fibres are identified via their large centrally located single nuclei; the numbers of interstitial cells has diminished. (C) Regenerating fibres are now larger, with smaller centrally located nuclei; of which there may be more than one per fibre. (D) Regenerated fibres are of a round morphology and are heterogeneous in size. The retention of central nuclei is indicative of a fibre having regenerated and can be used to assess the level of regeneration in a section of muscle.

4.2 – RESULTS

4.2.1 – IHC and western blotting confirms the loss of caveolin-3 in the DM

Proteins were extracted from triceps and quadriceps muscles, separated via PAGE, transferred onto nitrocellulose membranes and probed with anti-caveolin-3 antibodies. Detection was enhanced through the use of biotinylated secondary antibodies/streptavidin and membranes visualised using the Odyssey Infrared Imaging System. Caveolin-3 is shown to be absent in all mice identified as DM, thus the phenotypes were confirmation of the genotypes (**Figures 4.2 B**). The levels of caveolin-3 in the muscles of DMhet mice is slightly variable, but similar to that of WT, it is always reduced when compared to *mdx* (**Figures 4.2 B; 4.3 A**), which when analysed using densitometry gave a P value of 0.007154 with n=4 using a two-tailed student's *t*-test (**Figure 4.2 C**). Caveolin-3 in *mdx* is shown to be increased by as much as seven fold when compared to WT (**Figure 4.2 C**). These observations are consistent with all ages of mice analysed (**Figures 4.2 A; 4.3 A**). As was seen with western blotting performed with embryos, there are perturbations in α -tubulin shown in all dystrophic mutants (**Figure 4.2 A**), with the greatest disturbances seen in *mdx* and DM which when compared to WT afford P values of 0.000565 and 0.009145 respectively with n=4 using a two-tailed student's *t*-test (**Figure 4.2 B**). Imperial protein stain was used as a loading control, which proved to be reliable (**Figure 4.2 A; 4.3 A**). To establish the levels of caveolin-3 localised to the sarcolemma, IHC was performed on 5 μ m sections of paraffin wax embedded nine weeks old triceps muscles (**Figure 4.3 B**). The increased levels are clearly seen in the muscle of *mdx*, evident by the intense brown staining around the

periphery of the muscle fibres which is less intense in WT and DMhet muscle sections. The complete lack of staining in the DM once more establishes the caveolin-3 deficiency in the DM; *cav3*^{-/-} samples were included as controls. The presence of centrally nucleated fibres can be seen in all three of the dystrophin-deficient mutants (**Figure 4.3 B**).

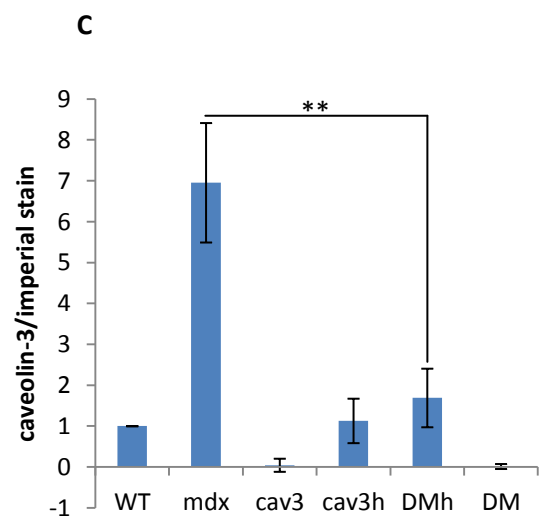
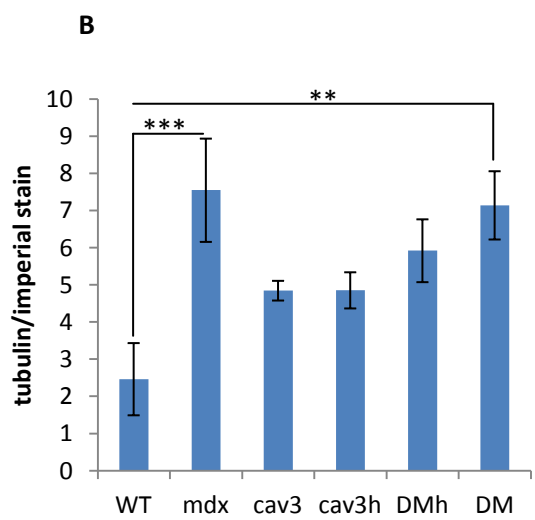
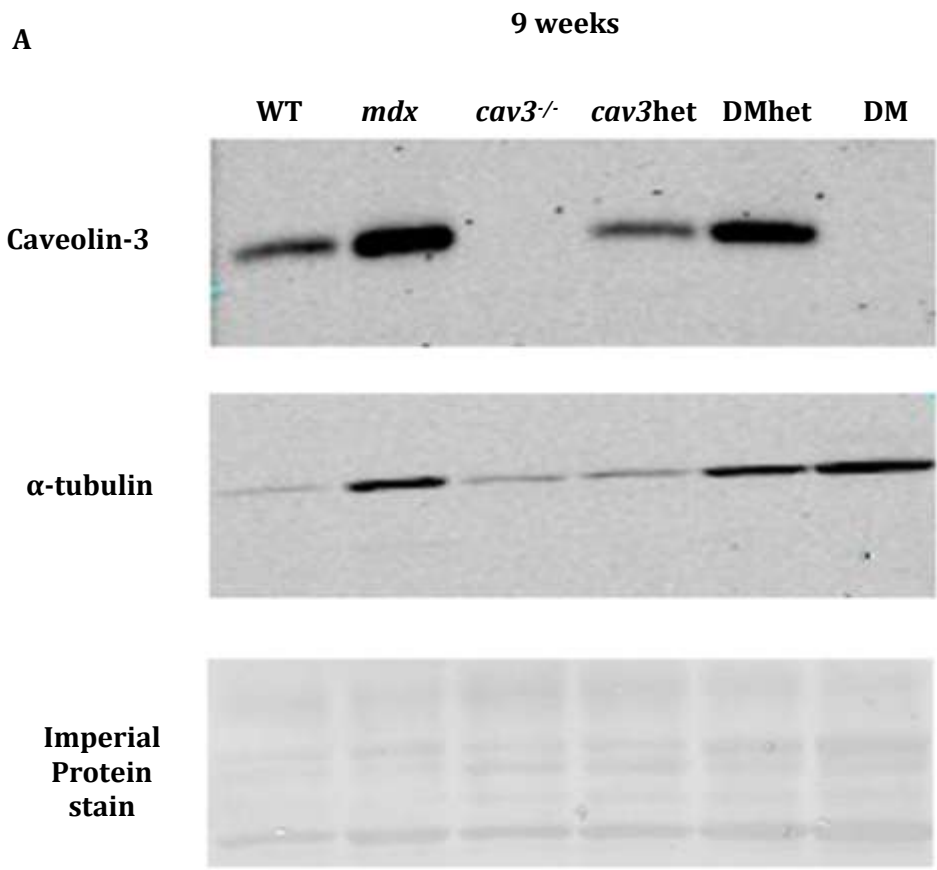


Figure 4.2

Membranes probed with antibodies to caveolin-3 and α -tubulin (A) As was demonstrated with embryos, α -tubulin protein levels appear to be disrupted in *mdx*, DMhet and DM postnatal proximal limb muscle tissue, with an increase in levels of the protein shown when compared to WT. Imperial protein stain provided a more reliable method of protein loading control. **(B)** Bar graph showing densitometric analysis of α -tubulin/Imperial protein stain from western blots of nine weeks old proximal limb muscle tissue samples. There is an increase of α -tubulin in all mutants when compared to WT; the greatest seen in *mdx* and DM where $P=0.000565$ and $P=0.009145$ respectively. **(C)** Densitometry of caveolin-3/Imperial protein stain shows nearly a seven fold increase in the caveolin-3 protein of *mdx* when compared to WT, there is no difference between WT caveolin-3 and DMhet, confirmed qualitatively by the western blot **(A)**. There is a statistically significant difference in caveolin-3 protein levels of *mdx* and DMhet, where $P=0.007154$; $n=4$, error bars: s.d. Asterisks' denotations ** = $P<0.01$, *** = $P<0.001$.

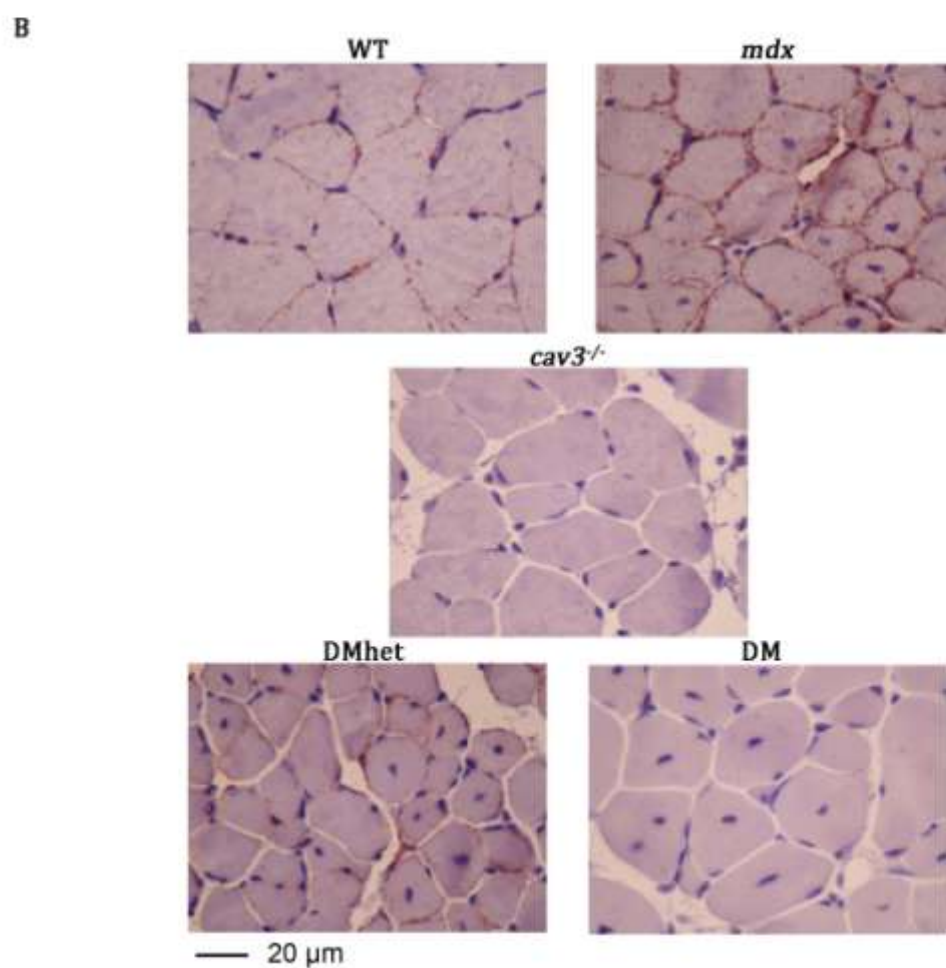
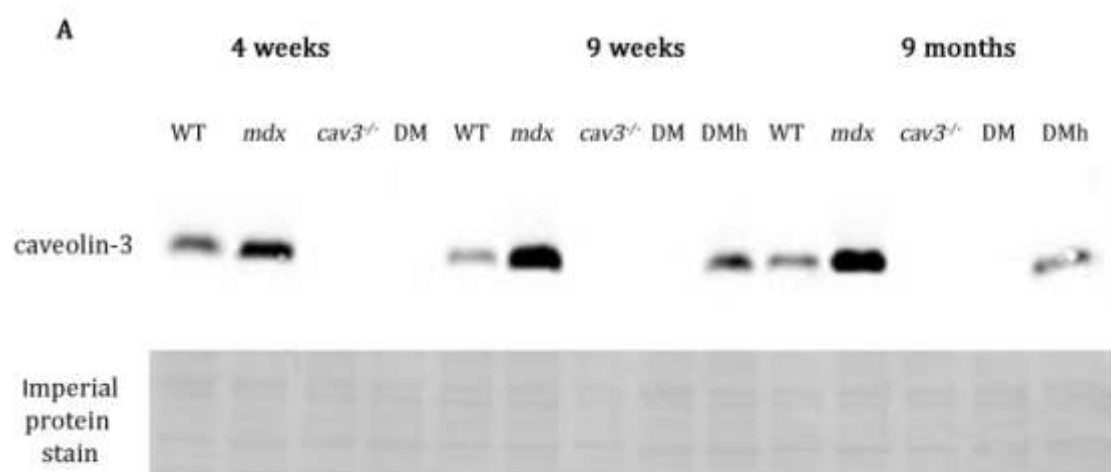


Figure 4.3

Caveolin-3 protein levels and localisation in WT, *mdx*, *cav3*^{-/-}, DMhet and DM. (A) membranes probed with anti-caveolin-3 antibodies show upregulation in *mdx* and an absence of caveolin-3 in DM and *cav3*^{-/-} at all stages; DMhets at nine weeks and nine months show levels comparable to WT but reduced when compared to *mdx*. (B) Caveolin-3 labelled paraffin wax embedded triceps muscles of nine weeks old WT, *mdx*, *cav3*^{-/-}, DMhet and DM show peripheral staining around fibres of WT, *mdx* and DMhet, the more intense staining seen in *mdx*; there is an absence of staining in both *cav3*^{-/-} and DM sections. The staining shown in the DMhet is comparable to WT but reduced when compared to *mdx*. Note the centrally located nuclei present in fibres of *mdx*, DMhet and DM muscle tissues.

4.2.2 – Macroscopic analysis of the DM

The DM mice generated display no signs of obvious pathogenesis while alive; they are indistinguishable from their WT and *mdx* counterparts, although WT animals appear to be slightly slimmer in comparison to the dystrophic mutants (**Figure 4.4 A**). There are no real differences between the live bodyweights of all four strains used although there is less variation shown between females than males (**Figure 4.5**). Their inquisitiveness and mobility around the cages is as would be expected for healthy mice and this does not appear to change as they age. In order to conduct a comparable examination of the muscularity of DM mice; WT, *mdx* and *cav3*^{-/-} specimens around nine months of age, were culled and their skins removed along with DM animals. With their skins removed, differences in the muscularity of all strains can be seen. Both *mdx* and DM display hypertrophy of all viewable skeletal muscles when compared to WT and *cav3*^{-/-}; which can be clearly seen in both the distal and proximal parts of the hindlimbs, where quadriceps, tibialis anterior, gluteal and biceps femoris display increased muscle mass (**Figure 4.4 B**). When skins of the dorsa are removed from *mdx*, *cav3*^{-/-} and DM, an excess of subcutaneous adipose tissue can be seen in *cav3*^{-/-}, particularly on the flanks and scapular regions, *mdx* and DM do not display this level of adiposity (**Figure 4.4 C**). When venters are viewed of *mdx*, *cav3*^{-/-} and DM, the increased adiposity that is seen on the back is consistent on the abdomen of *cav3*^{-/-}, *mdx* appears to be the leanest and the DM intermediate between *mdx* and *cav3*^{-/-} (**Figure 4.4 D**). The lumbodorsal fascia of *cav3*^{-/-} also appears to be thicker than that of *mdx* and DM (**Figure 4.4 C**).

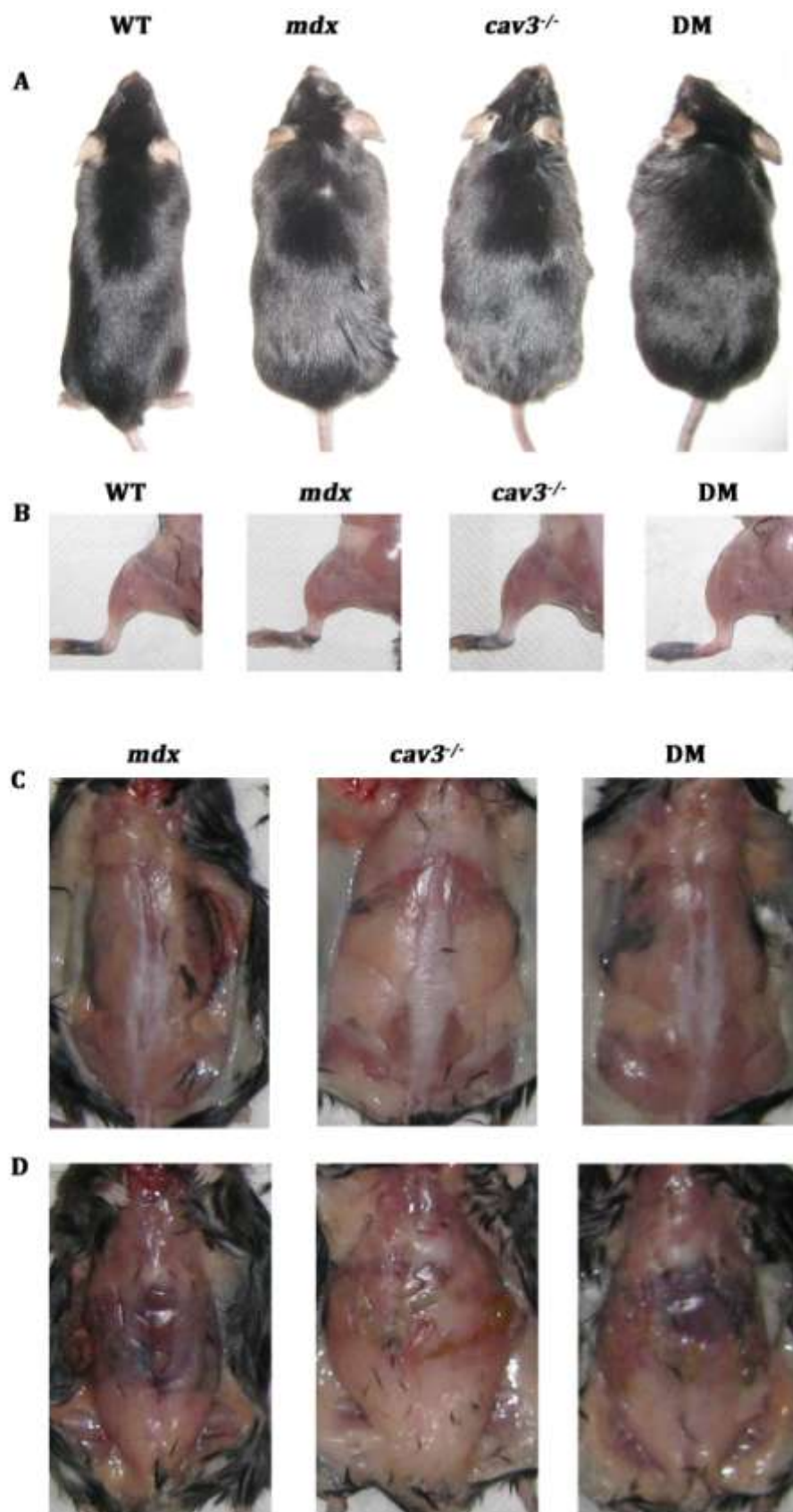


Figure 4.4

Macroscopic analysis of nine month old WT, *mdx*, *cav3*^{-/-} and DM somatotypes. (A)

All strains appear of a similar body size, the WT specimen being slightly slimmer than the others. **(B)** Dorsal view of skinned hindlimbs showing comparable muscle mass of all

strains. When compared to WT, *mdx* and particularly DM show hypertrophy of all viewable proximal and distal hindlimb muscles, including gluteal muscles. There appears to be no discernible difference between *cav3*^{-/-} and WT hindlimbs' muscle mass.

(C) Skinned *mdx*, *cav3*^{-/-} and DM dorsa showing subcutaneous adipose deposition; *cav3*^{-/-}

mutants show the highest level of subcutaneous fat, with larger depositions on the flanks and scapular regions than *mdx* and DM. The lumbodorsal fascia in *cav3*^{-/-} also

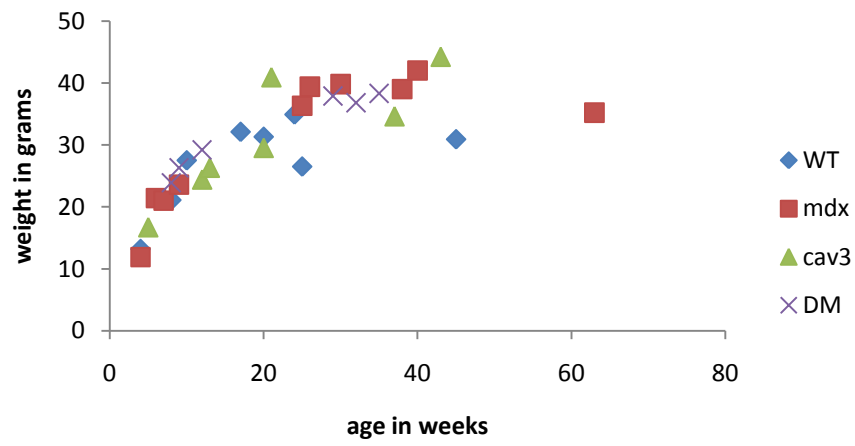
appears thicker than in *mdx* and DM. **(D)** Images of skinned venters show a greater

degree of abdominal adipose tissue present in *cav3*^{-/-}, the least in *mdx* and an intermediate degree exhibited by the DM. An excess of adipose tissue can also be seen

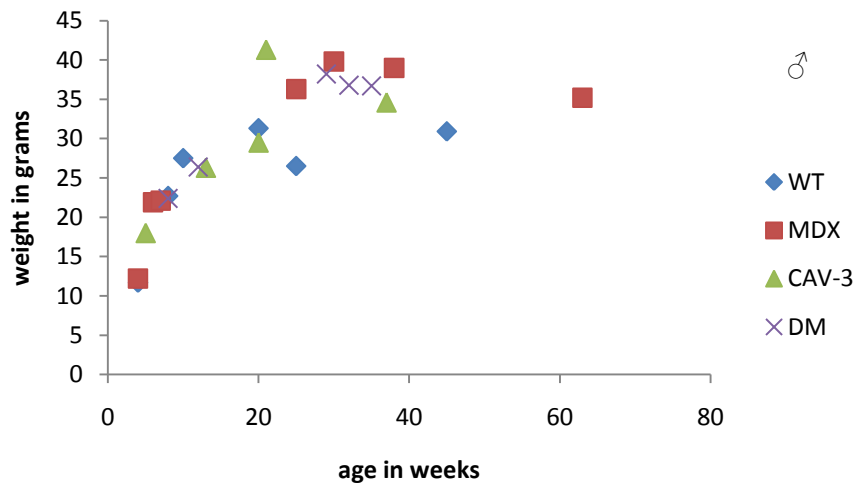
on the underside of skin lying bilaterally to the lower abdomen of *cav3*^{-/-}; with very little

present in *mdx* and once more the DM exhibiting an intermediate amount.

A



B



C

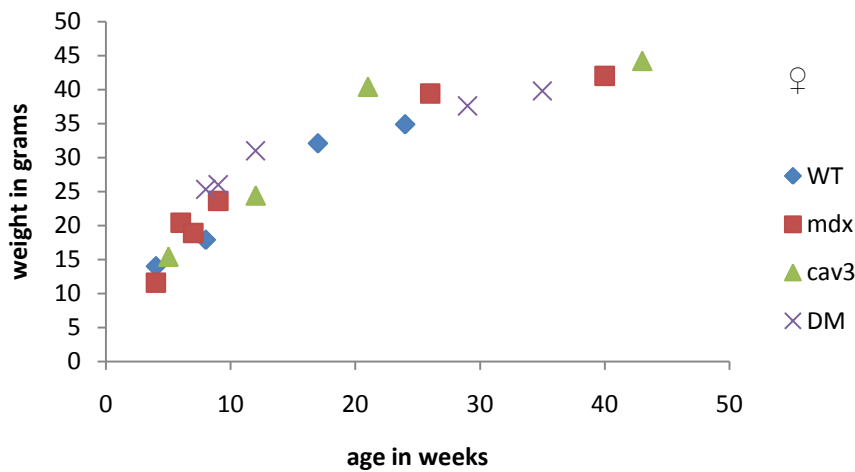


Figure 4.5

Line graphs showing live bodyweights of adult WT, *mdx*, *cav3*^{-/-} and DM colonies.

(A) Weights of both males and females were pooled resulting in a curve showing great variation in bodyweights. (B) Male bodyweights. The greatest variation of bodyweights is seen in males. (C) There is less variation seen between the bodyweights of females. The number of mice per strain used to generate data for each age group was between one and six (males and females separately).

4.2.3 - Regeneration of dystrophin-deficient proximal limb muscles

Paraffin wax embedded triceps and quadriceps muscles excised from WT, *mdx*, *cav3*^{-/-}, DM and DMhets of four weeks, nine weeks and nine months of age were cut into 5 µm sections, mounted onto slides and processed for staining using H&E. Muscle tissue stains pink and nucleic acids and therefore nuclei, stains blue/purple. Regeneration, due to the abundance of infiltrative cells associated with the process; which include myocytes, fibroblasts and monocytes, is easily identified using H&E staining as the regenerative areas exhibit extensive regions of blue/purple stained nuclei.

4.2.3.1 – Histology of four weeks triceps and quadriceps

At four weeks of age the extent of regeneration shown in *mdx* and DM, in both triceps and quadriceps is such that it is clearly observable at low magnification (**Figures 4.6 A-E; 4.7 A-C, F, G**). There are no extensive areas of regeneration, in either triceps or quadriceps, visible at low magnification in the four weeks old DMhet analysed (**Figures 4.6 F; 4.7 H**) and one of the DMs was seen to have no observable areas of regeneration in quadriceps analysed (**Figure 4.7 E**) . Analysis of triceps muscle taken from the same DM (**Figure 4.7 E**) was not possible due to the poor quality of the sections obtained.

When viewed at higher magnification (**Figures 4.8; 4.9**), areas of concentrated hypercellularity, indicative of the initial stage of muscle regeneration, can be seen in *mdx* (**Figures 4.8 E, F; 4.9 F**), DM (**Figures 4.8 L; 4.9 J, L**) and DMhet (**Figure 4.9 M, O**). Areas of regenerated muscle tissue can also be identified via the presence of centrally located myonuclei, which are shown in *mdx* (**Figures 4.8 D-F; 4.9 D, E**), DM (**Figures 4.8 J-L, O; 4.9 J-L**) and DMhet (**Figures 4.8 M, N; 4.9 N**) sections. There are no

hypercellular areas or centrally nucleated fibres shown in WT triceps or quadriceps muscle; the nuclei of WT are seen to locate to the peripheries of the muscle fibres' (**Figures 4.8 A-C; 4.9 A-C**), as do the myonuclei of *cav3*^{-/-} (**Figures 4.8 G-I; 4.9 G-I**). Of the images presented of *cav3*^{-/-}, only one fibre exhibits central myonucleation (**Figure 4.8 G**). N=4 per strain except DMhet where n=1. Images shown are of n=3, except where stated in the figure legend

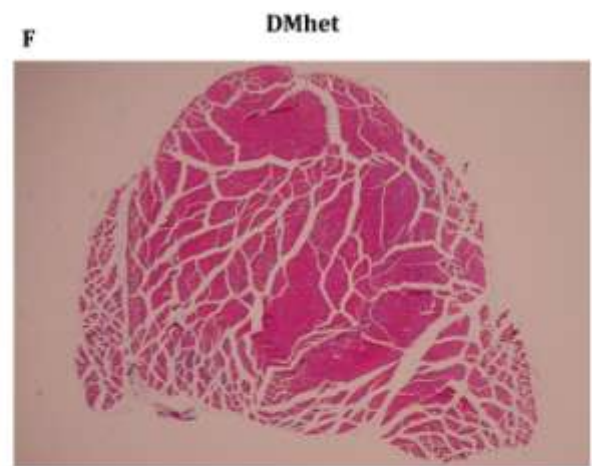
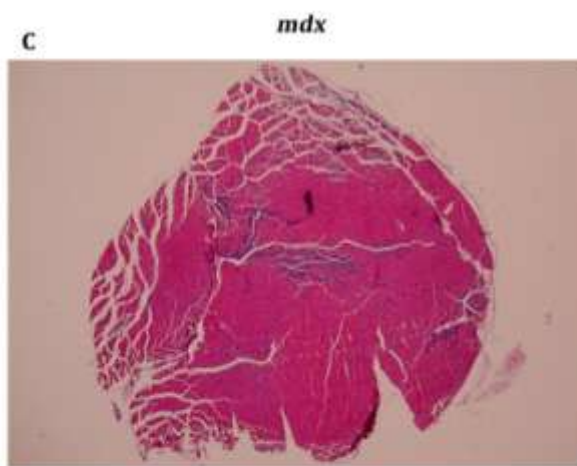
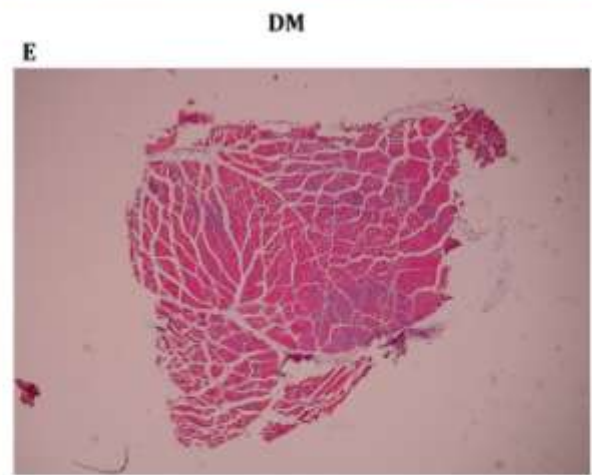
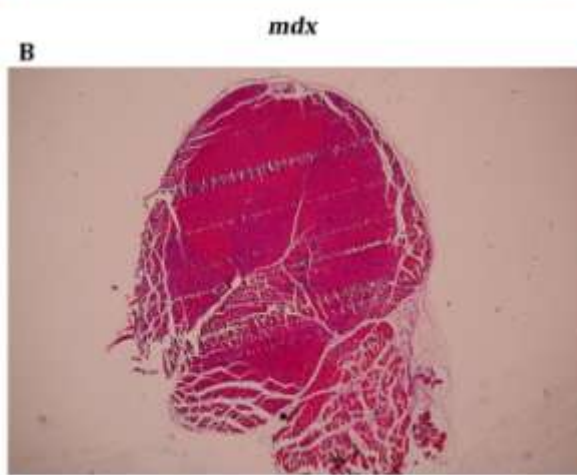
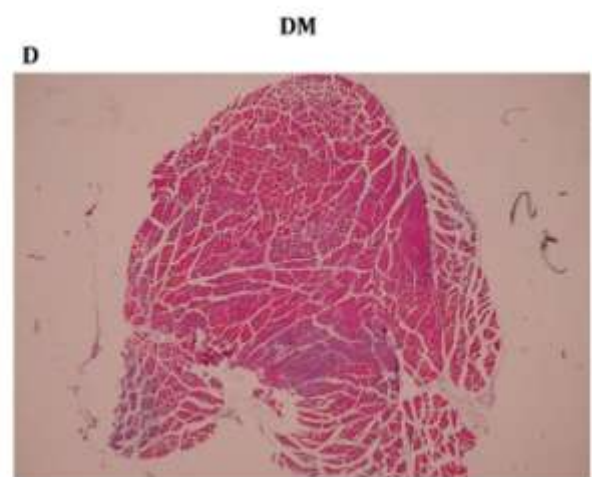
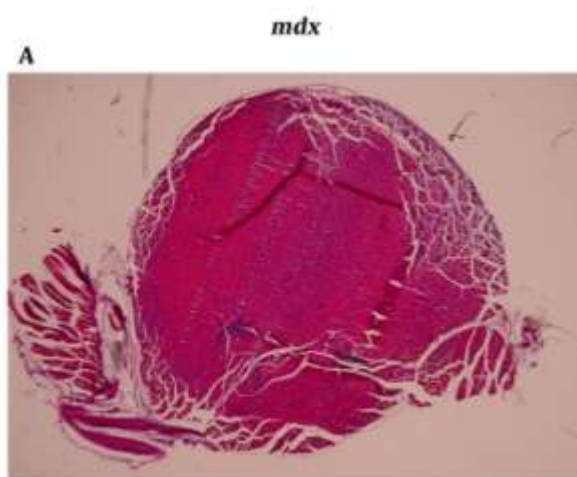


Figure 4.6

H&E stained four weeks old triceps. Transverse sections 5 μ m in thickness, were cut from paraffin wax embedded triceps muscles of four weeks old *mdx*, DM and DMhet mice and processed for H&E staining. Areas of regeneration are stained purple/blue. Gross histology shows regeneration in both *mdx* (**A-C**) and DM (**D, E**), but not in the DMhet (**F**). Images taken are of different mice. Only one DMhet was available at four weeks of age.

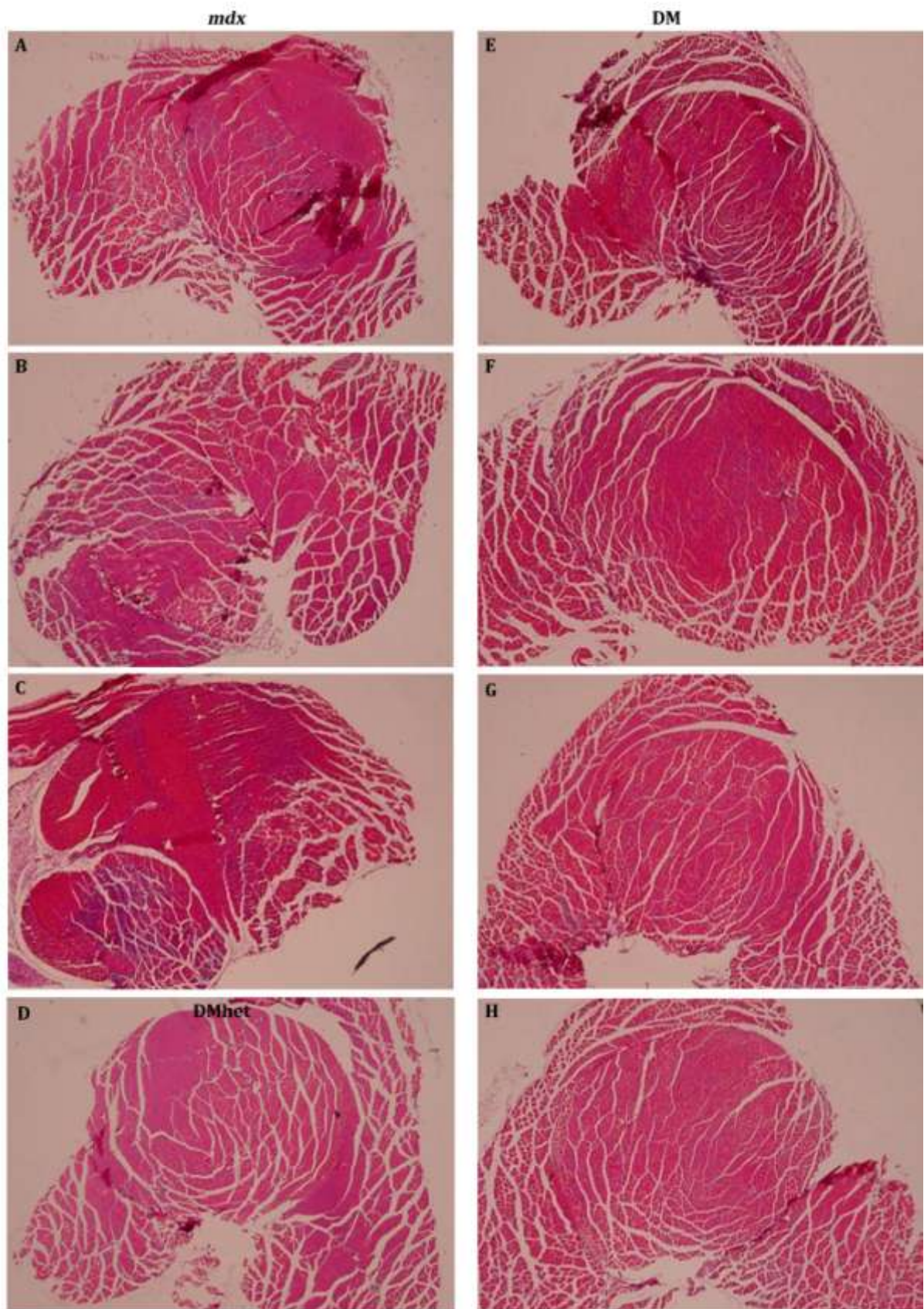


Figure 4.7

H&E stained four weeks old quadriceps. Transverse sections 5 μ m in thickness, were cut from paraffin wax embedded quadriceps muscles of four weeks old *mdx*, DM and DMhet mice and processed for H&E staining. (A-C) *mdx*; (D) DMhet; (E-H) DM. Areas of regeneration are stained purple/blue. At low magnification only *mdx* (C) shows obvious areas of regeneration, although regeneration can be seen in *mdx* (A,B) and DM (F,G). Images taken are of different mice. Only one DMhet was available at four weeks of age.

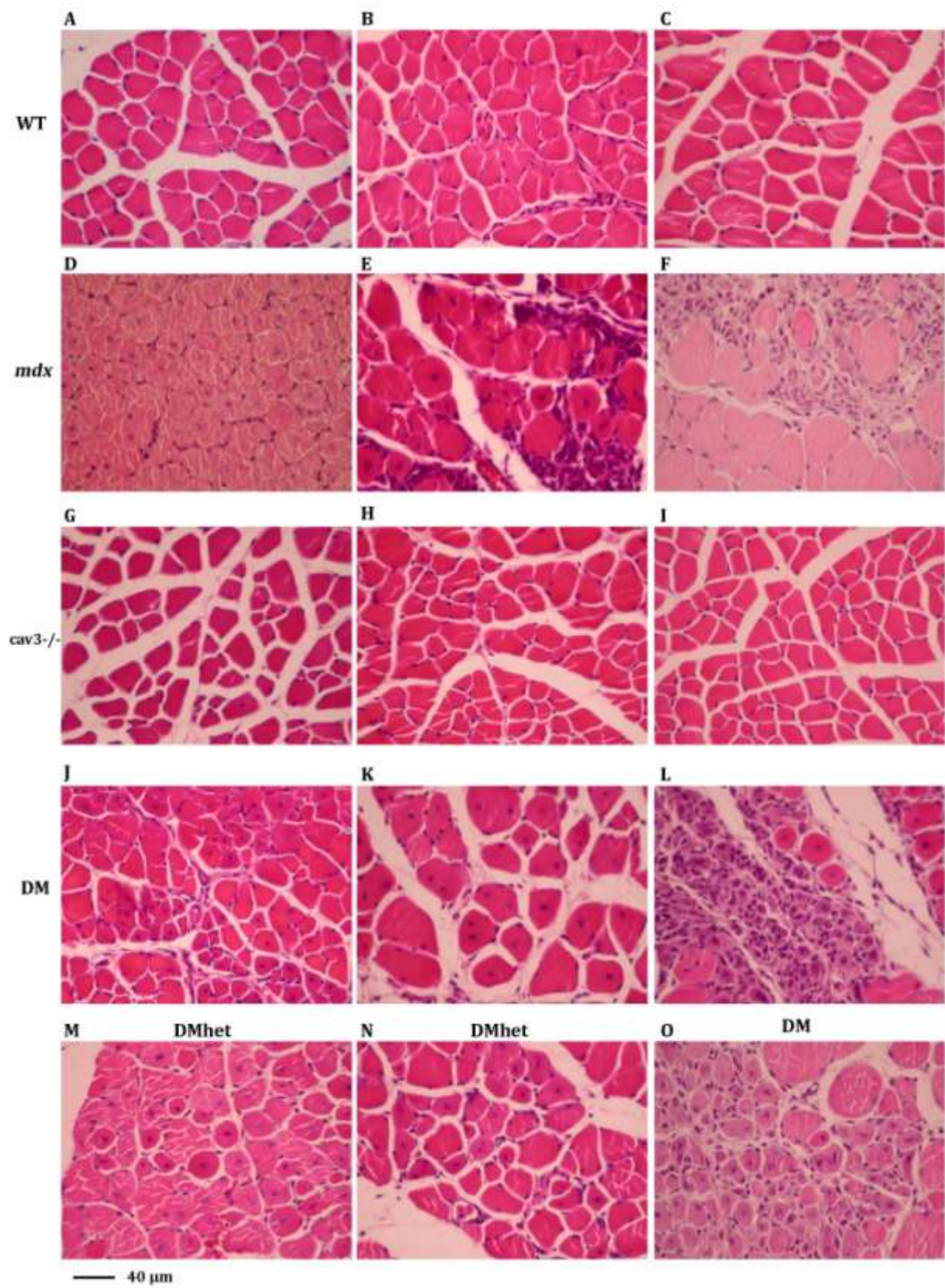


Figure 4.8

Images of four weeks old H&E stained triceps muscles. Transverse sections 5 μm in thickness, were cut from paraffin wax embedded triceps muscles of four weeks old WT, *mdx*, *cav3*^{-/-}, DM and DMhet mice and processed for H&E staining. **(A-C)** WT fibres are of a uniform size with myonuclei positioned at the fibres' peripheries; *cav3*^{-/-} fibres appear morphologically identical to those of WT **(G-I)**. Centrally located myonuclei and heterogeneity of fibre sizes are shown in *mdx* **(D-F)**, DM **(J-L, O)** and DMhet **(M, N)**. Areas of regeneration (characterised by hypercellularity) are evident in *mdx* **(E, F)** and DM **(L, O)**. All images shown are of three different mice per strain, except for DMhet where only one was available. Scale bar = 40 μm .

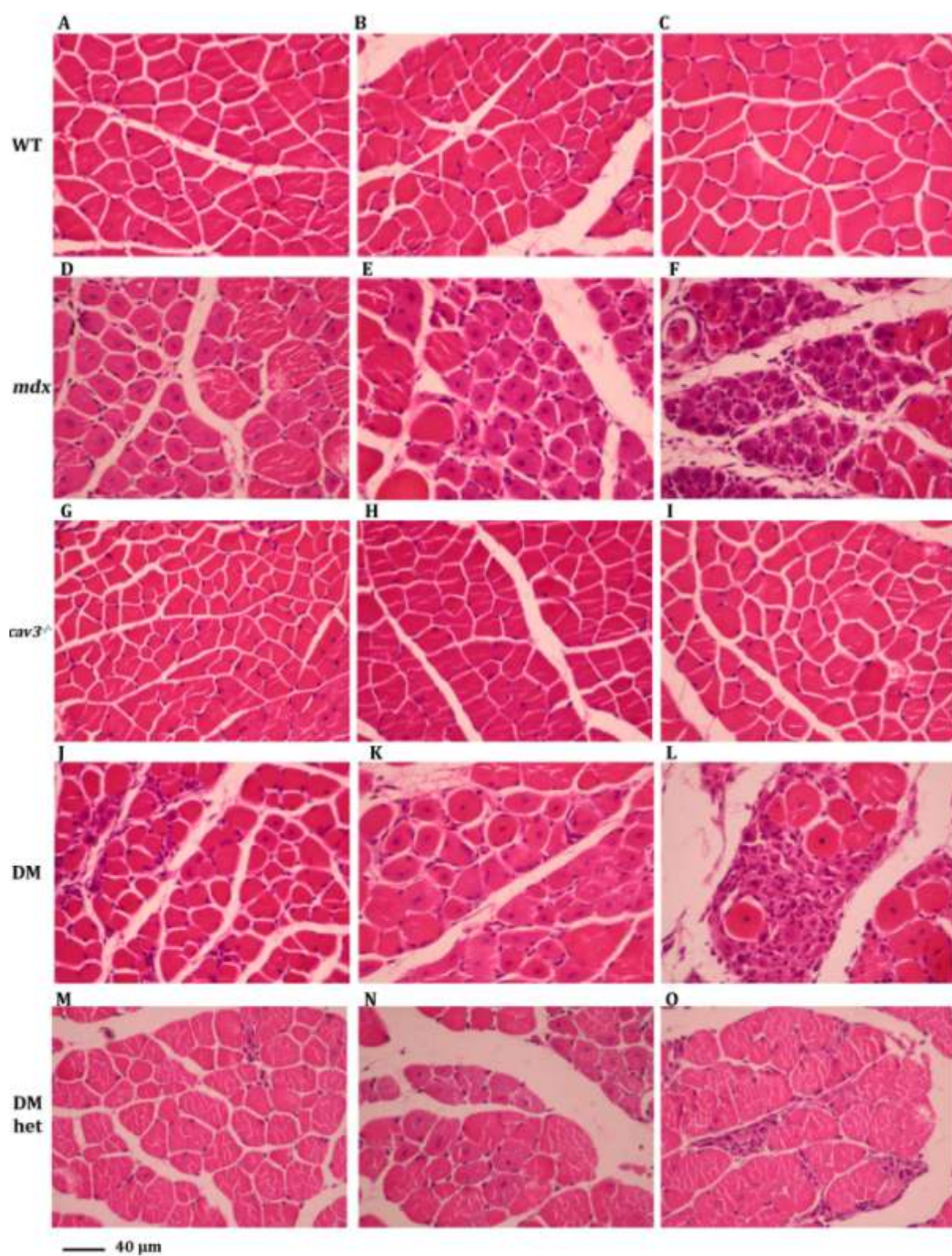


Figure 4.9

Images of four weeks old H&E stained quadriceps muscles. 5 µm thick transverse sections were cut from paraffin wax embedded quadriceps muscles of four weeks old WT, *mdx*, *cav3*^{-/-}, DM and DMhet mice and processed for H&E staining. **(A-C)** WT fibres are of a uniform size with myonuclei positioned at the fibres' peripheries; *cav3*^{-/-} fibres appear morphologically identical to those of WT **(G-I)**. Centrally located myonuclei are shown in *mdx* **(D, E)**, DM **(J-L)** and DMhet **(N)**. Areas of regeneration (characterised by hypercellularity) are evident in *mdx* **(E, F)**, DM **(J, L)** and DMhet **(O)**. All images shown are of three different mice per strain, except for DMhet where only one was available. Scale bar = 40 µm.

4.2.3.2 – Histology of nine weeks triceps and quadriceps

At nine weeks of age areas of regeneration in triceps and quadriceps of *mdx* (**Figures 4.10 A-C; 4.11 A-C**), DM (**Figures 4.10 D-F; 4.11 D-F**) and DMhets (**Figures 4.10 G, H; 4.11 G, H**) can be seen in images taken at low magnification. There does not appear to be any discernible differences at nine weeks when compared to triceps and quadriceps of *mdx*, DM and DMhet at four weeks of age (**Figures 4.6; 4.7**); neither is there any obvious observable differences in the level of regeneration between the three dystrophin-deficient mutants.

Higher magnification images show areas of hypercellularity and many centrally located nuclei in triceps and quadriceps of *mdx* (**Figures 4.12 D-F; 4.13 D-F**), DM (**Figures 4.12 J-L; 4.13 I-K**) and DMhets (**Figures 4.12 M-O; 4.13 L, M**), neither of which are present in the same muscles of WT (**Figures 4.12 A-C; 4.13 A-C**) or *cav3*^{-/-} (**Figures 4.12 G-I; 4.13 G, H**) at nine weeks of age.

Many of the muscle fibres seen in DM and DMhet triceps and quadriceps are of a rounded morphology, in contrast to the fibres of WT and *cav3*^{-/-} muscle, which have a more angular morphology (**Figures 4.12 A-C, G-I; 4.13 A-C, G, H**). This phenotype is also shown in *mdx* (**Figures 4.12 D-F; 4.13 D-F**). Fibres of *mdx*, DM and DMhets also exhibit heterogeneity within their fibre sizes, with hypertrophic fibres juxtaposed next to very small fibres; the nuclei of which may or may not be centrally located (**Figure 4.12 D, J, M**). Fibres of WT and *cav3*^{-/-} appear to be of a more uniform size, although *cav3*^{-/-} fibres are seen to be less dense than those of WT. N=3 per strain, except for DMhet where n=2. Images shown are of n=3, except where stated in the figure legend.

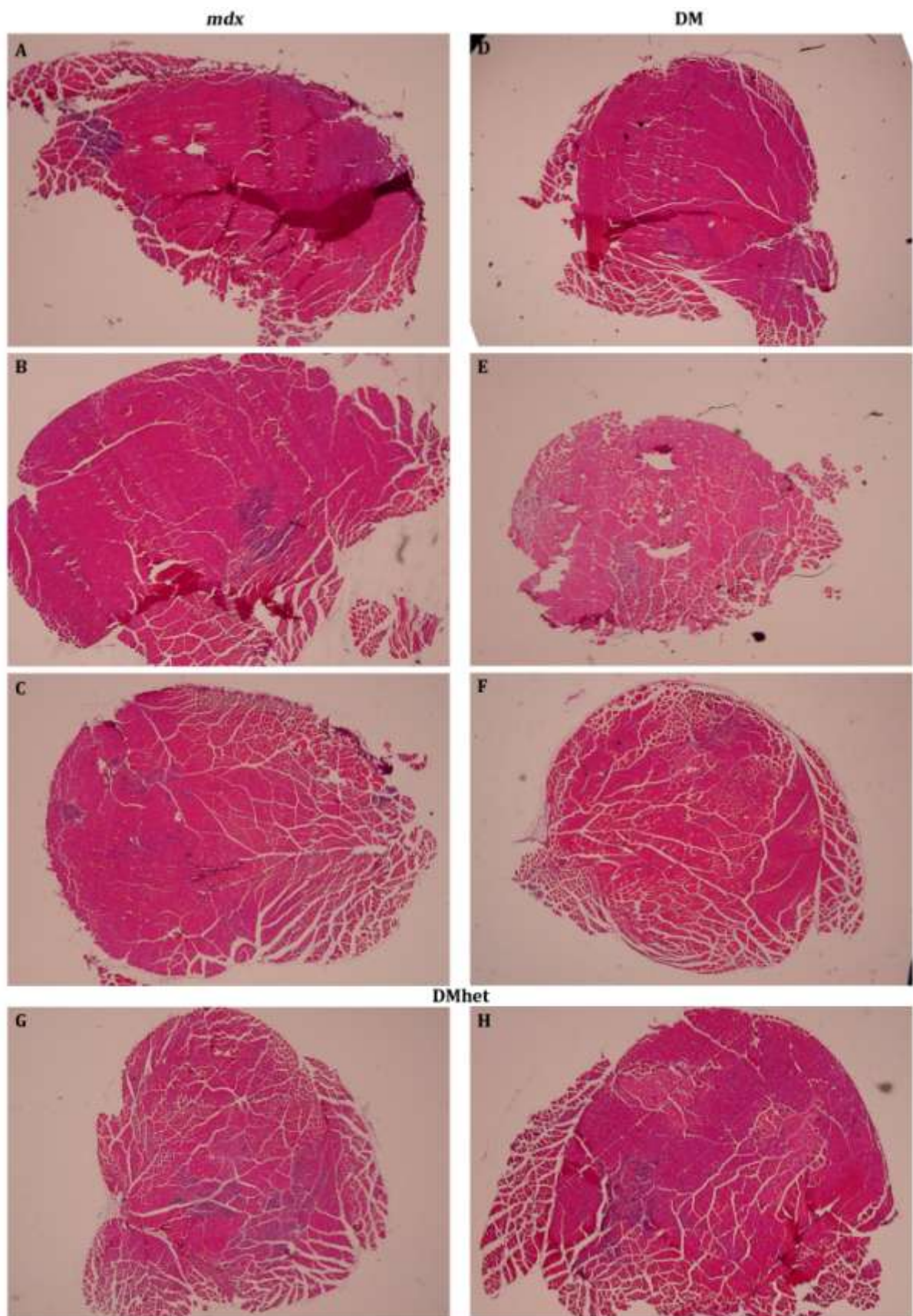


Figure 4.10

H&E stained nine weeks old triceps. Transverse sections 5 μm in thickness, were cut from paraffin wax embedded triceps muscles of nine weeks old *mdx*, DM and DMhet mice and processed for H&E staining. Areas of regeneration are stained purple/blue. Gross histology shows regenerative areas in *mdx* (**A-C**), DM (**D-F**) and DMhet (**G, H**). Images taken are of different mice.

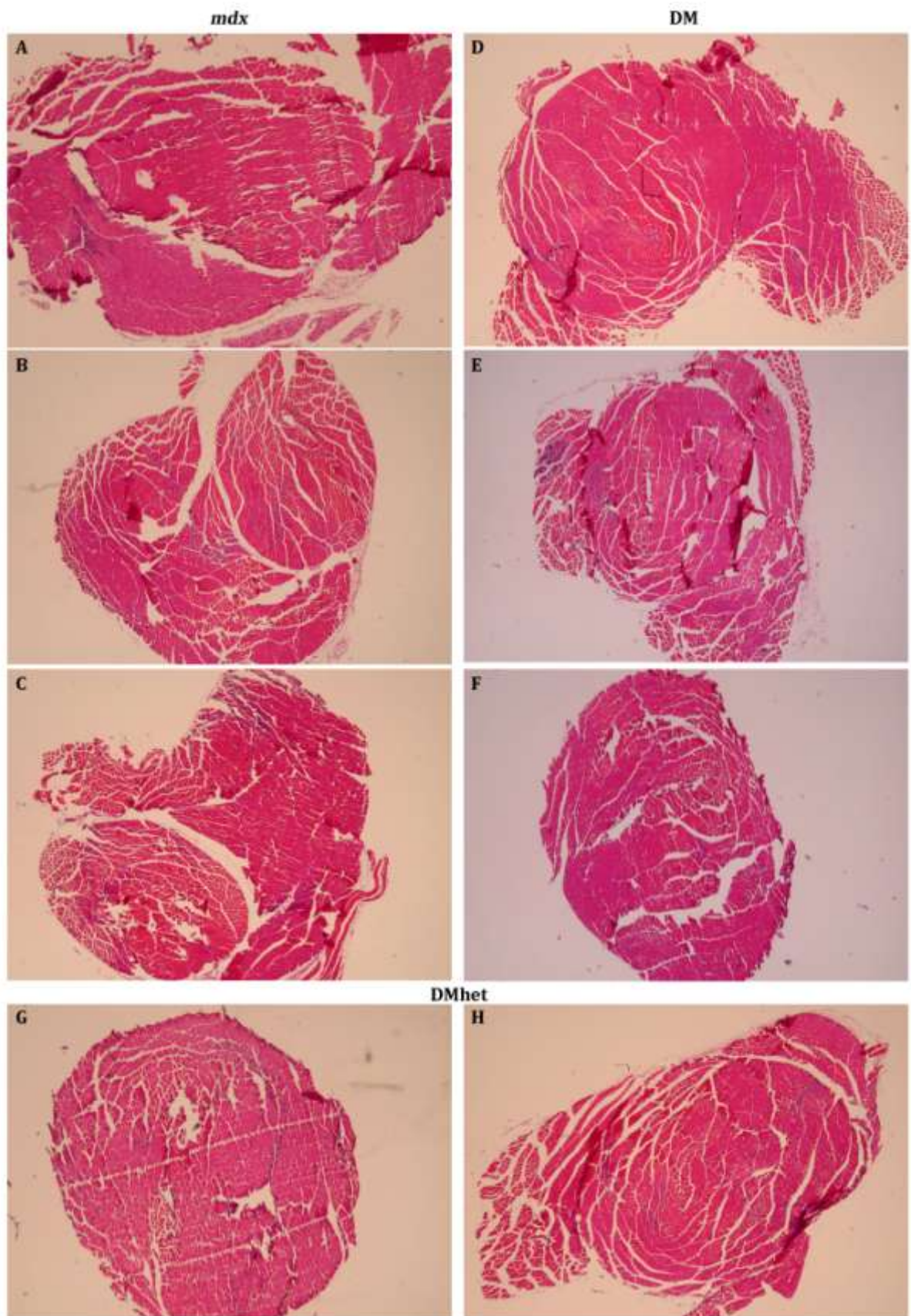


Figure 4.11

H&E stained nine weeks old quadriceps. Transverse sections 5 μ m in thickness, were cut from paraffin wax embedded quadriceps muscles of nine weeks old *mdx*, DM and DMhet mice and processed for H&E staining. Areas of regeneration are stained purple/blue. Gross histology shows regeneration in all mutants; *mdx* (**A-C**), DM (**D-F**) and DMhet (**G, H**). Images taken are of different mice.

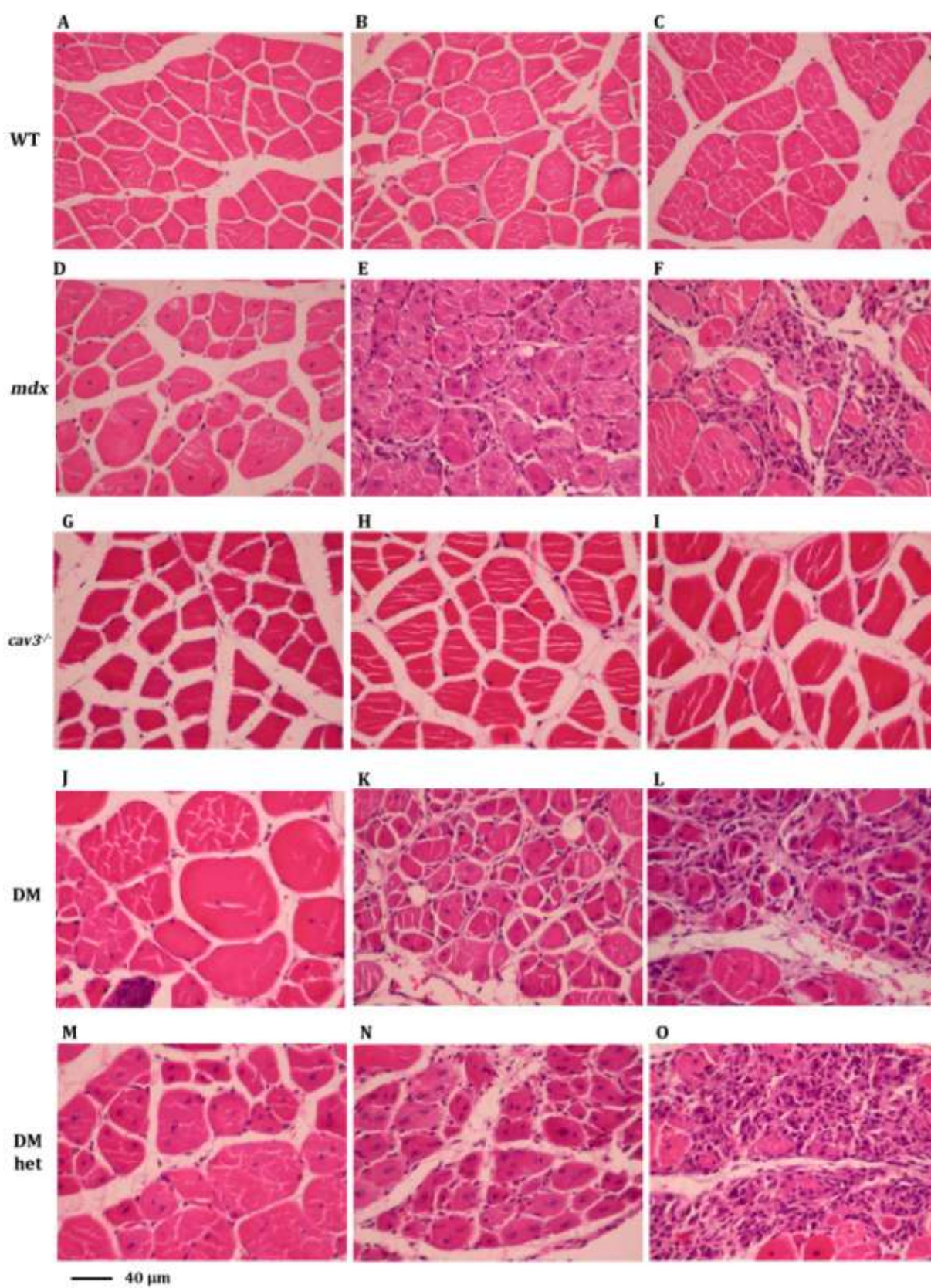


Figure 4.12

Images of nine weeks old H&E stained triceps. 5 μ m thick transverse sections were cut from paraffin wax embedded triceps muscles of nine weeks old WT, *mdx*, *cav3*^{-/-}, DM and DMhet mice and processed for H&E staining. WT fibres are of a uniform size with myonuclei positioned at the fibres' peripheries (**A-C**). The fibres of *cav3*^{-/-} muscle although uniform in size as in WT, appear less dense than those of WT (**G-I**). Centrally located myonuclei and heterogeneity of fibre sizes are shown in *mdx* (**D-F**), DM (**J-L**) and DMhet (**M-O**). Areas of regeneration (characterised by hypercellularity) are evident in *mdx* (**E, F**), DM (**K, L**) and DMhet (**M-O**). Images taken of two different WT and DMhets and three different *mdx*, *cav3*^{-/-} and DM. Scale bar = 40 μ m.

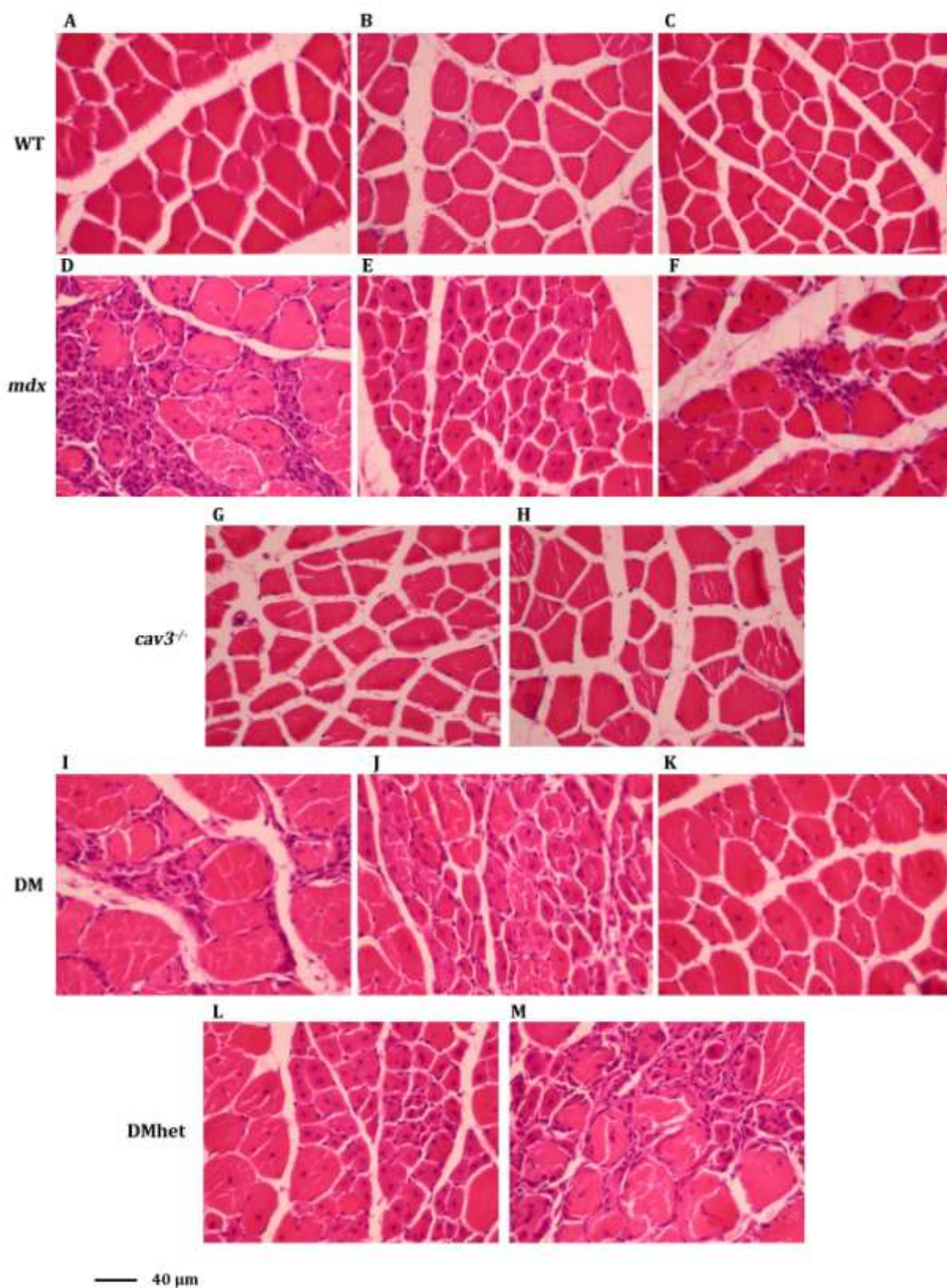


Figure 4.13

Images of nine weeks old H&E stained quadriceps. 5 µm thick transverse sections were cut from paraffin wax embedded quadriceps muscles of nine weeks old WT, *mdx*, *cav3*^{-/-}, DM and DMhet mice and processed for H&E staining. **(A-C)** WT fibres are of a uniform size with myonuclei positioned at the fibres' peripheries; *cav3*^{-/-} fibres appear morphologically identical to those of WT, with no signs of any pathogenesis **(G, H)**. Centrally located myonuclei are shown in *mdx* **(D-F)**, DM **(J, K)** and DMhet **(L, M)**. Areas of regeneration (characterised by hypercellularity) are evident in *mdx* **(D, F)**, DM **(I)** and DMhet **(L, M)**. Variations in fibre sizes can be seen in *mdx* **(D)**, DM **(I, J)** and DMhet **(L, M)**. Images were taken from three WT, three *mdx*, two *cav3*^{-/-}, three DM and one DMhet. Scale bar = 40 µm.

4.2.3.3 – Histology of nine months triceps and quadriceps

Triceps muscles at nine months of age show no regenerative areas that can be seen at low magnification in any of the dystrophin-deficient mutants, WT or *cav3*^{-/-} sections (**Figure 4.14**). In muscles of the quadriceps, small areas of hypercellularity can be seen in a single *mdx* (**Figure 4.15 B**) and a single DM section (**Figure 4.15 D**). There were no *mdx* sections of sufficient quality to photograph.

Images that were taken at higher magnification show that there are regenerative areas present in *mdx* (**Figure 4.17 C**), DM (**Figure 4.17 F**) and DMhet (**Figure 4.16 F**) sections. Many of the fibres of *mdx* (**Figure 4.17 B, D**), DM (**Figures 4.16 E, F; 4.17 F-H**) and DMhets (**Figures 4.16 G, H; 4.17 I-K**) at this age have centrally located nuclei and are hypertrophic, although there is an observable heterogeneity of fibre sizes in all of the dystrophin-deficient mutants (**Figures 4.16 E-H; 4.17 B-D, F-K**). WT and *cav3*^{-/-} fibres are shown to be of a uniform size (**Figures 4.16 A, C, D; 4.17 A, E**). In both triceps and quadriceps of DMhet sections there are clusters of non-muscle cells that may be adipocytes (**Figures 4.16 F; 4.17 J**), but as appropriate labelling was not performed to ascertain the identity of the cells, this is purely speculative. A smaller number of what appears to be the same cell type can be seen in a DM section image (**Figure 4.16 E**). N=1 WT, n=2 *cav3*^{-/-}, n=3 *mdx*, DM, DMhet.

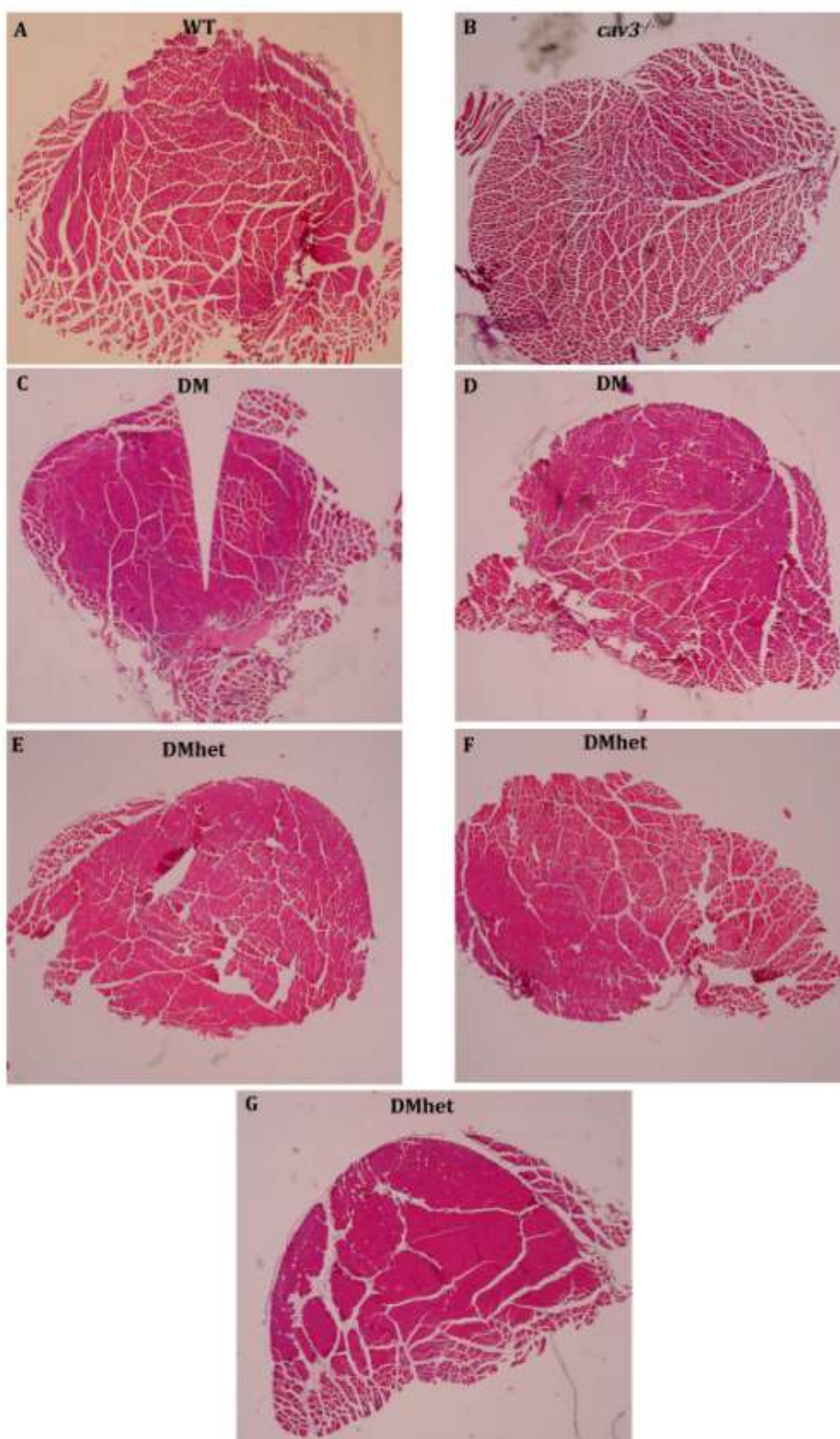


Figure 4.14

H&E stained nine months old triceps. 5 µm thick transverse sections were cut from paraffin wax embedded triceps muscles of nine months old WT, *mdx*, *cav3*^{-/-}, DM and DMhet mice and processed for H&E staining. At this low magnification there appears to be no obvious signs of pathogenesis in any of the dystrophic mutants. Images taken are of different mice.

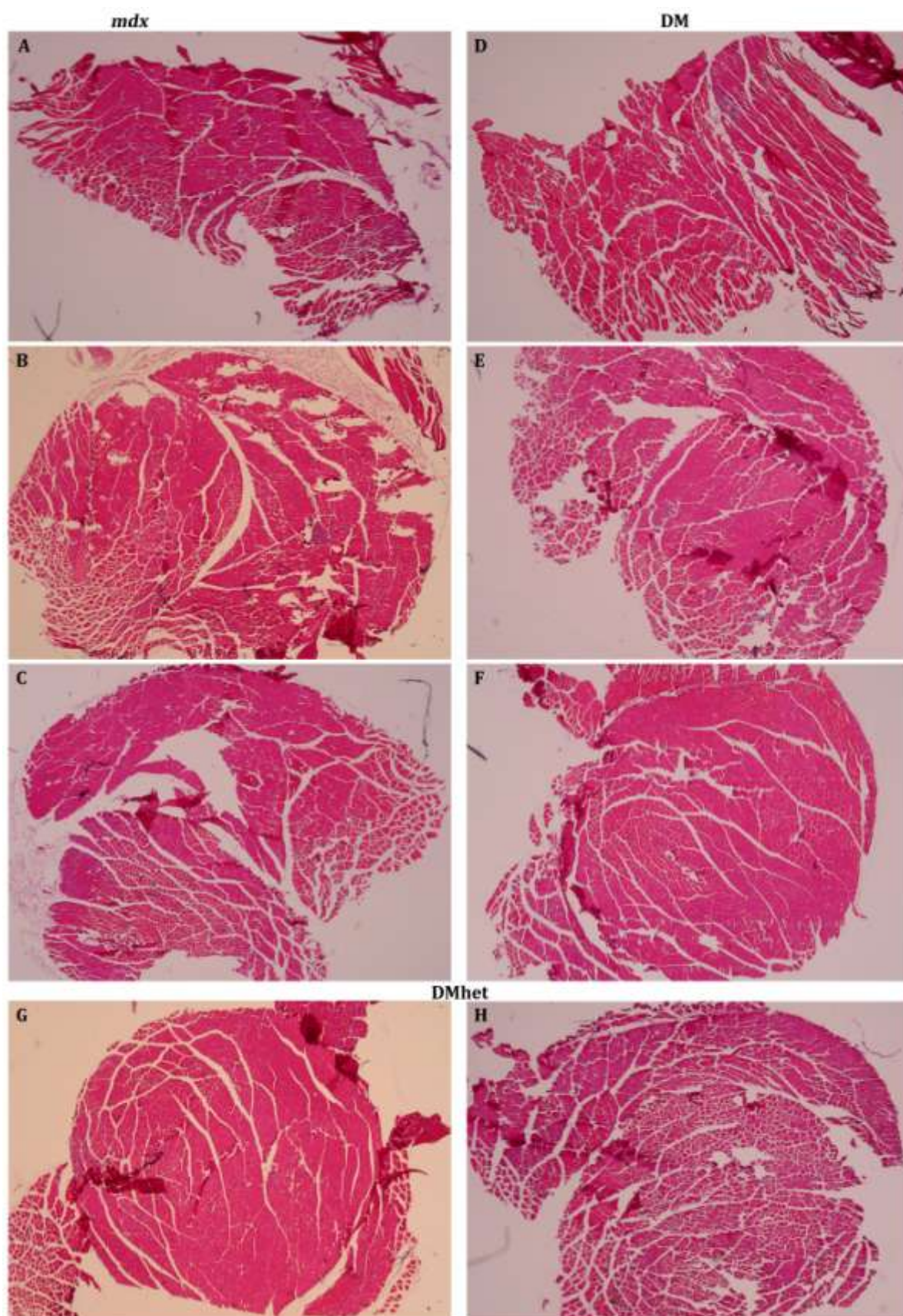


Figure 4.15

H&E stained nine months old quadriceps muscles. Transverse sections 5 μm in thickness, were cut from paraffin wax embedded quadriceps muscles of nine months old *mdx*, DM and DMhet mice and processed for H&E staining. Areas of regeneration are stained purple/blue. There appears to be small regenerative areas in *mdx* (**B**) and DM (**D**). Images taken are of different mice.

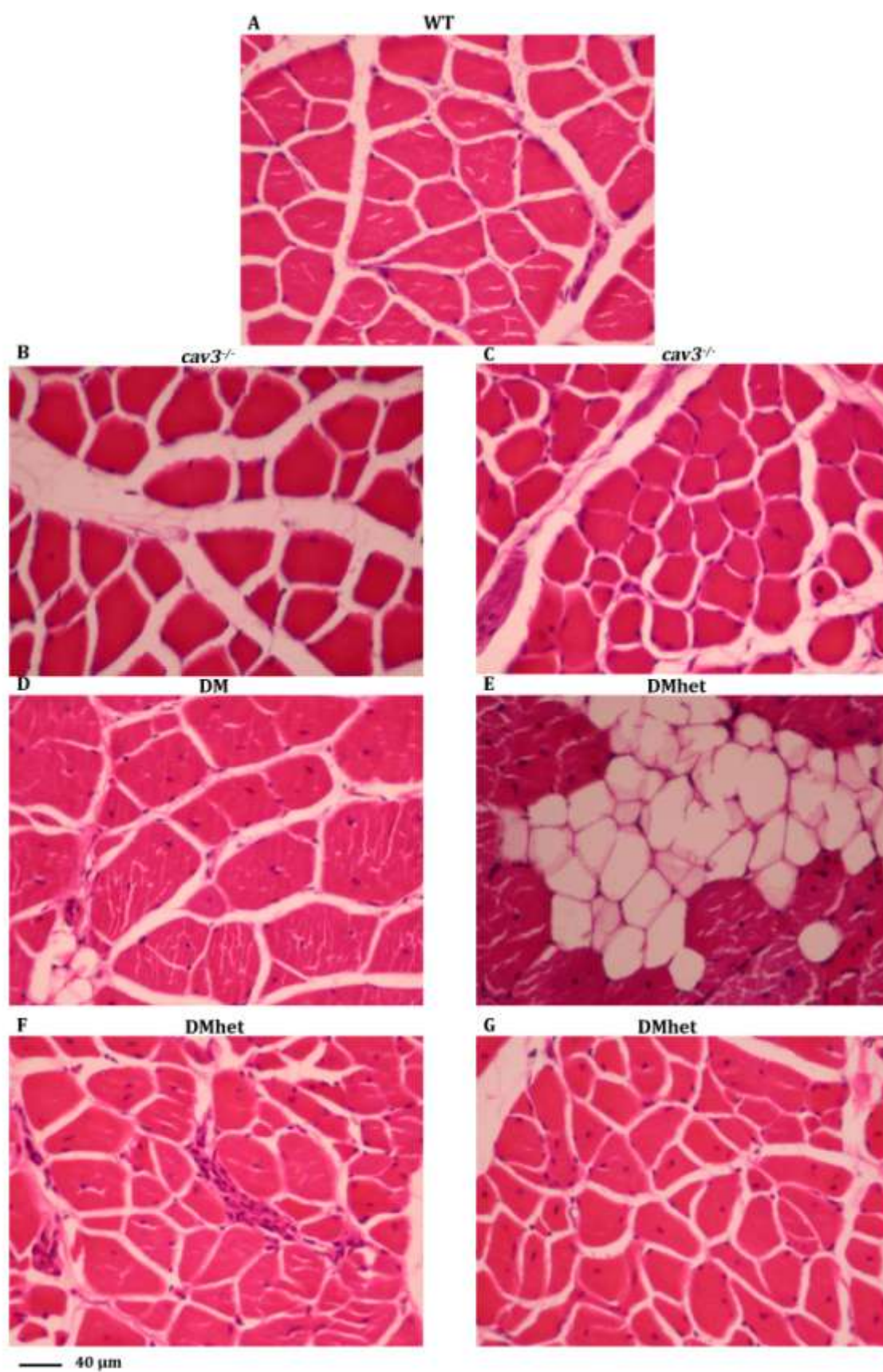


Figure 4.16

Images of nine months old H&E stained triceps. 5 μ m thick transverse sections were cut from paraffin wax embedded triceps muscles of nine months old WT, *cav3*^{-/-}, DM and DMhet mice and processed for H&E staining. WT fibres are of a uniform size with myonuclei positioned at the fibres' peripheries (**A**); there is no discernible difference seen in *cav3*^{-/-} when compared to WT, although there are a couple of centrally located myonuclei shown in the images presented (**B,C**). Hypertrophic fibres when compared to WT are seen in DM and these fibres display centrally located myonuclei (**D**) as do DMhet fibres (**E-G**). Areas of regeneration (characterised by hypercellularity) are evident only in DMhet (**F**). Non muscle cells can be seen in DM (**D**) and in particular DMhet (**E**), these cells may be adipocytes, not usually present in muscles of the limbs of *mdx*. Images were taken from one WT, one *cav3*^{-/-}, one DM and two DMhets. Scale bar = 40 μ m.

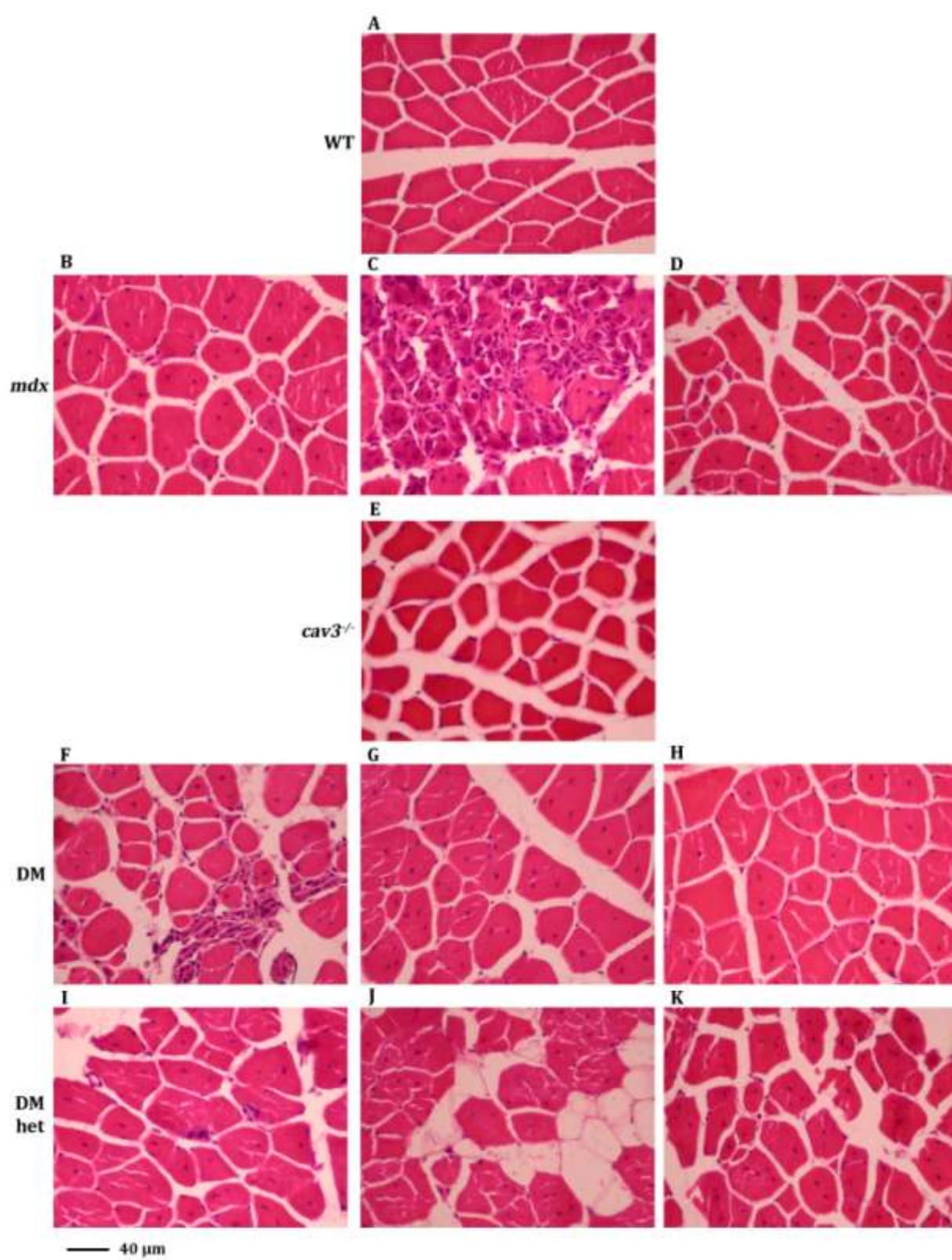


Figure 4.17

Images of nine months old H&E stained quadriceps. Transverse sections 5 μm in thickness were cut from paraffin wax embedded quadriceps muscles of nine months old WT, *mdx*, *cav3*^{-/-}, DM and DMhet mice and processed for H&E staining. WT fibres are of a uniform size with myonuclei peripherally positioned within the fibres' (**A**). There appears to be no histopathology in *cav3*^{-/-} tissue, however there does appear to be a greater degree of interstitium between *cav3*^{-/-} fibres (**E**) when compared to those of WT (**A**). Centrally located myonuclei are shown in *mdx* (**B, D**), DM (**F-H**) and DMhet (**I-K**). Areas of regeneration (characterised by hypercellularity) are evident in *mdx* (**C**) and DM (**F**), but not in DMhet (**I-K**). Variations in fibre sizes can be seen in *mdx* (**B, D**), DM (**F, G**) and DMhet (**K**). There are also non muscle cells shown in DMhet (**J**), which may be adipocytes. Images were taken from one WT, two *mdx*, one *cav3*^{-/-}, two DMs and three DMhets. Scale bar = 40 μm .

4.2.4 - Respiratory muscles

4.2.4.1 - intercostals

Sections of thoracic cages were excised from WT, mice at four weeks, nine weeks and nine months of age and embedded in paraffin wax. Sections 5 µm thick were cut, mounted and processed for staining with H&E.

When seen at low magnification, there appears to be no discernible differences in any of the strains at four weeks (**Figure 4.18 A1-E1**), nine weeks (**Figure 4.18 F1-J1**) or nine months of age (**Figure 4.18 K1-O1**) and as the quality of the sections shown varies, accurate analyses of these data is difficult. However, there are no obvious signs of pathogenesis seen in any of the dystrophic mutants, i.e. *mdx* (**Figure 4.18 B1, G1, L1**), *cav3^{-/-}* (**Figure 4.18 C1, H1, M1**), DM (**Figure 4.18 D1, I1, N1**) or DMhet (**Figure 4.18 E1, J1, O1**) when compared to WT images of the same ages (**Figure 4.18 F1, K1**).

At higher magnification (**Figure 4.18 A2-E2, F2-J2, K2-O2**), areas undergoing regeneration are shown in *mdx* (**Figure 4.18 B2**) and DMhet (**Figure 4.18 E2**) at four weeks of age; *mdx* (**Figure 4.18 G2**), DM (**Figure 4.18 I2**) and DMhet (**Figure 4.18 J2**) at nine weeks of age and DM only (**Figure 4.18 N2**) at nine months of age. Centrally located myonuclei can be seen in a few fibres of *mdx* (**Figure 4.18 B2**), DM (**Figure 4.18 D2**) and DMhet (**Figure 4.18 E2**) at four weeks, but as centrally nucleated fibres are also present in WT of the same age (**Figure 4.18 A2**), this phenotype cannot be attributed to their dystrophic condition. There are many more centrally located myonuclei seen at nine weeks of age in *mdx* (**Figure 4.18 G2**), DM (**Figure 4.18 I2**) and DMhet (**Figure 4.18 J2**) and at nine months of age in *mdx* (**Figure 4.18 L2**) and DMhet (**Figure 4.18**

02), but as they are more numerous than that which was shown at four weeks of age, are indicative of regenerated fibres

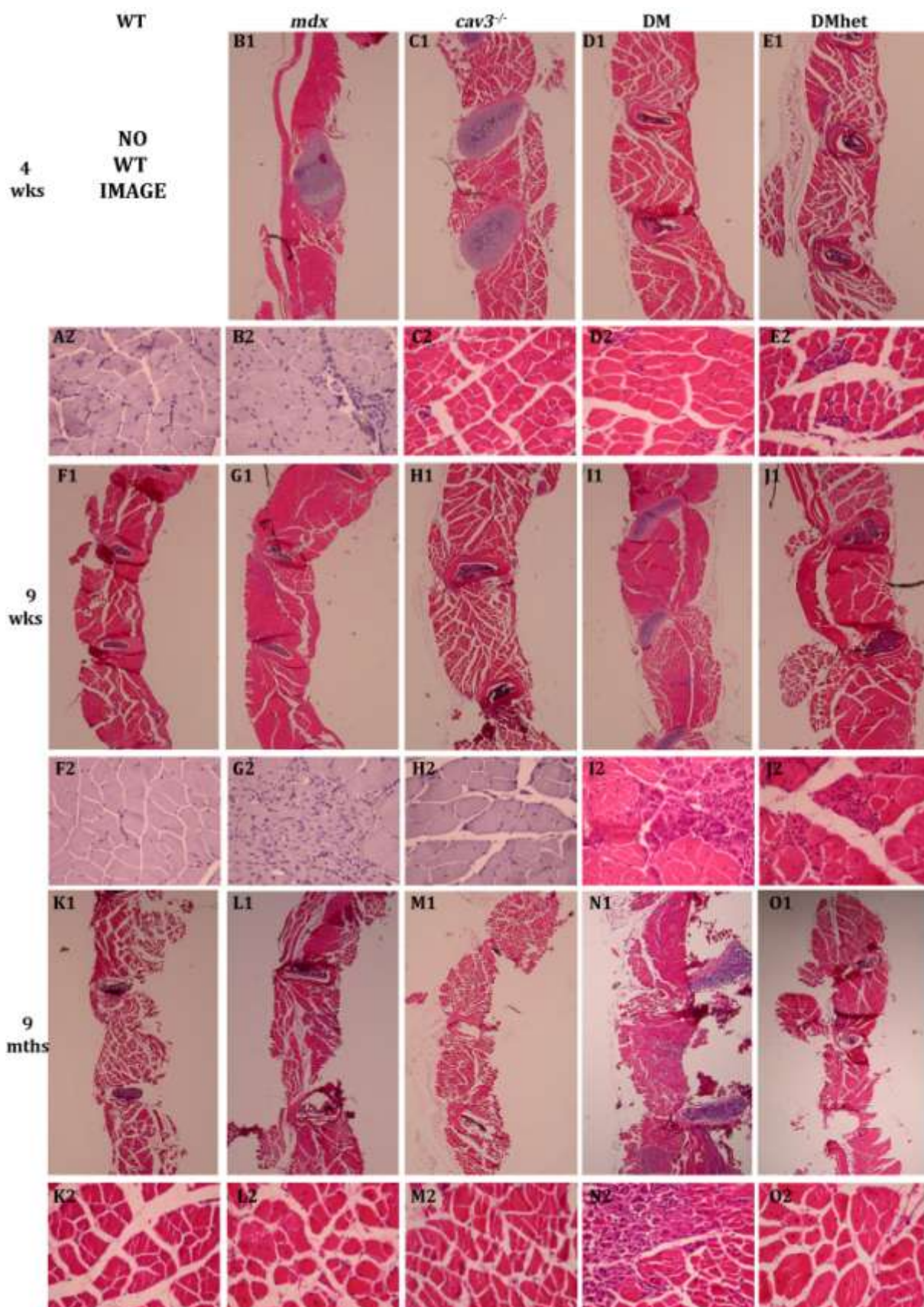


Figure 4.18

H&E stained intercostal muscles. 5 μ m thick sections of paraffin wax embedded thoracic cages from four weeks, nine weeks and nine months old WT, *mdx*, *cav3^{-/-}*, DM and DMhet were processed for H&E staining. At low magnification there appears to be no discernible differences in any of the strains at four weeks (**B1-E1**), nine weeks (**F1-J1**) or nine months of age (**K1-O1**). Higher magnification images show areas undergoing regeneration (areas of hypercellularity) in *mdx* (**B2**) and DMhet (**E2**) at four weeks of age; *mdx* (**G2**), DM (**I2**) and DMhet (**J2**) at nine weeks of age and DM (**N2**) at nine months of age. Central nucleation of fibres can be seen in very few fibres at four weeks in *mdx* (**B2**), DM (**D2**) and DMhet (**E2**); there are also a couple of centrally nucleated WT fibres shown at four weeks of age (**A2**). There are many more centrally located myonuclei seen at nine weeks in *mdx* (**G2**), DM (**I2**) and DMhet (**J2**); and at nine months of age in *mdx* (**L2**) and DMhet (**O2**) images.

4.2.4.2 - Diaphragm

Diaphragm muscles were removed from WT, *mdx*, *cav3*^{-/-}, DM and DMhet mice at four weeks and nine weeks of age and embedded in paraffin wax. 5 µm thick sections were cut, mounted and then processed for staining with H&E.

Areas of regeneration are shown in *mdx* (**Figure 4.19 B**), DM (**Figure 4.19 D**) and DMhet (**Figure 4.19 E**) at four weeks of age; *cav3*^{-/-} (**Figure 4.19 C**) diaphragm appears as WT (**Figure 4.19 A**) at the same age. At nine weeks of age hypercellularity is shown in *mdx* (**Figure 4.19 I**) and DMhet (**Figure 4.19 L, M**) diaphragm muscles, although the cells seen in DMhet muscle are spread evenly throughout the muscle fibres' interstitium rather than aggregated as in *mdx*. Most of the fibres shown in DMhet have centrally located myonuclei. The most severe diaphragmatic pathogenesis is shown in the DM where adipocytes appear to be seen within the section (**Figure 4.19 K**).

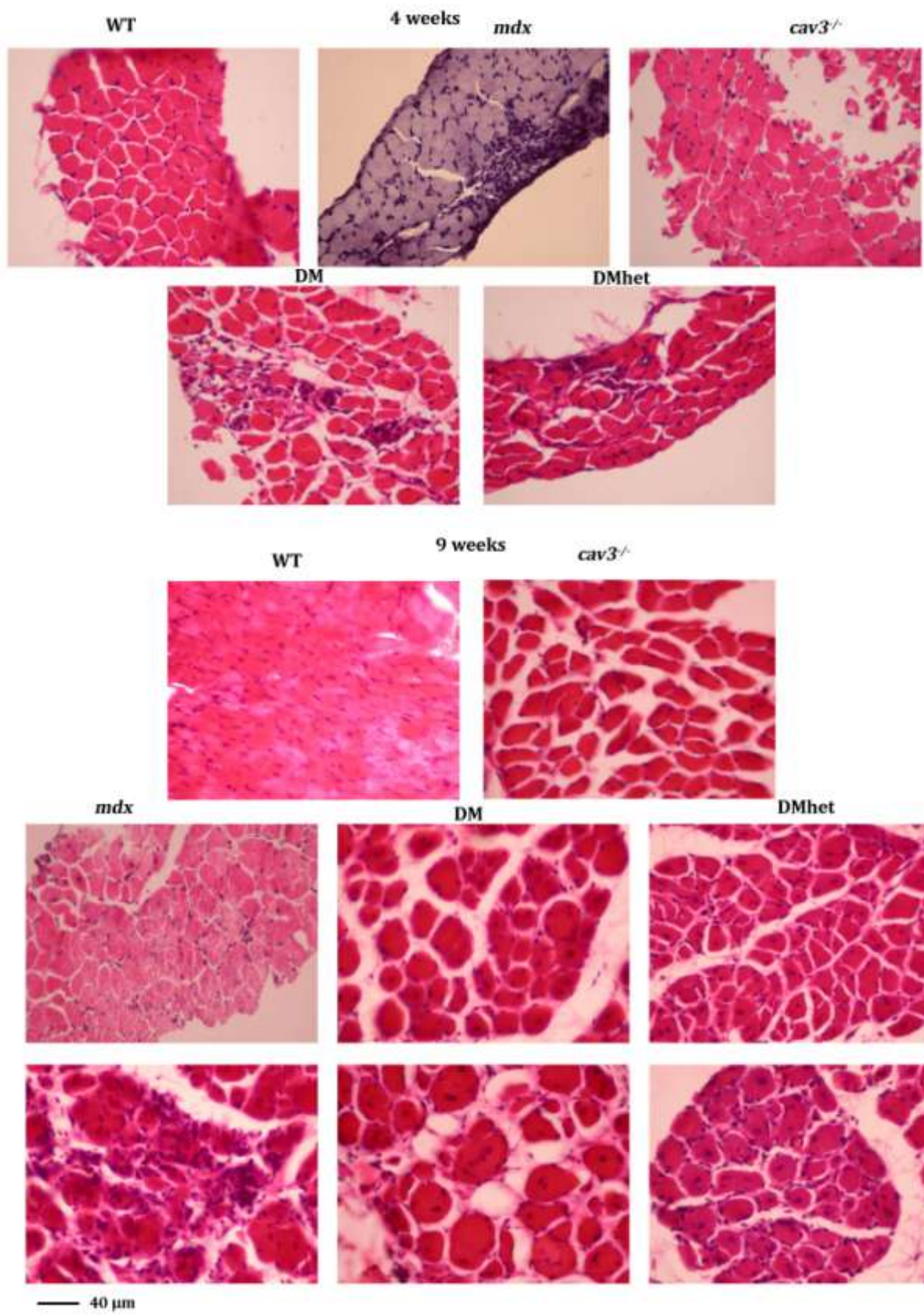


Figure 4.19

H&E stained diaphragm muscle. 5 μm thick sections of paraffin wax embedded diaphragm muscles from four weeks, nine weeks and nine months old WT, *mdx*, *cav3*^{-/-}, DM and DMhet were processed for H&E staining. At four weeks of age, areas of regeneration (hypercellular regions) are shown in *mdx* (**B**), DM (**D**) and DMhet (**E**). At nine weeks of age hypercellularity is obvious in *mdx* (**I**) and although not aggregated as shown in *mdx*, extra-myonuclei can be seen in DMhet (**L, M**); there is also an abundance of centrally located myonuclei seen in DMhet. The most severe diaphragmatic pathogenesis is shown in the DM where there appears to be adipocytes within the section (**K**).

4.2.5 - Fibre diameter variation in dystrophin-deficient mutants

Following histological analyses of sections from WT, *mdx*, *cav3*^{-/-}, DM and DMhets, it was noted that all three dystrophin-deficient mutants exhibited heterogeneity of fibre sizes, whereas their WT and *cav3*^{-/-} age matched counterparts, possessed fibres that were of a more uniform size. With the use of a stage mounted scale micrometer, diameters of nine weeks old WT, *mdx*, *cav3*^{-/-}, DM and DMhet triceps muscle fibres were measured. Nine weeks was chosen as there appeared to be greater variation in fibre sizes at this age and triceps were chosen as the quality of the sections cut from these muscles were better and this would allow for more accurate measurements to be taken.

WT fibres range between 15 µm and 85 µm in diameter (**Figure 4.20 A**), the modal size being 30 µm and 85 % ranging between 25 µm and 55 µm (**Figure 4.21 A**). The fibres of *mdx*, although showing a greater range, 10 µm - 100 µm (**Figure 4.20 A-C**), like WT have a modal diameter of 30 µm, with 62 % of these fibres ranging between 25 µm and 55 µm (**Figure 4.21 B**). Both DM and DMhets have approximately 50 % of their fibres between 25 µm and 55 µm (**Figure 4.21 C, D**), with ranges of 10 µm -125 µm and 10 µm -115 µm for DM and DMhets respectively (**Figure 4.20 A-C**). The modal size for DM is 60 µm and for DMhets 40 µm. The fibres of *cav3*^{-/-} triceps range between 20 µm -95 µm (**Figure 4.20 A**), 71 % of these fibres are between 25 µm and 55 µm in diameter (**Figure 4.21 E**), *cav3*^{-/-} fibres have a modal size of 40 µm. All four dystrophic mutants exhibit hypertrophic fibres; 26 % of *mdx* and *cav3*^{-/-} fibres have diameters between 60 µm and 125 µm and 42 % and 40 % of fibres are within this range for DM and DMhets respectively. Fewer than 10 % of WT fibres are of this size. Not only do dystrophin-deficient mutants possess larger fibres than WT or *cav3*^{-/-}, they also have a higher

proportion of small sized fibres too. Around 11 % of fibres in *mdx* and DMhet and 7 % in DM have diameters between 10 μm and 20 μm (**Figure 4.21 B, C, D**), compared to WT where 5 % of fibres are within this range (**Figure 4.21 A**). 3 % of *cav3*^{-/-} muscle fibres are 10 μm - 20 μm in diameter (**Figure 4.21 E**).

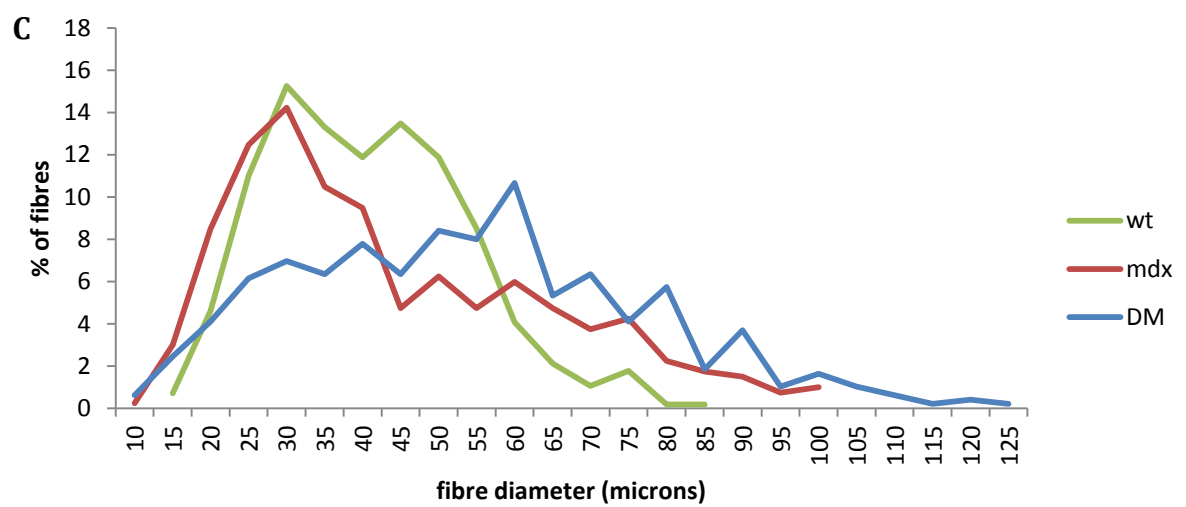
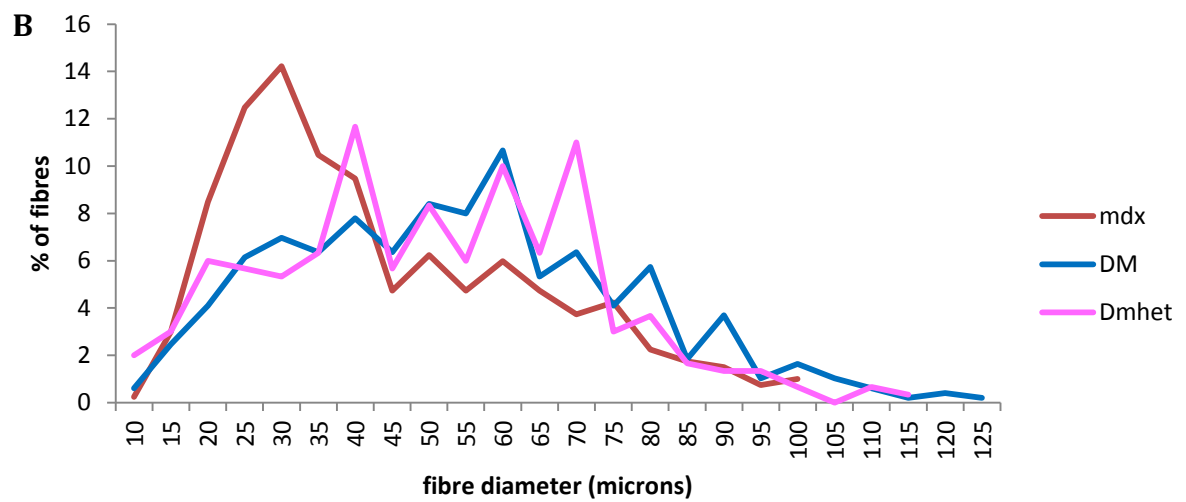
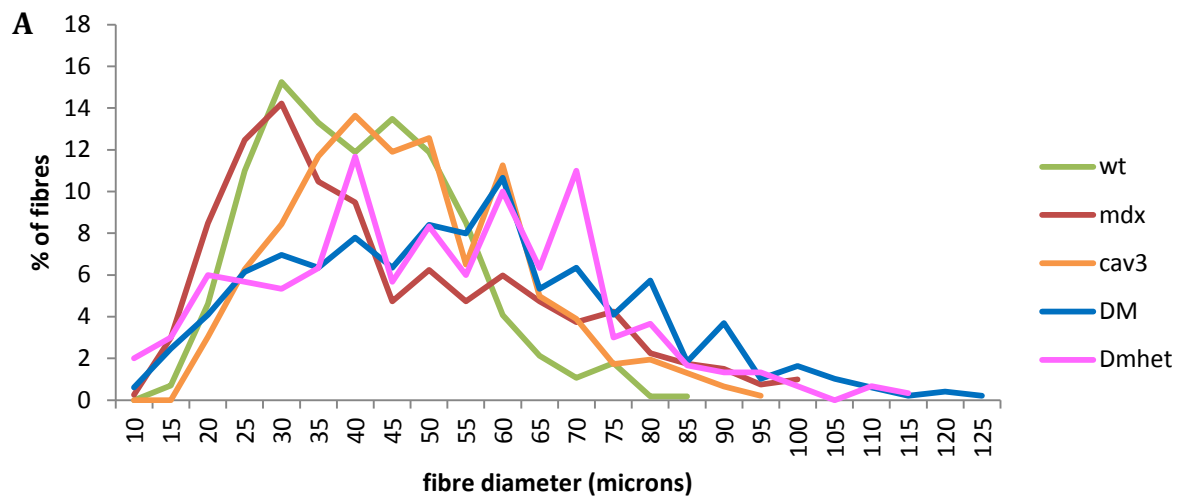


Figure 4.20

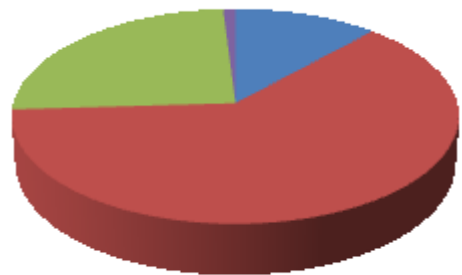
Graphical representation of fibre diameter sizes of nine weeks triceps muscles.

(A) Line graph showing fibre diameter sizes of WT, *mdx*, *cav3*^{-/-} DMhet and DM. Fibre sizes range between 15 - 85 μm for WT, 10 - 100 μm for *mdx*, 20 - 95 μm for *cav3*^{-/-}, 10 - 125 μm for DM and 10 - 115 μm for DMhet. 85 % of WT fibres are between 25 μm and 55 μm in diameter; DM and DMhets have approximately 50 % of their fibres between these measurements whereas 62 % and 71 % of fibres are between these sizes for *mdx* and *cav3*^{-/-} respectively. A higher percentage of fibres are seen between 15 μm and 40 μm in *mdx* than in any of the other strains and there are more fibres between 45 μm and 100 μm (with the exception of those measuring 75 μm) in DM than *mdx*. (B,C) The same data comparing the three dystrophin-deficient mutants (B) and WT, *mdx* and DM (C). WT n=2, *mdx* n=3, *cav3*^{-/-} n=3, DM n=3, DMhet n=2.

A **WT**



B *mdx*



C **DM**



D **DMhet**



E *cav3*^{-/-}

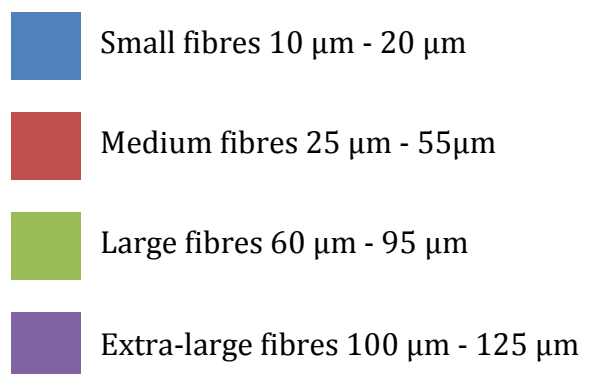
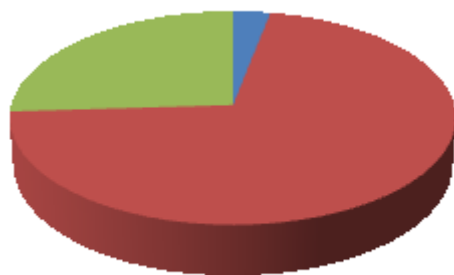


Figure 4.21

Pie charts showing proportions of small, medium, large and extra-large muscle fibres in nine weeks old WT, *mdx*, *cav3*^{-/-} and DM triceps muscles. (A) WT triceps consisted of 5.3 % small fibres (10 µm – 20 µm), 85.3 % medium fibres (25 µm – 55 µm) and 9.4 % large fibres (60 µm – 95 µm). (B) *mdx* triceps consisted of 11.7 % small fibres, 62.3 % medium fibres, 24.9 % large fibres and 1 % extra-large fibres. (C) *cav3*^{-/-} consisted of 3 % small fibres, 71 % medium fibres and 26 % large fibres. (D) DM consisted of 7.2 % small fibres, 50 % medium fibres, 38.7 % large fibres and 4.1 % extra-large fibres. DMhet consisted of 11 % small fibres, 49 % medium fibres, 38.3 % large fibres and 1.7 % extra-large fibres.

4.2.6 - Quantification of muscle regeneration

4.2.6.1 - Hypercellular aggregation

In order to quantify the level of regeneration occurring in dystrophin-deficient mutants, regenerating regions were calculated as percentages of the sections' total areas. H&E stained sections were used for the analyses, as regenerative areas stain a deep blue/purple and are therefore easily identifiable. Newly regenerating fibres, characterised by large centrally located nuclei, were not included in the counts, only the initial hypercellular regions, which contain leukocytes, fibroblasts and myocytes, were counted (**Figure 4.22 A**). H&E stained triceps and quadriceps sections of *mdx* and DM at four weeks and nine weeks of age were used for the analyses.

The levels of regeneration, as percentages of total areas, appear to be greater in *mdx* than in DM at both four weeks and nine weeks of age. This trend is seen in triceps muscles and quadriceps muscles (**Figure 4.22 B, C**); although error bars attest to the huge variation observed between *mdx* triceps sections of four weeks of age (**Figure 4.22 B**). At nine weeks of age, differences seen between the levels of regeneration in *mdx* and DM triceps is just outside of statistical significance, with a P value of 0.053578. Based on bars of the graph (**Figure 4.22 B**) representative of averages, both dystrophin-deficient mutants exhibit similar temporal patterns of muscle regeneration; the greater regeneration occurring at four weeks of age. The opposite is seen in quadriceps muscles, where the bars show the greater average levels of regeneration at nine weeks of age (**Figure 4.22 C**). Although none of these data are statistically significant, there does appear to be a trend where there is more regeneration occurring in *mdx* than in DM.

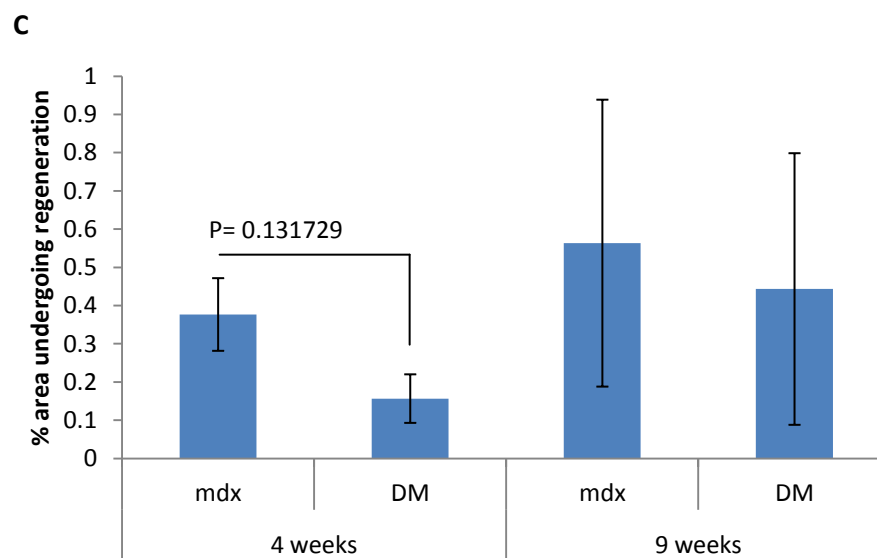
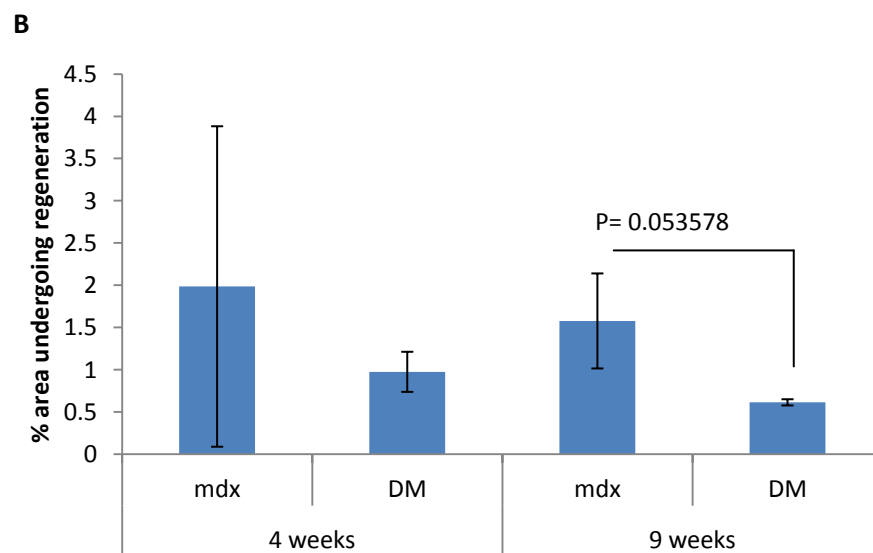
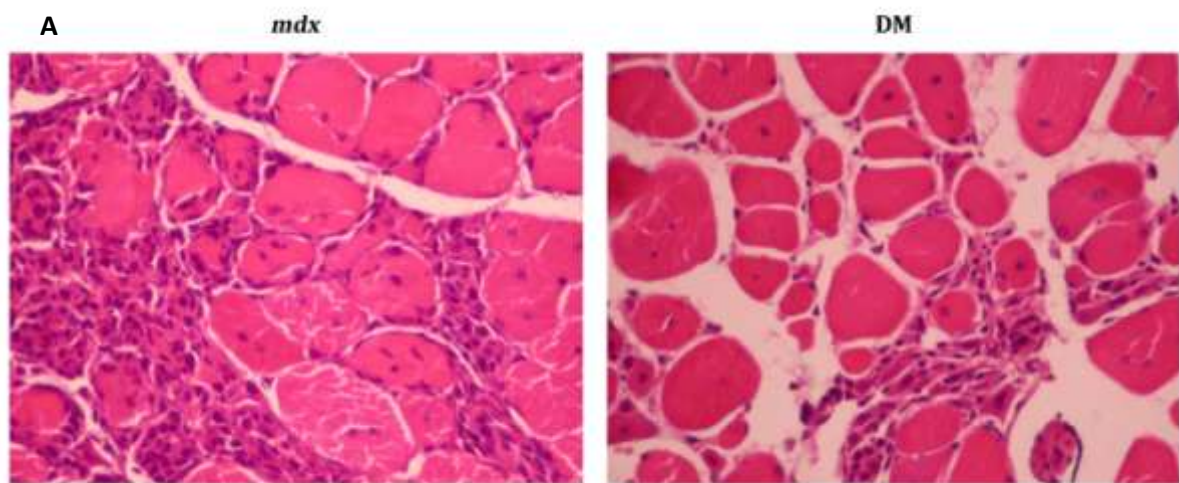


Figure 4.22

Regeneration in *mdx* and DM triceps and quadriceps muscles. (A) Areas showing concentrated extra-myonuclei hypercellularity associated with regeneration. These areas are graphically represented as percentages of total sections' areas. (B) Bar graph showing percentage area of triceps undergoing regeneration at four weeks and nine weeks of age. At both stages the level of regeneration is greater in *mdx* than DM; although there is a huge variation seen at four weeks in *mdx*. At nine weeks the difference between regeneration in *mdx* and DM falls just outside statistical significance, with a P value of 0.053578. Both *mdx* and DM exhibit very similar temporal patterns of regeneration with more extensive areas of regeneration seen at four weeks than at nine weeks. (C) Bar graph showing percentage area of quadriceps undergoing regeneration at four weeks and nine weeks of age. As with triceps muscles, there appears to be more regeneration in *mdx* than DM, although the greater regeneration is shown at nine weeks as opposed to four weeks in both mutants. The difference shown between *mdx* and DM was not statistically significant, with a P value of 0.131729. Error bars s.d. n=3 per strain. Student's *t*-test used.

4.2.6.2 - Centrally located myonuclei

To further access any differences pertaining to the regeneration of muscle tissue in *mdx* and DM mice, muscle fibres with centrally located nuclei and extra-myonuclei were counted in *mdx* and DM triceps muscles. Sections taken from four weeks and nine weeks old mice were analysed; three different mice from each strain and age being used for the analyses.

At four weeks of age there is no difference observed in the percentage of fibres with centrally located nuclei (**Figure 4.23 A**), with 28 % and 34 % of fibres having centrally located nuclei, for *mdx* and DM respectively. At nine weeks of age there is an increase seen in the central nucleation of myofibres, whereby 85 % of *mdx* and 75 % of DM fibres are centrally nucleated (**Figure 4.23 A**), this equates to an approximate fold increase of three and two, for *mdx* and DM respectively. Although a 10 % difference is shown between *mdx* and DM at nine weeks of age, this difference is not statistically significant, with a P value of 0.077256.

4.2.6.3 - Extra-myonuclei in dystrophin-deficient mutants

Aside from the increased, aggregated cellularity observed in regenerative areas of muscle tissue, an increase in the numbers of interstitial cells was seen in *mdx* and DM (**Figure 4.23 B**). Between 5 % and 10 % of the total cells in WT and *cav3^{-/-}* triceps at four weeks and nine weeks of age are interstitially located, compared to 24 % – 34 % for *mdx* and DM respectively; many of which are located in areas of regeneration. There is

no difference in the extra-myonuclei content shown between four weeks and nine weeks *mdx* and DM muscle.

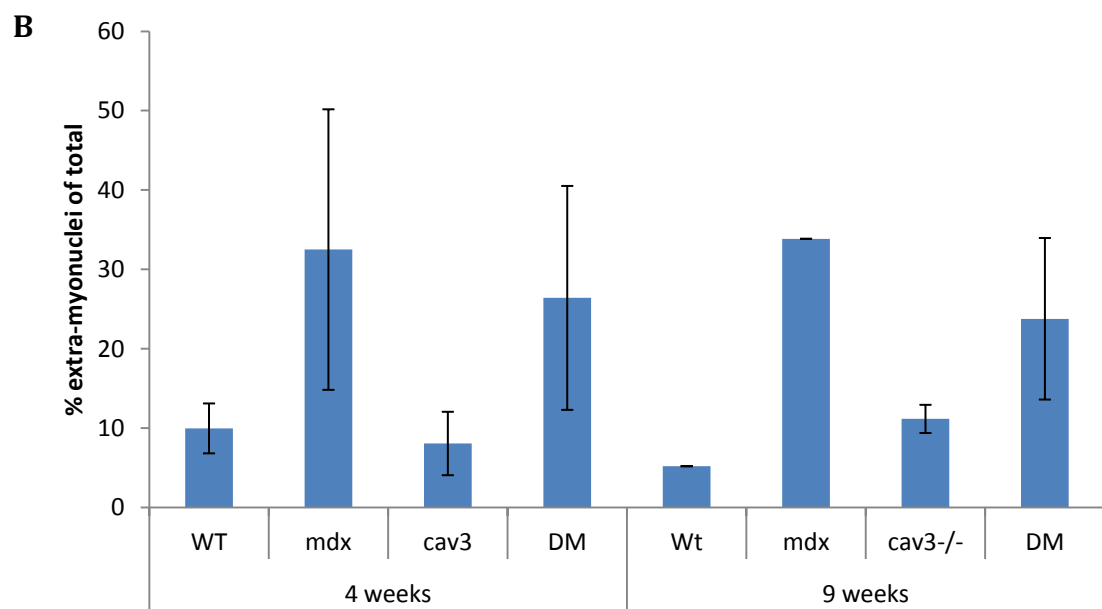
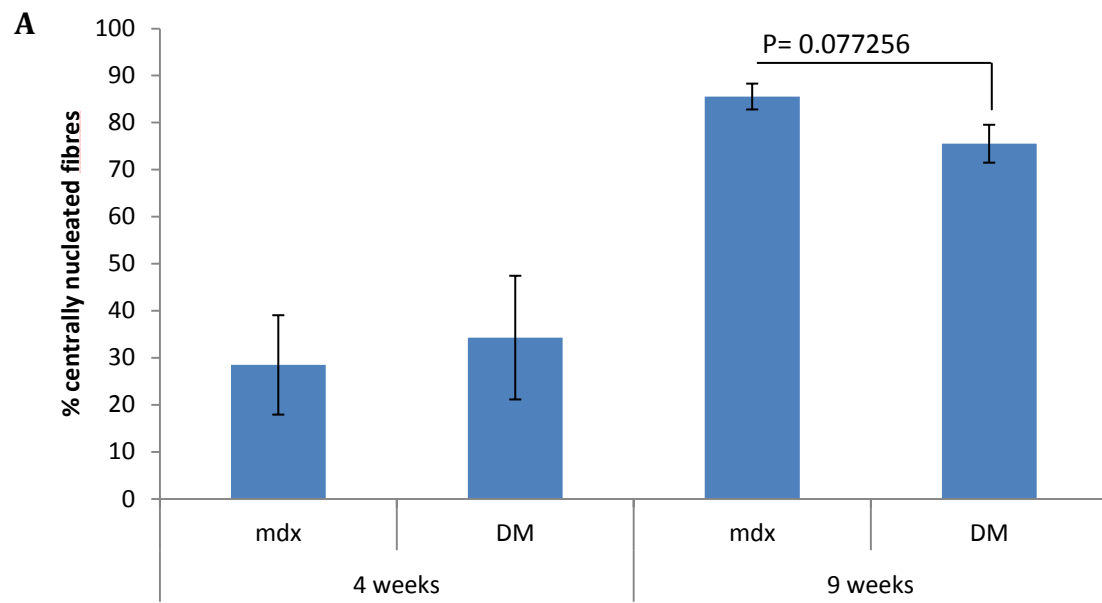


Figure 4.23

Graphical representation of central nucleated myofibres and extra-myonuclei.

(A) Bar graph showing percentages of centrally located myonuclei in four weeks and nine weeks old *mdx* and DM triceps. Although no real difference can be seen between *mdx* and DM at four weeks, there appears to be a difference at nine weeks; although this difference is not statistically significant, with a P value of 0.077256. A greater percentage of centrally located nuclei are seen in fibres at nine weeks of age than at four weeks of age; n= 3 per strain. (B) Bar graph showing percentages of extra-myonuclei as percentages of total nuclei in triceps muscles of four weeks and nine weeks old WT, *mdx*, *cav3*^{-/-} and DM. There are no differences seen in the percentages of extra-myonuclei at four weeks and at nine weeks of age. At both ages, there are greater percentages of extra-myonuclei seen in *mdx* and DM, between 24 % and 34 %, when compared to WT and *cav3*^{-/-}, where between 5 % and 10 % of nuclei are interstitially located. No statistical significance was shown at four weeks and as only one WT was used at nine weeks, statistical analysis could not be applied; n= 3 for four weeks; n=1 WT, *mdx*, n=3 *cav3*^{-/-}, DM for nine weeks. Error bars s.d. Student's *t*-test.

4.3 – DISCUSSION

The generation of DM and DMhet mice enabled direct comparisons to be made between *mdx* mice with varying levels of caveolin-3 and thus establish a role, if any, that caveolin-3 may have in the pathogenesis of the *mdx* mouse. A line of mice deficient in both dystrophin and caveolin-3 had been developed previously by a group researching the expression levels of *Opn* (osteopontin) in dystrophic mice (Hagiwara *et al.*, 2006). Although the pathology of the muscles of the different dystrophic models wasn't studied extensively, they did make some observations regarding the degeneration/regeneration of tibialis anterior muscles in *mdx* and DM, or double-deficient mice, as they were referred to.

4.3.1 – The macroscopic analysis of DM mice

4.3.1.1 – Mobility and general appearance

It is known that the malady of the *mdx* mouse does not impair the mobility of the animals in any way and their movement is indistinguishable from that of WT mice; Hagiwara's group reported that the movement of DM mice was akin to *mdx*, as was their lifespan (Dangain and Vrbova, 1984; Tanabe *et al.*, 1986; Hagiwara *et al.*, 2006). Although observations pertaining to the mobility of our DM mice concur with that which has been previously published, i.e. no impairment, no definitive concurrence or disputation can be given regarding their longevity, as our line was not established long enough for senescence to occur.

4.3.1.2 – Muscle mass

An increase in muscle mass is a phenotype obvious to anybody who has ever worked closely with *mdx*. This increase, compared to WT controls, has been previously documented to be between 9 % and 42 %, dependent on age (Lynch *et al.*, 2001). Although there is an increase in the cross-sectional areas of *mdx* muscles, the force of contractions when normalised to areas are no greater than that of WT animals; thus, muscle hypertrophy is believed to occur as a compensatory mechanism for the loss of contractile force generated by *mdx* muscles, which is around 20 % lower than that of WT (Coulton *et al.*, 1988; Williams *et al.*, 1993; Lynch *et al.*, 2001; Chan *et al.*, 2007). There has been uncertainty as to whether the increased muscle size observed in *mdx* is due to muscle hypertrophy or hyperplasia, yet Lynch found a 35 % increase in the numbers of fibres in soleus and extensor digitorum longus (EDL) *mdx* muscles when compared to age matched controls, but these data may have included branched fibres which have been found to increase with ageing in *mdx* (Lynch *et al.*, 2001; Chan *et al.*, 2007). The DM mice generated for this study showed profound muscle hypertrophy, even when compared with *mdx* of similar ages, though their bodyweights were no heavier than that of *mdx* or WT; this is consistent with data pertaining to the bodyweights of *mdx* in relationship to the less muscular WT animals (Tanabe *et al.*, 1986). Interestingly, the caveolin-3 null mice we used for our work, *cav3*^{-/-}, did not appear to be any less muscular than WT animals, in contrast to the caveolin-3 null mice (TgCAV3M1) generated and used by the Sunada group of Japan, which exhibited a marked reduction in hindlimbs muscle mass when compared to WT controls (Ohsawa *et al.*, 2006). The difference in the generation of these two murine models for LGMD-1C being that *cav3*^{-/-} had the region of DNA encoding the scaffolding and membrane

spanning domains of exon 2 replaced with a *neo* cassette, while TgCAV3M1 mice had the P104L mutation, shown to result in the human myopathy LGMD-1C, transgenically inserted. Whether or not the methods used to generate these two models for LGMD-1C resulted in any phenotypic difference regarding the pathogenicity of their myopathies is open to debate, but the mode of inheritance for the two models shows that *cav3*^{-/-} mice transmit the disease in a manner associated with a type-2 LGMD, i.e. recessively, whereas TgCAV3M1 transmit in the dominant manner of a type-1 LGMD (Minetti *et al.*, 1998; Hagiwara *et al.*, 2000; Sunada *et al.*, 2001).

The pronounced skeletal muscle hypertrophy exhibited by the DM mice generated for this study, could be seen as contradictory to data suggesting that caveolin-3 inhibits myostatin signalling, a negative regulator of skeletal muscle mass; a consequence of which sees mice lacking caveolin-3 present with atrophied skeletal muscles, which can be rescued by myostatin inhibition (McPherron *et al.*, 1997; Ohsawa *et al.*, 2006). The effects of increased myostatin signalling on the muscle mass of DM mice, assuming data presented by Ohsawa *et al.* to be correct, appears to be of no consequence, the only variable being the absence of dystrophin. This suggests that dystrophin or any one of the proteins of the DGC, may be required by myostatin to optimally convey its signal, or required for *Mstn* be optimally expressed. Another reason for the observed hypertrophy could be due to an increase in the growth factor Igf1, which unlike Igf2 is not affected by the upregulation of *Mstn* and has been shown to be upregulated in regenerating *mdx* muscle fibres, having a hypertrophic effect on skeletal muscle mass (De Lucca *et al.*, 1999; Lalani *et al.*, 2000; Miyake *et al.*, 2010; Shavlakadze *et al.*, 2010).

Whatever the reason for the observed muscle hypertrophy of DM mice, it is beyond the scope of this project, but may provide the basis for some interesting future work.

4.3.1.3 – Fat deposition

Although fat deposition has not been studied in murine models of MD, observed differences between *mdx*, *cav3*^{-/-} and DM mice regarding subcutaneous levels of fat warrant a brief mention. Fat deposition of nine month old *cav3*^{-/-} mice used in this study was by far in excess to that of WT, *mdx* and DM mice of similar ages. These observations are consistent with a study that found *cav3*^{-/-} mice developed insulin resistance in their skeletal muscles; they concluded that caveolin-3, unlike other caveolins which are signal suppressors, enhances insulin signalling (Hulit *et al.*, 2000; Oshikawa *et al.*, 2004; Rodriguez *et al.*, 2009). Insulin resistance invariably results in an increase in adipogenesis and consequently, increases in fat deposition (reviewed in (Holland *et al.*, 2007)). One possible explanation for the leaner somatotypes of DMs over that of *cav3*^{-/-} mice, is the signalling of Igf1 through insulin receptors (IR); though not its cognate receptor, Igf1 can bind to and convey a signal via the IR (Gauguin *et al.*, 2007). This hypothesis is backed up in that DM mice are not as lean as their *mdx* counterparts; who have increased *Igf1* expression and by virtue of increased levels of caveolin-3, (possibly) have enhanced insulin signalling also.

4.3.2 – Muscle regeneration in DM mice

4.3.2.1 – Cell infiltration into regenerating areas

During the initial stages of muscle regeneration in *mdx* mouse there is an infiltration of various cell types, including resident satellite cells and extravasated leukocytes, into the regenerating areas; a process that begins with the apoptosis of muscle fibres (Carnwath and Shotton, 1987; Smith *et al.*, 1995; Tidball *et al.*, 1995). When sections of muscles are stained with haematoxylin, these infiltrated hypercellular areas appear blue/purple in colour and due to the concentrated numbers of cells, are easily identified as areas of regeneration. Muscle regeneration is invariably preceded by muscle degeneration, thus an area of regeneration conversely, is representative of an area of degeneration. It has been well documented that episodes or ‘bouts’ of degeneration followed by regeneration begin at around three weeks of age and continue until around twelve weeks of age, at which point they occur less frequently; maximal regenerative activity occurs around eight weeks of age when many regeneration associated genes also peak (Bullfield *et al.*, 1984; Tanabe *et al.*, 1986; Porter *et al.*, 2004; Turk *et al.*, 2005). It should be noted however that three weeks of age signals the onset of the dystrophic condition regarding observable degeneration/regeneration, as phenotypic differences in dystrophic embryos when compared to WT have been presented in this study (**Chapter 3**) and previously (Merrick *et al.*, 2007; Merrick *et al.*, 2009).

Cell infiltration and therefore regeneration observed in DMs during this study were akin to that of *mdx* at the three ages studied, i.e. four weeks, nine weeks and nine

months, at which point hypercellularity was only observable (with the exception of two quadriceps sections, *mdx* and DM) at higher magnification. This observation is consistent with that of Hagiwara's group, who concluded there were no differences in the patterns of degeneration and regeneration between their double-deficient mice and *mdx* (Hagiwara *et al.*, 2006). As there was an absence of any areas of gross regeneration at four weeks in DMhet it would be easy to grasp at this as a real piece of data. However, as only one DMhet was available at this age, it would not be prudent to view this as a phenotypic difference, as higher magnification images showed that there were indeed areas that were regenerating and areas that had regenerated as the presence of centrally located nuclei attested to. When hypercellular areas were quantified, there appeared to be a trend (P value of 0.053578 for nine weeks triceps) suggesting a greater level of regeneration in *mdx* than in DM, this was consistent for four weeks and nine weeks of age in both muscles analysed. Given a greater sample size, this difference may well have been significant and as such would have fitted in with data regarding the increased expression levels of *Opn* (osteopontin) in *mdx*. *Opn* has been shown to be secreted by many cell types, including macrophages where it may have chemotactic properties, attracting inflammatory cells to areas of muscle degeneration (Weber *et al.*, 1996; Barbosa-Souza *et al.*, 2011). It has been shown that muscle fibres of *mdx*, express greater levels of *Opn* than do those of DM; this would affect the numbers of mononuclear cells infiltrating areas of degeneration, i.e. there would be more infiltration in *mdx* muscles (Hagiwara *et al.*, 2006). Independent studies regarding *OPN* expression in DMD muscle have shown increases of 46 fold and 146 fold; another study showed that in WT mouse TA muscle, an increase of 118 fold, 48 hours following cardiotoxin induced injury was observed (Haslett *et al.*, 2002; Porter *et*

al., 2002; Hirata *et al.*, 2003). DMD subjects using the anti-inflammatory drug prednisolone exhibited no increase in the expression of *OPN* ('t Hoen *et al.*, 2011).

4.3.2.2 – Centrally nucleated fibres are more prevalent in *mdx*

The central positioning of nuclei in regenerating *mdx* muscle fibres persists with the fibres' maturity and thus centronucleation can be used as a cumulative index for muscle regeneration, although the validity of its use has been disputed (Karpati *et al.*, 1988; Williams *et al.*, 1993; Totsuka *et al.*, 1998). Centronucleation in *mdx* mouse has been well documented and re-confirmed by those generating various *mdx* crosses (Bullfield *et al.*, 1984; Tanabe *et al.*, 1986; Carnwath and Shotton, 1987; Deconinck *et al.*, 1997; Hagiwara *et al.*, 2006). It has been shown that centrally nucleated fibres are more resistant to mechanical stress than *mdx* fibres with peripherally located myonuclei, suggesting centronucleation occurs as a compensatory mechanism in dystrophic muscle fibres, although there are no differences in the contractile properties of the two (Williams *et al.*, 1993; Narita and Yorifuji, 1999).

The progressive increase of centrally nucleated fibres shown in *mdx* and DM mice used in this study is typical of what has been shown historically. With 85 % of *mdx* fibres and 75 % of DM fibres centronucleated at nine weeks, these figures concur with previously published data that showed 80 % of *mdx* fibres at 60 days of age had centrally located nuclei (Karpati *et al.*, 1988). Although not statistically significant, with a P value of 0.077256 using a sample size of n=3, the 10 % increase shown in centronucleated *mdx* fibres over those of DM, could be an important observation regarding the involvement

of caveolin-3 in dystrophin-deficient muscle regeneration. When taken together with data pertaining to cell infiltration into regenerating areas (**section 4.3.2.1**), the increased centronucleation seen in *mdx* suggests a greater occurrence of regeneration and therefore preliminary degeneration in dystrophin-deficient muscle in the presence of caveolin-3.

An elevation in muscle fibre degeneration in *mdx* may be caused by an increased autoimmune response due to the supraphysiological levels of caveolin-3 present. Caveolin-1 has 65 % identity and 85 % similarity to caveolin-3 and has been shown to play a role in the activation of CD26⁺ T-cells through their interaction with the lipid rafts of caveolae; moreover, satellite cells have been shown to express *Cav-1* (Smart *et al.*, 1999; Ishii *et al.*, 2001; Volonte *et al.*, 2005; Ohnuma *et al.*, 2006). It could be postulated that the increased levels of caveolin-3 and caveolae in *mdx* muscle along with an abundance of caveolin-1^{+ve} satellite cells, at a time when an infiltration of leukocytes are prevalent, provide an abundance of lipid rafts with which to interact, thus prolonging the regenerative process. It has also been shown that HLA class I antigens, though usually absent from muscle fibres, are expressed on muscle fibres of DMD, targeting them for destruction by cytotoxic T-lymphocytes, it has been suggested that this may exacerbate the dystrophic condition (Arahata and Engel, 1984; Appleyard *et al.*, 1985). When the chemotactic properties of osteopontin, which is increased in *mdx* when compared to DM, is taken together with the interaction of CD26⁺ T-cells with caveolin of lipid rafts and data presented in this study regarding the observed increases in regeneration and centronucleation, it could be suggested that the

increased levels of caveolin-3 in *mdx* muscle may impede regeneration through an increased and prolonged inflammatory response.

4.3.3 – The histopathogenesis of respiratory muscles in dystrophin-deficient mutants

Perhaps the most important muscles in terms of the pathology of *mdx* are the respiratory muscles. It is the degeneration of the intercostals and diaphragm and the resultant respiratory failure that is the main cause of death for DMD patients (Calvert *et al.*, 2006). There have been conflicting reports as to whether the dystrophic condition of the diaphragm precedes or begins contemporaneously with that of the limbs, where unlike muscles of the limbs, degenerated fibres are replaced with fibrous connective tissue; this results in a collagen content that is ten times greater than in that of the limbs (Stedman *et al.*, 1991; Deconinck *et al.*, 1997).

The severely reduced intercostals muscle fibre density that was shown in late gestation embryos of DMhet mice and to a lesser degree in *mdx* (**Chapter 3**), was not evident in adult animals. The sections obtained from the intercostals of most of the mouse strains were of insufficient quality to enable accurate analyses to be performed, but those that were obtained appeared to be similar in all three of the dystrophin-deficient mutants.

4.3.4 - Muscle fibre calibre variations in dystrophin-deficient mutants

Regenerated *mdx* muscle-tissue invariable consists of fibres of varying sizes, which may or may not be centronucleated (Bullfield *et al.*, 1984; Tanabe *et al.*, 1986). As previously mentioned (**section 4.3.1.2**), *mdx* muscles are larger but their overall contractile force is no different to that of WT muscles (Coulton *et al.*, 1988; Williams *et al.*, 1993; Lynch *et al.*, 2001). It has also been shown that the contractile properties of individual *mdx* fibres when compared to WT fibres are surprisingly similar, with a statistically significant reduction seen only in the fibres of soleus muscles, these experiments were performed on single unbranched fibres and fibre-branching has been shown to reduce the force of contractions (Williams *et al.*, 1993; Chan *et al.*, 2007).

The DM and DMhet mice showed the same heterogeneity of fibre sizes that have been previously reported with *mdx* and *mdx* crosses (Bullfield *et al.*, 1984; Tanabe *et al.*, 1986; Deconinck *et al.*, 1997; Anderson *et al.*, 2006). However, the absence of caveolin-3 in DM muscle resulted in a 14 % increase above that of *mdx* in fibres with calibres above 60 μm and a four-fold increase in fibres with calibres over 100 μm in diameter; the differences in DMhet were more subtle. It has been suggested that fibres with calibres of less than 20 μm are not subject to necrosis as are larger fibres (based on the centronuclear index) and this could be the reason for the small calibre fibres seen in *mdx* and other dystrophic myopathies; it has also been shown that although most regenerated fibres have larger diameters than non-regenerated fibres, they are not prone to repeated bouts of necrosis (Karpati *et al.*, 1988; Massa *et al.*, 1997). The data presented in this study showed the proportions of small calibre fibres were 11.7 %, 7.2 % and 11 % and for fibres above 100 μm , 1 %, 4.1 % and 1.7 % for *mdx*, DM and DMhet

respectively; it also showed a correlation between caveolin-3 levels and fibre-size in the absence of dystrophin, whereby a reduction of caveolin-3 results in an increase in the percentages of large fibres and a reduction in the percentage of small fibres.

A recent paper showed that caveolae act as stress sinks to buffer membrane tension caused by mechanical stresses, when membrane tension increased, the caveolae would disassemble to effectively increase the surface area of the membrane and relieve tension. In cells which were deficient in caveolin and thus caveolae, there was no buffering and as a consequence, their membranes were ruptured (Sinha *et al.*, 2011). The upregulation of caveolin-3 in *mdx* muscle fits in with this model rather well, as it has been shown that the lack of dystrophin in contracting *mdx* muscle results in sarcolemmal ruptures that are directly proportionate to the magnitude of the applied stress (Petrof *et al.*, 1993). The increased caveolae would help to buffer this stress to some extent. The DM mice do not have the luxury of the buffering system afforded by caveolae, so they may compensate by growing larger muscles. Larger muscle fibres are less likely to have sarcolemmal ruptures than smaller calibre fibres as they are capable of more forceful contractions and therefore increased workloads. The intermediate fibre size of the DMhet adds validity to this hypothesis. The extreme hypertrophic phenotype of the DM could also be attributed to an increased fusion of myoblasts during the regenerative process as it has been shown that in myoblasts deficient in caveolin-3 there is an increase in myotube fusion, conversely in the same report it was shown that myoblasts that overexpressed *Cav3* showed a reduction in myotube fusion (Volonte *et al.*, 2003).

Whatever the reason for the differences observed, it is beyond the scope of this report to elucidate. But the data collected herein suggests that caveolin-3 has a role in determining sizes of regenerated fibres in dystrophin-deficient muscle and may in fact exacerbate the inflammatory response in leukocyte infiltrated regenerating dystrophin-deficient muscle tissue.

Table 4.1 – Summary of results. The four dystrophic mouse strains along with the most significant results are summarised. All results are compared with WT, therefore – denotes < WT; +- denotes =WT; + denotes >WT; n/d denotes no data.

Mouse strain	Caveolin-3 protein	Muscle mass	Sub-cut. adiposity	Fibre size	Central nuclei
<i>mdx</i>	+	+	-	++	85 %
<i>cav3^{-/-}</i>	0	+-	++	+	n/d
DMhet	+-	n/d	n/d	+++	n/d
DM	0	++	+	++++	75 %

CHAPTER 5 - CONCLUSIONS AND FUTURE WORK

5.1 - Conclusions

5.1.1 - Caveolin-3 in embryonic myogenesis

Although the increased caveolin-3 protein in DMD and the mouse model of the disease, *mdx* has been known of for more than a decade, there has been very little research into how this may affect the pathogenesis observed in these dystrophinopathies (Vaghy *et al.*, 1998; Repetto *et al.*, 1999). The data presented in this thesis has shown that in the skeletal muscles of the developing *mdx* embryo the affect of reduced levels of caveolin-3 is profound. The global attrition of pax7⁺ cells in DMhet embryos, when taken with the more severe reduction of intercostals muscles fibre-density, strongly suggests the increased protein levels of caveolin-3 in *mdx* may occur as a compensatory mechanism in the absence of dystrophin, which may help ameliorate the dystrophic condition of *mdx*. This appears to contradict data which showed transgenic mice that overexpress *Cav3* have a more severe DMD-like phenotype than *mdx*, although this particular study was conducted using adult mice (Galbiati *et al.*, 2000). This implied that it was the increase in caveolin-3 rather than the deficiency in dystrophin that was the primary cause of the pathogenesis observed in dystrophin-deficient muscle.

5.1.2 - Caveolin-3 in adult myoregeneration

However, the contradiction leans towards concurrence with the pathogenesis of adult muscle tissue. Based on the initial gross histological analysis of both triceps and quadriceps muscles, whether caveolin-3 is increased compared to WT, as in *mdx*; at WT

levels, as in DMhet; or completely absent, as in DM; the histopathogenesis of dystrophin-deficient muscles it seems is neither exacerbated nor ameliorated to a statistically significant extent. The quantitative data, although not significant, did show a trend in that there was a greater level of regeneration, assessed by the area of tissue with aggregated hypercellularity and centronucleated fibres, in *mdx* muscles. This suggests that the increased levels of caveolin-3 do in fact contribute slightly to the dystrophic phenotype of *mdx*. As discussed in **chapter 4**, this could be due to an increased inflammatory response.

5.1.3 – Heterogeneity of muscle fibre calibres

The greater variation in the sizes of muscle fibres shown in DM muscle would suggest that caveolin-3 has a role in the regulation of muscle fibre calibre size. However, as all three dystrophin-deficient mice present with the same phenotype and all have different levels of caveolin-3, it is very difficult to draw any conclusions. There was a correlation between caveolin-3 levels and fibre-size in that a decrease in caveolin-3 was accompanied by an increase in fibre sizes. As mentioned in the discussion of **chapter 4**, this does support Volonte's paper which showed caveolin-3 deficient myoblasts exhibited an increase in fusion, the bouts of regeneration and lack of dystrophin would possibly disrupt the process somewhat but the correlation is seen in the three dystrophin-deficient mutants (Volonte *et al.*, 2003).

5.2 - Future work

The following section briefly describes work that would have been conducted if given considerably more time.

The late acquisition of DM mice did not allow for the analysis of DM embryos, so the effect of a caveolin-3 deficiency in dystrophin-deficient embryonic muscle unfortunately could not be ascertained. This is an area of work that if given considerably more time I would have pursued.

With the DM line established during the final six months of the project, the sample sizes available were limited. The quantitative data shows that several analyses were just outside of statistical significance; given more samples these data would more than likely have been significant. In the samples that were analysed there were great degrees of variation regarding regenerating areas exhibited by all of the dystrophin-deficient mutants. A fixed section of muscle tissue is merely a snapshot of what was occurring in a microscopic area of muscle at a precise time-point. The same muscle, if cut just a couple of millimetres further up or down could produce an entirely different set of results. The only way to be sure of any slight difference there may be would be to section entire muscles, from insertions to origins, of at least ten different mice of each dystrophin-deficient mutant. Although very onerous and time consuming, the data generated would be robust.

I find it extremely difficult to believe that the increased levels of caveolin-3 in *mdx* mouse have no functional purpose, particularly in light of recent data regarding caveolae as plasmalemma stress reservoirs (Sinha *et al.*, 2011). Given time I would

have generated exercised induce muscle damage on all dystrophin-deficient strains along with WT controls. Downhill treadmill running would be employed to induce a greater degree of muscle damage and repeated grip strength tests would be performed too as a form of anaerobic eccentric exercise and to evaluate muscle strength. Following injections with Evans blue dye, muscles would be eventually excised and histologically examined.

Finally, it would be worth establishing a DM cell line derived from muscle explants, *in vitro* experiments could be performed and cell signalling pathways elucidated in a dystrophin and caveolin-3 deficient cell-line.

REFERENCES

- 't Hoen, P. A. C., Nadarajah, V. D., van Putten, M., Chaouch, A., Garrood, P., Straub, V., Ginjaar, H. B., Aartsma-Rus, A. M., van Ommen, G.-J. B., Den Dunnen, J. T. and Lochmuller, H. (2011) serum matrix metalloproteinase-9 (MMP-9) as a biomarker for monitoring Duchenne muscular dystrophy (DMD) disease progression. *Neuromuscular Disorders* 21(9-10 16th International Congress of The World Muscle Society): 656.
- Aartsma-Rus, A., Janson, A. A. M., van Ommen, G.-J. B. and van Deutekom, J. C. T. (2007) Antisense-induced exon skipping for duplications in Duchenne muscular dystrophy. *BMC Medical Genetics* 8: 43-51.
- Aartsma-Rus, A., Van Deutekom, J. C., Fokkema, I. F., Van Ommen, G. J. and Den Dunnen, J. T. (2006) Entries in the Leiden Duchenne muscular dystrophy mutation database: an overview of mutation types and paradoxical cases that confirm the reading-frame rule. *Muscle and Nerve* 34: 135-144.
- Acakpo-Satchivi, L. J., Edelmann, W., Sartorius, C., Lu, B. D., Wahr, P. A., Watkins, S. C., Metzger, J. M., Leinwand, L. and Kucherlapati, R. (1997) Growth and muscle defects in mice lacking adult myosin heavy chain genes. *J Cell Biol* 139: 1219-29.
- Andersen, D. C., Petersson, S. J., Jørgensen, L. H., Bollend, P., Jensen, P. B., Teisner, B., Schroeder, H. D. and Jensen, C. H. (2009) Characterization of DLK1+ cells emerging during skeletal muscle remodeling in response to myositis, myopathies, and acute injury *Stem Cells* 27: 898 -908.
- Anderson, C. L., De Repentigny, Y., Cifelli, C., Marshall, P., Renaud, J.-M., Worton, R. G. and Kothary, R. (2006) The mouse dystrophin muscle promoter/enhancer drives expression of mini-dystrophin in transgenic mdx mice and rescues the dystrophy in these mice. *Molecular Therapy* 14: 724-734.
- Anderson, J. L., Head, S. I., Rae, C. and Morley, J. W. (2002) Brain function in Duchenne muscular dystrophy. *Brain* 125: 4-13.
- Appleyard, S. T., Dubowitz, V., Dunn, M. J. and Rose, M. L. (1985) Increased expression of HLA ABC class I antigens by muscle fibres in Duchenne muscular dystrophy, inflammatory myopathy and other neuromuscular disorders. *The Lancet* 1: 361-363.
- Arahata, K. and Engel, A. G. (1984) Monoclonal antibody analysis of mononuclear cells in myopathies. I: Quantitation of subsets according to diagnosis and sites of accumulation and demonstration and counts of muscle fibers invaded by T cells. *Annals of Neurology* 16: 193-208.
- Arnold, H.-H. and Braun, T. (1996) Targeted inactivation of myogenic factor genes reveals their role during mouse myogenesis: a review. *International Journal of Developmental Biology* 40: 345-363.
- Baracos, V. E. (2001) Management of muscle wasting in cancer-associated cachexia. *CANCER Supplement* 92: 1669-1677.
- Barbosa-Souza, V., Contin, D. K., Filho, W. B., de Aravjo, A. L., Irazuska, S. P. and de Cruz-Hofling, M. A. (2011) Osteopontin, a chemotactic protein with cytokine-like properties, is up-regulated

in muscle injury caused by *Bothrops lanceolatus* (fer-de-lance) snake venom. *Toxicon* 58: 398-409.

Bober, E., Lyons, G. E., Braun, T., Cossu, G., Buckingham, M. and Arnold, H.-H. (1991) The muscle regulatory gene, myf-6, has a biphasic pattern of expression in early mouse development. *Journal of Cell Biology* 113: 1255-1265.

Bonifati, M. D., Ruzza, G., Bonometto, P., Berardinelli, A., Gorni, K., Orcesi, S., Lanzi, G. and Angelini, C. (2000) A multicenter, double-blind, randomized trial of deflazacort versus prednisone in Duchenne muscular dystrophy. *Muscle & Nerve* 23: 1344-1347.

Braun, T. and Arnold, H.-H. (1995) Inactivation of Myf-6 and Myf-5 genes in mice leads to alterations in skeletal muscle development. *EMBO Journal* 14: 1176-1186.

Braun, T., Bober, E., Winter, B., Rosenthal, N. and Arnold, H. H. (1990) Myf-6, a new member of the human gene family of myogenic determination factors: evidence for a gene cluster on chromosome 12. *Embo Journal* 9: 821-831.

Braun, T., Buschhausen-Denker, G., Bober, E., Tannich, E. and Arnold, H. H. (1989) A novel human muscle factor related to but distinct from MyoD1 induces myogenic conversion in 10T1/2 fibroblasts. *Embo Journal* 8: 701-709.

Braun, T., Rudnicki, M. A., Arnold, H.-H. and Jaenisch, R. (1992) Targeted inactivation of the muscle regulatory gene Myf-5 results in abnormal rib development and perinatal death. *Cell* 71: 369-382.

Buckingham, M. and Relaix, F. (2007) The role of Pax genes in the development of tissues and organs: Pax3 and Pax7 regulate muscle progenitor cell functions. *Annual Review of Cell and Developmental Biology* 23: 645-673.

Bullfield, G., Siller, W. G., Wight, P. A. L. and Moore, K. J. (1984) X-chromosome linked muscular dystrophy (*mdx*) in the mouse. *Proceedings of the National Academy of Sciences of the United States of America* 81: 1189-1192.

Calvert, L. D., McKeever, T. M., Kinnear, W. J. M. and Britton, J. R. (2006) Trends in survival from muscular dystrophy in England and Wales and impact on respiratory services. *Respiratory Medicine* 100: 1058-1063.

Carnwath, J. W. and Shotton, D. M. (1987) Muscular dystrophy in the *mdx* mouse: histopathology of the soleus and extensor digitorum longus muscles. *Journal of the Neurological Sciences* 80: 39-54.

Cash, J. N., Rejon, C. A., McPherron, A. C., Bernard, D. J. and Thompson, T. B. (2009) The structure of myostatin: follistatin 288: insights into receptor utilization and heparin binding. *The EMBO Journal* 28: 2662-2676.

Castro-Gago, M., Blanco-Barca, M. O., Eiris-Punal, J., Carneiro, I., Arce, V. M. and Devesa, J. (2006) Myostatin expression in muscular dystrophies and mitochondrial encephalomyopathies. *Pediatric Neurology* 34: 281-284.

Cerletti, M., Negri, T., Cozzi, F., Colpo, R., Andreetta, F., Croci, D., Davies, K. E., Cornelio, F., Pozza, O., Karpatis, G., Gilbert, R. and Mora, M. (2003) Dystrophic phenotype of canine X-linked muscular dystrophy is mitigated by adenovirus-mediated utrophin gene transfer *Gene Therapy* 10: 750-757.

Chamberlain, J. S., Metzger, J., Reyes, M., Townsend, D. and Faulkner, J. A. (2007) Dystrophin-deficient mdx mice display a reduced life span and are susceptible to spontaneous rhabdomyosarcoma. *The FASEB Journal* 21: 2195-2204.

Chan, S., Head, S. I. and Morley, J. W. (2007) Branched fibers in dystrophic mdx muscle are associated with a loss of force following lengthening contractions. *Am J Physiol Cell Physiol* 293: C985-92.

Chen, J.-F., Mandel, E. M., Thomson, J. M., Wu, Q., Callis, T. E., Hammond, S. M., Conlon, F. L. and Wang, D.-Z. (2005) The role of microRNA-1 and microRNA-133 in skeletal muscle proliferation and differentiation. *Nature Genetics* 38: 228 - 233.

Choi, J., Costa, M. L., Mermelstein, C. S., Chagas, C., Holtzer, S. and Holtzer, H. (1990) MyoD converts primary dermal fibroblasts, chondroblasts, smooth muscle, and retinal pigmented epithelial cells into striated mononucleated myoblasts and multinucleated myotubes. *PNAS* 87: 7988-7992.

Christ, B. and Ordahl, C. P. (1995) Early stages of chick somite development *Anatomy and Embryology* 191: 381-396.

Collins, C. A. and Morgan, J. E. (2003) Duchenne's muscular dystrophy: animal models used to investigate pathogenesis and develop therapeutic strategies. *International Journal of Experimental Pathology* 84: 165-172.

Cooper, B. J., Winand, N. J., Stedman, H., Valentine, B. A., Hoffman, E. P., Kunkel, L. M., Scott, M.-O., Fischbeck, K. H., Kornegay, J. N., Avery, R. J., Williams, J. R., Schmickel, R. D. and Sylvester, J. E. (1988) The homologue of the Duchenne locus is defective in X-linked muscular dystrophy of dogs. *Nature* 334: 154-156.

Corrado, K., Mills, P. L. and Chamberlain, J. S. (1994) Deletion analysis of the dystrophin-actin binding domain. *FEBS Lett* 344: 255-60.

Cossu, G. and Borello, U. (1999) Wnt signaling and the activation of myogenesis in mammals. *The EMBO Journal* 18: 6867- 6872.

Coulton, G. R., Curtin, N. A., Morgan, J. E. and Partridge, T. A. (1988) The mdx mouse skeletal muscle myopathy: II. Contractile properties. *Neuropathology and Applied Neurobiology* 14: 299-314.

Cox, G. F. and Kunkel, L. M. (1997) Dystrophies and heart disease. *Current Opinions in Cardiology* 12: 329-343.

Crosbie, R. H., Yamada, H., Venzke, D. P., Lisanti, M. P. and Campbell, K. P. (1998) Caveolin-3 is not an integral component of the dystrophin glycoprotein complex. *Febs Letters* 427: 279-282.

Dangain, J. and Vrbova, G. (1984) Muscle development in *mdx* mutant mice. *Muscle & Nerve* 7: 700-704.

- Davies, K. E., Pearson, P. L., Harper, P. S., Murray, J. M., O'Brien, T., Sarfarazi, M. and Williamson, R. (1983) Linkage analysis of two cloned DNA sequences flanking the Duchenne muscular dystrophy locus on the short arm of the human X chromosome. *Nucleic Acids Research* 11 2303-2312.
- Davis, R. L., Weintraub, H. and Lassar, A. B. (1987) Expression of a single transfected cDNA converts fibroblasts to myoblasts. *Cell* 51: 987-1000.
- De Lucca, A., Pierno, S., Camerino, C., Cocchib, D. and Camerino, D. C. (1999) Higher content of insulin-like growth factor-I in dystrophic mdx mouse: potential role in the spontaneous regeneration through an electrophysiological investigation of muscle function. *Neuromuscular Disorders* 9: 11-18
- Deconinck, A. E., Rafael, J. A., Skinner, J. A., Brown, S. C., Potter, A. C., Metzinger, L., Watt, D. J., Dickson, J. G., Tinsley, J. M. and Davies, K. E. (1997) Utrophin-dystrophin-deficient mice as a model for Duchenne muscular dystrophy. *Cell* 90: 717-27.
- Dey, B. R., Frick, K., Lopaczynski, W., Nissley, S. P. and Furlanetto, R. W. (1996) Evidence for the direct interaction of the insulin-like growth factor I receptor with IRS-1, Shc, and Grb10. *Molecular Endocrinology* 10: 631-641.
- Doherty, T. J. (2003) Invited Review: Aging and sarcopenia *Journal of Applied Physiology* 95: 1717-1727.
- Eagle, M., Baudouin, S. V., Chandler, C., Giddings, D. R., Bullock, R. and Bushby, K. (2002) Survival in Duchenne muscular dystrophy: improvements in life expectancy since 1967 and the impact of home nocturnal ventilation. *Neuromuscular Disorders* 12: 926-929.
- Edmondson, D. G. and Olson, E. N. (1989) A gene with homology to the myc similarity region of MyoD1 is expressed during myogenesis and is sufficient to activate the muscle differentiation program. *Genes and Development* 51: 628-640.
- Emery, A. H. (1977) Muscle histology and creatine kinase levels in the foetus in Duchenne muscular dystrophy *Nature* 266: 472 - 473.
- Ervasti, J. M. and Campbell, K. P. (1991) Membrane organization of the dystrophin-glycoprotein complex. *Cell* 66: 1121-1131.
- Ervasti, J. M., Ohlendieck, K., Kahl, S. D., Gaver, M. G. and Campbell, K. P. (1990) Deficiency of a glycoprotein component of the dystrophin complex in dystrophic muscle. *Nature* 345: 315-319.
- Fletcher, S., Honeyman, K., Fall, A. M., Harding, P. L., Johnsen, R. D., Steinhaus, J. P., Moulton, H. M., Iversen, P. L. and Wilton, S. D. (2007) Morpholino oligomer-mediated exon skipping averts the onset of dystrophic pathology in the mdx mouse. *Molecular Therapy* 15: 1587-1592.
- Foley, J. W., Bercurry, S. D., Finn, P., Cheng, S. H., Scheule, R. K. and Ziegler, R. J. (2010) Evaluation of systemic follistatin as an adjuvant to stimulate muscle repair and improve motor function in pompe mice. *Molecular Therapy*: 1584-1591.

- Galbiati, F., Volonte, D., Chu, J. B., Li, M., Fine, S. W., Fu, M. F., Bermudez, J., Pedemonte, M., Weidenheim, K. M., Pestell, R. G., Minetti, C. and Lisanti, M. P. (2000) Transgenic overexpression of caveolin-3 in skeletal muscle fibers induces a Duchenne-like muscular dystrophy phenotype. *Proceedings of the National Academy of Sciences of the United States of America* 97: 9689-9694.
- Gauguin, L., Klaproth, B., Sajid, W., Andersen, A. S., McNeil, K. A., Forbes, B. E. and De Meyts, P. (2007) Structural basis for the lower affinity of the insulin-like growth factors for the insulin receptor. *The Journal of Biological Chemistry* 283: 2604-2613.
- George Carlson, C., Bruemmer, K., Sesti, J., Stefanski, C., Curtis, H., Ucran, J., Lachey, J. and Seehra, J. S. (2011) Soluble activin receptor type IIB increases forward pulling tension in the mdx mouse. *Muscle & Nerve* 43: 694-699.
- Giordani, J., Bajard, L., Demignon, J., Daubas, P., Buckingham, M. and Maire, P. (2007) Six proteins regulate the activation of *Myf5* expression in embryonic mouse limbs. *PNAS* 104: 11310-11315.
- Gordon, E., Pegorara, E. and Hoffman, E. P. (revised 2009) Limb-girdle muscular dystrophy overview. *GeneReviews*: University of Washington, Seattle.
- Grifone, R., Demignon, J., Giordani, J., Niro, C., Souil, E., Bertin, F., Laclef, C., Xu, P.-X. and Maire, P. (2007) *Eya1* and *Eya2* proteins are required for hypaxial somitic myogenesis in the mouse embryo. *Developmental Biology* 302: 602-616.
- Hagiwara, Y., Fujita, M., Imamura, M., Noguchi, S. and Sasaoka, T. (2006) Caveolin-3 deficiency decreases the gene expression level of osteopontin in mdx mouse skeletal muscle. *Acta Myologica* 25: 53-61.
- Hagiwara, Y., Toshikuni, S., Araishi, K., Imamura, M., Yorifuji, H., Nonaka, I., Ozawa, E. and Kikuchi, T. (2000) Caveolin-3 deficiency causes muscle degeneration in mice. *Human Molecular Genetics* 9: 3047-3054.
- Haslett, J. N., Sanoudou, D., Kho, A. T., Bennett, R. R., Greenberg, S. A., Kohane, I. S., Beggs, A. H. and Kunkel, L. M. (2002) Gene expression comparison of biopsies from Duchenne muscular dystrophy (DMD) and normal skeletal muscle. *PNAS* 99: 15000-15005.
- Hasty, P., Bradley, A., Morris, J. H., Edmondson, D. G., Venuti, J. M., Olson, E. N. and Klein, W. H. (1993) Muscle deficiency and neonatal death in mice with a targeted mutation in the myogenin gene. *Nature* 364: 501-506.
- Hirata, A., Masuda, S., Tamura, T., Kai, K., Ojima, K., Fukase, A., Motoyoshi, K., Kamakura, K., Miyagoe-Suzuki, Y. and Takeda, S. (2003) Expression profiling of cytokines and related genes in regenerating skeletal muscle after cardiotoxin injection: a role for osteopontin. *American Journal of Pathology* 163: 203-215.
- Hoffman, E. P., Brown, R. H. J. and Kunkel, L. M. (1987) Dystrophin: the protein product of the Duchenne muscular dystrophy locus. *Cell* 51: 919-928.
- Holland, W. L., Knotts, T. A., Chavez, J. A., Wang, L.-P., Hoehn, K. L. and Summers, S. A. (2007) Lipid mediators of insulin resistance. *Nutrition Reviews* 65: S39-S56.

- Hulit, J., Bash, T., Fu, M. F., Galbiati, F., Albanese, C., Sage, D. R., Schlegel, A., Zhurinsky, J., Shtutman, M., Ben-Ze'ev, A., Lisanti, M. P. and Pestell, R. G. (2000) The cyclin D1 gene is transcriptionally repressed by caveolin-1. *Journal of Biological Chemistry* 275: 21203-21209.
- Ishii, T., Ohnuma, K., Murakami, A., Takasawa, N., Kobayashi, S., Dang, N., H. , Schlossman, S. F. and Morimoto, C. (2001) CD26-mediated signaling for T cell activation occurs in lipid rafts through its association with CD45RO. *PNAS* 98: 12138-12143.
- Janssen, I., Heymsfield, S. B., Wang, Z. and Ross, R. (2000) Skeletal muscle mass and distribution in 468 men and women aged 18-88 yr. *Journal of Applied Physiology* 89: 81-88.
- Jung, D., Yang, B., Meyer, J., Chamberlain, J. S. and Campbell, K. P. (1995) Identification and characterization of the dystrophin anchoring site on beta-dystroglycan. *Journal of Biological Chemistry* 270: 27305-27310.
- Karpati, G., Carpenter, S. and Prescott, S. (1988) Small-caliber skeletal muscle fibers do not suffer necrosis in mdx mouse dystrophy. *Muscle & Nerve* 11: 795-803.
- Kassar-Duchossoy, L., Gayraud-Morel, B., Gomès, D., Rocancourt, D., Buckingham, M., Shinin, V. and Tajbakhsh, S. (2004) Mrf4 determines skeletal muscle identity in Myf5:Myod double-mutant mice. *Nature* 431: 466-471.
- Kleopa, K. A., Drousiotou, A., Mavrikiou, E., Ormiston, A. and Kyriakides, T. (2006) Naturally occurring utrophin correlates with disease severity in Duchenne muscular dystrophy. *Human Molecular Genetics* 15: 1623-1628.
- Koenig, M., Monaco, A. P. and Kunkel, L. M. (1988) The complete sequence of dystrophin predicts a rod-shaped cytoskeletal protein. *Cell* 53: 219-228.
- Kota, J., Handy, C. R., Haidet, A. M., Montgomery, C. L., Eagle, A., Rodino-Klapac, L. R., Tucker, D., Shilling, C. J., Therlfall, W. R., Walker, C. M., Weisbrode, S. E., Janssen, P. M. L., Clark, K. R., Sahenk, Z., Mendell, J. R. and Kaspar, B. K. (2009) Follistatin Gene Delivery Enhances Muscle Growth and Strength in Nonhuman Primates *Science Translational Medicine* 1: 6-15.
- Kuang, S. H., Kuroda, K., Le Grand, F. and Rudnicki, M. A. (2007) Asymmetric self-renewal and commitment of satellite stem cells in muscle. *Cell* 129: 999-1010.
- Kunieda, T., Xian, M. W., Kobayashi, E., Imamichi, T., Moriwaki, K. and Toyoda, Y. (1992) Sexing of mouse preimplantation embryos by detection of Y-chromosome specific sequences using polymerase chain reaction. *Biology of Reproduction* 46: 692-697.
- Lalani, R., Bhasin, S., Byhower, F., Tarnuzzer, R., Grant, M., Shen, R., Asa, S., Ezzat, S. and Gonzalez-Cadavid, N. F. (2000) Myostatin and insulin-like growth factor-I and -II expression in the muscle of rats exposed to the microgravity environment of the NeuroLab space shuttle flight. *J Endocrinol* 167: 417-28.
- Lebakken, C. S., Venzke, D. P., Hrstka, R. F., Consolino, C. M., Faulkner, J. A., Williamson, R. A. and Campbell, K. P. (2000) Sarcospan-deficient mice maintain normal muscle function *Molecular and Cellular Biology* 20: 1669-1677.

- Lepper, C., Conway, S. J. and Fan, C. M. (2009) Adult satellite cells and embryonic muscle progenitors have distinct genetic requirements. *Nature* 460: 627-31.
- Lindenbaum, R. H., Clarke, G., Patel, C., Moncrieff, M. and Hughes, J. T. (1979) Muscular dystrophy in an X; 1 translocation female suggests that Duchenne locus is on X chromosome short arm. *Journal of Medical Genetics* 16: 389-392.
- Liu, F. and Roth, R. A. (1995) Grb-IR: a SH2-domain-containing protein that binds to the insulin receptor and inhibits its function. *Proc Natl Acad Sci* 93: 10287-10291.
- Lynch, G. S., Hinkle, R. T., Chamberlain, J. S., Brooks, S. V. and Faulkner, J. A. (2001) Force and power output of fast and slow skeletal muscles from mdx mice 6-28 months old *Journal of Physiology* 535: 591-600.
- Lyons, G. E., Ontell, M., Cox, R., Sassoon, D. and Buckingham, M. (1990) The expression of myosin genes in developing skeletal muscle in the mouse embryo. *The Journal of Cell Biology* 111: 1465-1476.
- Mann, C. J., Honeyman, K., Cheng, A. J., Ly, T., Lloyd, F., Fletcher, S., Morgan, J. E., Partridge, T. A. and Wilton, S. D. (2001) Antisense-induced exon skipping and synthesis of dystrophin in the mdx mouse. *PNAS* 98: 42-47.
- Manzur, A. Y., Kuntzer, T., Pike, M. and Swan, A. (2008) Glucocorticoid corticosteroids for Duchenne muscular dystrophy. *Cochrane Database of Systematic Reviews*(1): 65.
- Markham, L. W., Kinnet, K., Wong, B. L., Benson, D. W. and Cripe, L. H. (2008) Corticosteroid treatment retards development of ventricular dysfunction in Duchenne muscular dystrophy. *Neuromuscular Disorders* 18: 365-370.
- Massa, R., Silvestri, G., Zeng, Y. C., Martorana, A., Sancesario, G. and Bernardi, G. (1997) Muscle regeneration in mdx mice: resistance to repeated necrosis is compatible with myofiber maturity. *Basic and Applied Myology* 7: 387-394.
- Mathews, K. D. and Moore, S. A. (2003) Limb-girdle muscular dystrophy. *Current Neurology and Neuroscience Reports* 3: 78-85.
- Mauro, A. (1961) Satellite cells of skeletal muscle fibers. *Journal of Biophysical and Biochemical Cytology* 9: 493-495.
- McCroskery, S., Thomas, M., Maxwell, L., Sharma, M. and Kambadur, R. (2003) Myostatin negatively regulates satellite cell activation and self-renewal. *J Cell Biol* 162: 1135-47.
- McFarlane, C., Hennebry, A., Thomas, M., Plummer, E., Ling, N., Sharma, M. and Kambadur, R. (2008) Myostatin signals through Pax7 to regulate satellite cell self-renewal. *Exp Cell Res* 314: 317-29.
- McNally, E. M., de Sa Moreira, E., Duggan, D. J., Bonnemann, C. G., Lisanti, M. P., Lidov, H. G. W., Vainzof, M., Passos-Bueno, M. R., Hoffman, E. P., Zatz, M. and Kunkel, L. M. (1998) Caveolin-3 in muscular dystrophy. *Human Molecular Genetics* 7: 871-877.
- McPherron, A. C., Lawler, A. M. and Lee, S. J. (1997) Regulation of skeletal muscle mass in mice by a new TGF-beta superfamily member. *Nature* 387(6628): 83-90.

Merrick, D., Stadler, L. K. J., Larner, D. and Smith, J. (2009) Muscular dystrophy begins early in embryonic development and derives from stem cell loss and disrupted skeletal muscle formation. *Disease Models and Mechanisms* 2: 374-388.

Merrick, D., Ting, T., Stadler, L. K. J. and Smith, J. (2007) A role for Insulin-like growth factor 2 in specification of the fast skeletal muscle fibre. *Bmc Developmental Biology* 7: 16.

Meryon, E. (1851) On granular and fatty degeneration of the voluntary muscles. *Read to the Royal Medical and Chirurgical Society of London, Dec. 9th 1851*.

Michelson, A. M., Russell, E. S. and Harman, P. J. (1955) Dystrophia muscularis: a hereditary primary myopathy in the house mouse. *PNAS* 41: 1079-1084.

Miner, J. H. and Wold, B. (1990) Herculin, a forth member of the MyoD family of myogenic genes. *Proceedings of the National Academy of Sciences* 87: 1089-1093.

Minetti, C., Sotgia, F., Bruno, C., Scartezzini, P., Broda, P., Bado, M., Masetti, E., Mazzocco, M., Egeo, A., Donati, M. A., Volonte, D., Galbiati, F., Cordone, G., Bricarelli, F. D., Lisanti, M. P. and Zara, F. (1998) Mutations in the caveolin-3 gene cause autosomal dominant limb-girdle muscular dystrophy. *Nature Genetics* 18: 365-368.

Miyake, M., Hayashi, S., Taketa, Y., Iwasaki, S., Watanabe, K., Ohwada, S., Aso, H. and Yamaguchi, T. (2010) Myostatin down-regulates the IGF-2 expression via ALK-Smad signaling during myogenesis in cattle. *Anim Science Journal* 81: 223-9.

Moore, J. W., Dionne, C., Jaye, M. and Swain, J. L. (1991) The messenger-RNAs encoding acidic FGF, basic FGF and FGF receptor are coordinately down-regulated during myogenic differentiation. *Development* 111: 741-748.

Muntoni, F., Fisher, I., Morgan, J. E. and Abraham, D. (2002) Steroids in Duchenne muscular dystrophy: from clinical trials to genomic research. *Neuromuscular Disorders* 12(S162-S165).

Murray, J. M., Davies, K. E., Harper, P. S., Meredith, L., Mueller, C. R., Williamson, R. and (1982) Linkage relationship of a cloned DNA sequence on the short arm of the X chromosome to Duchenne muscular dystrophy. *Nature* 300: 69-71.

Nabeshima, Y., Hanaoka, K., Hayasaka, M., Esumi, E., Li, S., Nonaka, I. and Nabeshima, Y.-I. (1993) Myogenin gene disruption results in perinatal lethality because of severe muscle defect. *Nature* 364: 532-535.

Naidu, P. S., Ludolph, D. C., To, R. Q., Hinterberger, T. J. and Konieczny, S. F. (1995) Myogenin and MEF2 function synergistically to activate the MRF4 promoter during myogenesis. *Molecular and Cellular Biology* 15: 2707-2718.

Narita, S. and Yorifuji, H. (1999) Centrally nucleated fibers (CNFs) compensate the fragility of myofibers in mdx mouse. *Neuroreport* 10: 3233-3235.

Nigro, V., Okazaki, Y., Belsito, A., Piluso, G., Matsuda, Y., Politano, L., Nigro, G., Ventura, C., Abbondanza, C., Molinari, A. M., Acampora, D., Nishimura, M., Hayashizaki, Y. and Puca, G. A. (1997) Identification of the Syrian hamster cardiomyopathy gene *Human Molecular Genetics* 6: 601-607.

Noguchi, S., Tsukahara, T., Fujita, M., Kurokawa, R., Tachikawa, M., Toda, T., Tsujimoto, A., Arahata, K. and Nishino, I. (2003) cDNA microarray analysis of individual Duchenne muscular dystrophy patients. *Human Molecular Genetics* 12: 595-600.

Nueda, M. L., García-Ramírez, J. J., Laborda, J. and Baladrón, V. (2008) Dlk1 specifically interacts with insulin-like growth factor binding protein 1 to modulate adipogenesis of 3T3-L1 cells. *J Mol Biol* 379: 428-442.

Ohlendieck, K. and Campbell, K. P. (1991) Dystrophin-associated proteins are greatly reduced in skeletal muscle from mdx mice. *Journal of Cell Biology* 115: 1685-1694.

Ohnuma, K., Inoue, H., Uchiyama, M., Yamochi, T., Hosono, O., Dang, N. H. and Morimoto, C. (2006) T-cell activation via CD26 and caveolin-1 in rheumatoid synovium. *Modern Rheumatology* 16: 3-13.

Ohsawa, Y., Hagiwara, H., Nakatani, M., Yasue, A., Moriyama, K., Murakami, T., Tsuchida, K., Noji, S. and Sunada, Y. (2006) Muscular atrophy of caveolin-3-deficient mice is rescued by myostatin inhibition. *The Journal of Clinical Investigation* 116: 2924-2934.

Ohsawa, Y., Toko, H., Katsura, M., Morimoto, K., Yamada, H., Ichikawa, Y., Murakami, T., Ohkuma, S., Komuro, I. and Sunada, Y. (2004) Overexpression of P104L mutant caveolin-3 in mice develops hypertrophic cardiomyopathy with enhanced contractility in association with increased endothelial nitric oxide synthase activity. *Human Molecular Genetics* 13: 151-157.

Olguin, H. C. and Olwin, B. B. (2004) Pax-7 up-regulation inhibits myogenesis and cell cycle progression in satellite cells: a potential mechanism for self-renewal. *Developmental Biology* 275: 375-388.

Olson, E. N. and Klein, W. H. (1994) bHLH factors in muscle development: dead lines and commitments, what to leave in and what to leave out. *Genes and Development* 8: 1-8.

Onopiuk, M., Brutkowski, W., Wierzbicka, K., Wojciechowska, S., Szczepanowska, J., Fronk, J., Lochmüller, H., Górecki, D. C. and Zabłocki, K. (2009) Mutation in dystrophin-encoding gene affects energy metabolism in mouse myoblasts. *Biochemical and Biophysical Research Communications* 386: 463-466.

Ooi, J., Yajnik, V., Immanuel, D., Gordon, M., Moskow, J. J., Buchberg, A. M. and Margolis, B. (1995) The cloning of Grb10 reveals a new family of SH2 domain proteins. *Oncogene* 10: 1621-30.

Oshikawa, J., Otsu, K., Toya, Y., Tsunematsu, T., Hankins, R., Kawabe, J., Minamisawa, S., Umemura, S., Hagiwara, Y. and Ishikawa, Y. (2004) Insulin resistance in skeletal muscles of caveolin-3-null mice. *Proceedings of the National Academy of Sciences of the United States of America* 101: 12670-12675.

Ott, M. O., Bober, E., Lyons, G., Arnold, H. and Buckingham, M. (1991) Early expression of the myogenic regulatory gene, myf-5, in precursor cells of skeletal muscle in the mouse embryo. *Development* 111: 1097-1107.

Oustanina, S., Hause, G. and Braun, T. (2004) Pax7 directs postnatal renewal and propagation of myogenic satellite cells but not their specification

The Embo Journal 23: 3430-3439.

Patapoutian, A., Yoon, J. K., Miner, J. H., Wang, S., Stark, K. and Wold, B. (1995) Disruption of the mouse MRF4 gene identifies multiple waves of myogenesis in the myotome. *Development* 121: 3347-3358.

Petrof, B. J., Shrager, J. B., Stedman, H. H., Kelly, A. M. and Sweeney, H. L. (1993) Dystrophin protects the sarcolemma from stresses developed during muscle-contraction. *Proceedings of the National Academy of Sciences of the United States of America* 90: 3710-3714.

Petrof, B. J., Stedman, H. H., Shrager, J. B., Eby, J., Sweeney, H. L. and Kelly, A. M. (1993) Adaptations in myosin heavy chain expression and contractile function in dystrophic mouse diaphragm. *American Journal of Physiology* 265: C834-C841.

Pistilli, E. E., Bogdanovich, S., Goncalves, M. D., Ahima, R. S., Lachey, J., Seehra, J. and Khurana, T. (2011) Targeting the activin type IIB receptor to improve muscle mass and function in the mdx mouse model of Duchenne muscular dystrophy. *The American Journal of Pathology* 178: 1287-1297.

Porter, J. D., Khanna, S., Kaminski, H. J., Rao, J. S., Merriam, A. P., Richmonds, C. R., Leahy, P., Li, J., Guo, W. and Andrade, F. H. (2002) A chronic inflammatory response dominates the skeletal muscle molecule signature dystrophin deficient mdx *Human Molecular Genetics* 11: 263-272.

Porter, J. D., Merriam, A. P., Leahy, P., Gong, B., Feuerman, J., Cheng, G. and Khanna, S. (2004) Temporal gene expression profiling of dystrophin-deficient (mdx) mouse diaphragm identifies conserved and muscle group-specific mechanisms in the pathogenesis of muscular dystrophy *Human Molecular Genetics* 13: 257-269.

Pownall, M. E., Gustafsson, M. K. and Emerson Jr., C. P. (2002) Myogenic regulatory factors and the specification of muscle progenitors in vertebrate embryos. *Annual Review of Cell and Developmental Biology* 18: 747-783.

Rando, T. A. (2001) The dystrophin-glycoprotein complex, cellular signaling, and the regulation of cell survival in the muscular dystrophies. *Muscle & Nerve* 24: 1575-1594.

Relaix, F., Rocancourt, D., Mansouri, A. and Buckingham, M. (2005) A pax3/pax7-dependent population of skeletal muscle progenitor cells. *Nature* 435: 948-953.

Rentschler, S., Linn, H., Deininger, K., Bedford, M. T., Espanel, X. and Sudol, M. (1999) The WW domain of dystrophin requires EF-hands region to interact with beta-dystroglycan. *Biological Chemistry* 380: 431-442.

Repetto, S., Bado, M., Broda, P., Lucania, G., Masetti, E., Sotgia, F., Carbone, I., Pavan, A., Bonilla, E., Cordone, G., Lisanti, M. P. and Minetti, C. (1999) Increased number of caveolae and caveolin-3 overexpression in Duchenne muscular dystrophy. *Biochemical and Biophysical Research Communications* 261: 547-550.

Rhodes, S. J. and Konieczny, S. F. (1989) Identification of MRF4: a new member of the muscle regulatory factor gene family. *Genes and Development* 3: 2050-2061.

Ríos, R., Carneiro, I., Arce, V. M. and Devesa, J. (2001) Myostatin is an inhibitor of myogenic differentiation *Am J Physiol Cell Physiol* 282: 993-999.

- Rodriguez, D. A., Tapia, J. C., Fernandez, J. G., Torres, V. A., Munoz, N., Galleguillos, D., Leyton, L. and Quest, A. F. G. (2009) Caveolin-1-mediated suppression of cyclooxygenase-2 via a beta-catenin-Tcf/Lef-dependent transcriptional mechanism reduced prostaglandin E-2 production and Survivin expression. *Molecular Biology of the Cell* 20: 2297-2310.
- Rudnicki, M. A., Braun, T., Hinuma, S. and Jaenisch, R. (1992) Inactivation of MyoD in mice leads to up-regulation of the myogenic HLH gene Myf-5 and results in apparently normal muscle development. *Cell* 71: 383-390.
- Rudnicki, M. A., Schnegelsberg, P. N. J., Stead, R. H., Braun, T., Arnold, H. H. and Jaenisch, R. (1993) MyoD or Myf-5 is required for the formation of skeletal muscle. *Cell* 75: 1351-1359.
- Sassoon, D., Lyons, G., Wright, W. E., Lin, V., Lassar, A., Weintraub, H. and Buckingham, M. (1989) Expression of two myogenic regulatory factors myogenin and MyoDl during mouse embryogenesis. *Nature* 341: 303-307.
- Schmalbruch, H. (2006) The satellite cell of skeletal muscle fibres. *Brazilian Journal of Morphological Science* 23: 159-172.
- Schultz, E., Gibson, M. C. and Champion, T. (1978) Satellite cells are mitotically quiescent in mature mouse muscle - EM and autoradiographic study. *Journal of Experimental Zoology* 206: 451-456.
- Seale, P., Sabourin, L. A., Girgis-Gabardo, A., Mansouri, A., Gruss, P. and Rudnicki, M. A. (2000) Pax7 is required for the specification of myogenic satellite cells. *Cell* 102: 777-786.
- Shavlakadze, T., Chai, J., Maley, K., Cozens, G., Grounds, G., Winn, N., Rosenthal, N. and Grounds, M. D. (2010) A growth stimulus is needed for IGF-1 to induce skeletal muscle hypertrophy in vivo. *Journal of Cell Science* 123: 960-971.
- Sicinski, P., Geng, Y., Rydercook, A. S., Barnard, E. A., Darlison, M. G. and Barnard, P. J. (1989) The molecular-basis of muscular dystrophy in the mdx mouse - a point mutation. *Science* 244: 1578-1580.
- Simonds, A. K., Muntoni, F., Heather, S. and Fielding, S. (1998) Impact of nasal ventilation on survival in hypercapnic Duchenne muscular dystrophy. *Thorax* 53: 949-952.
- Sinha, B., Koster, D., Ruez, R., Gonnord, P., Bastiani, M., Abankwa, D., Stan, R. V., Butler-Browne, G., Védie, B., Johannes, L., Morone, N., Parton, R. G., Raposo, G., Senz, P., Lamaze, C. and Nassoy, P. (2011) Cells respond to mechanical stress by rapid disassembly of caveolae. *Cell* 144: 402-413.
- Smart, E. J., Graf, G. A., McNiven, M. A., Sessa, W. C., Engelman, J. A., Scherer, P. E., Okamoto, T. and Lisanti, M. P. (1999) Caveolins, liquid-ordered domains, and signal transduction. *Mol Cell Biol* 19: 7289-304.
- Smith, J., Fowkes, G. and Schofield, P. N. (1995) Programmed cell death in dystrophic (mdx) muscle is inhibited by IGF-II. *Cell Death and Differentiation* 2: 243-251.

- Smith, J., Goldsmith, C., Ward, A. and LeDieu, R. (2000) IGF-II ameliorates the dystrophic phenotype and coordinately down-regulates programmed cell death. *Cell Death and Differentiation* 7: 1109-1118.
- Song, K. S., Scherer, P. E., Tang, Z. L., Okamoto, T., Li, S. W., Chafel, M., Chu, C., Kohtz, D. S. and Lisanti, M. P. (1996) Expression of caveolin-3 in skeletal, cardiac, and smooth muscle cells - Caveolin-3 is a component of the sarcolemma and co-fractionates with dystrophin and dystrophin-associated glycoproteins. *Journal of Biological Chemistry* 271: 15160-15165.
- Sotgia, F., Lee, J. K., Das, K., Bedford, M., Petrucci, T. C., Macioce, P., Sargiacomo, M., Bricarelli, F. D., Minetti, C., Sudol, M. and Lisanti, M. P. (2000) Caveolin-3 directly interacts with the C-terminal tail of beta-dystroglycan - Identification of a central WW-like domain within caveolin family members. *Journal of Biological Chemistry* 275: 38048-38058.
- Stedman, H. H., Sweeney, H. L., Shrager, J. B., Maguire, H. C., Panettieri, R. A., Petrof, B., Narusawa, M., Leferovich, J. M., Sladky, J. T. and Kelly, A. M. (1991) The mdx mouse diaphragm reproduces the degenerative changes of Duchenne muscular dystrophy. *Nature* 352: 536-9.
- Straub, V., Ettinger, A. J., Durbeej, M., Venzke, D. P., Cutshall, S., Sanes, J. R. and Campbell, K. P. (1999) ϵ -Sarcoglycan replaces α -sarcoglycan in smooth muscle to form a unique dystrophin-glycoprotein complex. *The Journal of Biological Chemistry* 274: 27989-27996.
- Summerbell, D., Halai, C. and Rigby, P. W. J. (2002) Expression of the myogenic regulatory factor MRF4 precedes or is contemporaneous with that of myf5 in the somitic bud. *Mechanisms of Development* 117: 331-335.
- Sun, D., Li, H. and Zolkiewska, A. (2008) The role of Delta-like 1 shedding in muscle cell self-renewal and differentiation. *Journal of Cell Science* 121: 3815-3823.
- Sunada, Y., Ohi, H., Hase, A., Ohi, H., Hosono, T., Arata, S., Higuchi, S., Matsumura, K. and Shimizu, T. (2001) Transgenic mice expressing mutant caveolin-3 show severe myopathy associated with increased nNOS activity. *Human Molecular Genetics* 10: 173-178.
- Tanabe, Y., Esaki, K. and Nomura, T. (1986) Skeletal muscle pathology in X chromosome-linked muscular dystrophy (mdx) mouse. *Acta Neuropathol* 69: 91-5.
- Tang, Z. L., Scherer, P. E., Okamoto, T., Song, K., Chu, C., Kohtz, D. S., Nishimoto, I., Lodish, H. F. and Lisanti, M. P. (1996) Molecular cloning of caveolin-3, a novel member of the caveolin gene family expressed predominantly in muscle. *Journal of Biological Chemistry* 271: 2255-2261.
- Tennyson, C. N., Klamut, H. J. and Worton, R. G. (1995) The human dystrophin gene requires 16 hours to be transcribed and is cotranscriptionally spliced. *Nature Genetics* 9: 184 - 190.
- Thomas, M., Langley, B., Berry, C., Sharma, M., Kirk, S., Bass, J. and Kambadur, R. (2000) Myostatin, a negative regulator of muscle growth, functions by inhibiting myoblast proliferation. *J Biol Chem* 275: 40235-40243.
- Tidball, J. G., Albrecht, D. E., Lokensgard, B. E. and Spencer, M. J. (1995) Apoptosis precedes necrosis of dystrophin-deficient muscle. *Journal of Cell Science* 108: 2197-2204.

Tinsley, J., Deconinck, N., Fisher, R., Kahn, D., Phelps, S., Gillis, J.-M. and Davies, K. E. (1998) Expression of full-length utrophin prevents muscular dystrophy in mdx mice. *Nature Medicine* 4: 1441-1444.

Tinsley, J. M., Fairclough, R. J., Storer, R., Wilkes, F. J., Potter, A. C., Squire, S. E., Powell, D. S., Cozzoli, A., Capogrosso, R. F., Lambert, A., Wilson, F. X., Wren, S. P., De Luca, A. and Davies, K. E. (2011) Daily treatment with SMT1100, a novel small molecule utrophin upregulator, dramatically reduces the dystrophic symptoms in the *mdx* mouse. *PLoS ONE* 6: e19189.

Tinsley, J. M., Potter, A. C., Phelps, S. R., Fisher, R., Trickett, J. I. and Davies, K. E. (1996) Amelioration of the dystrophic phenotype of mdx mice using a truncated utrophin transgene. *Nature* 384: 349-353.

Totsuka, T., Watanabe, K., Uramoto, J., Sakuma, K. and Mizutani, T. (1998) Muscular dystrophy: centronucleation may reflect a compensatory activation of defective myonuclei. *Journal of Biomedical Science* 5: 54-61.

Turk, R., Sterrenburg, E., de Meijer, E. J., van Ommen, G.-J. B., den Dunnen, J. T. and 't Hoen, P. A. C. (2005) Muscle regeneration in dystrophin-deficient mdx mice studied by gene expression profiling. *BMC Genomics* 6.

Vaghy, P. L., Fang, J., Wu, W. R. and Vaghy, L. P. (1998) Increased caveolin-3 levels in mdx mouse muscles. *Febs Letters* 431: 125-127.

Venema, V. J., Ju, H., Zou, R. and Venema, R. C. (1997) Interaction of neuronal nitric-oxide synthase with caveolin-3 in skeletal muscle. *The American Society for Biochemistry and Molecular Biology* 272: 28187-28190.

Volonte, D., Liu, Y. and Galbiati, F. (2005) The modulation of caveolin-1 expression controls satellite cell activation during muscle repair. *The FASEB Journal* 19: 237-239.

Volonte, D., Peoples, A. J. and Galbiati, F. (2003) Modulation of myoblast fusion by caveolin-3 in dystrophic skeletal muscle cells: implications for Duchenne muscular dystrophy and limb-girdle muscular dystrophy-1C. *Molecular Biology of the Cell* 14: 4075-4088.

Walton, J. N. (1956) The inheritance of muscular dystrophy: further observations. *Annals of Human Genetics* 21: 40-58.

Walton, J. N. and Nattrass, F. J. (1954) On the classification, natural history and treatment of the myopathies. *Brain* 77: 169-231.

Weber, G. F., Ashkar, S., Glimcher, M. J. and Cantor, H. (1996) Receptor-ligand interaction between CD44 and osteopontin (Eta-1). *Science* 271: 509-512.

Weintraub, H., Davis, R., Tapscott, S., Thayer, M., Krause, M., Benze, R., Blackwell, T. K., Turner, D., Rupp, R., Hollenberg, S., Zhuang, Y. and Lassar, A. (1991) The myoD gene family: nodal point during specification of the muscle cell lineage. *Science* 251: 761-766.

Weiss, A. and Leinwand, L. A. (1996) The mammalian myosin heavy chain gene family. *Annu Rev Cell Dev Biol* 12: 417-39.

Welch, E. M., Barton, E. R., Zhuo, J., Tomizawa, Y., Friesen, W. J., Trifillis, P., Paushkin, S., Patel, M., Trotta, C. R., Hwang, S., Wilde, R. G., Karp, G., Takasugi, J., Chen, G., Jones, S., Ren, H., Moon, Y. C., Corson, D., Turpoff, A. A., Campbell, J. A., Conn, M. M., Khan, A., Almstead, N. G., Hedrick, J., Mollin, A., Risher, N., Weetall, M., Yeh, S., Branstrom, A. A., Colacino, J. M., Babiak, J., Ju, W. D., Hirawat, S., Northcutt, V. J., Miller, L. L., Spatrick, P., He, F., Kawana, M., Feng, H., Jacobson, A., Peltz, S. W. and Sweeney, H. L. (2007) PTC124 targets genetic disorders caused by nonsense mutations. *Nature* 447: 87-91.

Wernig, A., Bone, M., Irintchev, A., Schafer, R. and Cullen, M. J. (2004) M-cadherin is a reliable marker of quiescent satellite cells in mouse skeletal muscle. *Basic Applied Myol.* 14: 161-168.

Williams, D. A., Head, S. I., Lynch, G. S. and Stephenson, D. G. (1993) Contractile properties of skinned muscle fibres from young and adult normal and dystrophic (*mdx*) mice. *Journal of Physiology* 460: 51-67.

Williamson, R. A., Henry, M. D., Daniels, K. J., Hrstka, R. F., Lee, J. C., Sunada, Y., IbraghimovBeskrovnaya, O. and Campbell, K. P. (1997) Dystroglycan is essential for early embryonic development: Disruption of Reichert's membrane in *Dag1*-null mice. *Human Molecular Genetics* 6: 831-841.

Wong, B. L. Y. and Christopher, C. (2002) Corticosteroids in Duchenne muscular dystrophy: a reappraisal. *17*: 183-190.

Wright, W. E., Sassoon, D. A. and Lin, V. K. (1989) Myogenin, a factor regulating myogenesis, has a domain homologous to MyoD. *Cell* 56: 607-617.

Wu, J. Y., Kuban, K. C. K., Allred, E., Shapiro, F. and Darras, B. T. (2005) Association of Duchenne muscular dystrophy with autism spectrum disorder. *Journal of Child Neurology* 20: 790-795.

Xu, H., Christmas, P., Wu, X.-R., Wewer, U. M. and Engvall, E. (1994) Defective muscle basement membrane and lack of M-laminin in the dystrophic *dy/dy* mouse. *PNAS* 91: 5572-5576.

Yagami-Hiromasa, T., Sato, T., Kurisaki, T., Kamijo, K., Nabeshima, Y.-i. and Fujisawa-Sehara, A. (2002) A metalloprotease-disintegrin participating in myoblast fusion. *Nature* 377: 652 - 656.

Zatz, M., Vianna-Morgante, A. M., Campos, P. and Diament, A. J. (1981) Translocation (X;6) in a female with Duchenne muscular dystrophy: implications for the localisation of the DMD locus. *Journal of Medical Genetics* 18: 442-447.

Zellweger, H. and Antonik, A. (1975) Newborn screening for Duchenne muscular dystrophy. *Pediatrics* 55: 30 -34.

Zhang, W., Behringer, R. R. and Olson, E. N. (1995) Inactivation of the myogenic bHLH gene MRF4 results in upregulation of myogenin and rib anomalies. *Genes and Development* 9: 1388-1399.

Zhu, X., Hadhazy, M., Wehling, M., Tidball, J. G. and McNally, E. M. (2000) Dominant negative myostatin produces hypertrophy without hyperplasia in muscle. *Febs Letters* 474: 71-75.

Zubrzycka-Gaarn, E. E., Bulman, D. E., Karpati, G., Burghes, A. H. M., Belfall, B., Klamut, H. J., Talbot, J., Hodges, R. S., Ray, P. N. and Worton, R. G. (1988) The Duchenne muscular dystrophy gene product is localized in sarcolemma of human skeletal muscle *Nature* 333: 466-469.

APPENDICES

APPENDIX 1 – Suppliers of Chemicals and Equipment

Alta Biosciences (Building Y10, University of Birmingham, Edgbaston, Birmingham, B15 2TT, UK).

Primers:

CAV3: F (D72502DL) – 5' ATT-CCT-GTT-CGC-CTG-TAT-C- 3' R (D72501DL) – 5' AGG-ACC-AAC-CGA-ATC-TTC-TG- 3'

Dystrophin mdx: F (D71047DL) – 5' CTT-CTG-TGA-TGT-GAG-GAC-ATA- 3' R (D71048DL) – 5' CTA-GCT-TTT-GGC-AGC-TTT-CC- 3'

NEO: F – 5' GCA-CGC-AGG-TTC-TCC-GGC- 3' R – 5' GTC CTG ATA GCG GTC CGC C- 3'

SRY: F (D64053DL) – 5' TCT-TAA-ACT-CTG-AAG-AAG-AGA-C- 3' R (D64054DL) – 5' GTC-TTG-CCT-GTA-TGT-GAT-GG- 3'

Applied Biosystems (Life Technologies Corporation (Headquarters), 5791 Van Allen Way, PO Box 6482, Carlsbad, California 92008, USA).

Capillary Sequencer ABI 3730

Sequence Scanner Software v1.0

BD Biosciences (Edmund Halley Road - Oxford Science Park, Oxford, OX4 4DQ)

50 mL Falcon tubes (Cat. No. 352070)

BDH

Eosin Yellowish (Cat. No. 341972Q)

Sodium Hydroxide Pearl (Cat. No. 104384F)

Bibby Scientific Limited, Beacon Road, Stone, Staffordshire ST15 0SA, UK
Digital block heater (Cat. No. SBH200D)

Techne DB-2A Dri-Block Heater (Cat. No. FDB02AD)

BioLine Ltd (Unit 16, The Edge Business Centre, Humber Road, London, NW2

6EW, UK)

Agarose Molecular Grade (Cat. No. BIO-41025)

**Bio-Rad Laboratories Ltd (Bio-Rad House,
Maxted Road, Hemel Hempstead, Hertfordshire, HP2 7DX, UK)**

Mini Protean II Electrophoresis Cell (Cat No. 165-3301)

Mini Trans-blot blotting Cell (Cat No. 170-3930)

**Carl Zeiss Ltd. (15-20 Woodfield Road, Welwyn Garden City, Hertfordshire, AL7
1JQ, UK)**

Stemi 1000 dissecting microscope

**Dako UK Ltd (Cambridge House, St Thomas Place, Ely, Cambridgeshire, CB7 4EX,
UK)**

DAB Chromogen (Cat. No. S3000)

**Developmental Studies Hybridoma Bank (University of Iowa, Department of
Biology, 028 Biology Building East, Iowa City, Iowa, 52242-1324, USA)**

Mouse monoclonal anti-pax7 antibody

Mouse monoclonal anti-pan myosin antibody (MF20)

**DJB Labcare Ltd. (20 Howard Way, Interchange Business Park, Newport Pagnell,
Buckinghamshire, MK16 9QS, UK.)**

Hettich Mikro 20 centrifuge

**Eppendorf UK Ltd (Endurance House, Chivers Way, Histon, Cambridge, CB24 9ZR,
UK)**

Centrifuge (Cat. No. 5415 C)

**Fisher Scientific UK Ltd (Bishop Meadow Road, Loughborough, Leicestershire,
LE11 5RG, UK)**

Boric acid (Cat. No. B/3800/53)

Chloroform (Cat. No. C/0354/17)

Diaminoethanetetra-acetic acid disodium salt (Cat. No. D/0700/53)

Ethanol, absolute (Cat. No. E/0650DF/17)

Glacial acetic acid (Cat. No. A/0360/PB17)

Glycine (Cat. No. G/P460/53)

Hydrochloric acid (Cat. No. 101252F)
Methanol (Cat. No. M/4000/17)
Propan-2-ol (Cat. No. P/7490/17)
Shandon Histoplast paraffin wax (Cat. No. SD6774006)
Sodium Chloride (Cat. No. S/3160/53)
Sodium dodecyl sulphate (Cat. No. S/5200/53)
Stirring hotplate (Cat. No. 11-503-50SH)
Tri-Sodium Citrate (Cat. No. S/3320/53)
TRIS (hydroxymethyl methylamine; Cat. No. T/P630/53)
Xylene, (Cat. No. X/0250/17)

GE Healthcare UK Ltd (Amersham Place, Little Chalfont, Buckinghamshire HP7 9NA, UK)

Amersham™ Hybond™ - ECL Nitrocellulose membrane. (Cat. No. RPN203D)
Goat-anti-mouse IgG biotinylated whole antibody (Cat. No. RPN1177V1)

Geneflow Ltd (Fradley Business Centre, WoodEnd Lane, Fradley, Staffordshire, WS13 8NF, UK)

Protogel, 30% Acrylamide, 0.8% (w/v) Bis-Acrylamide Stock Solution (37.5:1)

Gilson Inc. (3000 Parmenter Street, P.O. Box 620027, Middleton, WI 53562-0027, USA)

Pipette tips

Grants Instruments (Cambridge) Ltd, UK (29 Station Road, Shepreth, Cambridgeshire, SG8 6GB, UK)

Water bath

Jenkons Scientific Ltd. (Cherrycourt Way, Stanbridge Road, Leighton Buzzard, Bedfordshire, LU7 4UA, UK)

U-1800 Spectrophotometer, DigLab, Hitachi

Kendro Laboratory Products Plc (Stortford Hall Park, Bishop's Stortford, Hertfordshire, CM23 5GZ, UK)

Heraeus Incubator

Leica Microsystems Ltd, UK (Davy Avenue, Knowlhill, Milton Keynes, MK5 8LB, UK)

Inverted microscope - Leica DMIRB

1150/Autocut Microtome

Premier International Foods (UK) Ltd (Bridge Road, Long Sutton, Spalding, Lincs, PE12 9EQ, UK)

Marvel dried skimmed milk

Merck (Boulevard Industrial Park, Padge Road, Beeston, Nottingham, NG9 2JR)

Haematoxylin solution modified acc. To Gill III (Cat. No. 1.05174.0500)

Molecular Devices Ltd. (135 Wharfedale Road, Winnersh Triangle, Winnersh, Wokingham, RG41 5RB, UK)

Emax microplate reader

Nikon UK Ltd (380 Richmond Road, Kingston Upon Thames, Surrey, KT2 5PR, UK)

Nikon Eclipse E600 Microscope

Novocastra Laboratories Ltd (Balliol Business Park West, Benton Lane, Newcastle upon Tyne, NE12 8EW, UK)

Anti-developmental Myosin Antibody (Cat. No. NCL-MHCd)

Nunc Plasticware (Life Technologies Ltd, 3 Fountain Drive, Ichinnan Business Park, Paisley, PA4 9RF, UK)

96-well plates (Cat No. 167008A)

Petri-dishes

Panasonic UK Ltd. (Panasonic House, Willoughby Road, Bracknell, Berkshire, RG12 8FP, UK)

Microwave oven

Pechiney Plastic Packaging (Menasha, WI 549252, USA)

Parafilm, laboratory Film (PM-996)

Perkin Elmer (Saxon Way Bar Hill, Cambridge, Cambridgeshire, CB23 8SL, UK)

Biotinyl Tyramide solution plus amplification diluent (Cat. No. SAT700001EA)

Streptavidin-HRP (Cat. No. NEL 750001EA)

Pierce (Perbio Sciences UK Ltd, Century House, High Street, Tattenhall, Cheshire, CH3 9RJ, UK)

Albumin Standard Ampules (Cat. No. 23209)

Coomassie® Protein Assay Reagent (Cat. No. 1856209)

Supersignal® West Pico Chemiluminescent substrate kit (Cat. No. 34080)

Polysciences Inc. (Park Scientific Ltd., 24 Low Farm Place, Moulton Park, GB-NN3 6HY, Northampton, UK)

Peel-A-Way® Disposable Embedding Molds (Cat. No. 18646A-1)

Reichert-Jung (Germany)

1150/Autocut microtome

Roche Diagnostic Ltd (Charles Avenue, Burgess Hill, RH15 9RY, UK)

Complete mini Protease Inhibitor Cocktail tablets (Cat. No. 11836153001)

Santa Cruz Biotechnology, Inc (Bergheimer Str. 89-2 69115, Heidelberg, Germany)

Anti-rabbit IgG-HRP (Cat no. sc-2004; Lot No. K159)

Goat anti-mouse IgG-HRP (Cat No. sc-2005; Lot No. J1802)

Sigma-Aldrich (Sigma-Aldrich Company Ltd, Fancy Road, Poole, Dorset, BD12 4QH, UK)

Anti-fast skeletal Myosin primary antibody (Cat No. M-4276; Clone MY-32))

Anti-tubulin primary antibody (Cat No. T9026)

Ammonium Persulfate (APS) (Cat No. A3678; Lot No. 022K1258)

Bromphenol Blue (3',3'',5',5'' Tetrabromophenolsulfonephthalein) (Cat No. B-5525; Lot No. 47H3638)

Deoxycolic Acid (Cat No. D-6750; Lot No. 110K0192)

Diaminoethanetetra-acetic acid disodium salt (Cat No. D/0700/53; Lot No. 0113456)

Dimethyl Sulfoxide (DMSO) (Cat. No. D2650)

Ethidium Bromide (E-1510)

Hydrogen Peroxide 30 wt.% sol. In water (Cat. No. H1009)

Paraformaldehyde (Cat No. EC-890; Lot No. 10-02-29)

Potassium Chloride KCl (Cat No. P9333; Lot No. 7447407)

SDS Sample buffer , Laemmli (Cat No. S-3401; Lot No. 20K9342)

0.0075 M Potassium Chloride (KCl) solution (Cat No. P9327; Lot No. 22K2424)
TEMED (Cat No. T-9281; Lot No. 38H0438)

Tween® 20 (Cat. No. P7949)

Sony (Pipersway, Thatcham, Berkshire RG19 4LZ, UK)

Gel imaging camera, video graphic printer (UP-860LE)

Stuart Scientific Co Ltd (Holmethorpe Industrial Estate, Redhill, Surrey RH1 2NB, UK)

Gyro-Rocker® Shaker (STR9)
Hybridisation oven/shaker S120H

Swann-Morton Ltd, UK (Owlerton Green, Sheffield, S6 2BJ, UK)

Sterile Scalpels.

Tefal (PO Box 467; Slough PDO, Berkshire SL3 8WD, UK)

'Kwisto' Pressure cooker

Terumo UK Ltd. (3 Unily Grove, Off School Lane, Knowsley Industrials Park, Knowsley, Merseyside, L34 9GI, UK)

18 gauge needles (Cat No. NN-1838R)

Upstate Biotechnology Incorporated (199 Saranac Avenue, Lake Placid, New York, 12946, USA)

Anti-Igf2 IgG₁ Mouse Monoclonal. (Cat Number 05-166; Lot No. 05166)

Vector Laboratories Ltd (3 Accent Park, Blakewell Road, Orton Southgate, Peterborough, PE2 6XS, UK)

ImmEdge Hydrophobic Barrier Pen™ (Cat. No. H-4000)

VWR International (Merk Ltd, Hunter Boulevard, Magna Park, Lutterworth, Leics, LE17 4XN, UK)

Depex Mounting medium 'Gurr' (Cat No. 361252B; Lot No. OB327384)

Eosin (Cat No. 341972Q; Lot No. K28531926205)

Glass Coverslips 22 x 64 mm (Cat No. 406/0188/52)

Glass Homogeniser (1-5 ml; Cat No. 409/1435/09)

Paramat, wax (Cat No. 36/144V; Lot No. 114080)

Sodium Hypochlorite Solution (Cat. No. 301696S)

Sodium dodecyl sulphate (Cat No. S/5200/53; Batch No. 0398855)

Superfrost Plus Microscope Slides (Cat No. 406/0179/00)

X-Ograph Imaging Systems Ltd (Xograph House, Hampton Street, Tetbury, Gloucestershire, GL8 8LD, UK)

X-Ograph X2 machine

CHEMICAL SOLUTIONS

4% Paraformaldehyde (PFA)

4 g Paraformaldehyde (Sigma-Aldrich, UK) – weigh with care, wearing a facemask

100 ml PBS (see above)

Heated to 70°C, in a fumehood, to allow powder to go in to solution, ensuring temperature did not go above 70°C, as PFA is explosive at high temperatures.

0.5 M EDTA

16.4 g EDTA (Fisher Scientific Ltd, UK)

100 ml dH₂O

pH 7.5 with concentrated HCl (Fisher Scientific Ltd, UK)

Immunohistochemistry (IHC)

Sodium Citrate Buffer

4.7 g Sodium Citrate (Fisher Scientific Ltd, UK)

1.6 L dH₂O

pH 6 with Conc HCl (Fisher Scientific Ltd, UK)

Washing Buffer (PBS + 0.05% Tween20)

2 l PBS (See above)

1 ml Tween20 (Sigma-Aldrich, UK)

TNB

0.61 g TRIS (Fisher Scientific Ltd, UK) in 100 ml dH₂O, pH 7.5

0.44 g NaCl (Fisher Scientific Ltd, UK)

0.25 g Blocking Reagent (TSA Kit, PerkinElmer Life Sciences)

DAB

1 x 10 mg DAB tablet (DAKO, UK)

10 ml PBS (See above)

Allowed to dissolve (on ice).

(All work involving DAB was carried out in the confines of a tray covered in aluminium foil. Two pairs of gloves were worn at all times. Anything that came in contact with DAB (i.e. pipette tip) was placed in bleach overnight. After overnight exposure to bleach at room temperature, the DAB was safe and was flushed down the sink with copious amounts of water (half life of DAB in solution at RT is <20 minutes). The content of the tray was then autoclaved).

Scott's Water

50 µl 10 M Sodium Hydroxide (Fisher Scientific, UK)

400 ml tap water

Acid-Alcohol

400 ml 70 % Ethanol (Fisher Scientific, UK)

2 ml concentrated HCl (Fisher Scientific, UK)

Protein Extraction and blotting

Lysis Buffer (850 µl) and Protease inhibitors (150 µl) (RIPA Buffer)

Lysis Buffer (store at 4°C for 2-3 months)

50 mM Tris (Fisher Scientific, UK)

150 mM NaCl (Fisher Scientific, UK)

1% Nonide-P40 (Roche Diagnostic Ltd, UK)

0.5% deoxycolic acid (Sigma Aldrich, UK)

Made up to 100 ml with sterile dH₂O

Protease Inhibitors (store at -20°C for 2-3 months)

1 protease inhibitor tablet (Roche Diagnostic Ltd, UK)

1.5 ml sterile H₂O

Running Buffer

3 g TRIS (Fisher Scientific Ltd, UK)

14.42 Glycine (Fisher Scientific Ltd, UK)

1 g SDS (Fisher Scientific Ltd, UK)

Made up to 1 litre with dH₂O

Transfer Buffer

3.03 g TRIS (Fisher Scientific Ltd, UK)

14.4 g Glycine (Fisher Scientific Ltd, UK)

200ml Methanol (Fisher Scientific Ltd, UK)

Made up to 1 litre with dH₂O

pH to 8.5 with Conc HCl (Fisher Scientific Ltd, UK)

1.5 M TRIS-HCl

18.17 g TRIS (Fisher Scientific Ltd, UK)

Made to 100 ml with dH₂O

pH to 8.8 with concentrated HCl (Fisher Scientific Ltd, UK)

0.5 M TRIS-HCl

6.05 g TRIS (Fisher Scientific Ltd, UK)

Made up to 100 ml with dH₂O

pH to 6.8 with concentrated HCl (Fisher Scientific Ltd, UK)

10% SDS

10 g SDS Made up to 100 ml with dH₂O

10X TBS

24.2 g TRIS

80 g NaCl

Made up to 100 ml with dH₂O

pH to 7.6 with Conc HCl (Fisher Scientific Ltd, UK)

Blocking Buffer

15 ml 10X TBS (see above)

135 ml dH₂O

7.5 g non-fat dry milk (Marvel, UK)

0.15 ml Tween20 (Sigma-Aldrich, UK)

Stripping Buffer

7.5 g Glycine (Fisher Scientific Ltd, UK)

Made up to 1 litre with dH₂O

pH to 2.5 with Conc HCl (Fisher Scientific Ltd, UK)

Wash Buffer (TBS/T)

100 ml 10X TBS (see above)

900 ml dH₂O

1 ml Tween20 (Sigma-Aldrich, UK)

Primary Antibody Dilution Buffer

2 ml 10X TBS

18 ml dH₂O

1 g BSA (Sigma-Aldrich, UK)

20 µl Tween20 (Sigma-Aldrich, UK)

6X loading buffer

30% glycerol (Sigma-Aldrich, UK)

0.25 % Xylene cyanole (Sigma-Aldrich, UK)

0.25 % Bromphenol blue (Sigma-Aldrich, UK)